

World Journal of *Gastroenterology*

World J Gastroenterol 2019 April 14; 25(14): 1640-1782



**REVIEW**

- 1640** Precision surgical approach with lymph-node dissection in early gastric cancer
Kinami S, Nakamura N, Tomita Y, Miyata T, Fujita H, Ueda N, Kosaka T

MINIREVIEWS

- 1653** Update on hepatocellular carcinoma: Pathologists' review
El Jabbour T, Lagana SM, Lee H
- 1666** Application of artificial intelligence in gastroenterology
Yang YJ, Bang CS

ORIGINAL ARTICLE**Basic Study**

- 1684** Clinical significance of programmed death 1/programmed death ligand 1 pathway in gastric neuroendocrine carcinomas
Yang MW, Fu XL, Jiang YS, Chen XJ, Tao LY, Yang JY, Huo YM, Liu W, Zhang JF, Liu PF, Liu Q, Hua R, Zhang ZG, Sun YW, Liu DJ
- 1697** Functional role of long non-coding RNA CASC19/miR-140-5p/CEMIP axis in colorectal cancer progression *in vitro*
Wang XD, Lu J, Lin YS, Gao C, Qi F
- 1715** Seven-senescence-associated gene signature predicts overall survival for Asian patients with hepatocellular carcinoma
Xiang XH, Yang L, Zhang X, Ma XH, Miao RC, Gu JX, Fu YN, Yao Q, Zhang JY, Liu C, Lin T, Qu K

Case Control Study

- 1729** Chronic functional constipation is strongly linked to vitamin D deficiency
Panarese A, Pesce F, Porcelli P, Riezzo G, Iacovazzi PA, Leone CM, De Carne M, Rinaldi CM, Shahini E

Retrospective Study

- 1741** Clinical characteristics of non-alcoholic fatty liver disease in Chinese adult hypopituitary patients
Yuan XX, Zhu HJ, Pan H, Chen S, Liu ZY, Li Y, Wang LJ, Lu L, Yang HB, Gong FY

Observational Study

- 1753** Measurement of prostaglandin metabolites is useful in diagnosis of small bowel ulcerations
Matsuno Y, Umeno J, Esaki M, Hirakawa Y, Fuyuno Y, Okamoto Y, Hirano A, Yasukawa S, Hirai F, Matsui T, Hosomi S, Watanabe K, Hosoe N, Ogata H, Hisamatsu T, Yanai S, Kochi S, Kurahara K, Yao T, Torisu T, Kitazono T, Matsumoto T

Prospective Study

- 1764** Endoscopic response to tumor necrosis factor inhibitors predicts long term benefits in Crohn's disease
Alfaro I, Masamunt MC, Planell N, López-García A, Castro J, Gallego M, Barastegui R, Giner A, Vara A, Salas A, Ricart E, Panés J, Ordás I

CASE REPORT

- 1775** Application of a 3D-printed "fistula stent" in plugging enteroatmospheric fistula with open abdomen: A case report
Xu ZY, Ren HJ, Huang JJ, Li ZA, Ren JA

ABOUT COVER

Editorial board member of *World Journal of Gastroenterology*, Jun-Te Hsu, MD, Professor, Surgeon, Surgical Oncologist, Department of Surgery, Chang Gung Memorial Hospital, Taoyuan County and Chang Gung Medicine College, Tao Yuan 333, Taiwan

AIMS AND SCOPE

World Journal of Gastroenterology (*World J Gastroenterol*, *WJG*, print ISSN 1007-9327, online ISSN 2219-2840, DOI: 10.3748) is a peer-reviewed open access journal. The *WJG* Editorial Board consists of 642 experts in gastroenterology and hepatology from 59 countries.

The primary task of *WJG* is to rapidly publish high-quality original articles, reviews, and commentaries in the fields of gastroenterology, hepatology, gastrointestinal endoscopy, gastrointestinal surgery, hepatobiliary surgery, gastrointestinal oncology, gastrointestinal radiation oncology, etc. The *WJG* is dedicated to become an influential and prestigious journal in gastroenterology and hepatology, to promote the development of above disciplines, and to improve the diagnostic and therapeutic skill and expertise of clinicians.

INDEXING/ABSTRACTING

The *WJG* is now indexed in Current Contents®/Clinical Medicine, Science Citation Index Expanded (also known as SciSearch®), Journal Citation Reports®, Index Medicus, MEDLINE, PubMed, PubMed Central, Scopus and Directory of Open Access Journals. The 2018 edition of Journal Citation Report® cites the 2017 impact factor for *WJG* as 3.300 (5-year impact factor: 3.387), ranking *WJG* as 35th among 80 journals in gastroenterology and hepatology (quartile in category Q2).

RESPONSIBLE EDITORS
FOR THIS ISSUE

Responsible Electronic Editor: Han Song

Proofing Editorial Office Director: Ze-Mao Gong

NAME OF JOURNAL

World Journal of Gastroenterology

ISSN

ISSN 1007-9327 (print) ISSN 2219-2840 (online)

LAUNCH DATE

October 1, 1995

FREQUENCY

Weekly

EDITORS-IN-CHIEF

Subrata Ghosh, Andrzej S Tarnawski

EDITORIAL BOARD MEMBERS

<http://www.wjgnet.com/1007-9327/editorialboard.htm>

EDITORIAL OFFICE

Ze-Mao Gong, Director

PUBLICATION DATE

April 14, 2019

COPYRIGHT

© 2019 Baishideng Publishing Group Inc

INSTRUCTIONS TO AUTHORS

<https://www.wjgnet.com/bpg/gerinfo/204>

GUIDELINES FOR ETHICS DOCUMENTS

<https://www.wjgnet.com/bpg/GerInfo/287>

GUIDELINES FOR NON-NATIVE SPEAKERS OF ENGLISH

<https://www.wjgnet.com/bpg/gerinfo/240>

PUBLICATION MISCONDUCT

<https://www.wjgnet.com/bpg/gerinfo/208>

ARTICLE PROCESSING CHARGE

<https://www.wjgnet.com/bpg/gerinfo/242>

STEPS FOR SUBMITTING MANUSCRIPTS

<https://www.wjgnet.com/bpg/GerInfo/239>

ONLINE SUBMISSION

<https://www.f6publishing.com>



Precision surgical approach with lymph-node dissection in early gastric cancer

Shinichi Kinami, Naohiko Nakamura, Yasuto Tomita, Takashi Miyata, Hideto Fujita, Nobuhiko Ueda, Takeo Kosaka

ORCID number: Shinichi Kinami (0000-0001-9867-3120); Naohiko Nakamura (0000-0002-5542-0163); Yasuto Tomita (0000-0001-8019-7058); Takashi Miyata (0000-0002-0348-2637); Hideto Fujita (0000-0002-6702-8011); Nobuhiko Ueda (0000-0002-7862-3967); Takeo Kosaka (0000-0002-8213-8155).

Author contributions: Kinami S is responsible for the scientific context and wrote the manuscript; Nakamura N, Tomita Y, Miyata T, Fujita H, Ueda N, and Kosaka T contributed literature review and analysis, drafting, editing and critical revision, and approval of the final version.

Conflict-of-interest statement: The authors declare no conflicts of interest related to the publication of the study.

Open-Access: This article is an open-access article which was selected by an in-house editor and fully peer-reviewed by external reviewers. It is distributed in accordance with the Creative Commons Attribution Non Commercial (CC BY-NC 4.0) license, which permits others to distribute, remix, adapt, build upon this work non-commercially, and license their derivative works on different terms, provided the original work is properly cited and the use is non-commercial. See: <http://creativecommons.org/licenses/by-nc/4.0/>

Manuscript source: Invited manuscript

Shinichi Kinami, Naohiko Nakamura, Yasuto Tomita, Takashi Miyata, Hideto Fujita, Nobuhiko Ueda, Takeo Kosaka, Department of Surgical Oncology, Kanazawa Medical University, Ishikawa 920-0293, Japan

Corresponding author: Shinichi Kinami, MD, PhD, Professor, Department of Surgical Oncology, Kanazawa Medical University, 1-1 Daigaku, Uchinada-machi, Kahoku-gun, Ishikawa 920-0293, Japan. kinami@kanazawa-med.ac.jp

Telephone: +81-76-2862211

Fax: +81-76-2864626

Abstract

The gravest prognostic factor in early gastric cancer is lymph-node metastasis, with an incidence of about 10% overall. About two-thirds of early gastric cancer patients can be diagnosed as node-negative prior to treatment based on clinic-pathological data. Thus, the tumor can be resected by endoscopic submucosal dissection. In the remaining third, surgical resection is necessary because of the possibility of nodal metastasis. Nevertheless, almost all patients can be cured by gastrectomy with D1+ lymph-node dissection. Laparoscopic or robotic gastrectomy has become widespread in East Asia because perioperative and oncological safety are similar to open surgery. However, after D1+ gastrectomy, functional symptoms may still result. Physicians must strive to minimize post-gastrectomy symptoms and optimize long-term quality of life after this operation. Depending on the location and size of the primary lesion, preservation of the pylorus or cardia should be considered. In addition, the extent of lymph-node dissection can be individualized, and significant gastric-volume preservation can be achieved if sentinel node biopsy is used to distinguish node-negative patients. Though the surgical treatment for early gastric cancer may be less radical than in the past, the operative method itself seems to be still in transition.

Key words: Stomach neoplasms surgery; Gastrectomy methods; Recovery of function; Sentinel lymph node surgery; Gastric cancer

©The Author(s) 2019. Published by Baishideng Publishing Group Inc. All rights reserved.

Core tip: The surgical treatment for early gastric cancer seems to be appropriately radical, because almost all patients can be cured by gastrectomy with lymph-node dissection up to D1+. However, after D1+ gastrectomy, multiple functional symptoms are caused by the loss of the stomach. Physicians must strive to reduce post-gastrectomy symptoms and

Received: February 15, 2019**Peer-review started:** February 17, 2019**First decision:** February 26, 2019**Revised:** March 9, 2019**Accepted:** March 16, 2019**Article in press:** March 16, 2019**Published online:** April 14, 2019**P-Reviewer:** Demetrashvili Z, Norero E**S-Editor:** Yan JP**L-Editor:** A**E-Editor:** Song H

optimize quality of life. About two-thirds of early gastric cancers are node-negative and can be resected by endoscopic submucosal dissection. The extent of lymph-node dissection can be individualized, and significant gastric preservation can be achieved, with sentinel-node biopsy. The operative method itself is still in transition.

Citation: Kinami S, Nakamura N, Tomita Y, Miyata T, Fujita H, Ueda N, Kosaka T. Precision surgical approach with lymph-node dissection in early gastric cancer. *World J Gastroenterol* 2019; 25(14): 1640-1652

URL: <https://www.wjgnet.com/1007-9327/full/v25/i14/1640.htm>

DOI: <https://dx.doi.org/10.3748/wjg.v25.i14.1640>

INTRODUCTION

Gastric cancer is a public health concern worldwide, and especially in Asia^[1,2]. Therefore, Japanese and South Korean physicians have focused on early detection of gastric cancer^[3]. For decades, half of the gastric cancers detected in Japan and Korea have been early-stage cancer^[4]. The outcome of surgical resection for early gastric cancer is excellent, and most clinicians recognize that early gastric cancer is curable. The focus of recent topical discussion of early gastric cancer is minimally invasive treatment. Many early gastric cancers have been resected endoscopically^[5]. Less invasive approaches such as laparoscopic gastrectomy and robotic gastrectomy have also been widely carried out^[6-8]. On the other hand, standard surgery for early gastric cancer is distal partial gastrectomy (DG) or total gastrectomy (TG), with lymph-node dissection^[9], so, even with a laparoscopic approach, post-gastrectomy symptoms and functional effects cannot be ignored^[10]. In this article, we reconsider surgical treatment options for early gastric cancer and discuss the most appropriate treatment.

THE CHARACTERISTICS OF EARLY GASTRIC CANCER

Early gastric cancer is defined as carcinoma in which depth of invasion is restricted to the mucosal layer or submucosa^[11]. The presence or absence of lymph-node metastasis is irrelevant to the classification^[11]. Most early gastric cancers are asymptomatic. Early gastric cancer is often detected with gastroscopy or barium meal during a health-screening checkup^[12]. Advanced gastric cancer is frequently associated with hematogenous or peritoneal metastases, while in contrast, early gastric cancer has few such distant metastases. On the other hand, early gastric cancer is rarely associated with lymph-node metastasis. The frequency of lymph-node metastasis is 2%-3% in mucosal cancer and 15%-20% in submucosal cancer^[13-21]. Numerous previous studies have examined the location of these lymph node metastases. In the classification of gastric carcinoma of the Japanese Gastric Cancer Association^[22], the regional lymph nodes of the stomach are classified in detail and numbered. Currently, the extent of lymph-node metastasis has been evaluated in terms of the number of metastases, but in the past, regional nodes were grouped according to the location of the cancer, and the degree of lymph-node metastasis was evaluated based on which group of nodes the metastasis had reached. The precise data of nodal metastasis of early gastric cancer described in a representative literature are summarized in Table 1^[23-26]. Most nodal metastasis in early gastric cancer was found to be limited to perigastric nodes and nodes number 7, 8a, and 9. Based on these results, the Japanese Gastric Cancer Association established D1+^[27], the extent of lymph-node dissection for submucosal cancer (Figure 1). The disease-specific survival of D1+ gastrectomy for early gastric cancer is often given as 96%-98% in articles investigating the outcome of laparoscopic gastrectomy^[28-30].

In summary, the characteristics of early gastric cancer are as follows: there are few hematogenous and peritoneal metastases; the determining prognostic factor is lymph node metastasis; the incidence of nodal metastasis is about 10% overall; and even with nodal metastases, almost all patients can be cured by gastrectomy with D1+ lymph-node dissection.

ADVENT OF ENDOSCOPIC TREATMENT

Table 1 Summary of representative literature on the precise incidence of nodal metastasis in early gastric cancer

Nodal location	Total cases	Perigastric nodes (%)						aLGA (%)	Suprapancreatic nodes (%)				SpH (%)	aPH A (%)	PAN (%)
Station NO		1	2	3	4	5	6	7	8a	9	11p	11d	10	12a	16
Kitamura <i>et al</i> ^[23]	634				8.2			1.6	0.94	0.31	0.31	0.00	0.00	0.16	0.16
Tanaka <i>et al</i> ^[24]	2368	0.97	0.08	4.6	3.2	0.51	2.4	1.4	0.63	0.72	0.42	0.00	0.00	0.00	0.00
Nakajima <i>et al</i> ^[25]	3630	0.90	0.11	5.9	3.9	0.47	3.4	1.1	1.1	1.1	0.36	0.03	0.08	0.06	0.25
Yoshikawa <i>et al</i> ^[26] ¹	715 ¹				19.0 ¹			2.0 ¹	1.8 ¹	0.13 ¹	0.13 ¹	0.00 ¹	0.00 ¹	0.00 ¹	0.00 ¹

¹Study of submucosal cancer. Percentages represent proportion of patients with metastasis in lymph nodes of given station. All articles but Yoshikawa include both mucosal cancer and submucosal cancer; Yoshikawa includes only submucosal cancer cases. aLGA: Nodes along left gastric artery; SpH: Nodes at the hilum of spleen; aPHA: Nodes along hepatic artery proper; PAN: Paraaortic nodes.

However, after D1+ gastrectomy, several functional symptoms are caused by the loss of the stomach. Reduction of gastric acid secretion impairs food digestive capacity. The amount of food intake decreases, nutritional status worsens, and body weight decreases. In addition, patients suffer from various postgastrectomy symptoms (PGS). They include reflux esophagitis, dumping syndrome, defecation abnormalities, anorexia, and abdominal pain. These symptoms are thought to compromise patients' quality of life (QOL). In addition, several long-term aftereffects may occur, such as iron deficiency anemia, pernicious anemia, bone metabolic disorders, gastric stump cancer, cholelithiasis, and ileus^[31-37]. Taking these disadvantages into consideration, if there is another therapeutic option, we would like to adopt it to avoid gastrectomy.

There are endoscopic treatments. The endoscopic treatments are alternatives to surgery using gastrofibroscopy. Gastroscopy was developed in Japan, and endoscopic treatments for gastric tumor were also invented and developed in Japan. The beginning of endoscopic treatment is endoscopic mucosal resection (EMR). EMR is a method of injecting physiological saline into the submucosal layer to lift the lesion, narrowing the mucosa with a snare, and removing the mucosa by applying a high frequency current^[38]. During the same period, endoscopic treatments using lesion cauterization with laser, heating probe, argon plasma discharge, etc., had been attempted. These therapies have some advantages and serious disadvantages, and they have not attained therapeutic value sufficient to replace surgical treatment^[39,40]. However, this situation has changed with the advent of endoscopic submucosal dissection (ESD) technique^[40]. ESD is the method of dissecting and removing the specimen after incision of the mucosa around the entire circumference using a dedicated device. In ESD, the specimen is removed in one piece, which secures a safety margin, the treatment outcome is equal to prior surgical treatments, and it is possible for the patient to enjoy the same QOL as before the treatment. The greatest disadvantage of ESD was its technical difficulty, though this difficulty was decreased by the development of electrocautery equipment and advancements in the dedicated device. Nowadays, ESD is not just an alternative to surgery, it is becoming a complete replacement for certain types of surgery^[40]. The indication for ESD is a case in which the clinic-pathological data available prior to treatment is presumed to be negative for nodal metastasis. The frequency of nodal metastasis is 2%-3% in mucosal cancer and 15%-20% in submucosal cancer. Therefore, ESD is indicated in most mucosal cancers. Gotoda *et al*^[41] proposed an indication for ESD from a study of surgical cases of two Japanese high-volume centers. Since the probability of nodal metastasis was set not to exceed the mortality rate after surgical resection, these criteria includes cases with a very low, but not zero, percentage probability of nodal metastasis. Recently, the long-term prognosis of the cases who underwent ESD according to this indication has been reported, and it has been confirmed that it is equal to the prognosis of the surgical resection^[42-44]. Current indications for ESD are shown in Tables 2 and 3. These are new recommendations, stated in Japanese gastric cancer treatment guidelines for 2018^[9]. In the table of indications (Table 2), Zone A is a former absolute indication. Zone B is newly added absolute indication proven by prospective observational trial JCOG 0607. Zone C is the expanded indication. Although this area is considered to be sufficiently curable, caution is necessary because the proof of the prospective observational trial JCOG1009/1010 has not been completed yet. Zone D is labeled "relative indication". This zone comprises an alternative treatment to surgery, reserved only for patients unable to endure surgical treatment. The guideline also defines the evaluation of curability after resection (Table 3). If the specimen is diagnosed as eCuraA or eCureB, the cancer is considered completely resected and no

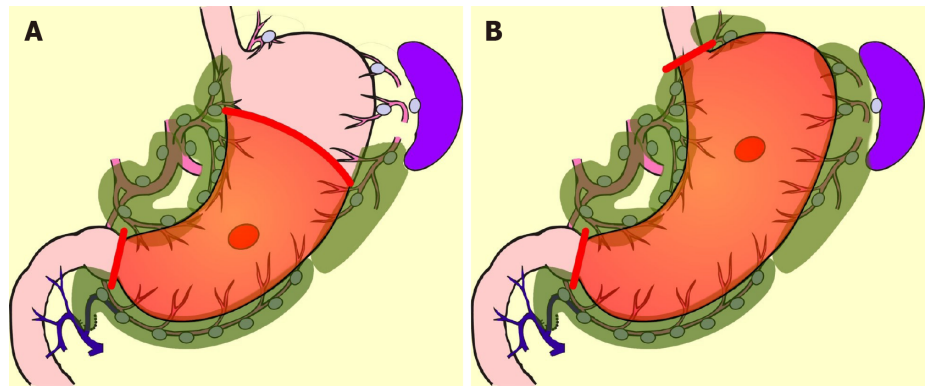


Figure 1 Standard surgery for early gastric cancer. A: Distal partial gastrectomy D1+; B: Total gastrectomy D1+.

additional treatment is required. On the other hand, for eCuraC it is considered that the cancer has not been completely resected, and additional treatment is necessary. The lesion of eCuraC-1 needs additional local treatment, and in the case of cCuraC-2 surgical treatment with lymph-node dissection should be added.

LESS INVASIVE SURGICAL TREATMENT

In cases where ESD is not indicated, surgical resection is necessary because of the possibility of nodal metastasis^[20,41]. In East Asia, most surgical treatment for early gastric cancer is laparoscopic D1+ gastrectomy. Laparoscopic gastrectomy was introduced in Japan in 1991^[45]. At the time, the quality of laparoscopic views was poor, and the instruments were inadequate to the task. Therefore, lymph-node dissection was extremely difficult. Laparoscopic surgeries for early gastric cancer at that time consisted of local resection (LR) without lymphadenectomy^[46], and intra-gastric surgery dissecting the mucosa^[47]. Though the pioneers also attempted laparoscopic DG, the extent of nodal dissection was confined to peri-gastric nodes^[45]. The indication for these treatments were cases in which lymph-node metastasis was presumed to be absent based on clinico-pathological features^[45-47]. These approaches gradually disappeared with the advent of ESD. Subsequently, the invention of ultrasonic activated devices and technological advancements by surgeons have enabled laparoscopic lymph-node dissection comparable to conventional open surgery. Therefore, laparoscopic DG or TG with D1+ or D2 came to be performed as daily practice, and gradually replaced conventional open surgery.

There are many articles comparing laparoscopic gastrectomy and conventional open gastrectomy for patients with early gastric cancer^[48,49], and a meta-analysis of prospective trials has also been conducted^[49]. Perioperative surgical safety and oncological safety are considered similar^[48,49]. The advantages of laparoscopic gastrectomy over conventional open surgery are as follows: the smaller size of the incision; lower number of times analgesic is required; lesser amount of intraoperative hemorrhage; and fewer occurrences of wound dehiscence and respiratory complications. On the other hand, the drawbacks are high cost and longer operation time^[49]. Although it is difficult to conclusively establish the minimal invasiveness of laparoscopic gastrectomy, it is suggested by the shorter time to first flatus and shorter hospital stays.

THE PGS AND QOL AFTER GASTRECTOMY

Because the size of the wound is clearly visible, laparoscopic surgery is an attractive option for hospitals. The high degree of difficulty of the laparoscopic gastrectomy is an attractive challenge for young surgeons. Thus, laparoscopic gastrectomy has become widespread in East Asia. However, the benefits of laparoscopic gastrectomy in the long term have not yet been sufficiently examined.

Various PGS occur after gastrectomy^[34-37], and, these symptoms seem to worsen QOL^[35]. The severity of these PGS and the deterioration of QOL are subjective measures, and objective evaluations are difficult. These items are patient-reported outcomes whose scientific validation must be performed using definitive questionnaires that have already been validated psychometrically. DAUGS^[50] and PGSAS-

Table 2 Updated preoperative indications for endoscopic submucosal dissection in Japanese gastric cancer treatment guidelines 2018

Depth of invasion (preoperative)	Clinical mucosal cancer			
Intra-tumoral ulcer or ulcer scar	UL 0		UL 1	
Tumor size (Long axis)	2 cm	> 2 cm	3 cm	> 3 cm
Differentiated	A	B	B	D
Undifferentiated	C	D	D	D

A: Absolute indication for both endoscopic mucosal resection and endoscopic submucosal dissection; B: Absolute indication for endoscopic submucosal dissection; C: Expanded indication for endoscopic submucosal dissection; D: Relative indication (Alternative).

45^[34] have been reported as questionnaires specifically for post-gastrectomy patients. Of these, PGSAS-45 seems to be the de-facto standard to verify PGS and QOL, because it covers items that are considered important by gastrectomy specialists, it includes a short-form 8 (SF-8) for the assessment of generic QOL, and the standard values of Japanese patients are known based on data from more than 2500 cases^[34].

Kinami *et al.*^[51] evaluated the superiority in PGS and QOL at least 1 year after surgery of patients who underwent laparoscopic gastrectomy, using data from the PGSAS study for additional analysis. The outcome measures included in the PGSAS-45 are classified into three domains: the symptom domain, the living status domain, and the QOL domain^[34]. A few main outcome measures of PGSAS-45 were superior after laparoscopic, compared to conventional open, DG surgery. These measures were: The need of additional food; dissatisfaction with symptoms; and the mental component summary of SF-8. These items were of the living status or QOL domain, not the symptom domain. In contrast, for TG, there was no difference in the scores of main outcome measures between laparoscopic surgery and conventional open surgery. From this large-scale analysis, it was concluded that there is no advantage for laparoscopic TG from the viewpoint of the PGS^[51]. Generally, the only difference between laparoscopic surgery and conventional open surgery is the length of the incision. Therefore, a large difference in PGS between laparoscopic and open surgery would not be expected.

LIMITED SURGERY FOR EARLY GASTRIC CANCER

Even if the advantages are small, such as the size of the incision, the number of times analgesic is used, and a slight improvement in QOL, it is reasonable to apply laparoscopic gastrectomy to the early gastric cancer, if the surgical and oncological safety are equivalent. However, if other approaches can be used to prevent PGS, palliation of PGS should be prioritized to benefit patients in the long term, rather than focusing on the small incision size afforded by laparoscopic surgery. Limited surgery is a method expected to palliate PGS. Limited surgical approaches consist of reduced resection area of the stomach and smaller extent of nodal dissection. These include pylorus-preserving gastrectomy (PPG), proximal gastrectomy (PG), and LR. In performing LR, the unconventional decision to omit lymph-node dissection is necessary. Therefore, LR is rarely done today, while ESD is routinely performed^[52].

In comparison with DG, PPG is a pylorus-preserving procedure^[53]. Generally, the right gastric artery and pyloric branch of the vagus nerve are preserved to secure an antral cuff of about 3 cm. It is expected to be effective for preventing dumping symptoms, regurgitation of duodenal juice into the stomach, and gallstone formation after gastrectomy^[54,55]. This procedure is indicated in cases in which right gastric-artery lymph-node dissection can be omitted. Practically speaking, these patients will have tumors located at the middle part of the stomach with distal margins more than 4 cm from the pylorus^[9]. Even if PPG is adopted, lymph-node dissection at nodes other than those located at the right gastric artery area is possible, and D1+ for PPG is included in the Japanese gastric cancer treatment guidelines^[9] (Figure 2). The survival outcome of PPG is considered equal to that of DG^[54,55]. In the PGSAS study, it was confirmed that, in comparison with Billroth I cases, diarrhea and dumping symptoms and the necessity of additional food was lower in PPG cases^[56].

PG is an alternative to TG for early gastric cancer located in the stomach's upper third. Compared with TG, PG preserves over one-half of the distal stomach and is considered to be superior in improving nutritional status and preventing anemia because of higher dietary intake and preserved secretion of gastric acid, Castle

Table 3 Updated evaluation of curability after endoscopic submucosal dissection in Japanese gastric cancer treatment guidelines 2018

Updated evaluation of curability after endoscopic submucosal dissection	
eCuraA	<i>En-bloc</i> resection, predominantly differentiated adenocarcinoma, pathological mucosal cancer (pT1a), HM0, VM0, Ly0, V0 UL0 (regardless of size) UL1, under 3 cm in diameter If size of undifferentiated component is > 2 cm, tumor is diagnosed as eCuraC-2
eCuraB	<i>En-bloc</i> resection, HM0, VM0, Ly0, V0 UL0, under 2 cm in diameter, predominantly undifferentiated adenocarcinoma, pathological mucosal cancer (pT1a) UL1, under 3 cm in diameter, predominantly differentiated adenocarcinoma, pathological submucosal cancer within 500 μ m (pT1b1) If there is an undifferentiated component in the submucosal layer, tumor is diagnosed as eCuraC-2
eCuraC-1	Lesion meeting criteria of eCuraA or eCuraB except with positive lateral margin or non- <i>en-bloc</i> resection.
eCuraC-2	The lesion meets none of eCuraA, eCuraB, or eCuraC-1

intrinsic factor, and gastrin. It is reported that if the cancer lesion is limited to the upper-third of the stomach, dissection of the lymph nodes along the right gastric artery and right gastroepiploic artery can be omitted without compromising radicality^[57-60]. In the Japanese gastric cancer treatment guideline, D1+ for PG is set^[9] (Figure 3). In the PGSAS study, PG prevented diarrhea and dumping symptoms, slightly diminished weight loss, and lowered the necessity of additional food than TG^[36].

Though these limited surgeries are superior in terms of preserving some functions lost by gastrectomy, it is known that some patient dissatisfaction may result from PGS. PPG occasionally creates cases where the hospitalization period is extended due to either delayed gastric emptying or small-stomach symptoms^[61]. There are also many cases in which reflux esophagitis or gastric stasis are generated after PG^[62,63]. Due to these facts, such limited surgeries are sometimes considered difficult procedures. In a questionnaire survey conducted by gastric cancer specialists in Japan by the Japanese Society for Gastro-surgical Pathophysiology, only 30% of surgeons had adopted PPG and 70% of surgeons had adopted PG. Several attempts to reduce the aforementioned postoperative difficulties have been reported. In PPG, preservation of the infra-pyloric arteries and veins has been reported to be beneficial in preventing delayed gastric emptying^[64-66]. The PGSAS study also concluded that size of proximal remnant stomach, gastro-gastric anastomoses with hand sewing, and adequate size of the antral cuff were helpful in reducing postoperative disability^[67]. In PG, the reconstruction method is considered to be useful for the prevention of reflux esophagitis, and pyloroplasty and preservation of the hepatic and pyloric branches of vagus are considered to be useful for the reduction of gastric stasis. Reconstruction is particularly important, and various method to prevent reflux have been devised (Figure 4), but every method has its own advantages and disadvantages, and there is still no definitive operative method^[68-76]. Methods to reduce postoperative damage of PG were also studied in the PGSAS study, and it has been concluded that a large distal remnant stomach and a pyloric bougie were effective^[77].

Though PPG and PG are complicated procedures, reports of laparoscopic PPG and laparoscopic PG have increased recently^[78-82]. However, the results of PPG and PG performed laparoscopically are equivalent to conventional open surgery in terms of safety and radicality, while preservation of function is not yet fully proven. Regarding function preservation, a retrospective study comparing laparoscopic PPG with laparoscopic DG was reported, again with fewer cases presenting with diarrhea and dumping symptoms^[80]. However, reports comparing PPG or PG in conventional open surgery and laparoscopic surgery are not impressive^[82]. Kinami *et al*^[51] analyzed the data of the PGSAS study and found that laparoscopic PPG had better physical-component scores on SF-8 than open PPG, whereas there was no difference in the scores for main outcome measures between laparoscopic PG and open PG. From these results, it is concluded that the function preserved in PPG and PG in laparoscopic surgeries are equivalent to those in the conventional open surgeries. Thus, it appears that there is little long-term advantage in laparoscopic surgery.

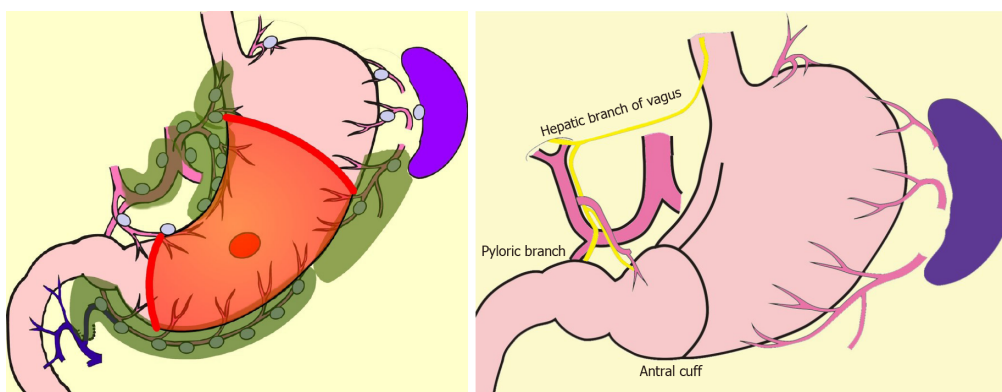


Figure 2 Pylorus-preserving gastrectomy D1+.

FUNCTION PRESERVING RADICAL GASTRECTOMY

As described above, studies of large cohorts using the PGSAS demonstrated that PPG and PG are superior in the occurrence rate of dumping symptoms and diarrhea, and the maintenance of eating habits. Nevertheless, comparing PPG and DG, or PG and TG, other functional outcomes were found to be similar^[36,56]. Therefore, more extensive gastric preservation is required to prevent more PGS outbreaks and improve QOL. The extent of resection of the stomach is inseparable from that of lymph-node dissection. Therefore, in order to carry out better function-preserving procedures, it is necessary to boldly omit the lymph-node dissection in order to preserve blood circulation to the stomach.

What is the lymph-node metastasis rate of surgical cases for early gastric cancer today, when ESD has become standard? In the latest version of the Japanese gastric-cancer treatment guideline (5th edition, in Japanese), the results of research on equalization and actual conditions of gastric-cancer medical treatment in Japan as of fiscal 2013 is reported^[9]. This study investigated the course of gastric-cancer treatment in 297 cancer hospitals in Japan. The total number of patients with gastric cancer was 44879, and the endoscopic treatment rate for pretreatment T1N0 gastric cancer was 64.1%. Therefore, at standard cancer treatment facilities in Japan, the number of primary surgical cases for T1N0 gastric cancer may be estimated to be approximately one-third. This is considering that 90% of early gastric cancers are negative for metastases. If all endoscopically treated cases are assumed to be node negative, 70% of surgical cases are calculated to be negative for metastasis. Therefore, only 30% of cases require D1+ (*i.e.*, are those in which the possibility of lymph-node metastasis cannot be ruled out). D1+ may be unnecessary in 70% of cases.

Currently, however, it is difficult to reduce the extent of dissection below D1+. The frequency of metastasis in group 2 lymph nodes is low. There are two opinions: one is that there is no large benefit from the prophylactic dissection^[16]; and the other is that there is a significant difference in the prognosis for D1 and D2^[17]. The general view of specialists is that the extent of lymph-node dissection should not be indiscriminately reduced. In addition, there is no large difference in gastrectomy extent between D1+ and D1. Reduction of nodal dissection from D1+ to D1 is of little value in terms of PGS prevention. To prevent PGS, intraoperative diagnosis of node-negative patients should be required to establish the appropriateness of omitting peri-gastric nodal dissection, with its benefits of preservation of gastric blood flow and reduction in the resection area of stomach.

SENTINEL NODE BIOPSY AND BASIN DISSECTION

Currently, the best reliable method of intraoperative nodal diagnosis is the sentinel-node biopsy^[83]. A sentinel node (SN) is defined as the node that receives lymphatic flow directly from a primary tumor. SN biopsy has been attempted most for gastric cancer among all gastrointestinal cancers^[84-88]. In a multicenter prospective clinical trial in Japan, the SN concept was proved valid in early gastric cancer^[85]. It is believed that the extent of lymph-node dissection can be reduced without compromising the radicality, if the node-negative patient is able to be diagnosed by SN biopsy^[89]. Unfortunately, unlike breast cancer, in gastric cancer there is no room for additional nodal dissection after initial surgery, the prognosis of micro-metastasis is unknown,

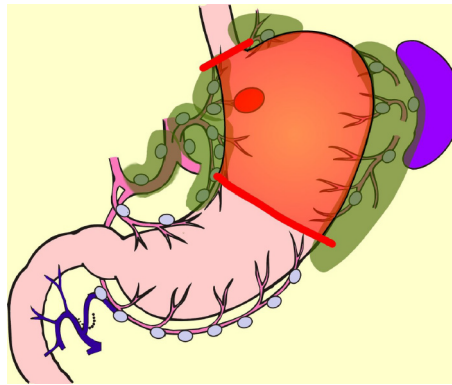


Figure 3 Proximal gastrectomy D1+.

and a method for predicting non-SN metastases in patients with positive SN metastases has not been established. Rapid intraoperative diagnostic methods for nodal metastasis which can diagnose to the micro-metastasis level has not been established either. Therefore, it is considered premature to omit all lymphadenectomy by utilizing SN biopsy in gastric cancer. Lymphatic-basin dissection has been proposed as a realistic solution for omitting the nodal dissection^[84-89]. This is a method for gastric SN biopsy, in which the lymphatic basin identified by dye mapping is removed *en-bloc*, and the SNs are identified *ex-vivo* after basin dissection, and is sent for intraoperative rapid diagnosis^[88]. After SN biopsy, D2 gastrectomy is added if the patient is diagnosed as node-positive, but if the patient is diagnosed as node negative, additional dissection is omitted, the gastric feeding artery outside the basin is preserved, and the resection area of stomach is minimized. Thus, by adopting the SN biopsy, a large-area stomach-sparing function-preserving radical gastrectomy, as shown in Figure 5, can be performed. Kinami *et al*^[88] reported that there was no recurrence in 174 cases in which nodal dissection outside the basin was omitted. Isozaki *et al*^[90] reported that PGS in cases involving function-preserving procedures according to this protocol were clearly better than standard procedures.

A large-scale prospective study is currently ongoing in Korea to verify survival prognoses after gastric-cancer SN biopsy^[91]. Additionally, a prospective trial to verify both prognosis and function-preservation effects of the function-preserving radical gastrectomy accompanied by basin dissection is on-going in Japan^[89]. In addition, attempts to reproduce this function-preserving radical gastrectomy using laparoscopic surgery have also been reported^[84,89,92]. If the two prospective studies described above show evidence supporting SN biopsy in gastric cancer, the surgery for early gastric cancer will eventually shift from the current laparoscopic D1+ gastrectomy to a laparoscopic, tailor-made, function-preserving radical gastrectomy, in which patients may be diagnosed as node-negative intraoperatively.

However, there are many problems to be solved in SN-directed, tailor-made function-preserving gastrectomy techniques. Solutions for the following issues are necessary: setting the proper range for lymphatic basin dissection; establishment of quick, convenient, universally-applicable intraoperative diagnosis method; and strategies for preventing dysfunction after surgery. Physicians should also pay attention to the risk of metachronous multiple gastric cancers when the remnant stomach area is large.

SUMMARY: OPTIMAL SURGICAL TREATMENT, NOW AND IN THE FUTURE

Early gastric cancer can be cured by surgical treatment, and physicians must be mindful of reduction of PGS and improvement of QOL over the long term after the operation. The authors intention in this article is to provide a roadmap for developing precision surgery for early gastric cancer from these three perspectives: Lymph-node dissection, function preservation, and a less invasive approach.

Lymph-node dissection: D1+ is an appropriate and standardized extent of dissection for early gastric cancer in view of radicality and safety. However, D1+ is not essential in all cases. The extent of lymph-node dissection can be individualized if SN biopsy is used to distinguish node-negative patients.

Function preserving: Depending on the location and size of the primary lesion,

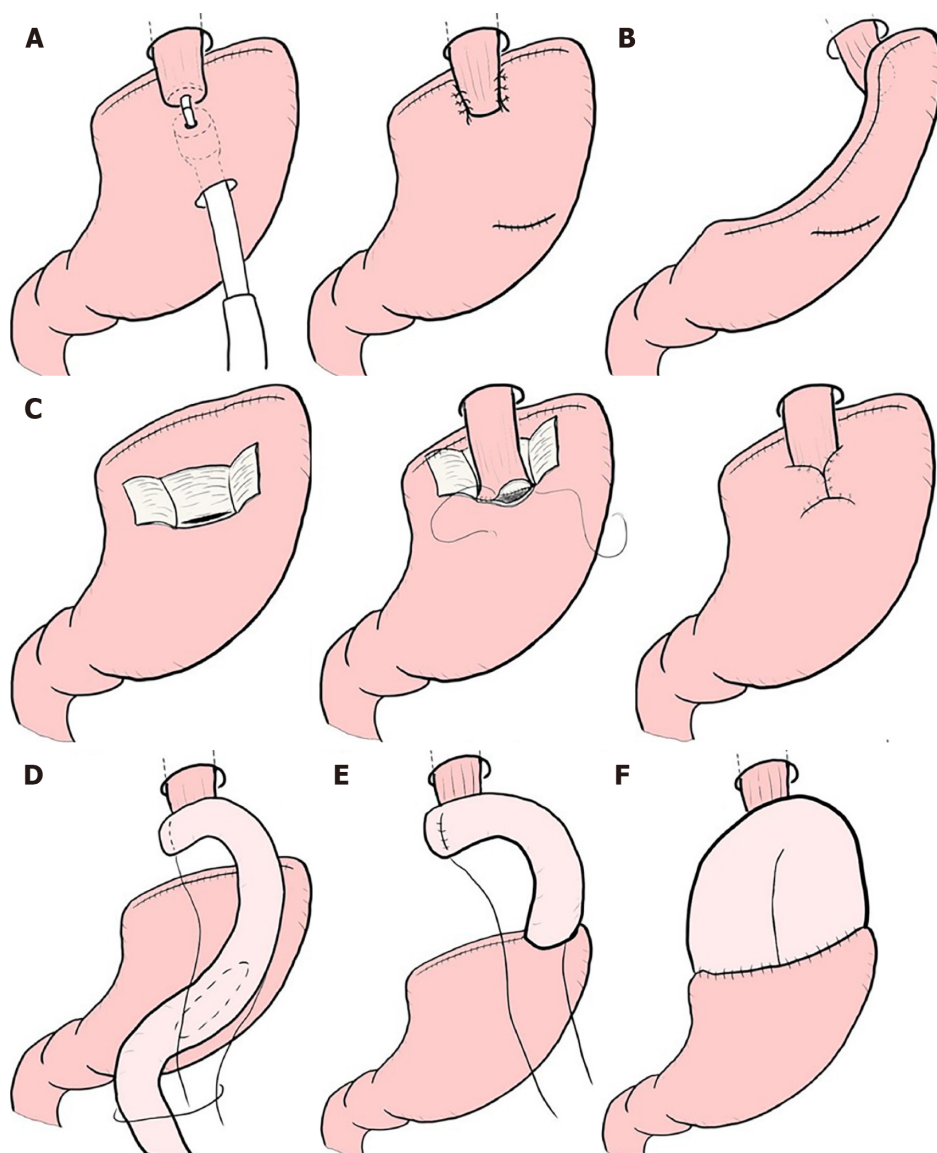


Figure 4 Reconstruction after proximal gastrectomy. A: Additional anti-reflux procedures for esophagogastric anastomosis; B: Gastric tube reconstruction; C: Double-flap technique (Kamikawa method); D: Double tract reconstruction; E: Jejunal interposition; F: Jejunal pouch interposition.

preservation of the pylorus or cardia should be considered. If the patient is diagnosed as node-negative by SN biopsy, significant, large-volume gastric preservation can be achieved.

Less invasive approach: There seems to be no problem with the use of laparoscopic surgery because the perioperative and oncological safety are similar to open surgery, but the physician should be aware that laparoscopic surgery is technically difficult. Prioritizing completion of laparoscopic surgery and forgoing conversion to limited or function-preserving open surgery is undesirable in terms of PGS reduction. However, if advances in surgical devices or technological innovations in robotic-assisted surgery are made, all operations will eventually be undertaken using a less invasive approach.

Though the surgical treatment for early gastric cancer is currently radical, the operative method itself seems to be still in a transitional stage. Evidence-based gastric-cancer SN biopsy and technological innovations in robotic-assisted surgery are sure to bring a new era of minimally invasive, significantly function-preserving surgery.

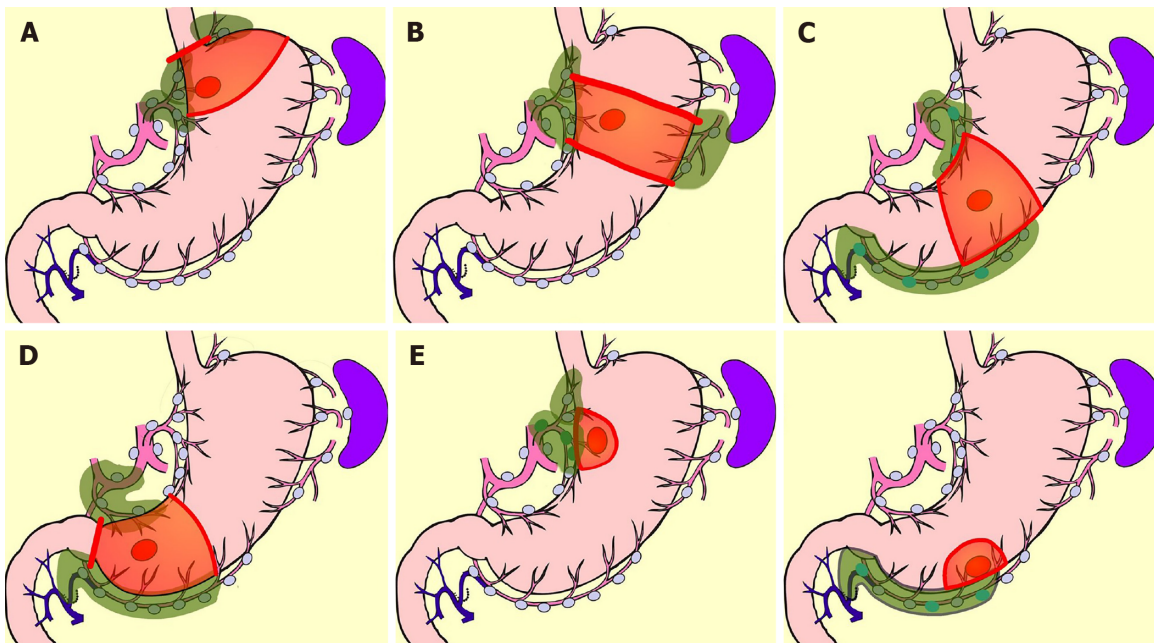


Figure 5 Function-preserving radical gastrectomy derived by sentinel node biopsy. A: Mini-proximal gastrectomy; B: High segmental gastrectomy; C: Segmental gastrectomy; D: Mini-distal gastrectomy; E: Local resection of stomach.

REFERENCES

- 1 **Bray F**, Ferlay J, Soerjomataram I, Siegel RL, Torre LA, Jemal A. Global cancer statistics 2018: GLOBOCAN estimates of incidence and mortality worldwide for 36 cancers in 185 countries. *CA Cancer J Clin* 2018; **68**: 394-424 [PMID: 30207593 DOI: 10.3322/caac.21492]
- 2 **Chen W**, Zheng R, Baade PD, Zhang S, Zeng H, Bray F, Jemal A, Yu XQ, He J. Cancer statistics in China, 2015. *CA Cancer J Clin* 2016; **66**: 115-132 [PMID: 26808342 DOI: 10.3322/caac.21338]
- 3 **Sumiyama K**. Past and current trends in endoscopic diagnosis for early stage gastric cancer in Japan. *Gastric Cancer* 2017; **20**: 20-27 [PMID: 27734273 DOI: 10.1007/s10120-016-0659-4]
- 4 **Sobue T**, Saika K. Epidemiology of stomach cancer (in Japanese with English abstract). *Stomach Intest* 2018; **53**: 522-524
- 5 **Nishizawa T**, Yahagi N. Endoscopic mucosal resection and endoscopic submucosal dissection: Technique and new directions. *Curr Opin Gastroenterol* 2017; **33**: 315-319 [PMID: 28704212 DOI: 10.1097/MOG.0000000000000388]
- 6 **Wang S**, Ling T, Zhao E, Cao H. The surgical treatment of gastric cancer in the era of minimally invasive surgery. *Minerva Chir* 2017; **72**: 334-346 [PMID: 28415834 DOI: 10.23736/S0026-4733.17.07347-3]
- 7 **Tokunaga M**, Kaito A, Sugita S, Watanabe M, Sunagawa H, Kinoshita T. Robotic gastrectomy for gastric cancer. *Transl Gastroenterol Hepatol* 2017; **2**: 57 [PMID: 28616612 DOI: 10.21037/tgh.2017.05.09]
- 8 **Caruso S**, Patrìti A, Roviello F, De Franco L, Franceschini F, Coratti A, Ceccarelli G. Laparoscopic and robot-assisted gastrectomy for gastric cancer: Current considerations. *World J Gastroenterol* 2016; **22**: 5694-5717 [PMID: 27433084 DOI: 10.3748/wjg.v22.i25.5694]
- 9 **Japanese Gastric Cancer Association**. Japanese gastric cancer treatment guidelines 2018 (ver. 5). Tokyo: Kanehara-shuppan 2018;
- 10 **Davis JL**, Ripley RT. Postgastrectomy Syndromes and Nutritional Considerations Following Gastric Surgery. *Surg Clin North Am* 2017; **97**: 277-293 [PMID: 28325187 DOI: 10.1016/j.suc.2016.11.005]
- 11 **Tasaka S**. National survey of early gastric cancer (Japanese). *Gastroenterol Endosc* 1962; **4**: 4-14
- 12 **Hosokawa O**, Shimizu M, Kaizaki Y, Miyanaga T, Asaumi Y, Ibe N, Hattori M, Dohden K, Hayashida Y, Hiranuma C. Current status of diagnosis for early gastric cancer (in Japanese with English abstract). *Stomach Intest* 2009; **44**: 455-464
- 13 **Takeda J**, Hashimoto K, Machi J, Hirai Y, Yoshida C, Ohmori Y, Kakegawa T. Clinical and pathological evaluation of early gastric cancer and lymph node metastasis. *Kurume Med J* 1987; **34**: 183-191 [PMID: 3455438 DOI: 10.2739/kurumemedj.34.183]
- 14 **Sasako M**, McCulloch P, Kinoshita T, Maruyama K. New method to evaluate the therapeutic value of lymph node dissection for gastric cancer. *Br J Surg* 1995; **82**: 346-351 [PMID: 7796005 DOI: 10.1002/bjs.1800820321]
- 15 **Isozaki H**, Okajima K, Ichinona T, Fujii K, Nomura E, Izumi N, Ohyama T. Distant lymph node metastasis of early gastric cancer. *Surg Today* 1997; **27**: 600-605 [PMID: 9306560 DOI: 10.1007/BF02388214]
- 16 **Yoshikawa T**, Tsuburaya A, Kobayashi O, Sairenji M, Motohashi H, Noguchi Y. Is D2 lymph node dissection necessary for early gastric cancer? *Ann Surg Oncol* 2002; **9**: 401-405 [PMID: 11986193 DOI: 10.1007/BF02573876]
- 17 **Miwa K**, Miyazaki I, Sahara H, Fujimura T, Yonemura Y, Noguchi M, Falla R. Rationale for extensive lymphadenectomy in early gastric carcinoma. *Br J Cancer* 1995; **72**: 1518-1524 [PMID: 8519670 DOI: 10.1038/bjc.1995.540]
- 18 **Seto Y**, Shimoyama S, Kitayama J, Mafune K, Kaminishi M, Aikou T, Arai K, Ohta K, Nashimoto A, Honda I, Yamagishi H, Yamamura Y. Lymph node metastasis and preoperative diagnosis of depth of

- invasion in early gastric cancer. *Gastric Cancer* 2001; **4**: 34-38 [PMID: [11706625](#) DOI: [10.1007/s101200100014](#)]
- 19 **Kurihara N**, Kubota T, Otani Y, Ohgami M, Kumai K, Sugiura H, Kitajima M. Lymph node metastasis of early gastric cancer with submucosal invasion. *Br J Surg* 1998; **85**: 835-839 [PMID: [9667719](#) DOI: [10.1046/j.1365-2168.1998.00743.x](#)]
 - 20 **Gotoda T**, Sasako M, Ono H, Katai H, Sano T, Shimoda T. Evaluation of the necessity for gastrectomy with lymph node dissection for patients with submucosal invasive gastric cancer. *Br J Surg* 2001; **88**: 444-449 [PMID: [11260114](#) DOI: [10.1046/j.1365-2168.2001.01725.x](#)]
 - 21 **Kwee RM**, Kwee TC. Predicting lymph node status in early gastric cancer. *Gastric Cancer* 2008; **11**: 134-148 [PMID: [18825308](#) DOI: [10.1007/s10120-008-0476-5](#)]
 - 22 **Japanese Gastric Cancer Association**. Japanese classification of gastric carcinoma 2017 (The 15th edition). Tokyo: Kanehara-shuppan 2018;
 - 23 **Kitamura K**, Yamaguchi T, Taniguchi H, Hagiwara A, Sawai K, Takahashi T. Analysis of lymph node metastasis in early gastric cancer: Rationale of limited surgery. *J Surg Oncol* 1997; **64**: 42-47 [PMID: [9040800](#)]
 - 24 **Tanaka N**, Katai H, Taniguchi H, Saka M, Morita S, Fukunaga T, Shimoda T. Surgical treatment for early gastric cancer (in Japanese with English abstract). *Stomach Intest* 2009; **44**: 700-706
 - 25 **Nakajima H**, Yamanaka K, Horii T, Nishina T, Ikeda T, Komeda M. A more comprehensive left ventricular repair for severely dilated cardiomyopathy. *J Card Surg* 2006; **21**: 62-64; discussion 65 [PMID: [16426350](#) DOI: [10.1111/j.1540-8191.2006.00170.x](#)]
 - 26 **Yoshikawa T**, Tsuburaya A, Kobayashi O, Sairenji M, Motohashi H, Noguchi Y. Indications of limited surgery for gastric cancer with submucosal invasion--analysis of 715 cases with special reference to site of the tumor and level 2 lymph nodes. *Hepatogastroenterology* 2003; **50**: 1727-1730 [PMID: [14571828](#)]
 - 27 **Japanese Gastric Cancer Association**. Japanese gastric cancer treatment guidelines 2010 (ver. 3). *Gastric Cancer* 2011; **14**: 113-123 [PMID: [21573742](#) DOI: [10.1007/s10120-011-0042-4](#)]
 - 28 **Kikuchi S**, Kuroda S, Nishizaki M, Kagawa T, Kanzaki H, Kawahara Y, Kagawa S, Tanaka T, Okada H, Fujiwara T. Management of early gastric cancer that meet the indication for radical lymph node dissection following endoscopic resection: A retrospective cohort analysis. *BMC Surg* 2017; **17**: 72 [PMID: [28637436](#) DOI: [10.1186/s12893-017-0268-0](#)]
 - 29 **Kitano S**, Shiraishi N, Uyama I, Sugihara K, Tanigawa N; Japanese Laparoscopic Surgery Study Group. A multicenter study on oncologic outcome of laparoscopic gastrectomy for early cancer in Japan. *Ann Surg* 2007; **245**: 68-72 [PMID: [17197967](#) DOI: [10.1097/01.sla.0000225364.03133.f8](#)]
 - 30 **Lee JH**, Yom CK, Han HS. Comparison of long-term outcomes of laparoscopy-assisted and open distal gastrectomy for early gastric cancer. *Surg Endosc* 2009; **23**: 1759-1763 [PMID: [19057958](#) DOI: [10.1007/s00464-008-0198-0](#)]
 - 31 **Bolton JS**, Conway WC 2nd. Postgastrectomy syndromes. *Surg Clin North Am* 2011; **91**: 1105-1122 [PMID: [21889032](#) DOI: [10.1016/j.suc.2011.07.001](#)]
 - 32 **Carvajal SH**, Mulvihill SJ. Postgastrectomy syndromes: Dumping and diarrhea. *Gastroenterol Clin North Am* 1994; **23**: 261-279 [PMID: [8070912](#)]
 - 33 **Harju E**. Metabolic problems after gastric surgery. *Int Surg* 1990; **75**: 27-35 [PMID: [2180835](#) DOI: [10.1007/BF00303284](#)]
 - 34 **Nakada K**, Ikeda M, Takahashi M, Kinami S, Yoshida M, Uenosono Y, Kawashima Y, Oshio A, Suzukamo Y, Terashima M, Koderia Y. Characteristics and clinical relevance of postgastrectomy syndrome assessment scale (PGSAS)-45: Newly developed integrated questionnaires for assessment of living status and quality of life in postgastrectomy patients. *Gastric Cancer* 2015; **18**: 147-158 [PMID: [24515247](#) DOI: [10.1007/s10120-014-0344-4](#)]
 - 35 **Nakada K**, Takahashi M, Ikeda M, Kinami S, Yoshida M, Uenosono Y, Kawashima Y, Nakao S, Oshio A, Suzukamo Y, Terashima M, Koderia Y. Factors affecting the quality of life of patients after gastrectomy as assessed using the newly developed PGSAS-45 scale: A nationwide multi-institutional study. *World J Gastroenterol* 2016; **22**: 8978-8990 [PMID: [27833389](#) DOI: [10.3748/wjg.v22.i40.8978](#)]
 - 36 **Takiguchi N**, Takahashi M, Ikeda M, Inagawa S, Ueda S, Nobuoka T, Ota M, Iwasaki Y, Uchida N, Koderia Y, Nakada K. Long-term quality-of-life comparison of total gastrectomy and proximal gastrectomy by postgastrectomy syndrome assessment scale (PGSAS)-45: A nationwide multi-institutional study. *Gastric Cancer* 2015; **18**: 407-416 [PMID: [24801198](#) DOI: [10.1007/s10120-014-0377-8](#)]
 - 37 **Terashima M**, Tanabe K, Yoshida M, Kawahira H, Inada T, Okabe H, Urushihara T, Kawashima Y, Fukushima N, Nakada K. Postgastrectomy Syndrome Assessment Scale (PGSAS)-45 and changes in body weight are useful tools for evaluation of reconstruction methods following distal gastrectomy. *Ann Surg Oncol* 2014; **21** Suppl 3: S370-S378 [PMID: [24590434](#) DOI: [10.1245/s10434-014-03583-z](#)]
 - 38 **Tada M**, Murakami A, Karita M, Yanai H, Okita K. Endoscopic resection of early gastric cancer. *Endoscopy* 1993; **25**: 445-450 [PMID: [8261986](#) DOI: [10.1055/s-2007-1010365](#)]
 - 39 **Ono H**, Kondo H, Gotoda T, Shirao K, Yamaguchi H, Saito D, Hosokawa K, Shimoda T, Yoshida S. Endoscopic mucosal resection for treatment of early gastric cancer. *Gut* 2001; **48**: 225-229 [PMID: [11156645](#) DOI: [10.1136/gut.48.2.225](#)]
 - 40 **Gotoda T**. Endoscopic resection of early gastric cancer. *Gastric Cancer* 2007; **10**: 1-11 [PMID: [17334711](#) DOI: [10.1007/s10120-006-0408-1](#)]
 - 41 **Gotoda T**, Yanagisawa A, Sasako M, Ono H, Nakanishi Y, Shimoda T, Kato Y. Incidence of lymph node metastasis from early gastric cancer: Estimation with a large number of cases at two large centers. *Gastric Cancer* 2000; **3**: 219-225 [PMID: [11984739](#) DOI: [10.1007/PL00011720](#)]
 - 42 **Hirasawa T**, Gotoda T, Miyata S, Kato Y, Shimoda T, Taniguchi H, Fujisaki J, Sano T, Yamaguchi T. Incidence of lymph node metastasis and the feasibility of endoscopic resection for undifferentiated-type early gastric cancer. *Gastric Cancer* 2009; **12**: 148-152 [PMID: [19890694](#) DOI: [10.1007/s10120-009-0515-x](#)]
 - 43 **Hatta W**, Gotoda T, Oyama T, Kawata N, Takahashi A, Yoshifuku Y, Hoteya S, Nakamura K, Hirano M, Esaki M, Matsuda M, Ohnita K, Shimoda R, Yoshida M, Dohi O, Takada J, Tanaka K, Yamada S, Tsuji T, Ito H, Hayashi Y, Nakamura T, Shimosegawa T. Is radical surgery necessary in all patients who do not meet the curative criteria for endoscopic submucosal dissection in early gastric cancer? A multi-center retrospective study in Japan. *J Gastroenterol* 2017; **52**: 175-184 [PMID: [27098174](#) DOI: [10.1007/s00535-016-1210-4](#)]
 - 44 **Kawata N**, Kakushima N, Takizawa K, Tanaka M, Makuuchi R, Tokunaga M, Tanizawa Y, Bando E, Kawamura T, Sugino T, Kusafuka K, Shimoda T, Nakajima T, Terashima M, Ono H. Risk factors for lymph node metastasis and long-term outcomes of patients with early gastric cancer after non-curative

- endoscopic submucosal dissection. *Surg Endosc* 2017; **31**: 1607-1616 [PMID: 27495338 DOI: 10.1007/s00464-016-5148-7]
- 45 **Kitano S**, Iso Y, Moriyama M, Sugimachi K. Laparoscopy-assisted Billroth I gastrectomy. *Surg Laparosc Endosc* 1994; **4**: 146-148 [PMID: 8180768 DOI: 10.1007/BF00590967]
 - 46 **Ohgami M**, Otani Y, Kumai K, Kubota T, Kim YI, Kitajima M. Curative laparoscopic surgery for early gastric cancer: Five years experience. *World J Surg* 1999; **23**: 187-192; discussion 192-193 [PMID: 9880430 DOI: 10.1007/PL00013167]
 - 47 **Ohashi S**. Laparoscopic intraluminal (intragastic) surgery for early gastric cancer. A new concept in laparoscopic surgery. *Surg Endosc* 1995; **9**: 169-171 [PMID: 7597587 DOI: 10.1007/BF00191960]
 - 48 **Katai H**, Sasako M, Fukuda H, Nakamura K, Hiki N, Saka M, Yamaue H, Yoshikawa T, Kojima K; JCOG Gastric Cancer Surgical Study Group. Safety and feasibility of laparoscopy-assisted distal gastrectomy with suprapancreatic nodal dissection for clinical stage I gastric cancer: A multicenter phase II trial (JCOG 0703). *Gastric Cancer* 2010; **13**: 238-244 [PMID: 21128059 DOI: 10.1007/s10120-010-0565-0]
 - 49 **Zhang CD**, Yamashita H, Zhang S, Seto Y. Reevaluation of laparoscopic versus open distal gastrectomy for early gastric cancer in Asia: A meta-analysis of randomized controlled trials. *Int J Surg* 2018; **56**: 31-43 [PMID: 29860125 DOI: 10.1016/j.ijsu.2018.05.733]
 - 50 **Nakamura M**, Hosoya Y, Umeshita K, Yano M, Doki Y, Miyashiro I, Dannoue H, Mori M, Kishi K, Lefor AT. Postoperative quality of life: Development and validation of the "Dysfunction After Upper Gastrointestinal Surgery" scoring system. *J Am Coll Surg* 2011; **213**: 508-514 [PMID: 21862356 DOI: 10.1016/j.jamcollsurg.2011.07.007]
 - 51 **Kinami S**, Takahashi M, Urushihara T, Ikeda M, Yoshida M, Uenosono Y, Oshio A, Suzukamo Y, Terashima M, Kodera Y, Nakada K. Background factors influencing postgastrectomy syndromes after various types of gastrectomy. *World J Clin Cases* 2018; **6**: 1111-1120 [PMID: 30613669 DOI: 10.12998/wjcc.v6.i16.1111]
 - 52 **Kinami S**, Funaki H, Fujita H, Nakano Y, Ueda N, Kosaka T. Local resection of the stomach for gastric cancer. *Surg Today* 2017; **47**: 651-659 [PMID: 27342746 DOI: 10.1007/s00595-016-1371-z]
 - 53 **Maki T**, Shiratori T, Hatafuku T, Sugawara K. Pylorus-preserving gastrectomy as an improved operation for gastric ulcer. *Surgery* 1967; **61**: 838-845 [PMID: 5338114]
 - 54 **Nunobe S**, Sasako M, Saka M, Fukagawa T, Katai H, Sano T. Symptom evaluation of long-term postoperative outcomes after pylorus-preserving gastrectomy for early gastric cancer. *Gastric Cancer* 2007; **10**: 167-172 [PMID: 17922094 DOI: 10.1007/s10120-007-0434-7]
 - 55 **Morita S**, Katai H, Saka M, Fukagawa T, Sano T, Sasako M. Outcome of pylorus-preserving gastrectomy for early gastric cancer. *Br J Surg* 2008; **95**: 1131-1135 [PMID: 18690631 DOI: 10.1002/bjs.6295]
 - 56 **Fujita J**, Takahashi M, Urushihara T, Tanabe K, Kodera Y, Yumiba T, Matsumoto H, Takagane A, Kunisaki C, Nakada K. Assessment of postoperative quality of life following pylorus-preserving gastrectomy and Billroth-I distal gastrectomy in gastric cancer patients: Results of the nationwide postgastrectomy syndrome assessment study. *Gastric Cancer* 2016; **19**: 302-311 [PMID: 25637175 DOI: 10.1007/s10120-015-0460-9]
 - 57 **Katai H**, Morita S, Saka M, Taniguchi H, Fukagawa T. Long-term outcome after proximal gastrectomy with jejunal interposition for suspected early cancer in the upper third of the stomach. *Br J Surg* 2010; **97**: 558-562 [PMID: 20169569 DOI: 10.1002/bjs.6944]
 - 58 **Ikeguchi M**, Kader A, Takaya S, Fukumoto Y, Osaki T, Saito H, Tatebe S, Wakatsuki T. Prognosis of patients with gastric cancer who underwent proximal gastrectomy. *Int Surg* 2012; **97**: 275-279 [PMID: 23113860 DOI: 10.9738/CC150.1]
 - 59 **Sugoor P**, Shah S, Dusane R, Desouza A, Goel M, Shrikhande SV. Proximal gastrectomy versus total gastrectomy for proximal third gastric cancer: Total gastrectomy is not always necessary. *Langenbecks Arch Surg* 2016; **401**: 687-697 [PMID: 27143021 DOI: 10.1007/s00423-016-1422-3]
 - 60 **Wen L**, Chen XZ, Wu B, Chen XL, Wang L, Yang K, Zhang B, Chen ZX, Chen JP, Zhou ZG, Li CM, Hu JK. Total vs. proximal gastrectomy for proximal gastric cancer: A systematic review and meta-analysis. *Hepatogastroenterology* 2012; **59**: 633-640 [PMID: 22328267 DOI: 10.5754/hge11834]
 - 61 **Michiura T**, Nakane Y, Kanbara T, Nakai K, Inoue K, Yamamichi K, Kamiyama Y. Assessment of the preserved function of the remnant stomach in pylorus-preserving gastrectomy by gastric emptying scintigraphy. *World J Surg* 2006; **30**: 1277-1283 [PMID: 16794905 DOI: 10.1007/s00268-005-7983-x]
 - 62 **Yoo CH**, Sohn BH, Han WK, Pae WK. Long-term results of proximal and total gastrectomy for adenocarcinoma of the upper third of the stomach. *Cancer Res Treat* 2004; **36**: 50-55 [PMID: 20396565 DOI: 10.4143/crt.2004.36.1.50]
 - 63 **Nakane Y**, Michiura T, Inoue K, Sato M, Nakai K, Ioka M, Yamamichi K. Role of pyloroplasty after proximal gastrectomy for cancer. *Hepatogastroenterology* 2004; **51**: 1867-1871 [PMID: 15532846]
 - 64 **Nakabayashi T**, Mochiki E, Garcia M, Haga N, Suzuki T, Asao T, Kuwano H. Pyloric motility after pylorus-preserving gastrectomy with or without the pyloric branch of the vagus nerve. *World J Surg* 2002; **26**: 577-583 [PMID: 12098048 DOI: 10.1007/s00268-001-0270-6]
 - 65 **Nishizawa N**, Hosoda K, Moriya H, Mieno H, Ema A, Ushiku H, Ishii S, Tanaka T, Washio M, Yokoi K, Harada H, Watanabe M, Yamashita K. Patients' preoperative background causes gastric stasis after laparoscopy-assisted pylorus-preserving gastrectomy. *Asian J Endosc Surg* 2018; **11**: 337-345 [PMID: 29573227 DOI: 10.1111/ases.12477]
 - 66 **Kiyokawa T**, Hiki N, Nunobe S, Honda M, Ohashi M, Sano T. Preserving infrapyloric vein reduces postoperative gastric stasis after laparoscopic pylorus-preserving gastrectomy. *Langenbecks Arch Surg* 2017; **402**: 49-56 [PMID: 27815708 DOI: 10.1007/s00423-016-1529-6]
 - 67 **Namikawa T**, Hiki N, Kinami S, Okabe H, Urushihara T, Kawahira H, Fukushima N, Kodera Y, Yumiba T, Oshio A, Nakada K. Factors that minimize postgastrectomy symptoms following pylorus-preserving gastrectomy: Assessment using a newly developed scale (PGSAS-45). *Gastric Cancer* 2015; **18**: 397-406 [PMID: 24760336 DOI: 10.1007/s10120-014-0366-y]
 - 68 **Sakuramoto S**, Yamashita K, Kikuchi S, Futawatari N, Katada N, Moriya H, Hirai K, Watanabe M. Clinical experience of laparoscopy-assisted proximal gastrectomy with Toupet-like partial fundoplication in early gastric cancer for preventing reflux esophagitis. *J Am Coll Surg* 2009; **209**: 344-351 [PMID: 19717038 DOI: 10.1016/j.jamcollsurg.2009.04.011]
 - 69 **Tokunaga M**, Ohyama S, Hiki N, Hoshino E, Nunobe S, Fukunaga T, Seto Y, Yamaguchi T. Endoscopic evaluation of reflux esophagitis after proximal gastrectomy: Comparison between esophagogastric anastomosis and jejunal interposition. *World J Surg* 2008; **32**: 1473-1477 [PMID: 18264827 DOI: 10.1007/s00268-007-9459-7]

- 70 **Nomura E**, Lee SW, Kawai M, Yamazaki M, Nabeshima K, Nakamura K, Uchiyama K. Functional outcomes by reconstruction technique following laparoscopic proximal gastrectomy for gastric cancer: Double tract versus jejunal interposition. *World J Surg Oncol* 2014; **12**: 20 [PMID: [24468278](#) DOI: [10.1186/1477-7819-12-20](#)]
- 71 **Takagawa R**, Kunisaki C, Kimura J, Makino H, Kosaka T, Ono HA, Akiyama H, Endo I. A pilot study comparing jejunal pouch and jejunal interposition reconstruction after proximal gastrectomy. *Dig Surg* 2010; **27**: 502-508 [PMID: [21079403](#) DOI: [10.1159/000321224](#)]
- 72 **Mochiki E**, Fukuchi M, Ogata K, Ohno T, Ishida H, Kuwano H. Postoperative functional evaluation of gastric tube after laparoscopic proximal gastrectomy for gastric cancer. *Anticancer Res* 2014; **34**: 4293-4298 [PMID: [25075061](#) DOI: [10.1016/j.urolonc.2014.05.010](#)]
- 73 **Hayami M**, Hiki N, Nunobe S, Mine S, Ohashi M, Kumagai K, Ida S, Watanabe M, Sano T, Yamaguchi T. Clinical Outcomes and Evaluation of Laparoscopic Proximal Gastrectomy with Double-Flap Technique for Early Gastric Cancer in the Upper Third of the Stomach. *Ann Surg Oncol* 2017; **24**: 1635-1642 [PMID: [28130623](#) DOI: [10.1245/s10434-017-5782-x](#)]
- 74 **Yamashita Y**, Yamamoto A, Tamamori Y, Yoshii M, Nishiguchi Y. Side overlap esophagogastrostomy to prevent reflux after proximal gastrectomy. *Gastric Cancer* 2017; **20**: 728-735 [PMID: [27942874](#) DOI: [10.1007/s10120-016-0674-5](#)]
- 75 **Nakamura M**, Yamaue H. Reconstruction after proximal gastrectomy for gastric cancer in the upper third of the stomach: A review of the literature published from 2000 to 2014. *Surg Today* 2016; **46**: 517-527 [PMID: [25987497](#) DOI: [10.1007/s00595-015-1185-4](#)]
- 76 **Tomita R**, Fujisaki S, Tanjoh K, Fukuzawa M. A novel operative technique on proximal gastrectomy reconstructed by interposition of a jejunal J pouch with preservation of the vagal nerve and lower esophageal sphincter. *Hepatogastroenterology* 2001; **48**: 1186-1191 [PMID: [11490830](#)]
- 77 **Inada T**, Yoshida M, Ikeda M, Yumiba T, Matsumoto H, Takagane A, Kunisaki C, Fukushima R, Yabusaki H, Nakada K. Evaluation of QOL after proximal gastrectomy using a newly developed assessment scale (PGSAS-45). *World J Surg* 2014; **38**: 3152-3162 [PMID: [25135173](#) DOI: [10.1007/s00268-014-2712-y](#)]
- 78 **Jiang X**, Hiki N, Nunobe S, Fukunaga T, Kumagai K, Nohara K, Katayama H, Ohya S, Sano T, Yamaguchi T. Long-term outcome and survival with laparoscopy-assisted pylorus-preserving gastrectomy for early gastric cancer. *Surg Endosc* 2011; **25**: 1182-1186 [PMID: [20844895](#) DOI: [10.1007/s00464-010-1336-z](#)]
- 79 **Ueda Y**, Shiroshita H, Etoh T, Inomata M, Shiraishi N. Laparoscopic proximal gastrectomy for early gastric cancer. *Surg Today* 2017; **47**: 538-547 [PMID: [27549773](#) DOI: [10.1007/s00595-016-1401-x](#)]
- 80 **Hosoda K**, Yamashita K, Sakuramoto S, Katada N, Moriya H, Mieno H, Watanabe M. Postoperative quality of life after laparoscopy-assisted pylorus-preserving gastrectomy compared With laparoscopy-assisted distal gastrectomy: A cross-sectional postal questionnaire survey. *Am J Surg* 2017; **213**: 763-770 [PMID: [27751530](#) DOI: [10.1016/j.amjsurg.2016.09.041](#)]
- 81 **Ahn SH**, Lee JH, Park DJ, Kim HH. Comparative study of clinical outcomes between laparoscopy-assisted proximal gastrectomy (LAPG) and laparoscopy-assisted total gastrectomy (LATG) for proximal gastric cancer. *Gastric Cancer* 2013; **16**: 282-289 [PMID: [22821182](#) DOI: [10.1007/s10120-012-0178-x](#)]
- 82 **Kinoshita T**, Gotohda N, Kato Y, Takahashi S, Konishi M, Kinoshita T. Laparoscopic proximal gastrectomy with jejunal interposition for gastric cancer in the proximal third of the stomach: A retrospective comparison with open surgery. *Surg Endosc* 2013; **27**: 146-153 [PMID: [22736285](#) DOI: [10.1007/s00464-012-2401-6](#)]
- 83 **Morton DL**, Wen DR, Wong JH, Economou JS, Cagle LA, Storm FK, Foshag LJ, Cochran AJ. Technical details of intraoperative lymphatic mapping for early stage melanoma. *Arch Surg* 1992; **127**: 392-399 [PMID: [1558490](#) DOI: [10.1001/archsurg.1992.01420040034005](#)]
- 84 **Kinami S**, Kosaka T. Laparoscopic sentinel node navigation surgery for early gastric cancer. *Transl Gastroenterol Hepatol* 2017; **2**: 42 [PMID: [28616598](#) DOI: [10.21037/tgh.2017.05.02](#)]
- 85 **Kitagawa Y**, Takeuchi H, Takagi Y, Natsugoe S, Terashima M, Murakami N, Fujimura T, Tsujimoto H, Hayashi H, Yoshimizu N, Takagane A, Mohri Y, Nabeshima K, Uenosono Y, Kinami S, Sakamoto J, Morita S, Aikou T, Miwa K, Kitajima M. Sentinel node mapping for gastric cancer: A prospective multicenter trial in Japan. *J Clin Oncol* 2013; **31**: 3704-3710 [PMID: [24019550](#) DOI: [10.1200/JCO.2013.50.3789](#)]
- 86 **Miwa K**. Sentinel node concept and its application for cancer surgery. *Nihon Geka Gakkai Zasshi* 2000; **101**: 307-310 [PMID: [10773998](#)]
- 87 **Miwa K**, Kinami S, Taniguchi K, Fushida S, Fujimura T, Nonomura A. Mapping sentinel nodes in patients with early-stage gastric carcinoma. *Br J Surg* 2003; **90**: 178-182 [PMID: [12555293](#) DOI: [10.1002/bjs.4031](#)]
- 88 **Kinami S**, Fujimura T, Ojima E, Fushida S, Ojima T, Funaki H, Fujita H, Takamura H, Ninomiya I, Nishimura G, Kayahara M, Ohta T, Yoh Z. PTD classification: Proposal for a new classification of gastric cancer location based on physiological lymphatic flow. *Int J Clin Oncol* 2008; **13**: 320-329 [PMID: [18704632](#) DOI: [10.1007/s10147-007-0755-x](#)]
- 89 **Takeuchi H**, Goto O, Yahagi N, Kitagawa Y. Function-preserving gastrectomy based on the sentinel node concept in early gastric cancer. *Gastric Cancer* 2017; **20**: 53-59 [PMID: [27714472](#) DOI: [10.1007/s10120-016-0649-6](#)]
- 90 **Isozaki H**, Matsumoto S, Murakami S, Takama T, Sho T, Ishihara K, Sakai K, Takeda M, Nakada K, Fujiwara T. Diminished Gastric Resection Preserves Better Quality of Life in Patients with Early Gastric Cancer. *Acta Med Okayama* 2016; **70**: 119-130 [PMID: [27094837](#) DOI: [10.18926/AMO/54191](#)]
- 91 **Park JY**, Kim YW, Ryu KW, Nam BH, Lee YJ, Jeong SH, Park JH, Hur H, Han SU, Min JS, An JY, Hyung WJ, Cho GS, Jeong GA, Jeong O, Park YK, Jung MR, Yoon HM, Eom BW. Assessment of laparoscopic stomach preserving surgery with sentinel basin dissection versus standard gastrectomy with lymphadenectomy in early gastric cancer-A multicenter randomized phase III clinical trial (SENORITA trial) protocol. *BMC Cancer* 2016; **16**: 340 [PMID: [27246120](#) DOI: [10.1186/s12885-016-2336-8](#)]
- 92 **Kinami S**, Oonishi T, Fujita J, Tomita Y, Funaki H, Fujita H, Nakano Y, Ueda N, Kosaka T. Optimal settings and accuracy of indocyanine green fluorescence imaging for sentinel node biopsy in early gastric cancer. *Oncol Lett* 2016; **11**: 4055-4062 [PMID: [27313740](#) DOI: [10.3892/ol.2016.4492](#)]



Update on hepatocellular carcinoma: Pathologists' review

Tony El Jabbour, Stephen M Lagana, Hwajeong Lee

ORCID number: Tony El Jabbour (0000-0002-6823-1919); Stephen Lagana (0000-0002-1533-368X); Hwajeong Lee (0000-0001-7005-6278).

Author contributions: El Jabbour T and Lee H drafted the manuscript; Lagana SM and Lee H contributed to the editing of the manuscript; El Jabbour T and Lagana SM provided the microscopic images; Lagana SM contributed to critical review of the manuscript; El Jabbour T, Lagana SM, and Lee H gave final approval of the version to be published and is agreeable to be accountable for all aspects of the work in ensuring that questions that arise are investigated and the information is accurate.

Conflict-of-interest statement: No potential conflicts of interest.

Open-Access: This article is an open-access article which was selected by an in-house editor and fully peer-reviewed by external reviewers. It is distributed in accordance with the Creative Commons Attribution Non Commercial (CC BY-NC 4.0) license, which permits others to distribute, remix, adapt, build upon this work non-commercially, and license their derivative works on different terms, provided the original work is properly cited and the use is non-commercial. See: <http://creativecommons.org/licenses/by-nc/4.0/>

Manuscript source: Invited manuscript

Received: February 12, 2019

Peer-review started: February 14, 2019

First decision: March 5, 2019

Tony El Jabbour, Hwajeong Lee, Department of Pathology and Laboratory Medicine, Albany Medical College, Albany, NY 12208, United States

Stephen M Lagana, Department of Pathology and Cell Biology, College of Physicians and Surgeons, Columbia University, New York, NY 10032, United States

Corresponding author: Hwajeong Lee, MD, Associate Professor, Department of Pathology and Laboratory Medicine, Albany Medical College, 47 New Scotland Ave., MC81, Albany, NY 12208, United States. leeh5@amc.edu

Telephone: +1-518-2626254

Fax: +1-518-2623663

Abstract

Histopathologic diversity and several distinct histologic subtypes of hepatocellular carcinoma (HCC) are well-recognized. Recent advances in molecular pathology and growing knowledge about the biology associated with distinct histologic features and immuno-profile in HCC allowed pathologists to update classifications. Improving sub-classification will allow for more clinically relevant diagnoses and may allow for stratification into biologically meaningful subgroups. Therefore, immuno-histochemical and molecular testing are not only diagnostically useful, but also are being incorporated as crucial components in predicting prognosis of the patients with HCC. Possibilities of targeted therapy are being explored in HCC, and it will be important for pathologists to provide any data that may be valuable from a theranostic perspective. Herein, we review and provide updates regarding the pathologic sub-classification of HCC. Pathologic diagnostic approach and the role of biomarkers as prognosticators are reviewed. Further, the histopathology of four particular subtypes of HCC: Steatohepatitic, clear cell, fibrolamellar and scirrhous - and their clinical relevance, and the recent consensus on combined HCC-cholangiocarcinoma is summarized. Finally, emerging novel biomarkers and new approaches to HCC stratification are reviewed.

Key words: Hepatocellular carcinoma; Subtype; Classification; Review; Update

©The Author(s) 2019. Published by Baishideng Publishing Group Inc. All rights reserved.

Core tip: We summarize the updated classifications of hepatocellular carcinoma. Immunohistochemistry and molecular pathology are becoming crucial components of prognostication and theranostics. Pathologic and molecular features of clinically relevant subtypes to include steatohepatitic, clear cell, fibrolamellar and scirrhous hepatocellular carcinomas are reviewed. Recent consensus on the combined hepatocellular carcinoma-

Revised: March 12, 2019
Accepted: March 24, 2019
Article in press: March 25, 2019
Published online: April 14, 2019

P-Reviewer: Jin C, Namisaki T, Sitkin S

S-Editor: Yan JP

L-Editor: A

E-Editor: Song H



cholangiocarcinoma, a controversial pathologic entity, is summarized.

Citation: El Jabbour T, Lagana SM, Lee H. Update on hepatocellular carcinoma: Pathologists' review. *World J Gastroenterol* 2019; 25(14): 1653-1665

URL: <https://www.wjgnet.com/1007-9327/full/v25/i14/1653.htm>

DOI: <https://dx.doi.org/10.3748/wjg.v25.i14.1653>

INTRODUCTION

Hepatocellular neoplasms constitute a heterogeneous group of disorders that encompasses benign, dysplastic and malignant lesions. These lesions demonstrate a wide morphologic spectrum and include newly identified morphologic subtypes. Knowledge about molecular signatures, provisional classifications, and clinical correlates continues to evolve. A careful synthesis of all clinical, radiologic and pathologic data is essential to establish a proper diagnosis and devise a treatment plan.

This review aims to address the most common questions brought to our (pathologists') attention by our clinical colleagues. Firstly, the current classification of hepatocellular carcinoma (HCC) will be reviewed. Secondly, the utility of ancillary tests to include immunohistochemistry (IHC) including prognostic biomarkers, and molecular testing will be reviewed. Next, a few subtypes of non-conventional HCC that are deemed clinically relevant will be briefly reviewed. Further, we will summarize the recent consensus on combined HCC-cholangiocarcinoma (cHCC-CCA). Finally, novel diagnostic and/or prognostic biomarkers and comprehensive genomic and epigenomic stratification of HCC are briefly reviewed.

EVOLUTION OF THE HISTOLOGIC (MORPHOLOGIC) CLASSIFICATION OF HEPATOCELLULAR CARCINOMA

The 4th edition of WHO classification of the tumors of the digestive system was published in 2010. In this edition, in addition to the conventional HCC, the WHO recognized 5 morphological subtypes of HCC: Fibrolamellar HCC (FL-HCC), scirrhous HCC (S-HCC), undifferentiated carcinoma, lymphoepithelioma-like carcinoma and sarcomatoid HCC. Several architectural growth patterns and cytological variation of HCC were also described to aid in establishing a diagnosis. These architectural and cytologic variations were not recognized as individual subtypes. The following architectural patterns were described: trabecular (plate-like) pattern, pseudoglandular (acinar) pattern and compact pattern. The cytological variations included pleomorphic cells (bizarre multinucleated, mononuclear giant cells or osteoclast-like giant cells), clear cells, fatty change, bile production, hyaline bodies (Mallory-Denk bodies), pale bodies and ground glass inclusions^[1].

Since the publication of the 4th edition WHO classification of the tumors of the digestive system, additional morphologic variations of HCC have been reported in the literature, some with characteristic molecular signature. It was suggested that for a tumor with specific morphologic variation to qualify for a subtype, the following criteria should be met: the tumor should have reproducible microscopic pattern, immuno-histochemical and molecular tests that help in the subcategorization of the tumor should be available, and there should be a particular clinical correlate regarding the proposed subtype.

This approach has led to 12 proposed subtypes and 6 provisional entities, constituting approximately 35% of HCC. In a decreasing order of frequency, these morphologic subtypes are: Steatohepatic, clear cell, scirrhous, cirrhotomimetic, fibrolamellar carcinoma, combined hepatocellular-cholangiocarcinoma, combined hepatocellular and neuroendocrine, granulocyte colony-stimulating factor producing, sarcomatoid, carcinosarcoma, carcinosarcoma with osteoclast-like giant cells and lymphocyte rich. Out of the 6 provisional entities, chromophobe subtype is the most common. The remaining 5 provisions are of equal frequency: Combined hepatocellular-cholangiocarcinoma with stem cell features, lipid rich, myxoid, syncytial giant cell and transitional cell^[2,3]. A subset of the proposed subtypes and provisional entities is likely to be endorsed in the 5th edition WHO classification of the tumors of the digestive system, which is to be released in 2019.

ROLE OF IMMUNOHISTOCHEMISTRY IN HEPATOCELLULAR CARCINOMA DIAGNOSIS

Both well differentiated and poorly differentiated hepatocellular neoplastic lesions pose diagnostic challenge. “Well differentiated” implies that the histomorphology of the tumor closely resembles the native tissue the tumor originates from. Therefore, a well differentiated HCC recapitulates benign liver tissue, mimicking the following benign and pre-neoplastic entities: hepatocellular adenoma, focal nodular hyperplasia (FNH), regenerative nodule, and dysplastic nodule in cirrhotic liver. In order to demonstrate malignancy in a well-differentiated HCC that morphologically resembles benign hepatocytic lesions, IHC such as CD34 (showing diffuse sinusoidal capillarization), and a panel of glutamine synthetase (GS), glypican-3 (GPC-3) and heat shock protein 70 (HSP-70) may be helpful^[4,5]. Reticulin special stain remains a very useful test, as the aforementioned benign and pre-neoplastic entities generally retain a reticulin network, whereas HCC does not.

However, these stains are neither 100% specific nor 100% sensitive^[6]. Thus, careful review of histomorphology and stringent application of cytomorphologic criteria of malignancy, and clinical and imaging correlation is essential to establish a firm diagnosis of well-differentiated HCC. For example, when immuno-histochemical stains are not helpful in demonstrating malignancy, focal loss of reticulin framework in conjunction with cytomorphologic features of malignancy may be the only adjunctive in arriving at the diagnosis. Yet, differentiating between high grade dysplastic nodule and small, early well-differentiated HCC may be extremely challenging in a biopsy specimen^[7].

At the other end of the spectrum, “poor differentiation” implies that a tumor lacks resemblance to the native tissue that the tumor originates from. Consequently, a poorly differentiated HCC would morphologically resemble poorly differentiated carcinomas (malignancy of epithelial origin) from any other site, including metastasis to the liver and poorly differentiated intrahepatic cholangiocarcinoma. While it would be relatively straightforward to document malignancy based on histomorphology, documenting that the tumor demonstrates immuno-histochemical evidence of hepatocellular phenotype, and excluding other lines of differentiation are necessary in arriving at the correct diagnosis of HCC. Several immuno-histochemical markers including hepatocyte in paraffin 1 (HepPar1), Arginase-1, CD10, polyclonal carcinoembryonic antigen, bile salt export pump and GPC-3 have been utilized in this setting with variable sensitivities and specificities depending on the degree of differentiation of HCC^[3,4,7,8]. One study suggested that a combination of Arginase 1 and GPC-3 has the highest sensitivity in determining a hepatocellular origin of a poorly differentiated carcinoma^[9].

Some HCCs aberrantly express non-hepatocellular immuno-histochemical markers of origin and further confound the diagnosis. Shah *et al* reported that CDX2, an immuno-histochemical marker indicative of intestinal origin, is expressed in 5.2% of HCCs. In their cohort, the aberrant CDX2 expression was common in poorly differentiated HCC^[10]. Also, aberrant CK20 expression has been described in 14% of HCCs^[11]. Furthermore, a case of poorly differentiated HCC co-expressing CDX2 and CK20 has been recently reported^[12]. This would pose a diagnostic pitfall especially when metastatic colorectal carcinoma is a clinical and radiologic differential diagnosis for a liver mass.

Likewise, CK7 expression in HCC is not uncommon. Ward *et al* compared the immuno-histochemical profile of 22 cases of FL-HCC and 50 non-FL type HCC using tissue microarrays. When “positive” was defined as > 15% of tumor cells staining and “focal positive” as < 15%, 28% and 32% of non-FL type HCC were positive and focal positive for CK7, respectively. All FL-HCCs were positive for CK7^[13]. Albumin *in situ* hybridization (Albumin-ISH) is another promising test. Albumin-ISH is positive in tumors of liver origin such as HCC and intrahepatic cholangiocarcinoma with > 95% and 80%-95% sensitivity, respectively, and is negative in metastatic tumors to the liver^[3,8,14].

MOLECULAR BASIS OF HEPATOCELLULAR CARCINOMA AND TARGETED THERAPY

Identification of molecular alterations and signaling pathways that are involved in tumorigenesis is critical for personalized medicine. In HCC, however, it is challenging to identify genetic alterations that are directly related to tumorigenesis, as HCC usually arises in a background of chronic liver disease of many years. The ongoing inflammation and injury lead to the accumulation of a multitude of genetic alterations

prior to the development of HCC. The alterations differ between patients with different underlying liver diseases, and between tumor foci within a same patient. This phenomenon is known as “field effect”, and is considered an obstacle in developing a therapy targeting a single mutation^[15].

Several studies attempted to classify HCCs according to their molecular signature, but the attempts have not been successfully adopted in the clinical practice^[16-19]. However, these attempts are making a significant progress in identifying distinct morphologic subtypes corresponding to specific molecular profiles and clinical correlates. For example, scirrhous subtype, one of the histologic subtypes that were recognized in 2010 WHO, is associated with *TSC1/TSC2* mutations. Also, the authors recognized new morphological subtype, “macrotrabecular-massive” subtype, associated with *TP53* mutations, *FGF19* amplifications and with poor survival and high serum alpha-fetoprotein (AFP) level^[20].

The Cancer Genome Atlas Research Network analyzed a total of 559 cases of HCC, and identified 26 genes with significant alterations including some that are promising therapy targets. This study also showed that the promotor region of *TERT* (regulating cell survival), *TP53* (a gene that is frequently involved in carcinogenesis), or *CTNNB1* (regulating cell growth and differentiation) is altered in 77% of HCC. However, the authors recognized that it is unlikely to have one therapeutic agent that would effectively target most HCC, given the variety of mutations identified in a given patient (requiring a combination of treatments to target different mutations)^[21].

Sorafenib is one of the first generation fms-like tyrosine kinase 3 inhibitors approved for the first-line treatment of advanced HCC. Several protocols and clinical trials reported modest results with survival benefit, especially in patients with hepatitis C^[22-24]. Other multikinase inhibitors, regorafenib and cabozantinib, also showed survival benefit as a second-line treatment compared to placebo group in phase 3 clinical trials^[23,25,26]. Recent phase 1/2 trial of nivolumab, an immune checkpoint inhibitor, in patients with advanced HCC with or without chronic viral hepatitis reported promising responses^[27].

PATHOLOGIC PROGNOSTIC BIOMARKERS

Variable parameters such as serum AFP level, des-gamma-carboxy prothrombin level, tumor size and number, margin status, major vessel invasion, tumor stage, Edmonson-Steiner grade, Child-Pugh score, portal hypertension and cirrhosis, are considered clinical prognosticators of HCC, depending on the treatment modalities and underlying liver diseases^[28-32]. Pathologically, the overall poor outcome of HCCs expressing stem cell markers such as keratin 19 (K19), epithelial cell adhesion molecule (EpCAM), and CD133 has been reported, potentially via hypoxia-induced epithelial to mesenchymal transition^[33-36]. For example, the expression of K19 was associated with high rate of recurrence following radiofrequency ablation, and the HCCs expressing K19, EpCAM or carbonic anhydrase-IX (marker of hypoxia) showed incomplete response to transarterial chemoembolization. The overexpression of CD133 and CD90 in HCCs predicted poor response to sorafenib^[37-39]. Histologic grade of HCC is useful in predicting long-term survival. In HCCs with different grades of tumor foci within a same lesion, the worst grade within the tumor appears to dictate its biologic behavior. Therefore, careful approach is warranted when dealing with limited biopsy sample^[40].

SELECTED SUBTYPES OF HEPATOCELLULAR CARCINOMA

Steatohepatitic HCC

A possible correlation between non-alcoholic fatty liver disease (NAFLD) and the development of HCC has long been recognized^[41]. Moreover, it has been documented that HCC arising in association with non-alcoholic steatohepatitis or metabolic syndrome can develop in non-cirrhotic livers^[42,43].

A steatohepatitic variant of HCC was described in 2010. In this study, the authors described multiple histologic features that can be seen in steatohepatitis including macrovesicular steatosis, ballooning, Mallory-Denk Bodies, inflammation and pericellular fibrosis in 35.5% (22 of 62) of HCC arising in HCV induced cirrhosis. 63.6% of patients with steatohepatitic HCC had risk factors of NAFLD (Figure 1). Furthermore, 63.6% of steatohepatitic HCC was associated with background NAFLD, suggesting a link between this variant of HCC and NAFLD^[44]. Subsequently the same group established a correlation between the steatohepatitic variant HCC and an underlying steatohepatitis or metabolic risk factors, and suggested a role of

steatohepatitis in human hepatocarcinogenesis^[45]. A minor subset of steatohepatitic HCC may arise in the absence of background fatty liver disease or metabolic syndrome^[46]. This histologic entity and the reports of HCC arising in non-cirrhotic steatohepatitis gained the attention of hepatologists and oncologists. With the increasing incidence of metabolic risk factors and NAFLD especially in the western world, recognition of steatohepatitis without cirrhosis as an additional risk factor for HCC could have significant bearing on HCC screening programs^[41,47].

The molecular profile and the pathway involved in the carcinogenesis of steatohepatitic subtype are different from conventional HCC. For example, *CTNNB1* mutation (beta catenin pathway alterations) are less frequent in steatohepatitic HCC compared to conventional HCC^[48]. The immune-histochemical profile of steatohepatitic HCC has been compared to the conventional type. While no significant differences in staining pattern with HNF-1 α , β -catenin, GS, GPC-3 and HSP-70 were seen between the two, the degree of staining with C-reactive protein and serum amyloid A was higher in steatohepatitic HCC^[49].

FNH arising in a background of steatotic liver may demonstrate at least focal, steatohepatitis-like features and mimic steatohepatitic HCC. Careful identification of the typical histologic features of FNH including thick walled blood vessels, ductular reaction and thick fibrous septa, will be helpful in ruling out a steatohepatitic HCC^[50]. A study conducted on a Japanese population showed that steatohepatitic HCC has a similar prognosis to conventional type^[51].

Clear cell HCC

Cytoplasmic clearing is a defining feature of the broad category of neoplasms so called “clear cell tumors”. It may be a consequence of accumulation of glycogen, cytoplasmic vesicles, lipopolysaccharides or mucopolysaccharides, or simply represent a processing artifact^[52]. Clear cell HCC is a well differentiated variant of HCC. Its cytoplasmic clearing is a result of glycogen and less frequently, fat storing in the cytoplasm^[53]. The minimum amount of neoplastic cells with clear cytoplasm required for the diagnosis of clear cell HCC varies in the literature; however a cut-off of minimum 50% has been advocated in the recent AFIP fascicle^[3].

Rarely, clear cells may be seen in other types of HCC, *i.e.*, clear cell variant of fibrolamellar HCC or lipid-rich HCC secondary to cytoplasmic lipid accumulation. Thus, assigning the right subtype for the tumor in question may be necessary but challenging, particularly when there is a difference in the outcome^[54]. Most studies comparing the prognosis of clear cell HCC versus conventional HCC showed a better prognosis of the former^[55,56], or at least similar outcomes for both^[57,58]. Interestingly, Lee *et al*^[59] reported the presence of *IDH1* mutation in 25% of clear cell HCC. These *IDH1* mutated clear cell HCCs showed a statistically significant worse prognosis compared to *IDH1* wild-type clear cell HCCs. Of note, *IDH1* mutations are not uncommon in intrahepatic cholangiocarcinoma, a tumor with a significantly worse prognosis than HCC^[60,61].

Cases of clear cell HCC in non-cirrhotic liver or liver without hepatitis are rarely reported in the literature^[62,63]. Therefore, when a liver tumor with clear cell features in an otherwise unremarkable background liver is encountered, a metastasis from another primary with clear cell components needs to be excluded. Most common scenario would be a metastatic clear cell renal cell carcinoma or a clear cell carcinoma from the ovaries mimicking clear cell HCC. While a panel of IHC will aid in establishing the diagnosis of a primary *vs* a metastatic process in the vast majority of cases^[64-66], some ovarian clear cell carcinomas may stain with HepPar-1, posing a diagnostic pitfall^[65].

Fibrolamellar HCC

FL-HCC is a clinically, histologically and molecularly distinct subtype of HCC when compared to other subtypes of HCC. It frequently occurs in adolescents and young adults, and the mean age at the diagnosis is 25^[67-69]. The background liver typically lacks features of chronic hepatitis, inflammation, fibrosis, or preneoplastic lesions. Primarily due to the absence of cirrhosis in the background, the outcome of FL-HCC is usually better than the remaining subtypes. When non FL-HCCs arising in non-cirrhotic liver are compared, both show a similar outcome^[70].

The unique histology of FL-HCC was first described in 1956. FL-HCC consists of large, polygonal eosinophilic cells with abundant cytoplasm resembling hepatocytes. There are prominent nucleoli and pale inclusion bodies and pink bodies (hyaline bodies/globules) within the neoplastic cells, and the extensive intratumoral fibrosis is a characteristic feature. The thick collagenous bands within the tumor are often parallel and “lamellar”, but may be irregular and haphazard^[71] (Figure 2). Patchy areas of solid growth with little fibrosis may be noted within FL-HCC^[3]. Intratumoral cholestasis is common, and pseudoglandular growth with mucin production may be

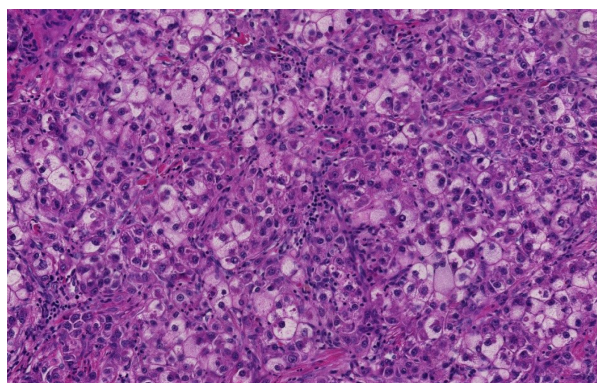


Figure 1 Steatohepatic hepatocellular carcinoma. Tumoral cells show features of steatohepatitis including steatosis, ballooning and Mallory-Denk bodies (Hematoxylin and eosin stain, $\times 200$).

seen, mimicking combined cholangiocarcinoma component^[3].

The immuno-profile of FL-HCC is also unique, and shows positivity for the biliary marker CK7^[13] and histiocytic marker CD68^[72]. Histologic differential diagnosis is S-HCC. Both are characterized by extensive intratumoral fibrosis. Kim *et al*^[73] studied the nature of the fibrous stroma in FL-HCC and S-HCC. The authors showed that the fibrous stroma in FL-HCC is composed of dense lamellated collagen whereas in S-HCC, the fibrous stroma represents aggressive and complex tumoral microenvironment enriched by cancer-associated fibroblasts and tumor-infiltrating macrophages. At the molecular level, FL-HCC harbors a characteristic fusion of *DNAJB1* and *PRKACA* on chromosome 19, secondary to chromosomal deletion in between these two genes^[74]. This fusion has been proven to be 100% specific for FL-HCC in the context of hepatic malignancy^[75].

Scirrhou S HCC

S-HCC is another rare subtype of HCC. The histomorphology of S-HCC is somewhat similar to FL-HCC with striking intratumoral fibrosis and oftentimes non-cirrhotic background liver. While the biologic behavior of S-HCC may be more aggressive than usual HCC with more portal vein invasion in the former, the long term outcome and prognosis of S-HCC is similar to, or better than those of usual HCC^[3,76].

The fibrosis involves at least 50% of the tumor and separates small nests of tumor cells^[2] (Figure 3). Due to the abundance of intratumoral fibrous stroma associated with thin trabecular pattern growth, S-HCC may, radiologically and pathologically, closely mimic cholangiocarcinoma^[3,76,77]. S-HCC is positive for CK7 similarly to FL-HCC^[78]. However, the distinction between these two can be made by co-expression of CD68^[72] and the fusion of *DNAJB1-PRKACA* genes in FL-HCC^[74]. On the other hand, *TSC1/TSC2* mutations and the overexpression of TGF-beta signaling have been identified in S-HCC^[20,79]. While S-HCC is a subtype of HCC, immuno-markers that are associated with adenocarcinoma such as CK7 and EpCAM are commonly expressed whereas HepPar1 expression is less common in S-HCC. A combination of GPC-3 and Arginase 1 was useful in distinguishing S-HCC from cholangiocarcinoma with 100% sensitivity for S-HCC^[80].

COMBINED HEPATOCELLULAR CARCINOMA-CHOLANGIOCARCINOMA

cHCC-CCA is primary liver cancer demonstrating morphologic and immuno-histochemical features of both HCC and CCA (Figure 4). Collision tumor or two separate primaries of HCC and CCA in the same liver do not qualify for cHCC-CCA diagnosis. Variable terminologies have been used in the literature for this entity, including hepatocholangiocarcinoma, biphenotypic HCC-CCA, mixed HCC-CCA, mixed hepatobiliary carcinoma, combined liver cell and bile duct carcinoma, HCC with dual phenotype, HCC with stem/progenitor cell immunophenotype, cholangiolocarcinoma, cholangiolocellular carcinoma (CLC), intermediate HCC and stem cell tumor, making it difficult to collect meaningful data^[3,81].

In 2010 WHO, cHCC-CCA was largely divided into two types: Classical type and a subtype with stem-cell features, wherein the latter was further subdivided into typical, intermediate, and cholangiocellular subtypes^[1]. However, subsequent studies showed that stem cell features are seen in many other types of HCC and CCA and the

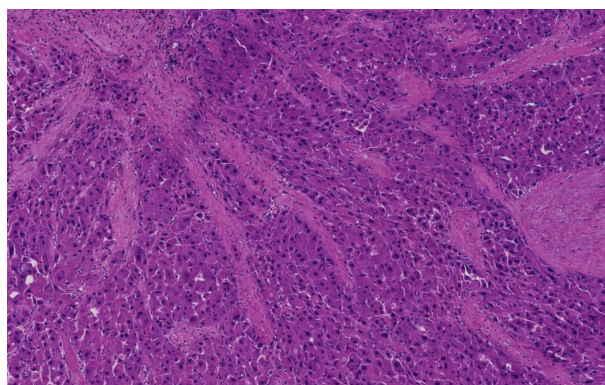


Figure 2 Fibrolamellar hepatocellular carcinoma. Multiple fibrous septa composed of parallel collagen fibers separate tumoral trabeculae (Hematoxylin and eosin stain, $\times 100$).

WHO criteria for stem cell subtypes are difficult to apply in practice. This observation has led to collaborative efforts and the publication of a consensus paper on working terminology and diagnostic criteria of cHCC-CCA in 2018 by international experts in the field consisting of pathologists, radiologists and clinicians^[81].

The consensus paper formally endorsed the terminology cHCC-CCA and recommended that the diagnosis of cHCC-CCA has to be primarily based on morphology on hematoxylin and eosin stain and immuno-histochemical stains are to be used as a supplemental purpose only. In addition, the panel recommended the term "intermediate cell carcinoma" for previous cHCC-CCA with "intermediate cell" stem cell features (primary liver cancer consisting purely of intermediate cells), as a separate entity. "CLC" was recommended as another separate entity with a cut off of 80% required for the diagnosis of pure CLC without mixed components. It was recommended that the morphologic and immuno-histochemical stem/progenitor cell features/phenotypes are to be noted in a comment, but not in the diagnostic line. Further, when more than one morphologic component is present within the same tumor, it was recommended that each component to be listed in the diagnostic line. Therefore, previous cHCC-CCA with "typical" and "cholangiolocellular" stem cell features are termed as cHCC-CCA and cHCC-CCA-CLC, respectively, and the percentage of each component is to be reported^[81].

Studies suggest that cHCC-CCA is likely a clonal lesion of stem/progenitor cell origin^[33,82,83]. The molecular phenotype of cHCC-CCA is heterogeneous^[84]; however, molecular features indicative of stem cell features have been documented^[85]. According to the current 8th edition American Joint Committee on Cancer cancer staging manual, cHCC-CCA is staged as intrahepatic CCA^[86]. Given the differing treatment options for HCC and CCA, biopsy sample of a large mass lesion needs to be interpreted with great caution and a resection specimen needs to be thoroughly sampled.

EMERGING BIOMARKERS AND COMPREHENSIVE STRATIFICATION OF HEPATOCELLULAR CARCINOMA

Novel diagnostic and/or prognostic biomarkers are emerging as key players in the field of HCC research. For example, annexin A2 is significantly increased in the serum of patients with HCC when compared to patients with chronic liver disease, thus may be diagnostically useful especially when combined with AFP^[87,88]. Additional biomarkers, such as osteopontin, Golgi protein-73, squamous cell carcinoma antigen, soluble urokinase plasminogen activator receptor, midkine, AXL, thioredoxins^[88], multifucosylated α -1-acid glycoprotein^[89], vascular endothelial growth factor, angiopoietin^[90], survivin^[91] and alpha-1 antitrypsin^[92], have shown potential for diagnostic and/or prognostic utility. Some of these are recognized by a major international hepatology society^[90].

Likewise, comprehensive genomic and epigenomic approaches are emerging as promising tools to stratify HCCs into clinically relevant subgroups. Bidkhori *et al*^[93] stratified HCCs into three subtypes: Altered kynurenine metabolism, WNT/ β -catenin-associated lipid metabolism and PI3K/AKT/mTOR signaling subtype based on the metabolic and signalling pathways and showed differences in survival. Shimada *et al*^[94] stratified HCCs into three major subtypes: Mitogenic and stem cell-

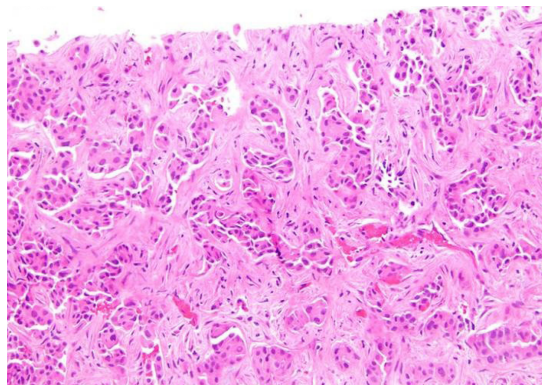


Figure 3 Scirrhous hepatocellular carcinoma. Bands of dense fibrosis separate cords and nests of tumoral cells (Hematoxylin and eosin stain, × 200).

like tumors with chromosomal instability (the proliferative subtype), *CTNNB1*-mutated tumors displaying immune suppression and metabolic disease-associated tumors by multi-platform analysis including transcriptome, exome and methylome profiles and public omics data, and showed a favorable prognosis in the "immuno-genic" subset of the metabolic disease-associated tumors.

CONCLUSION

Our understanding of the pathogenesis of HCC and diagnostic approach is evolving along with rapid advancement of diagnostic tools including molecular pathology. Updated pathologic classification of HCC is a reflection of the accrued knowledge and an effort to facilitate effective communication and collaborative studies. We hope that the effort further advances our understanding of the disease and ultimately improve patient care.

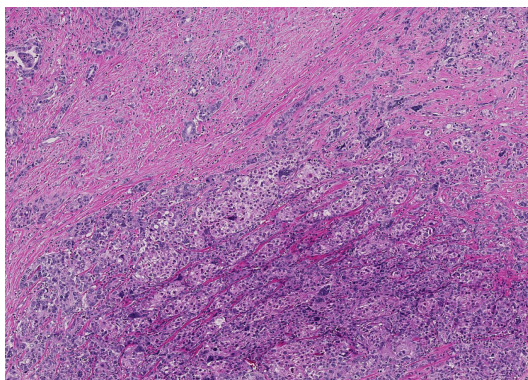


Figure 4 Combined hepatocellular carcinoma-cholangiocarcinoma. Areas of conventional hepatocellular carcinoma (lower mid to right) are admixed with areas of discrete glands formation (upper left) (Hematoxylin and eosin stain, × 40).

REFERENCES

- 1 **Bosman F**, Carneiro F, Hruban R, Theise N. WHO classification of tumours of the digestive system. 4th ed. Lyon: IARC 2010; 205-227
- 2 **Torbenson MS**. Morphologic Subtypes of Hepatocellular Carcinoma. *Gastroenterol Clin North Am* 2017; **46**: 365-391 [PMID: [28506370](#) DOI: [10.1016/j.gtc.2017.01.009](#)]
- 3 **Torbenson M**, Zen Y, Yeh MM. Tumors of the liver, AFIP Atlas of tumor pathology series 4. Washington (DC): American Registry of Pathology 2018; 39-112
- 4 **Koehne de Gonzalez AK**, Salomao MA, Lagana SM. Current concepts in the immunohistochemical evaluation of liver tumors. *World J Hepatol* 2015; **7**: 1403-1411 [PMID: [26052385](#) DOI: [10.4254/wjh.v7.i10.1403](#)]
- 5 **Di Tommaso L**, Destro A, Seok JY, Balladore E, Terracciano L, Sangiovanni A, Iavarone M, Colombo M, Jang JJ, Yu E, Jin SY, Morengi E, Park YN, Roncalli M. The application of markers (HSP70 GPC3 and GS) in liver biopsies is useful for detection of hepatocellular carcinoma. *J Hepatol* 2009; **50**: 746-754 [PMID: [19231003](#) DOI: [10.1016/j.jhep.2008.11.014](#)]
- 6 **Uthamalingam P**, Das A, Behra A, Kalra N, Chawla Y. Diagnostic Value of Glypican3, Heat Shock Protein 70 and Glutamine Synthetase in Hepatocellular Carcinoma Arising in Cirrhotic and Non-Cirrhotic Livers. *J Clin Exp Hepatol* 2018; **8**: 173-180 [PMID: [29892181](#) DOI: [10.1016/j.jceh.2017.09.005](#)]
- 7 **Choi WT**, Ramachandran R, Kakar S. Immunohistochemical approach for the diagnosis of a liver mass on small biopsy specimens. *Hum Pathol* 2017; **63**: 1-13 [PMID: [28087475](#) DOI: [10.1016/j.humpath.2016.12.025](#)]
- 8 **Koehne de Gonzalez A**, Lagana SM. Update on Ancillary Testing in the Evaluation of High-Grade Liver Tumors. *Surg Pathol Clin* 2018; **11**: 367-375 [PMID: [29751880](#) DOI: [10.1016/j.path.2018.02.004](#)]
- 9 **Nguyen T**, Phillips D, Jain D, Torbenson M, Wu TT, Yeh MM, Kakar S. Comparison of 5 Immunohistochemical Markers of Hepatocellular Differentiation for the Diagnosis of Hepatocellular Carcinoma. *Arch Pathol Lab Med* 2015; **139**: 1028-1034 [PMID: [26230595](#) DOI: [10.5858/arpa.2014-0479-OA](#)]
- 10 **Shah SS**, Wu TT, Torbenson MS, Chandan VS. Aberrant CDX2 expression in hepatocellular carcinomas: An important diagnostic pitfall. *Hum Pathol* 2017; **64**: 13-18 [PMID: [28089540](#) DOI: [10.1016/j.humpath.2016.12.029](#)]
- 11 **Mourra N**, Azizi L. CK20 positivity in hepatocellular carcinoma: A potential diagnostic pitfall in liver biopsy. *Appl Immunohistochem Mol Morphol* 2013; **21**: 94-95 [PMID: [22495366](#) DOI: [10.1097/PAL.0b013e31824c4c4a](#)]
- 12 **El Jabbour T**, Durie N, Lee H. Coexpression of CDX2 and CK20 in hepatocellular carcinoma, an exceedingly rare co-incidence with potential diagnostic pitfall. *Hum Pathol* 2018; **81**: 298 [PMID: [29953895](#) DOI: [10.1016/j.humpath.2018.04.031](#)]
- 13 **Ward SC**, Huang J, Tickoo SK, Thung SN, Ladanyi M, Klimstra DS. Fibrolamellar carcinoma of the liver exhibits immunohistochemical evidence of both hepatocyte and bile duct differentiation. *Mod Pathol* 2010; **23**: 1180-1190 [PMID: [20495535](#) DOI: [10.1038/modpathol.2010.105](#)]
- 14 **Shahid M**, Mubeen A, Tse J, Kakar S, Bateman AC, Borger D, Rivera MN, Ting DT, Deshpande V. Branched chain in situ hybridization for albumin as a marker of hepatocellular differentiation: Evaluation of manual and automated in situ hybridization platforms. *Am J Surg Pathol* 2015; **39**: 25-34 [PMID: [25353287](#) DOI: [10.1097/PAS.0000000000000343](#)]
- 15 **Hernandez-Gea V**, Toffanin S, Friedman SL, Llovet JM. Role of the microenvironment in the pathogenesis and treatment of hepatocellular carcinoma. *Gastroenterology* 2013; **144**: 512-527 [PMID: [23313965](#) DOI: [10.1053/j.gastro.2013.01.002](#)]
- 16 **Lee JS**, Chu IS, Heo J, Calvisi DF, Sun Z, Roskams T, Durnez A, Demetris AJ, Thorgeirsson SS. Classification and prediction of survival in hepatocellular carcinoma by gene expression profiling. *Hepatology* 2004; **40**: 667-676 [PMID: [15349906](#) DOI: [10.1002/hep.20375](#)]
- 17 **Boyault S**, Rickman DS, de Reyniès A, Balabaud C, Rebouissou S, Jeannot E, Hérault A, Saric J, Belghiti J, Franco D, Bioulac-Sage P, Laurent-Puig P, Zucman-Rossi J. Transcriptome classification of HCC is related to gene alterations and to new therapeutic targets. *Hepatology* 2007; **45**: 42-52 [PMID: [17187432](#) DOI: [10.1002/hep.21467](#)]
- 18 **Hoshida Y**, Nijman SM, Kobayashi M, Chan JA, Brunet JP, Chiang DY, Villanueva A, Newell P, Ikeda K, Hashimoto M, Watanabe G, Gabriel S, Friedman SL, Kumada H, Llovet JM, Golub TR. Integrative transcriptome analysis reveals common molecular subclasses of human hepatocellular carcinoma. *Cancer Res* 2009; **69**: 7385-7392 [PMID: [19723656](#) DOI: [10.1158/0008-5472.CAN-09-1089](#)]

- 19 **Désert R**, Rohart F, Canal F, Sicard M, Desille M, Renaud S, Turlin B, Bellaud P, Perret C, Clément B, Lê Cao KA, Musso O. Human hepatocellular carcinomas with a periportal phenotype have the lowest potential for early recurrence after curative resection. *Hepatology* 2017; **66**: 1502-1518 [PMID: [28498607](#) DOI: [10.1002/hep.29254](#)]
- 20 **Calderaro J**, Couchy G, Imbeaud S, Amadeo G, Letouzé E, Blanc JF, Laurent C, Hajji Y, Azoulay D, Bioulac-Sage P, Nault JC, Zucman-Rossi J. Histological subtypes of hepatocellular carcinoma are related to gene mutations and molecular tumour classification. *J Hepatol* 2017; **67**: 727-738 [PMID: [28532995](#) DOI: [10.1016/j.jhep.2017.05.014](#)]
- 21 **Cancer Genome Atlas Research Network**. Comprehensive and Integrative Genomic Characterization of Hepatocellular Carcinoma. *Cell* 2017; **169**: 1327-1341.e23 [PMID: [28622513](#) DOI: [10.1016/j.cell.2017.05.046](#)]
- 22 **Chan SL**, Wong AM, Lee K, Wong N, Chan AK. Personalized therapy for hepatocellular carcinoma: Where are we now? *Cancer Treat Rev* 2016; **45**: 77-86 [PMID: [26995632](#) DOI: [10.1016/j.ctrv.2016.02.008](#)]
- 23 **Forner A**, Reig M, Bruix J. Hepatocellular carcinoma. *Lancet* 2018; **391**: 1301-1314 [PMID: [29307467](#) DOI: [10.1016/S0140-6736\(18\)30010-2](#)]
- 24 **Bruix J**, Cheng AL, Meinhardt G, Nakajima K, De Sanctis Y, Llovet J. Prognostic factors and predictors of sorafenib benefit in patients with hepatocellular carcinoma: Analysis of two phase III studies. *J Hepatol* 2017; **67**: 999-1008 [PMID: [28687477](#) DOI: [10.1016/j.jhep.2017.06.026](#)]
- 25 **Bruix J**, Qin S, Merle P, Granito A, Huang YH, Bodoky G, Pracht M, Yokosuka O, Rosmorduc O, Breder V, Gerolami R, Masi G, Ross PJ, Song T, Bronowicki JP, Ollivier-Hourmand I, Kudo M, Cheng AL, Llovet JM, Finn RS, LeBerre MA, Baumhauer A, Meinhardt G, Han G; RESORCE Investigators. Regorafenib for patients with hepatocellular carcinoma who progressed on sorafenib treatment (RESORCE): A randomised, double-blind, placebo-controlled, phase 3 trial. *Lancet* 2017; **389**: 56-66 [PMID: [27932229](#) DOI: [10.1016/S0140-6736\(16\)32453-9](#)]
- 26 **Abou-Alfa GK**, Meyer T, Cheng AL, El-Khoueiry AB, Rimassa L, Ryoo BY, Cicin I, Merle P, Chen Y, Park JW, Blanc JF, Bolondi L, Klumpen HJ, Chan SL, Zagonel V, Pressiani T, Ryu MH, Venook AP, Hessel C, Borgman-Hagey AE, Schwab G, Kelley RK. Cabozantinib in Patients with Advanced and Progressing Hepatocellular Carcinoma. *N Engl J Med* 2018; **379**: 54-63 [PMID: [29972759](#) DOI: [10.1056/NEJMoa1717002](#)]
- 27 **El-Khoueiry AB**, Sangro B, Yau T, Crocenzi TS, Kudo M, Hsu C, Kim TY, Choo SP, Trojan J, Welling TH Rd, Meyer T, Kang YK, Yeo W, Chopra A, Anderson J, Dela Cruz C, Lang L, Neely J, Tang H, Dastani HB, Melero I. Nivolumab in patients with advanced hepatocellular carcinoma (CheckMate 040): An open-label, non-comparative, phase 1/2 dose escalation and expansion trial. *Lancet* 2017; **389**: 2492-2502 [PMID: [28434648](#) DOI: [10.1016/S0140-6736\(17\)31046-2](#)]
- 28 **Gu J**, Zhang X, Cui R, Zhang J, Wang Z, Jia Y, Miao R, Dong Y, Ma X, Fan H, Wang H, Ren L, Li Y, Niu W, Zhang J, Qu K, Liu C. Prognostic predictors for patients with hepatocellular carcinoma receiving adjuvant transcatheter arterial chemoembolization. *Eur J Gastroenterol Hepatol* 2019 [PMID: [30614882](#) DOI: [10.1097/MEG.0000000000001346](#)]
- 29 **Meguro M**, Mizuguchi T, Nishidate T, Okita K, Ishii M, Ota S, Ueki T, Akizuki E, Hirata K. Prognostic roles of preoperative α -fetoprotein and des- γ -carboxy prothrombin in hepatocellular carcinoma patients. *World J Gastroenterol* 2015; **21**: 4933-4945 [PMID: [25945007](#) DOI: [10.3748/wjg.v21.i16.4933](#)]
- 30 **Wang X**, Wang Z, Wu L. Combined measurements of tumor number and size helps estimate the outcome of resection of Barcelona clinic liver cancer stage B hepatocellular carcinoma. *BMC Surg* 2016; **16**: 22 [PMID: [27094483](#) DOI: [10.1186/s12893-016-0135-4](#)]
- 31 **Goh BK**, Chow PK, Teo JY, Wong JS, Chan CY, Cheow PC, Chung AY, Ooi LL. Number of nodules, Child-Pugh status, margin positivity, and microvascular invasion, but not tumor size, are prognostic factors of survival after liver resection for multifocal hepatocellular carcinoma. *J Gastrointest Surg* 2014; **18**: 1477-1485 [PMID: [24855028](#) DOI: [10.1007/s11605-014-2542-0](#)]
- 32 **Yilmaz C**, Karaca CA, Iakobadze Z, Farajov R, Kilic K, Doganay L, Kilic M. Factors Affecting Recurrence and Survival After Liver Transplantation for Hepatocellular Carcinoma. *Transplant Proc* 2018; **50**: 3571-3576 [PMID: [30577240](#) DOI: [10.1016/j.transproceed.2018.05.027](#)]
- 33 **Kim H**, Choi GH, Na DC, Ahn EY, Kim GI, Lee JE, Cho JY, Yoo JE, Choi JS, Park YN. Human hepatocellular carcinomas with "Stemness"-related marker expression: Keratin 19 expression and a poor prognosis. *Hepatology* 2011; **54**: 1707-1717 [PMID: [22045674](#) DOI: [10.1002/hep.24559](#)]
- 34 **Guo Z**, Li LQ, Jiang JH, Ou C, Zeng LX, Xiang BD. Cancer stem cell markers correlate with early recurrence and survival in hepatocellular carcinoma. *World J Gastroenterol* 2014; **20**: 2098-2106 [PMID: [24616575](#) DOI: [10.3748/wjg.v20.i8.2098](#)]
- 35 **Chan AW**, Tong JH, Chan SL, Lai PB, To KF. Expression of stemness markers (CD133 and EpCAM) in prognostication of hepatocellular carcinoma. *Histopathology* 2014; **64**: 935-950 [PMID: [24506513](#) DOI: [10.1111/his.12342](#)]
- 36 **Nahm JH**, Rhee H, Kim H, Yoo JE, San Lee J, Jeon Y, Choi GH, Park YN. Increased expression of stemness markers and altered tumor stroma in hepatocellular carcinoma under TACE-induced hypoxia: A biopsy and resection matched study. *Oncotarget* 2017; **8**: 99359-99371 [PMID: [29245907](#) DOI: [10.18632/oncotarget.22078](#)]
- 37 **Tsuchiya K**, Komuta M, Yasui Y, Tamaki N, Hosokawa T, Ueda K, Kuzuya T, Itakura J, Nakanishi H, Takahashi Y, Kurosaki M, Asahina Y, Enomoto N, Sakamoto M, Izumi N. Expression of keratin 19 is related to high recurrence of hepatocellular carcinoma after radiofrequency ablation. *Oncology* 2011; **80**: 278-288 [PMID: [21734420](#) DOI: [10.1159/000328448](#)]
- 38 **Rhee H**, Nahm JH, Kim H, Choi GH, Yoo JE, Lee HS, Koh MJ, Park YN. Poor outcome of hepatocellular carcinoma with stemness marker under hypoxia: Resistance to transarterial chemoembolization. *Mod Pathol* 2016; **29**: 1038-1049 [PMID: [27312064](#) DOI: [10.1038/modpathol.2016.111](#)]
- 39 **Kim BH**, Park JW, Kim JS, Lee SK, Hong EK. Stem Cell Markers Predict the Response to Sorafenib in Patients with Hepatocellular Carcinoma. *Gut Liver* 2018 [PMID: [30600675](#) DOI: [10.5009/gnl18345](#)]
- 40 **Han DH**, Choi GH, Kim KS, Choi JS, Park YN, Kim SU, Park JY, Ahn SH, Han KH. Prognostic significance of the worst grade in hepatocellular carcinoma with heterogeneous histologic grades of differentiation. *J Gastroenterol Hepatol* 2013; **28**: 1384-1390 [PMID: [23517197](#) DOI: [10.1111/jgh.12200](#)]
- 41 **Starley BQ**, Calcagno CJ, Harrison SA. Nonalcoholic fatty liver disease and hepatocellular carcinoma: A weighty connection. *Hepatology* 2010; **51**: 1820-1832 [PMID: [20432259](#) DOI: [10.1002/hep.23594](#)]
- 42 **Yasui K**, Hashimoto E, Komorizono Y, Koike K, Arai S, Imai Y, Shima T, Kanbara Y, Saibara T, Mori T, Kawata S, Uto H, Takami S, Sumida Y, Takamura T, Kawanaka M, Okanoue T; Japan NASH Study

- Group, Ministry of Health, Labour, and Welfare of Japan. Characteristics of patients with nonalcoholic steatohepatitis who develop hepatocellular carcinoma. *Clin Gastroenterol Hepatol* 2011; **9**: 428-433; quiz e50 [PMID: 21320639 DOI: 10.1016/j.cgh.2011.01.023]
- 43 **Paradis V**, Zalinski S, Chelbi E, Guedj N, Degos F, Vilgrain V, Bedossa P, Belghiti J. Hepatocellular carcinomas in patients with metabolic syndrome often develop without significant liver fibrosis: A pathological analysis. *Hepatology* 2009; **49**: 851-859 [PMID: 19115377 DOI: 10.1002/hep.22734]
- 44 **Salomao M**, Yu WM, Brown RS, Emond JC, Lefkowitz JH. Steatohepatic hepatocellular carcinoma (SH-HCC): A distinctive histological variant of HCC in hepatitis C virus-related cirrhosis with associated NAFLD/NASH. *Am J Surg Pathol* 2010; **34**: 1630-1636 [PMID: 20975341 DOI: 10.1097/PAS.0b013e3181f31caa]
- 45 **Salomao M**, Remotti H, Vaughan R, Siegel AB, Lefkowitz JH, Moreira RK. The steatohepatic variant of hepatocellular carcinoma and its association with underlying steatohepatitis. *Hum Pathol* 2012; **43**: 737-746 [PMID: 22018903 DOI: 10.1016/j.humpath.2011.07.005]
- 46 **Yeh MM**, Liu Y, Torbenson M. Steatohepatic variant of hepatocellular carcinoma in the absence of metabolic syndrome or background steatosis: A clinical, pathological, and genetic study. *Hum Pathol* 2015; **46**: 1769-1775 [PMID: 26410018 DOI: 10.1016/j.humpath.2015.07.018]
- 47 **Baffy G**, Brunt EM, Caldwell SH. Hepatocellular carcinoma in non-alcoholic fatty liver disease: An emerging menace. *J Hepatol* 2012; **56**: 1384-1391 [PMID: 22326465 DOI: 10.1016/j.jhep.2011.10.027]
- 48 **Ando S**, Shibahara J, Hayashi A, Fukayama M. β -catenin alteration is rare in hepatocellular carcinoma with steatohepatic features: Immunohistochemical and mutational study. *Virchows Arch* 2015; **467**: 535-542 [PMID: 26311355 DOI: 10.1007/s00428-015-1836-2]
- 49 **Taniai M**, Hashimoto E, Tobari M, Kodama K, Tokushige K, Yamamoto M, Takayama T, Sugitani M, Sano K, Kondo F, Fukusato T. Clinicopathological investigation of steatohepatic hepatocellular carcinoma: A multicenter study using immunohistochemical analysis of adenoma-related markers. *Hepatol Res* 2018; **48**: 947-955 [PMID: 30058778 DOI: 10.1111/hepr.13203]
- 50 **Deniz K**, Moreira RK, Yeh MM, Ferrell LD. Steatohepatitis-like Changes in Focal Nodular Hyperplasia, A Finding to Distinguish From Steatohepatic Variant of Hepatocellular Carcinoma. *Am J Surg Pathol* 2017; **41**: 277-281 [PMID: 28079599 DOI: 10.1097/PAS.0000000000000781]
- 51 **Shibahara J**, Ando S, Sakamoto Y, Kokudo N, Fukayama M. Hepatocellular carcinoma with steatohepatic features: A clinicopathological study of Japanese patients. *Histopathology* 2014; **64**: 951-962 [PMID: 24898917 DOI: 10.1111/his.12343]
- 52 **Kwon TJ**, Ro JY, Mackay B. Clear-cell carcinoma: An ultrastructural study of 57 tumors from various sites. *Ultrastruct Pathol* 1996; **20**: 519-527 [PMID: 8940759 DOI: 10.3109/01913129609016356]
- 53 **Bannasch P**, Ribback S, Su Q, Mayer D. Clear cell hepatocellular carcinoma: Origin, metabolic traits and fate of glycogenotic clear and ground glass cells. *Hepatobiliary Pancreat Dis Int* 2017; **16**: 570-594 [PMID: 29291777 DOI: 10.1016/S1499-3872(17)60071-7]
- 54 **Cheuk W**, Chan JK. Clear cell variant of fibrolamellar carcinoma of the liver. *Arch Pathol Lab Med* 2001; **125**: 1235-1238 [PMID: 11520281]
- 55 **Liu Z**, Ma W, Li H, Li Q. Clinicopathological and prognostic features of primary clear cell carcinoma of the liver. *Hepatol Res* 2008; **38**: 291-299 [PMID: 17877725 DOI: 10.1111/j.1872-034X.2007.00264.x]
- 56 **Ji SP**, Li Q, Dong H. Therapy and prognostic features of primary clear cell carcinoma of the liver. *World J Gastroenterol* 2010; **16**: 764-769 [PMID: 20135727 DOI: 10.3748/wjg.v16.i6.764]
- 57 **Yang SH**, Watanabe J, Nakashima O, Kojiro M. Clinicopathologic study on clear cell hepatocellular carcinoma. *Pathol Int* 1996; **46**: 503-509 [PMID: 8870006 DOI: 10.1111/j.1440-1827.1996.tb03645.x]
- 58 **Emile JF**, Lemoine A, Azoulay D, Debuire B, Bismuth H, Reynès M. Histological, genomic and clinical heterogeneity of clear cell hepatocellular carcinoma. *Histopathology* 2001; **38**: 225-231 [PMID: 11260303 DOI: 10.1046/j.1365-2559.2001.01096.x]
- 59 **Lee JH**, Shin DH, Park WY, Shin N, Kim A, Lee HJ, Kim YK, Choi KU, Kim JY, Yang YI, Lee CH, Sol MY. IDH1 R132C mutation is detected in clear cell hepatocellular carcinoma by pyrosequencing. *World J Surg Oncol* 2017; **15**: 82 [PMID: 28403884 DOI: 10.1186/s12957-017-1144-1]
- 60 **Lee H**, Ross JS. The potential role of comprehensive genomic profiling to guide targeted therapy for patients with biliary cancer. *Therap Adv Gastroenterol* 2017; **10**: 507-520 [PMID: 28567120 DOI: 10.1177/1756283X17698090]
- 61 **Lee WS**, Lee KW, Heo JS, Kim SJ, Choi SH, Kim YI, Joh JW. Comparison of combined hepatocellular and cholangiocarcinoma with hepatocellular carcinoma and intrahepatic cholangiocarcinoma. *Surg Today* 2006; **36**: 892-897 [PMID: 16998683 DOI: 10.1007/s00595-006-3276-8]
- 62 **Clayton EF**, Furth EE, Ziober A, Xu T, Yao Y, Hwang PG, Bing Z. A case of primary clear cell hepatocellular carcinoma in a non-cirrhotic liver: An immunohistochemical and ultrastructural study. *Rare Tumors* 2012; **4**: e29 [PMID: 22826786 DOI: 10.4081/rt.2012.e29]
- 63 **Takahashi A**, Saito H, Kanno Y, Abe K, Yokokawa J, Irisawa A, Kenjo A, Saito T, Gotoh M, Ohira H. Case of clear-cell hepatocellular carcinoma that developed in the normal liver of a middle-aged woman. *World J Gastroenterol* 2008; **14**: 129-131 [PMID: 18176975 DOI: 10.3748/wjg.14.129]
- 64 **Murakata LA**, Ishak KG, Nzeako UC. Clear cell carcinoma of the liver: A comparative immunohistochemical study with renal clear cell carcinoma. *Mod Pathol* 2000; **13**: 874-881 [PMID: 10955454 DOI: 10.1038/modpathol.3880156]
- 65 **Fan Z**, van de Rijn M, Montgomery K, Rouse RV. Hep par 1 antibody stain for the differential diagnosis of hepatocellular carcinoma: 676 tumors tested using tissue microarrays and conventional tissue sections. *Mod Pathol* 2003; **16**: 137-144 [PMID: 12591966 DOI: 10.1097/01.MP.0000052103.13730.20]
- 66 **Hou TC**, Wu CC, Yang CR, Wang J. Synchronous renal cell carcinoma and clear cell hepatocellular carcinoma mimicking metastatic disease. *Pathol Res Pract* 2010; **206**: 342-345 [PMID: 19608351 DOI: 10.1016/j.prp.2009.06.008]
- 67 **Craig JR**, Peters RL, Edmondson HA, Omata M. Fibrolamellar carcinoma of the liver: a tumor of adolescents and young adults with distinctive clinico-pathologic features. *Cancer* 1980; **46**: 372-379 [PMID: 6248194]
- 68 **Torbenson M**. Fibrolamellar carcinoma: 2012 update. *Scientifica (Cairo)* 2012; **2012**: 743790 [PMID: 24278737 DOI: 10.6064/2012/743790]
- 69 **Eggert T**, McGlynn KA, Duffy A, Manns MP, Greten TF, Altekruse SF. Fibrolamellar hepatocellular carcinoma in the USA, 2000-2010: A detailed report on frequency, treatment and outcome based on the Surveillance, Epidemiology, and End Results database. *United European Gastroenterol J* 2013; **1**: 351-357 [PMID: 24917983 DOI: 10.1177/2050640613501507]
- 70 **Kakar S**, Burgart LJ, Batts KP, Garcia J, Jain D, Ferrell LD. Clinicopathologic features and survival in

- fibrolamellar carcinoma: Comparison with conventional hepatocellular carcinoma with and without cirrhosis. *Mod Pathol* 2005; **18**: 1417-1423 [PMID: [15920538](#) DOI: [10.1038/modpathol.3800449](#)]
- 71 **Edmondson HA.** Differential diagnosis of tumors and tumor-like lesions of liver in infancy and childhood. *AMA J Dis Child* 1956; **91**: 168-186 [PMID: [13282629](#) DOI: [10.1001/archpedi.1956.02060020170015](#)]
- 72 **Ross HM, Daniel HD, Vivekanandan P, Kannangai R, Yeh MM, Wu TT, Makhlof HR, Torbenson M.** Fibrolamellar carcinomas are positive for CD68. *Mod Pathol* 2011; **24**: 390-395 [PMID: [21113139](#) DOI: [10.1038/modpathol.2010.207](#)]
- 73 **Kim YJ, Rhee H, Yoo JE, Alves VAF, Kim GJ, Kim HM, Herman P, Chagas A, Kim H, Park YN.** Tumour epithelial and stromal characteristics of hepatocellular carcinomas with abundant fibrous stroma: Fibrolamellar versus scirrhous hepatocellular carcinoma. *Histopathology* 2017; **71**: 217-226 [PMID: [28326574](#) DOI: [10.1111/his.13219](#)]
- 74 **Honeyman JN, Simon EP, Robine N, Chiaroni-Clarke R, Darcy DG, Lim II, Gleason CE, Murphy JM, Rosenberg BR, Teegan L, Takacs CN, Botero S, Belote R, Germer S, Emde AK, Vacic V, Bhanot U, LaQuaglia MP, Simon SM.** Detection of a recurrent DNAJB1-PRKACA chimeric transcript in fibrolamellar hepatocellular carcinoma. *Science* 2014; **343**: 1010-1014 [PMID: [24578576](#) DOI: [10.1126/science.1249484](#)]
- 75 **Graham RP, Jin L, Knutson DL, Kloft-Nelson SM, Greipp PT, Waldburger N, Roessler S, Longerich T, Roberts LR, Oliveira AM, Halling KC, Schirmacher P, Torbenson MS.** DNAJB1-PRKACA is specific for fibrolamellar carcinoma. *Mod Pathol* 2015; **28**: 822-829 [PMID: [25698061](#) DOI: [10.1038/modpathol.2015.4](#)]
- 76 **Lee JH, Choi MS, Gwak GY, Lee JH, Koh KC, Paik SW, Yoo BC, Choi D, Park CK.** Clinicopathologic characteristics and long-term prognosis of scirrhous hepatocellular carcinoma. *Dig Dis Sci* 2012; **57**: 1698-1707 [PMID: [22327241](#) DOI: [10.1007/s10620-012-2075-x](#)]
- 77 **Kurogi M, Nakashima O, Miyaaki H, Fujimoto M, Kojiro M.** Clinicopathological study of scirrhous hepatocellular carcinoma. *J Gastroenterol Hepatol* 2006; **21**: 1470-1477 [PMID: [16911695](#) DOI: [10.1111/j.1440-1746.2006.04372.x](#)]
- 78 **Matsuura S, Aishima S, Taguchi K, Asayama Y, Terashi T, Honda H, Tsuneyoshi M.** 'Scirrhous' type hepatocellular carcinomas: A special reference to expression of cytokeratin 7 and hepatocyte paraffin 1. *Histopathology* 2005; **47**: 382-390 [PMID: [16178893](#) DOI: [10.1111/j.1365-2559.2005.02230.x](#)]
- 79 **Seok JY, Na DC, Woo HG, Roncalli M, Kwon SM, Yoo JE, Ahn EY, Kim GI, Choi JS, Kim YB, Park YN.** A fibrous stromal component in hepatocellular carcinoma reveals a cholangiocarcinoma-like gene expression trait and epithelial-mesenchymal transition. *Hepatology* 2012; **55**: 1776-1786 [PMID: [22234953](#) DOI: [10.1002/hep.25570](#)]
- 80 **Krings G, Ramachandran R, Jain D, Wu TT, Yeh MM, Torbenson M, Kakar S.** Immunohistochemical pitfalls and the importance of glypican 3 and arginase in the diagnosis of scirrhous hepatocellular carcinoma. *Mod Pathol* 2013; **26**: 782-791 [PMID: [23348905](#) DOI: [10.1038/modpathol.2012.243](#)]
- 81 **Brunt E, Aishima S, Clavien PA, Fowler K, Goodman Z, Gores G, Gouw A, Kagen A, Klimstra D, Komuta M, Kondo F, Miksad R, Nakano M, Nakanuma Y, Ng I, Paradis V, Nyun Park Y, Quaglia A, Roncalli M, Roskams T, Sakamoto M, Saxena R, Sempoux C, Sirlin C, Stueck A, Thung S, Tsui WMS, Wang XW, Wee A, Yano H, Yeh M, Zen Y, Zucman-Rossi J, Theise N.** cHCC-CCA: Consensus terminology for primary liver carcinomas with both hepatocytic and cholangiocytic differentiation. *Hepatology* 2018; **68**: 113-126 [PMID: [29360137](#) DOI: [10.1002/hep.29789](#)]
- 82 **Durnez A, Verslype C, Nevens F, Fevery J, Aerts R, Pirenne J, Lesaffre E, Libbrecht L, Desmet V, Roskams T.** The clinicopathological and prognostic relevance of cytokeratin 7 and 19 expression in hepatocellular carcinoma. A possible progenitor cell origin. *Histopathology* 2006; **49**: 138-151 [PMID: [16879391](#) DOI: [10.1111/j.1365-2559.2006.02468.x](#)]
- 83 **Theise ND, Yao JL, Harada K, Hytioglou P, Portmann B, Thung SN, Tsui W, Ohta H, Nakanuma Y.** Hepatic 'stem cell' malignancies in adults: four cases. *Histopathology* 2003; **43**: 263-271 [PMID: [12940779](#) DOI: [10.1046/j.1365-2559.2003.01707.x](#)]
- 84 **Mocini A, Sia D, Zhang Z, Camprecios G, Stueck A, Dong H, Montal R, Torrens L, Martinez-Quetglas I, Fiel MI, Hao K, Villanueva A, Thung SN, Schwartz ME, Llovet JM.** Mixed hepatocellular cholangiocarcinoma tumors: Cholangiolocellular carcinoma is a distinct molecular entity. *J Hepatol* 2017; **66**: 952-961 [PMID: [28126467](#) DOI: [10.1016/j.jhep.2017.01.010](#)]
- 85 **Coulouarn C, Cavard C, Rubbia-Brandt L, Audebourg A, Dumont F, Jacques S, Just PA, Clément B, Gilgenkrantz H, Perret C, Terris B.** Combined hepatocellular-cholangiocarcinomas exhibit progenitor features and activation of Wnt and TGFβ signaling pathways. *Carcinogenesis* 2012; **33**: 1791-1796 [PMID: [22696594](#) DOI: [10.1093/carcin/bgs208](#)]
- 86 **Amin MB, Edge S, Greene F, Byrd DR, Brookland RK, Washington MK, Gershenwald JE, Compton CC, Hess KR, Sullivan DC, Jessup JM, Brierley JD, Gaspar LE, Schilsky RL, Balch CM, Winchester DP, Asare EA, Madera M, Gress DM, Meyer LR.** AJCC Cancer Staging Manual. 8th ed. Chicago: Springer International Publishing: American Joint Commission on Cancer 2017; 295-302
- 87 **El-Abd N, Fawzy A, Elbaz T, Hamdy S.** Evaluation of annexin A2 and as potential biomarkers for hepatocellular carcinoma. *Tumour Biol* 2016; **37**: 211-216 [PMID: [26189841](#) DOI: [10.1007/s13277-015-3524-x](#)]
- 88 **Tsuchiya N, Sawada Y, Endo I, Saito K, Uemura Y, Nakatsura T.** Biomarkers for the early diagnosis of hepatocellular carcinoma. *World J Gastroenterol* 2015; **21**: 10573-10583 [PMID: [26457017](#) DOI: [10.3748/wjg.v21.i37.10573](#)]
- 89 **Tanabe K, Kitagawa K, Kojima N, Iijima S.** Multifucosylated Alpha-1-acid Glycoprotein as a Novel Marker for Hepatocellular Carcinoma. *J Proteome Res* 2016; **15**: 2935-2944 [PMID: [27354006](#) DOI: [10.1021/acs.jproteome.5b01145](#)]
- 90 **European Association for the Study of the Liver.** EASL Clinical Practice Guidelines: Management of hepatocellular carcinoma. *J Hepatol* 2018; **69**: 182-236 [PMID: [29628281](#) DOI: [10.1016/j.jhep.2018.03.019](#)]
- 91 **Su C.** Survivin in survival of hepatocellular carcinoma. *Cancer Lett* 2016; **379**: 184-190 [PMID: [26118774](#) DOI: [10.1016/j.canlet.2015.06.016](#)]
- 92 **Abdel-Wahab R, Hassan M, Wolff RA, Lacin S, Al-Shamsi HO, Raghav KPS, Shalaby AS, Yao JC, Kaseb AO.** Association of elevated alpha-1 antitrypsin with advanced clinicopathologic features of hepatocellular carcinoma. *J Clin Oncol* 2017; **35**: 289-289 [DOI: [10.1200/JCO.2017.35.4_suppl.289](#)]
- 93 **Bidkhorji G, Benfeitas R, Kleivstig M, Zhang C, Nielsen J, Uhlen M, Boren J, Mardinglu A.** Metabolic network-based stratification of hepatocellular carcinoma reveals three distinct tumor subtypes. *Proc Natl*

- Acad Sci U S A* 2018; **115**: E11874-E11883 [PMID: [30482855](#) DOI: [10.1073/pnas.1807305115](#)]
- 94 **Shimada S**, Mogushi K, Akiyama Y, Furuyama T, Watanabe S, Ogura T, Ogawa K, Ono H, Mitsunori Y, Ban D, Kudo A, Arii S, Tanabe M, Wands JR, Tanaka S. Comprehensive molecular and immunological characterization of hepatocellular carcinoma. *EBioMedicine* 2019; **40**: 457-470 [PMID: [30598371](#) DOI: [10.1016/j.ebiom.2018.12.058](#)]



Application of artificial intelligence in gastroenterology

Young Joo Yang, Chang Seok Bang

ORCID number: Young Joo Yang (0000-0001-6325-1104); Chang Seok Bang (0000-0003-4908-5431).

Author contributions: Yang YJ collected the data and drafted the manuscript. Bang CS conceptualized, collected the data, drafted the manuscript, performed critical revision and approved the final manuscript.

Conflict-of-interest statement: The authors declare no conflicts of interest.

Open-Access: This article is an open-access article which was selected by an in-house editor and fully peer-reviewed by external reviewers. It is distributed in accordance with the Creative Commons Attribution Non Commercial (CC BY-NC 4.0) license, which permits others to distribute, remix, adapt, build upon this work non-commercially, and license their derivative works on different terms, provided the original work is properly cited and the use is non-commercial. See: <http://creativecommons.org/licenses/by-nc/4.0/>

Manuscript source: Invited manuscript

Received: February 9, 2019

Peer-review started: February 12, 2019

First decision: February 26, 2019

Revised: March 4, 2019

Accepted: March 16, 2019

Article in press: March 16, 2019

Published online: April 14, 2019

P-Reviewer: Chiu KW, Triantafyllou K

S-Editor: Ma RY

L-Editor: A

Young Joo Yang, Chang Seok Bang, Department of Internal Medicine, Hallym University College of Medicine, Chuncheon, Gangwon-do 24253, South Korea

Corresponding author: Chang Seok Bang, MD, PhD, Assistant Professor, Doctor, Department of Internal Medicine, Hallym University College of Medicine, Sakju-ro 77, Chuncheon, Gangwon-do 24253, South Korea. csbang@hallym.ac.kr

Telephone: +82-33-2405821

Fax: +82-33-2418064

Abstract

Artificial intelligence (AI) using deep-learning (DL) has emerged as a breakthrough computer technology. By the era of big data, the accumulation of an enormous number of digital images and medical records drove the need for the utilization of AI to efficiently deal with these data, which have become fundamental resources for a machine to learn by itself. Among several DL models, the convolutional neural network showed outstanding performance in image analysis. In the field of gastroenterology, physicians handle large amounts of clinical data and various kinds of image devices such as endoscopy and ultrasound. AI has been applied in gastroenterology in terms of diagnosis, prognosis, and image analysis. However, potential inherent selection bias cannot be excluded in the form of retrospective study. Because overfitting and spectrum bias (class imbalance) have the possibility of overestimating the accuracy, external validation using unused datasets for model development, collected in a way that minimizes the spectrum bias, is mandatory. For robust verification, prospective studies with adequate inclusion/exclusion criteria, which represent the target populations, are needed. DL has its own lack of interpretability. Because interpretability is important in that it can provide safety measures, help to detect bias, and create social acceptance, further investigations should be performed.

Key words: Artificial intelligence; Convolutional neural network; Deep-learning; Computer-assisted; Gastroenterology; Endoscopy

©The Author(s) 2019. Published by Baishideng Publishing Group Inc. All rights reserved.

Core tip: Artificial intelligence (AI) using deep-learning (DL) has emerged as a breakthrough computer technology. The convolutional neural network exhibited outstanding performance in image analysis. AI has been applied in the field of gastroenterology in terms of diagnosis, prognosis, and image analysis. However, potential inherent pitfalls of selection bias, overfitting, and spectrum bias (class imbalance) have the possibility of overestimating the accuracy and generalizing the

E-Editor: Song H



result. Therefore, external validation using unused datasets for model development, collected in a way that minimizes the spectrum bias, is mandatory. DL has its own lack of interpretability, and further investigations should be performed on this issue.

Citation: Yang YJ, Bang CS. Application of artificial intelligence in gastroenterology. *World J Gastroenterol* 2019; 25(14): 1666-1683

URL: <https://www.wjgnet.com/1007-9327/full/v25/i14/1666.htm>

DOI: <https://dx.doi.org/10.3748/wjg.v25.i14.1666>

INTRODUCTION

Recently, artificial intelligence (AI) using deep-learning (DL) has emerged as a breakthrough computer technology, and numerous research studies, using AI applications to identify or differentiate images in various medical fields including radiology, neurology, orthopedics, pathology, ophthalmology, and gastroenterology, have been published^[1]. However, AI, the display of intelligent behavior indistinguishable from that of a human being, was already mentioned in the 1950s^[2]. Although AI has waxed and waned over the past six decades with seemingly little improvement, it was constantly applied to the medical field using various models of machine learning (ML) including Bayesian inferences, decision trees, linear discriminants, support vector machines (SVM), logistic regression, and artificial neural networks (ANNs).

By the era of big data, the accumulation of enormous digital images and medical records drove a need for the utilization of AI to efficiently deal with these data, which also become fundamental resources for the machine to learn by itself. Furthermore, the evolution of computing power with graphic processing units can overcome the limitations of traditional ML, particularly overtraining for input data (overfitting). This led to a revival of AI, especially when using DL technology, a new form of ML. Among several DL methods, the convolutional neural network (CNN), which consists of multilayers of ANN with step-by-step minimal processing, showed outstanding performance in image analysis and has received attention in AI (Figure 1 and Table 1).

In the field of gastroenterology, physicians handle large amounts of clinical data and various kinds of image devices such as esophagogastroduodenoscopy (EGD), colonoscopy, capsule endoscopy (CE), and ultrasound equipment. AI has been applied in the field of gastroenterology when making a diagnosis, predicting a prognosis, and analyzing images. Previous studies reported remarkable results of AI in gastroenterology. The rapid progression of AI demands that gastroenterologists learn the utility, strengths, and pitfalls of AI. In addition, physicians should prepare for the changes and effects of AI on real clinical practice in the near future. Hence, in this review, we aim to (1) briefly introduce an ML technology; (2) summarize an AI application in the field of gastroenterology, which is divided into two categories (statistical analysis for recognition of diagnosis or prediction of prognosis, and analyze images for patient applications excluding animal studies); and (3) discuss the challenges for the application and future directions of AI.

ML TECHNOLOGY

Generally, AI is considered as a machine intelligence that has cognitive functions similar to those of humans including “learning” and “problem solving^[3]”. Currently, ML is the most common approach of AI. It automatically builds mathematical algorithms from given data (known as input training data) and predicts or makes decisions in uncertain conditions without human instructions (Figure 1A)^[4]. In the medical field, ML methods such as Bayesian networks, linear discriminants, SVMs, and ANNs have been used^[5]. A naïve Bayes classifier that represents the probabilistic relationship between input and output data is a typical classification model^[6]. The SVM, which was invented by Vladimir N Vapnik and Alexey Ya Chervonenkis in 1963^[7], is a discriminative model that uses a dividing hyperplane. Before DL development, SVM showed the best performance for classification and regression, which were achieved by optimizing a hyperplane with the largest functional margin (distance from the hyperplane in a high- or infinite-dimensional space to the nearest training data point of any class)^[8].

Table 1 Artificial intelligence terminology

Artificial intelligence	Machine intelligence that has cognitive functions similar to those of humans such as “learning” and “problem solving.”
Machine learning	Mathematical algorithms which is automatically built from given data (known as input training data) and predicts or makes decisions in uncertain conditions without being explicitly programmed
Support vector machines	Discriminative classifier formally defined by an optimizing hyperplane with the largest functional margin
Artificial neural networks	Multilayered interconnected network which consists of an input, hidden connection (between the input and output layer), and output layer
Deep learning	Subset of machine learning technique that composed of multiple-layered neural network algorithms
Convolutional neural networks	Specific class of artificial neural networks that consists of (1) convolutional and pooling layers, which are the two main components to extract distinct features; and (2) fully connected layers to make an overall classification
Overfitting	Modelling error which occurs when a certain learning model tailors itself too much on the training dataset and predictions are not well generalized to new datasets
Spectrum bias	Systematic error occurs when the dataset used for model development does not adequately represent or reflect the range of patients who will be applied in clinical practice (target population)

An ANN is a multilayered interconnected network inspired by the neuronal connections of the human brain. Although the ANN was introduced by McCulloch and Walter in 1943^[9], it was studied in 1957 by Frank Rosenblatt using the concept of the perceptron^[10]. The ANN as a hierarchical structure consists of an input, hidden connection (between the input and output layer), and output layer. The connection in the hidden layer has a strength (known as weight) that is used for the learning process of the network (Figure 1B). Through an appropriate training process (learning process), the network can adjust the value of the connection weight to optimize the best result (Figure 1C).

In the 1980s, an ANN with several hidden layers between the input and output layer was introduced. This was known as a DL (or a deep neural network). Although the ANN showed remarkable performance in managing nonlinear datasets regarding diagnosis and prognostic prediction in the medical field, the ANN revealed several weaknesses as well: a vanishing gradient, overfitting, insufficient computing capacity, and lack of training data. These weaknesses hampered the advancement of the ANN. Finally, the recent availability of big data provided sufficient input data for training, and the rapid progression of computing power allowed researchers to overcome prior limitations. Among several AI methods, DL received the attention of the public and has shown excellent performance in the computer vision area using CNNs.

A CNN consists of (1) convolutional and pooling layers, which are the two main components to extract distinct features; and (2) fully connected layers to make an overall classification. The input images were filtered to extract specialized features using numerous specific filters, and to create multiple feature maps. This preprocessing operation for filtering is called convolution. A learning process for the convolution filter to make the best feature maps is essential for success in a CNN. These feature maps are compressed to smaller sizes by pooling the pixels to capture a larger field of the image, and these convolutional and pooling layers are iterated many times. Finally, fully connected layers combine all features and produce the final outcomes (Figure 1B).

The rapid growth of the CNN was demonstrated at the ImageNet Large Scale Visual Recognition Competition (ILSVRC) in 2012 by Geoffrey Hinton, and several CNNs such as Inception from google and ResNet from Microsoft have shown excellent performance. A graphical summary of AI, ML, and DL development is shown in Figure 1.

APPLICATION OF AI IN GASTROENTEROLOGY

Recognition of diagnosis and prediction of prognosis

Although AI in the field of gastroenterology recently focused on image analysis, several ML models have shown promising results in the recognition of diagnosis and prediction of prognosis. The ANN is appropriate for dealing with complex datasets to overcome the drawbacks of traditional linear statistics. In addition, the ANN can

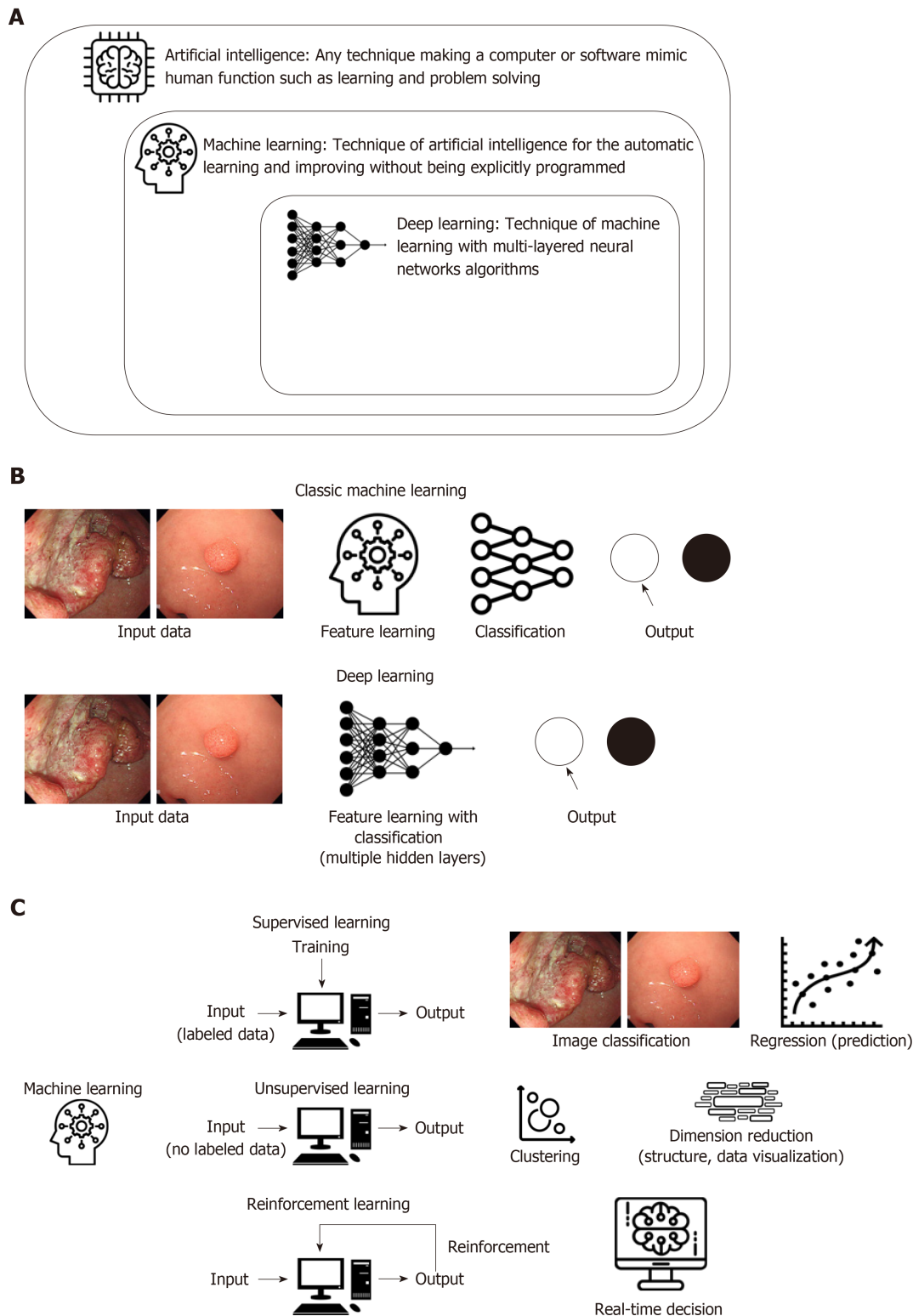


Figure 1 Schematic graphical summary for artificial intelligence, machine learning and deep learning development. A: Definition of artificial intelligence, machine learning (ML) and deep learning (DL). B: Comparison of process between classic ML and DL. C: Modes of learning and examples of ML.

stand for the sophisticated interactions between demographic, environmental, and clinical characteristics.

In terms of diagnosis, Pace *et al*^[11] demonstrated an ANN model in 2005 that made a diagnosis of gastroesophageal reflux disease using only 45 clinical variables in 159 cases with an accuracy of 100%. Lahner *et al*^[12] performed a similar pilot study to recognize atrophic gastritis solely by using clinical and biochemical variables from 350 outpatients by using ANNs and linear discriminant analysis. This study showed great accuracy.

Regarding the prediction of prognosis, in 1998, Pofahl *et al*^[13] compared an ANN

model to the Ranson criteria and the Acute Physiologic and Chronic Health Evaluation (APACHE II) scoring system to predict the length of stay for patients with acute pancreatitis. The authors used a backpropagation neural network that was trained using 156 patients. Although the highest specificity (94%) was observed in the Ranson criteria, the ANN model showed the highest sensitivity (75%) when predicting a length of stay more than 7 d. Similar accuracy was observed for the Ranson criteria and APACHE II scoring system^[13]. In 2003, Das *et al*^[14] used an ANN to predict the outcomes of acute lower gastrointestinal bleeding using 190 patients. The authors compared the performance of ANNs to a previously validated scoring system (BLEED), which revealed a significantly better predictive accuracy of mortality (87% *vs* 21%), recurrent bleeding (89% *vs* 41%), and the need for therapeutic intervention (96% *vs* 46%) in the ANN model.

Sato *et al*^[15] presented an ANN model in 2005 to predict 1-year and 5-year survival using 418 esophageal cancer patients. This ANN model showed improved accuracy compared to the conventional linear discriminant analysis model.

Recently, the number of input training data items for ANNs was increased from hundreds to thousands of patients. Rotondano *et al*^[16] compared the Rockall score to a supervised ANN model to predict the mortality of nonvariceal upper gastrointestinal bleeding using 2380 patients. This approach showed superior sensitivity (83.8% *vs* 71.4%), specificity (97.5% *vs* 52.0%), accuracy (96.8% *vs* 52.9%), and area under receiver operating characteristic (AUROC) of the predictive performance (0.95 *vs* 0.67) in the ANN model to those in the complete Rockall score.

Takayama *et al*^[17] established an ANN model for the prediction of prognosis in patients with ulcerative colitis after cytoapheresis therapy and achieved a sensitivity and specificity for the need of an operation of 96% and 97%, respectively. Hardalaç *et al*^[18] established an ANN model to predict mucosal healing by azathioprine therapy in patients with inflammatory bowel disease (IBD) and achieved 79.1% correct classifications. Peng *et al*^[19] used an ANN model to predict the frequency of the onset, relapse, and severity of IBD. The researchers achieved an average accuracy to predict the frequency of onset and severity of IBD but a high accuracy in predicting the frequency of relapse of IBD (mean square error = 0.009, mean absolute percentage error = 17.1%).

SVMs have been used to analyze data and recognize patterns in classification analyses. Recently, Ichimasa *et al*^[20] analyzed 45 clinicopathological factors in 690 endoscopically resected T1 colorectal cancer patients to predict lymph node metastasis using a SVM. This approach showed superior performance (sensitivity 100%, specificity 66%, accuracy 69%) compared to those of American (sensitivity 100%, specificity 44%, accuracy 49%), European (sensitivity 100%, specificity 0%, accuracy 9%), and Japanese (sensitivity 100%, specificity 0%, accuracy 9%) guidelines. A prediction model using a SVM model reduced the amount of unnecessary additional surgery (77%) when misdiagnosing lymph node metastasis than those of a prediction model using American (85%), European (91%), and Japanese guidelines (91%). Yang *et al*^[21] constructed an SVM-based model using clinicopathological features and 23 immunologic markers from 483 patients who underwent curative surgery for esophageal squamous cell carcinoma. This study revealed reasonable performance in identifying high-risk patients with postoperative distant metastasis [sensitivity 56.6%, specificity 97.7%, positive predictive value (PPV) 95.6%, negative predictive value (NPV) 72.3%, and overall accuracy 78.7%] (Table 2).

Analysis of images

Although endoscopic screening programs have reduced the mortality from gastrointestinal malignancies, they are still the leading cause of death worldwide and remain a global economic burden. To enhance the detection rate of gastrointestinal neoplasms and optimize the treatment strategies, a high-quality endoscopic examination for the recognition of gastrointestinal neoplasms and classifications between benign and malignant lesions are essential for the gastroenterologist. Thus, gastroenterologists are interested in the applications of AI, especially when using CNNs and SVMs for image analysis. Furthermore, AI has been increasingly adopted in terms of non-neoplastic gastrointestinal diseases including infection, inflammation, or hemorrhage.

Upper gastrointestinal field: Takiyama *et al*^[22] constructed a CNN model that could recognize the anatomical location of EGD images with AUROCs of 1.00 for the larynx and esophagus, and 0.99 for the stomach and duodenum. This CNN model could also recognize specific anatomical locations within the stomach, with AUROCs of 0.99 for the upper, middle, and lower stomach.

To assist in the discrimination of early neoplastic lesions in Barrett's esophagus, van der Sommen *et al*^[23] developed an automated algorithm to include specific

Table 2 Summary of clinical studies using artificial intelligence for recognition of diagnosis and prediction of prognosis

Ref.	Published year	Aim of study	Design of study	Number of subjects	Type of AI	Input variables (number/type)	Outcomes
Pace <i>et al</i> ^[11]	2005	Diagnosis of gastroesophageal reflux disease	Retrospective	159 patients (10 times cross validation)	"backpropagation" ANN	101/clinical variables	Accuracy: 100%
Lahner <i>et al</i> ^[12]	2005	Recognition of atrophic corpus gastritis	Retrospective	350 patients (subdivided several times into training and test set equally)	ANN	37 to 3 /clinical and biochemical variables (experiment 1 to 5)	Accuracy: 96.6%, 98.8%, 98.4%, 91.3% and 97.7% (experiment 1-5, respectively)
Pofahl <i>et al</i> ^[13]	1998	Prediction of length of stay for patients with acute pancreatitis	Retrospective	195 patients (training set: 156, test set: 39)	"backpropagation" ANN	71/clinical variables	Sensitivity: 75 % (for prediction of a length of stay more than 7 d)
Das <i>et al</i> ^[14]	2003	Prediction of outcomes in acute lower gastrointestinal bleeding	Prospective	190 patients (training set: 120, internal validation set: 70, external validation set: 142)	ANN	26/clinical variables	Accuracy (external validation set): 97% for death, 93% for, recurrent bleeding, 94% for need for intervention
Sato <i>et al</i> ^[15]	2005	Prediction of 1-year and 5-year survival of esophageal cancer	Retrospective	418 patients (training-: validation-: test set = 53%: 27%: 20%)	ANN	199/ clinicopathologic, biologic, and genetic variables	AUROC for 1 year- and 5 year survival prediction: 0.883 and 0.884, respectively
Rotondano <i>et al</i> ^[16]	2011	Prediction of mortality in nonvariceal upper gastrointestinal bleeding	Prospective, multicenter	2380 patients (5 × 2 cross-validation)	ANN	68/clinical variables	Accuracy: 96.8%, AUROC: 0.95, sensitivity: 83.8%, specificity: 97.5%,
Takayama <i>et al</i> ^[17]	2015	Prediction of prognosis in ulcerative colitis after cytoapheresis therapy	Retrospective	90 patients (training set: 54, test set: 36)	ANN	13/clinical variables	Sensitivity: 96.0%, specificity: 97.0%
Hardalaç <i>et al</i> ^[18]	2015	Prediction of mucosal healing by azathioprine therapy in IBD	Retrospective	129 patients (training set: 103, validation set: 13, test set: 13)	"feed-forward back-propagation" and "cascade-forward" ANN	6/clinical variables	Total correct classification rate: 79.1%
Peng <i>et al</i> ^[19]	2015	Prediction of frequency of onset, relapse, and severity of IBD	Retrospective	569 UC and 332 CD patients (training set: data from 2003-2010, validation set: data in 2011)	ANN	5/meteorological data	Accuracy in predicting the frequency of relapse of IBD (mean square error = 0.009, mean absolute percentage error = 17.1%)
Ichimasa <i>et al</i> ^[20]	2018	Prediction of lymph node metastasis, thus minimizing the need for additional surgery in T1 colorectal cancer	Retrospective	690 patients (training set: 590, validation set: 100)	SVM	45/ Clinicopathologic al variables	Accuracy: 69%, sensitivity: 100%, specificity: 66%
Yang <i>et al</i> ^[21]	2013	Prediction of postoperative distant metastasis in esophageal squamous cell carcinoma	Retrospective	483 patients (training set: 319, validation set: 164)	SVM	30/7 clinicopathologica l variables and 23 immunomarkers	Accuracy: 78.7% sensitivity: 56.6%, specificity: 97.7%, PPV: 95.6%, NPV: 72.3%

AI: Artificial intelligence; ANN: Artificial neural network; AUROC: Area under receiver operating characteristic; IBD: Inflammatory bowel disease; UC: Ulcerative colitis; CD: Crohn's disease; SVM: Support vector machine; PPV: Positive predictive value; NPV: Negative predictive value.

textures, color filters, and ML from 100 endoscopic images. This algorithm reasonably detected early neoplastic lesions in a per-image analysis with a sensitivity and specificity of 83%. In 2017, the same group investigated a model to improve the detection rate of early neoplastic lesions in Barrett's esophagus by using 60 *ex vivo* volumetric laser endomicroscopy images. This novel computer model showed optimal performance compared with a clinical volumetric laser endomicroscopy prediction score with a sensitivity of 90% and specificity of 93%^[24].

Several studies evaluated the ML model using specialized endoscopy to differentiate neoplastic/dysplastic and non-neoplastic lesions. Kodashima *et al*^[25] showed that computer-based analysis can easily identify malignant tissue at the cellular level using endocytoscopic images, which enables the microscopic visualization of the mucosal surface. In 2015, Shin *et al*^[26] reported on an image analysis model to detect esophageal squamous dysplasia using high-resolution microendoscopy (HRME). The sensitivity and specificity of this model were 87% and 97%, respectively. During the following year, Quang *et al*^[27] from the same study group evolved this model, which was incorporated in tablet-interfaced HRME with full automation for real-time analysis. As a result, the model reduced the costs compared to previous laptop-interfaced HRME and showed good diagnostic yields of esophageal squamous cell carcinoma with a sensitivity and specificity of 95% and 91%, respectively. However, there was a limitation for the application of this model owing to the unavailability of specialized endoscopy.

Finally, Horie *et al*^[28] demonstrated the utility of AI using CNNs to make a diagnosis of esophageal cancer. This was trained with 8428 conventional endoscopic images including white-light images (WLIs) and narrow-band images (NBIs). This CNN model detected esophageal cancer with a sensitivity of 95% and could identify all small cancers of < 10 mm. This model also distinguished superficial esophageal cancer from advanced cancer with an accuracy of 98%.

Helicobacter pylori (*H. pylori*) infection is the most important risk factor of peptic ulcers and gastric cancer. Several researchers challenged AI to aid the endoscopic diagnosis of *H. pylori* infections. In 2004, Huang *et al*^[29] investigated the predictability of *H. pylori* infection by refined feature selection with a neural network using related gastric histologic features in endoscopic images. This model was trained and analyzed with 84 image parameters from 30 patients. The sensitivity and specificity for the detection of *H. pylori* infection were 85.4% and 90.9%, respectively. In addition, the accuracy of this model for identifying gastric atrophy, intestinal metaplasia, and predicting the severity of *H. pylori*-related gastric inflammation was higher than 80%.

Recently, two Japanese researchers reported on the application of a CNN to make a diagnosis of *H. pylori* infection^[30,31]. Itoh *et al*^[31] developed a CNN model to recognize *H. pylori* infections by using 596 endoscopic images after the data augmentation of a prior set of 149 images. This CNN model showed promising results with a sensitivity and specificity of 86.7% and 86.7%, respectively. Shichijo *et al*^[30] compared the performance of a CNN to that of 23 endoscopists for the diagnosis of *H. pylori* infection by using endoscopic images. The CNN model showed superior sensitivity (88.9% *vs* 79.0%), specificity (87.4% *vs* 83.2%), accuracy (87.7% *vs* 82.4%), and diagnostic time (194 s *vs* 230 s).

In 2018, a prospective pilot study was conducted for automated diagnosis of *H. pylori* infections using image-enhanced endoscopy such as blue laser imaging-bright and linked color imaging. The performance of the developed AI model was significantly higher with blue laser imaging-bright and linked color imaging training (AUROCs of 0.96 and 0.95) than WLI imaging training (0.66)^[32].

The utility of AI in the diagnosis of gastrointestinal neoplasms was classified into two main categories: detection and characterization. In 2012, Kubota *et al*^[33] first evaluated a computer-aided pattern recognition system to identify the depth of the wall invasion of gastric cancer using endoscopic images. They used 902 endoscopic images and created a backpropagation model after a 10-time cross validation. As a result, the diagnostic accuracy was 77.2%, 49.1%, 51.0%, and 55.3% for T1-4 staging, respectively. In particular, the accuracy of T1a (mucosal invasion) and T1b staging (submucosal invasion) was 68.9% and 63.6%, respectively. Hirasawa *et al*^[34] reported on the good performance of a CNN-based diagnostic system to detect gastric cancers in endoscopic images. The authors trained the CNN model using 13584 endoscopic images and tested it with 2296 images. The overall sensitivity was 92.2%. In addition, the detection rate with a diameter of 6 mm or more was 98.6%, and all invasive cancers were identified^[34]. All missed lesions were superficially depressed and differentiated-type intramucosal cancers that were difficult to distinguish from gastritis even for experienced endoscopists. However, 69.4% of the lesions that the CNN diagnosed as gastric cancer were benign, and the most common reasons for misdiagnosis were gastritis with redness, atrophy, and intestinal metaplasia^[34].

Zhu *et al*^[35] further applied a CNN system to discriminate the invasion depth of

gastric cancer (M/SM1 vs deeper than SM1) using conventional endoscopic images. They trained a CNN model with 790 images and tested it with another 203 images. The CNN model showed high accuracy (89.2%) and specificity (95.6%) when determining the invasion depth of gastric cancer. This result was significantly superior to that of experienced endoscopists. Kanesaka *et al*^[36] studied a computer-aided diagnosis system using a SVM to facilitate the use of magnifying NBI to distinguish early gastric cancer. The study reported on remarkable potential in terms of diagnostic performance (accuracy 96.3%, PPV 98.3%, sensitivity 96.7%, and specificity 95%) and the performance of area concordance (accuracy 73.8%, PPV 75.3%, sensitivity 65.5%, and specificity 80.8%).

In terms of hepatology, the ultrasound has been challenged for the application of AI. Gatos *et al*^[37] established a SVM diagnostic model of chronic liver disease using ultrasound shear wave elastography (70 patients with chronic liver disease and 56 healthy controls). The performance was promising, with an accuracy of 87.3%, sensitivity of 93.5%, and specificity of 81.2%, although the prospective validation was not conducted. Kuppli *et al*^[38] established a fatty liver detection and characterization model using a single-layer feed-forward neural network, and validated this model with a higher accuracy than the previous SVM-based model. These researchers used ultrasound images of 63 patients, and the gold standard for labeling for each patient was the pathologic results of a liver biopsy.

The determination of liver cirrhosis was also challenged with ML technology. Liu *et al*^[39] developed a CNN model with ultrasound liver capsule images (44 images from controls and 47 images from patients with cirrhosis), and classified these images using a SVM. The AUROC for the classification was 0.951, although the prospective validation was not conducted.

Lower gastrointestinal field: Among various gastrointestinal fields, the development of an AI model using colonoscopy has been the most promising area because polyp detection during colonoscopies is frequent. This provides sufficient sources for AI training, and a missed colorectal polyp is directly associated with interval colorectal cancer development.

In terms of polyp detection, Fernandez-Esparrach *et al*^[40] established an automated computer-vision method using an energy map to detect colonic polyps in 2016. They used 24 videos containing 31 polyps and showed acceptable performance with a sensitivity of 70.4% and a specificity of 72.4% for polyp detection (Table 3). Recently, this performance was improved with a DL application for polyp detection^[41,42]. Misawa *et al*^[41] designed a CNN model using 546 short videos from 73 full-length videos, which were divided into two groups of training data (105 polyp-positive videos and 306 polyp-negative videos) and test data (50 polyp-positive videos and 85 polyp-negative videos). The researchers showed the possibility of the automated detection of colonic polyps in real time, and the sensitivity and specificity were 90.0% and 63.3%, respectively. Urban *et al*^[42] also used a CNN system to identify colonic polyps. They used 8641 hand-labeled images and 20 colonoscopy videos in various combinations as training and test data. The CNN model detected polyps in real time with an AUROC of 0.991 and an accuracy of 96.4%. Moreover, it assisted in the identification of an additional nine polyps compared with expert endoscopists in the application of test colonoscopy videos.

Although there were many promising performances of the automated polyp detection models, a prospective validation was not conducted^[43-45]. However, Klare *et al*^[46] performed a prototype software validation under real-time conditions (55 routine colonoscopies), and the results were comparable between those of endoscopists and the established software. The endoscopists' polyp detection rates and adenoma detection rates were 56.4% and 30.9%, respectively, and these rates were 50.9% and 29.1% for the software, respectively). Wang *et al*^[47] established a DL algorithm by using data from 1290 patients, and validated this model with 27113 newly collected colonoscopy images from 1138 patients. This model showed remarkable performance with a sensitivity of 94.38%, specificity of 95.2%, and AUROC of 0.984 for at least one polyp detection^[47].

For AI applications of polyp characterization, magnifying endoscopic images, which is useful when discriminating pit or vascular patterns, was first adopted to enhance the performance of AI. Tischendorf *et al*^[48] developed an automated classification model of colorectal polyps by magnifying NBI images to evaluate vascular patterns in 2010. They reported that the overall accurate classification rates were 91.9% for a consensus decision between the human observers and 90.9% for a safe decision (classifying polyps as neoplastic in cases when there was an interobserver discrepancy)^[48]. In 2011, Gross *et al*^[49] compared the performances of a computer-based model for the differentiation of small colonic polyps of < 10 mm using NBI images. The expert endoscopists and computer-based model showed

Table 3 Summary of clinical studies using artificial intelligence in the upper gastrointestinal field

Ref.	Published year	Aim of study	Design of study	Number of subjects	Type of AI	Endoscopic or ultrasound modality	Outcomes
Takiyama <i>et al</i> ^[22]	2018	Recognition of anatomical locations of EGD images	Retrospective	Training set: 27335 images from 1750 patients. Validation set: 17081 images from 435 patients	CNN	White-light endoscopy	AUROC: 1.00 for the larynx and esophagus, and 0.99 for the stomach and duodenum recognition
van der Sommen <i>et al</i> ^[23]	2016	Discrimination of early neoplastic lesions in Barrett's esophagus	Retrospective	100 endoscopic images from 44 patients (leave-one-out cross-validation on a per-patient basis)	SVM	White-light endoscopy	Sensitivity: 83%, specificity: 83% (per-image analysis)
Swager <i>et al</i> ^[24]	2017	Identification of early Barrett's esophagus neoplasia on ex vivo volumetric laser endomicroscopy images.	Retrospective	60 volumetric laser endomicroscopy images	Combination of several methods (SVM, discriminant analysis, AdaBoost, random forest, etc)	Ex vivo volumetric laser endomicroscopy	Sensitivity: 90%, specificity: 93%
Kodashima <i>et al</i> ^[25]	2007	Discrimination between normal and malignant tissue at the cellular level in the esophagus	Prospective <i>ex vivo</i> pilot	10 patients	ImageJ program	Endocytoscopy	Difference in the mean ratio of total nuclei to the entire selected field, $6.4 \pm 1.9\%$ in normal tissues and $25.3 \pm 3.8\%$ in malignant samples
Shin <i>et al</i> ^[26]	2015	Diagnosis of esophageal squamous dysplasia	Prospective, multicenter	375 sites from 177 patients (training set: 104 sites, test set: 104 sites, validation set: 167 sites)	Linear discriminant analysis	HRME	Sensitivity: 87%, specificity: 97%
Quang <i>et al</i> ^[27]	2016	Diagnosis of esophageal squamous cell neoplasia	Retrospective, multicenter	Same data from reference number 26	Linear discriminant analysis	Tablet-interfaced HRME	Sensitivity: 95%, specificity: 91%
Horie <i>et al</i> ^[28]	2019	Diagnosis of esophageal cancer	Retrospective	Training set: 8428 images from 384 patients. Test set: 1118 images from 97 patients	CNN	White-light endoscopy with NBI	Sensitivity 98%
Huang <i>et al</i> ^[29]	2004	Diagnosis of <i>H. pylori</i> infection	Prospective	Training set: 30 patients. Test set: 74 patients	Refined feature selection with neural network	White-light endoscopy	Sensitivity: 85.4%, specificity: 90.9%
Shichijo <i>et al</i> ^[30]	2017	Diagnosis of <i>H. pylori</i> Infection	Retrospective	Training set: CNN1: 32208 images; CNN2: images classified according to 8 different locations in the stomach. Test set: 11481 images from 397 patients	CNN	White-light endoscopy	Accuracy: 87.7%, sensitivity: 88.9%, specificity: 87.4%, diagnostic time: 194 s.
Itoh <i>et al</i> ^[31]	2018	Diagnosis of <i>H. pylori</i> infection	Prospective	Training set: 149 images (596 images through data augmentation. Test set: 30 images)	CNN	White-light endoscopy	AUROC: 0.956, sensitivity: 86.7%, specificity: 86.7%

Nakashima <i>et al</i> ^[32]	2018	Diagnosis of <i>H. pylori</i> infection	Prospective pilot	222 patients (training set: 162, test set: 60)	CNN	White-light endoscopy and image-enhanced endoscopy, such as blue laser imaging-bright and linked color imaging	AUROC: 0.96 (blue laser imaging-bright), 0.95 (linked color imaging)
Kubota <i>et al</i> ^[33]	2012	Diagnosis of depth of invasion in gastric cancer	Retrospective	902 images (10 times cross validation)	"backpropagation" ANN	White-light endoscopy	Accuracy: 77.2%, 49.1%, 51.0%, and 55.3% for T1-4 staging, respectively
Hirasawa <i>et al</i> ^[34]	2018	Detection of gastric cancers	Retrospective	Training set: 13584 images. Test set: 2296 images.	CNN	White-light endoscopy, chromoendoscopy, NBI	Sensitivity: 92.2%, detection rate with a diameter of 6 mm or more: 98.6%
Zhu <i>et al</i> ^[35]	2018	Diagnosis of depth of invasion in gastric cancer (mucosa/SM1/deeper than SM1)	Retrospective	Training set: 790 images. Test set: 203 images	CNN	White-light endoscopy	Accuracy: 89.2%, AUROC: 0.94, sensitivity: 74.5%, specificity: 95.6%
Kanesaka <i>et al</i> ^[36]	2018	Diagnosis of early gastric cancer using magnifying NBI images	Retrospective	Training set: 126 images. Test set: 81 images	SVM	Magnifying NBI	Accuracy: 96.3%, sensitivity: 96.7%, specificity: 95%, PPV: 98.3%,
Gatos <i>et al</i> ^[37]	2017	Diagnosis of chronic liver disease	Retrospective	126 patients (56 healthy controls, 70 with chronic liver disease)	SVM	Ultrasound shear wave elastography imaging with a stiffness value-clustering	AUROC: 0.87, highest accuracy: 87.3%, sensitivity: 93.5%, specificity: 81.2%
Kuppili <i>et al</i> ^[38]	2017	Detection and characterization of fatty liver	Prospective	63 patients who underwent liver biopsy (10 times cross validation)	Extreme Learning Machine to train single-layer feed-forward neural network	Ultrasound liver images	Accuracy: 96.75%, AUROC: 0.97 (validation performance)
Liu <i>et al</i> ^[39]	2017	Diagnosis of liver cirrhosis	Retrospective	44 images from controls and 47 images from patients with cirrhosis	SVM	Ultrasound liver capsule images	AUROC: 0.951

AI: Artificial intelligence; EGD: Esophagogastroduodenoscopy; CNN: Convolutional neural network; AUROC: Area under receiver operating characteristic; SVM: Support vector machine; HRME: High-resolution microendoscopy; NBI: Narrow band image; *H. pylori*: *Helicobacter pylori*; ANN: Artificial neural network; PPV: Positive predictive value.

comparable diagnostic performance in sensitivity (93.4% *vs* 95.0%), specificity (91.8% *vs* 90.3%), and accuracy (92.7% *vs* 93.1%)^[49].

Takemura *et al*^[50] retrospectively compared the identification of pit patterns of a computer-based model with shape descriptors such as area, perimeter, fit ellipse, or circularity in reference to endoscopic diagnosis by using magnified endoscopic images with crystal violet staining in 2010. The accuracies of the type I, II, III_L, and IV pit patterns of colorectal lesions were 100%, 100%, 96.6%, and 96.7%, respectively. In 2012, the authors applied an upgraded version of a computer system *via* SVM to distinguish neoplastic and non-neoplastic lesions by using endoscopic NBI images, which showed a detection accuracy of 97.8%^[51]. They further demonstrated the availability of a real-time image recognition system in 2016, and the accuracy between the pathologic results of diminutive polyps and diagnosis by a real-time image recognition model was 93.2%^[52].

Byrne *et al*^[53] developed a CNN model for the real-time differentiation of diminutive colorectal polyps by using only NBI video frames in 2017. This model discriminated adenomas from hyperplastic polyps with an accuracy of 94%, and identified the adenoma with a sensitivity of 98% and a specificity of 83%^[53]. Likewise, Chen *et al*^[54] made a CNN model trained with 2157 images to identify neoplastic or hyperplastic polyps of < 5 mm with a PPV and NPV of 89.6% and 91.5%, respectively. In 2017, Komeda *et al*^[55] reported on the preliminary data of a CNN model to distinguish adenomas from non-adenomatous polyps. The CNN model was trained with 1800 conventional endoscopic images with WLI, NBI, and chromoendoscopy, and the accuracy of a 10-fold cross-validation was 75.1%.

To enhance the differentiation of polyps, a Japanese study group reported several articles for AI application with endocytoscopy images, which enables the observation of nuclei on site, and showed comparable diagnostic results to those of pathologic examinations. In 2015, these researchers first developed a computer-aided diagnosis system using endocytoscopy for the discrimination of neoplastic changes in small polyps. This approach showed a comparable sensitivity (92.0%) and accuracy (89.2%) with those of expert endoscopists^[56]. In 2016, this research team developed a second-generation model that could (1) evaluate both nuclei and ductal lumens, (2) use an SVM instead of multivariate analysis, (3) provide the confidence levels of the decisions, and (4) provide a more rapid process of discriminating neoplastic changes from 0.3 s to 0.2 s. The endocytoscopic microvascular patterns could be effectively evaluated by staining with dye^[57]. These researchers also developed endocytoscopy with NBI without staining to evaluate microvascular findings. This approach showed an overall accuracy of 90%^[57]. The same group performed a prospective validation of a real-time computer-aided diagnosis system using endocytoscopy with NBI or stained images to identify neoplastic diminutive polyps. The researchers reported a pathologic prediction rate of 98.1%, and the time required to assess one diminutive polyp was about 35 to 47 s^[59].

The application of a computer-aided ultrahigh (approximately 400 ×) magnification endocytoscopy system for the diagnosis of invasive colorectal cancers was investigated by Takeda *et al*^[60]. This system was trained with 5543 endocytoscopic images from 238 lesions and reported a sensitivity of 89.4%, specificity of 98.9%, and accuracy of 94.1% using 200 test images^[60].

For the application of AI in IBD, Maeda *et al*^[61] developed a diagnosis system using a SVM after refining previous computer-aided endocytoscopy systems^[56-58]. They evaluated the diagnostic performance of this model for the prediction of persistent histologic inflammation in ulcerative colitis patients. This model showed good performance with a sensitivity of 74%, specificity of 97%, and an accuracy of 91%^[61].

Currently, the resolution of images is relatively low in capsule endoscopy compared to other digestive endoscopies. Moreover, the interpretation and diagnosis of capsule endoscopy images highly depends on the reviewer's ability and effort. It is also a time-consuming process. Therefore, several conditions were attempted for the automated diagnosis of capsule endoscopy images including angiectasia, celiac disease, or intestinal hookworms, or for small intestinal motility characterization^[62-65].

Leenhardt *et al*^[62] developed a gastrointestinal angiectasia detection model using semantic segmentation images with a CNN. They used 600 control images and 600 typical angiectasia images to form 4166 small bowel capsule endoscopy videos, which were divided equally into training and test data sets. The CNN-based model revealed a high diagnostic performance with a sensitivity of 100%, specificity of 96%, PPV of 96%, and NPV of 100%^[62] (Table 4). Zhou *et al*^[63] established a CNN model for the classification of celiac disease from control with capsule endoscopy clips from six celiac disease patients and five controls. The researchers achieved 100% sensitivity and specificity for the test data set. Moreover, the evaluation confidence was related to the severity level of small bowel mucosal lesions, reflecting the potential for the quantitative measurement of the existence and degree of pathology throughout the small intestine^[63]. Intestinal hookworms are difficult to find with direct visualization because they have small tubular structures with a whitish color and semitransparent features similar to background intestinal mucosa. Moreover, the presence of intestinal secretory materials makes them difficult to detect. He *et al*^[64] established a CNN model for the detection of hookworms in capsule endoscopy images. The CNN-based model showed a reasonable performance with a sensitivity of 84.6%, specificity of 88.6% and only 15% hookworm images and 11% non-hookworm image were falsely detected.

The interpretation of wireless motility capsule endoscopy is a complex task. Seguí *et al*^[65] established a CNN model for small-intestine motility characterization and achieved a mean classification accuracy of 96% for six intestinal motility events ("turbid", "bubbles", "clear blob", "wrinkles", "wall", and, "undefined"). This outperformed the other classifiers by a large margin (a 14% relative performance increase).

CHALLENGES AND FUTURE DIRECTIONS FOR APPLICATION OF AI

Although many researchers have investigated the utility of AI and have shown promising results, most studies were designed in retrospective manner: as a case-control study from a single center, or by using endoscopic images that were chosen from specific endoscopic modalities unavailable from many institutions. Potential

Table 4 Summary of clinical studies using artificial intelligence in the lower gastrointestinal field

Ref.	Published year	Aim of study	Design of study	Number of subjects	Type of AI	Endoscopic modality	Outcomes
Fernandez-Esparrach <i>et al</i> ^[40]	2016	Detection of colonic polyps	Retrospective	24 videos containing 31 polyps	Window Median Depth of Valleys Accumulation maps	White-light colonoscopy	Sensitivity: 70.4%. Specificity: 72.4%
Misawa <i>et al</i> ^[41]	2018	Detection of colonic polyps	Retrospective	546 short videos (training set: 105 polyp-positive videos and 306 polyp-negative videos, test set: 50 polyp-positive videos and 85 polyp-negative videos) from 73 full length videos	CNN	White-light colonoscopy	Accuracy: 76.5%. Sensitivity: 90.0%. Specificity: 63.3%.
Urban <i>et al</i> ^[42]	2018	Detection of colonic polyps	Retrospective	8641 images with 20 colonoscopy videos	CNN	White-light colonoscopy with NBI	Accuracy: 96.4%. AUROC: 0.991
Klare <i>et al</i> ^[46]	2019	Detection of colonic polyps	Prospective	55 patients	Automated polyp detection software	White-light colonoscopy	Polyp detection rate: 50.9%. Adenoma detection rate: 29.1%
Wang <i>et al</i> ^[47]	2018	Detection of colonic polyps	Retrospective	Training set: 5545 images from 1290 patients. Validation set A: 27113 images from 1138 patients. Validation set B: 612 images. Validation set C: 138 video clips from 110 patients. Validation set D: 54 videos from 54 patients	CNN	White-light colonoscopy	Dataset A: AUROC: 0.98 for at least one polyp detection, per-image sensitivity: 94.4%, per-image specificity: 95.2%. Dataset B: per-image sensitivity: 88.2%. Dataset C: per-image sensitivity: 91.6%, per-polyp sensitivity: 100%. Dataset D: per-image specificity: 95.4%
Tischendorf <i>et al</i> ^[48]	2010	Classification of colorectal polyps on the basis of vascularization features.	Prospective pilot	209 polyps from 128 patients	SVM	Magnifying NBI images	Accurate classification rate: 91.9%
Gross <i>et al</i> ^[49]	2011	Differentiation of small colonic polyps of < 10 mm	Prospective	434 polyps from 214 patients	SVM	Magnifying NBI images	Accuracy: 93.1%. Sensitivity: 95.0%. Specificity: 90.3%.
Takemura <i>et al</i> ^[50]	2010	Classification of pit patterns	Retrospective	Training set: 72 images. Validation set: 134 images	HuPAS software version 1.3	Magnifying endoscopic images with crystal violet staining	Accuracies of the type I, II, III _L , and IV pit patterns of colorectal lesions: 100%, 100%, 96.6%, and 96.7%, respectively
Takemura <i>et al</i> ^[51]	2012	Classification of histology of colorectal tumors	Retrospective	Training set: 1519 images. Validation set: 371 images	HuPAS software version 3.1 using SVM	Magnifying NBI images	Accuracy: 97.8%
Kominami <i>et al</i> ^[52]	2016	Classification of histology of colorectal polyps	Prospective	Training set: 2247 images from 1262 colorectal lesion. Validation: 118 colorectal lesions	SVM with logistic regression	Magnifying NBI images	Accuracy: 93.2%, Sensitivity: 93.0%, Specificity: 93.3%, PPV: 93%, NPV: 93.3%
Byrne <i>et al</i> ^[53]	2017	Differentiation of histology of diminutive colorectal polyps	Retrospective	Training set: 223 videos, Validation set: 40 videos. Test set: 125 videos	CNN	NBI video frames	Accuracy: 94%, Sensitivity: 98%, Specificity: 83%

Chen <i>et al</i> ^[54]	2018	Identification of neoplastic or hyperplastic polyps of < 5 mm	Retrospective	Training set: 2157 images. Test set: 284 images	CNN	Magnifying NBI images	Sensitivity: 96.3%, specificity: 78.1%, PPV: 89.6%, NPV: 91.5%
Komeda <i>et al</i> ^[55]	2017	Discrimination adenomas from non-adenomatous polyps	Retrospective	1200 images from the endoscopic videos (10 times cross validation)	CNN	White-light colonoscopy with NBI and chromoendoscopy	Accuracy in validation: 75.1%
Mori <i>et al</i> ^[56]	2015	Discrimination of neoplastic changes in small polyps	Retrospective	Test set: 176 polyps from 152 patients	Multivariate regression analysis	Endocytoscopy	Accuracy: 89.2%, Sensitivity: 92.0%
Mori <i>et al</i> ^[57]	2016	Development of 2 nd generation model, which was mentioned in reference number 56	Retrospective	Test set: 205 small colorectal polyps (≤ 10 mm) from 123 patients	SVM	Endocytoscopy	Accuracy: 89% for both diminutive (< 5 mm) and small (< 10 mm) polyps
Misawa <i>et al</i> ^[58]	2016	Diagnosis of colorectal lesions using microvascular findings	Retrospective	Training set: 979 images, validation set: 100 images	SVM	Endocytoscopy with NBI	Accuracy: 90%
Mori <i>et al</i> ^[59]	2018	Diagnosis of neoplastic diminutive polyp	Prospective	466 diminutive polyps from 325 patients	SVM	Endocytoscopy with NBI and stained images	Prediction rate: 98.1%
Takeda <i>et al</i> ^[60]	2017	Diagnosis of invasive colorectal cancer	Retrospective	Training set: 5543 images from 238 lesions. Test set: 200 images	SVM	Endocytoscopy with NBI and stained images	Accuracy: 94.1% Sensitivity: 89.4%, Specificity: 98.9%, PPV: 98.8%, NPV: 90.1%
Maeda <i>et al</i> ^[61]	2018	Prediction of persistent histologic inflammation in ulcerative colitis patients	Retrospective	Training set: 12900 images. Test set: 9935 images	SVM	Endocytoscopy with NBI	Accuracy: 91%, Sensitivity: 74%, Specificity: 97%

AI: Artificial intelligence; CNN: Convolutional neural network; NBI: Narrow band image; AUROC: Area under receiver operating characteristic; SVM: Support vector machine; PPV: Positive predictive value; NPV: Negative predictive value.

inherent bias such as selection bias cannot be excluded in this situation. Therefore, it is crucial to meticulously validate the performance of AI before the application of AI in real clinical practice. To properly verify the accuracy of AI, physicians should understand the effects of overfitting and spectrum bias (class imbalance) on the performance of AI, and try to evaluate the performance by avoiding these biases.

Overfitting occurs when a learning model tailors itself too much on the training dataset and predictions are not well generalized to new datasets^[66] (Table 5). Although several methods were used to reduce overfitting in the development of DL models, they did not guarantee the resolution of this problem. In addition, datasets that were collected by case-control design are particularly vulnerable to spectrum bias. Spectrum bias occurs when the dataset used for model development does not adequately represent the range of patients who will be applied in clinical practice (target population)^[67].

Because overfitting and spectrum bias may lead to overestimation of the accuracy and generalization, external validation using unused datasets for model development, collected in a way that minimizes the spectrum bias, is mandatory. For more robust clinical verification, well-designed multicenter prospective studies with adequate inclusion/exclusion criteria that represent the target population are needed. Furthermore, DL technology has its own “black box” nature (lack of interpretability or explainability), which means the decision mechanism of AI is not clearly demonstrated (Figure 2). Because interpretability is important in that it can provide safety measures, help to detect bias, and establish social acceptance, further investigation to solve this issue should be performed. However, there have been some methods to complement “black box” characteristics, such as the attention map and saliency region^[68].

It is obvious that the efficiency and accuracy of ML increases as the amount of data increases; however, it is challenging to develop an efficient ML model owing to the paucity of human labeled data given the issue of privacy with regard to private

Table 5 Summary of clinical studies using artificial intelligence in the capsule endoscopy

Ref.	Published year	Aim of study	Design of study	Number of subjects	Type of AI	Outcomes
Leenhardt <i>et al</i> ^[62]	2019	Detection of gastrointestinal angiectasia	Retrospective	600 control images and 600 typical angiectasia images (divided equally into training and test datasets)	CNN	Sensitivity: 100%, specificity: 96%, PPV: 96%, NPV: 100%.
Zhou <i>et al</i> ^[63]	2017	Classification of celiac disease	Retrospective	Training set: 6 celiac disease patients, 5 controls. Test set: additional 5 celiac disease patients, 5 controls	CNN	Sensitivity: 100%, specificity: 100% (for test dataset)
He <i>et al</i> ^[64]	2018	Detection of intestinal hookworms	Retrospective	440000 images	CNN	Sensitivity: 84.6%, specificity: 88.6%
Seguí <i>et al</i> ^[65]	2016	Characterization of small intestinal motility	Retrospective	120000 images (training set: 100000, test set: 20000)	CNN	Mean classification accuracy: 96%

AI: Artificial intelligence; CNN: Convolutional neural network; PPV: Positive predictive value; NPV: Negative predictive value.

medical records. To overcome this issue, data augmentation strategies (with synthetically modified data) have been proposed^[69]. Spiking neural networks, which more closely mimic the real mechanisms of neurons, can potentially replace current ANN models with more powerful computing ability, although no effective supervised learning method currently exists^[70].

The precision of diagnosis or classification using AI does not always mean efficacy in real clinical practice. The actual benefit of the clinical outcome, the satisfaction of physicians, and the cost effectiveness beyond the academic performance must be proven by sophisticated investigation. Finally, the acquisition of reasonable regulations from responsible authorities and a reimbursement policy are essential for integrating AI technology in the current healthcare environment. Moreover, AI is not perfect. That's why "Augmented Intelligence" emerged emphasizing the fact that AI is designed to improve or enhance human intelligence rather than replace it. Although the aim of applying AI in medical practice is to improve the workflow with enhanced precision and to reduce the number of unintentional errors, established models with inaccuracy or exaggerated performance are likely to cause ethical issues owing to misdiagnosis or misclassification. Moreover, we do not know the impact of AI application on the doctor-patient relationship, which is an essential part of healthcare utilization and the practice of medicine. Therefore, ethical principles relevant to AI model development should be established in the current period when AI research begins to increase.

CONCLUSION

Since AI was introduced in the 1950s, it has been persistently challenged in terms of statistical or image analyses in the field of gastroenterology. Recent evaluation of big data and computer science enabled the dramatic development of AI technology, particularly DL, which showed promising potential. Now, there is no doubt that the implementation of AI in the gastroenterology field will progress in various healthcare services. To utilize AI wisely, physicians should make great effort to understand its feasibility and ameliorate the drawbacks through further investigation.

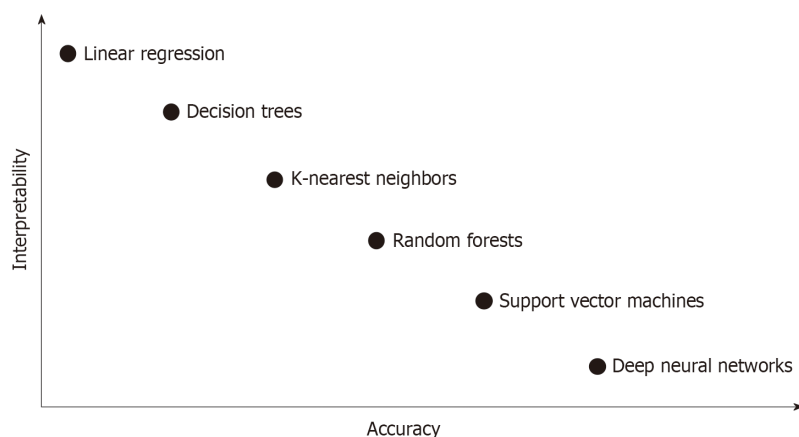


Figure 2 Interpretability-accuracy tradeoff in classification algorithms of machine learning.

REFERENCES

- 1 Topol EJ. High-performance medicine: the convergence of human and artificial intelligence. *Nat Med* 2019; **25**: 44-56 [PMID: 30617339 DOI: 10.1038/s41591-018-0300-7]
- 2 Turing AM. Computing machinery and intelligence. Oxford: Mind 1950; 433-460
- 3 Russell S, Norvig P. Artificial intelligence: a modern approach. 3rd ed. Harlow: Pearson Education 2009; 1-3
- 4 Kevin PM. Machine learning: a probabilistic perspective. 1st ed. Cambridge: The MIT Press 2012; 1-2
- 5 Bishop B. CM: Pattern recognition and machine learning. *J Electron Imaging* 2006; **16**: 140-155
- 6 Lee JG, Jun S, Cho YW, Lee H, Kim GB, Seo JB, Kim N. Deep Learning in Medical Imaging: General Overview. *Korean J Radiol* 2017; **18**: 570-584 [PMID: 28670152 DOI: 10.3348/kjr.2017.18.4.570]
- 7 Boser BE, Guyon IM, Vapnik VN. A training algorithm for optimal margin classifiers. Proceedings of the fifth annual workshop on Computational learning theory; 1992 July 1, Pittsburgh, US. New York: ACM 1992; 144-152
- 8 Hastie T, Tibshirani R, Friedman J. The elements of Statistical Learning. New York: Springer 2001;
- 9 McCulloch WS, Pitts W. A logical calculus of the ideas immanent in nervous activity. *Bull Math Biophys* 1943; **5**: 115-133
- 10 ROSENBLATT F. The perceptron: a probabilistic model for information storage and organization in the brain. *Psychol Rev* 1958; **65**: 386-408 [PMID: 13602029]
- 11 Pace F, Buscema M, Dominici P, Intraligi M, Baldi F, Cestari R, Passaretti S, Bianchi Porro G, Grossi E. Artificial neural networks are able to recognize gastro-oesophageal reflux disease patients solely on the basis of clinical data. *Eur J Gastroenterol Hepatol* 2005; **17**: 605-610 [PMID: 15879721]
- 12 Lahner E, Grossi E, Intraligi M, Buscema M, Corleto VD, Delle Fave G, Annibale B. Possible contribution of artificial neural networks and linear discriminant analysis in recognition of patients with suspected atrophic body gastritis. *World J Gastroenterol* 2005; **11**: 5867-5873 [PMID: 16270400]
- 13 Pofahl WE, Walczak SM, Rhone E, Izenberg SD. Use of an artificial neural network to predict length of stay in acute pancreatitis. *Am Surg* 1998; **64**: 868-872 [PMID: 9731816]
- 14 Das A, Ben-Menachem T, Cooper GS, Chak A, Sivak MV, Gonet JA, Wong RC. Prediction of outcome in acute lower-gastrointestinal haemorrhage based on an artificial neural network: internal and external validation of a predictive model. *Lancet* 2003; **362**: 1261-1266 [PMID: 14575969 DOI: 10.1016/S0140-6736(03)14568-0]
- 15 Sato F, Shimada Y, Selaru FM, Shibata D, Maeda M, Watanabe G, Mori Y, Stass SA, Imamura M, Meltzer SJ. Prediction of survival in patients with esophageal carcinoma using artificial neural networks. *Cancer* 2005; **103**: 1596-1605 [PMID: 15751017 DOI: 10.1002/cncr.20938]
- 16 Rotondano G, Cipolletta L, Grossi E, Koch M, Intraligi M, Buscema M, Marmo R; Italian Registry on Upper Gastrointestinal Bleeding (Progetto Nazionale Emorragie Digestive). Artificial neural networks accurately predict mortality in patients with nonvariceal upper GI bleeding. *Gastrointest Endosc* 2011; **73**: 218-226, 226.e1-226.e2 [PMID: 21295635 DOI: 10.1016/j.gie.2010.10.006]
- 17 Takayama T, Okamoto S, Hisamatsu T, Naganuma M, Matsuoka K, Mizuno S, Bessho R, Hibi T, Kanai T. Computer-Aided Prediction of Long-Term Prognosis of Patients with Ulcerative Colitis after Cytoapheresis Therapy. *PLoS One* 2015; **10**: e0131197 [PMID: 26111148 DOI: 10.1371/journal.pone.0131197]
- 18 Hardalaç F, Başaranoglu M, Yüksel M, Kutbay U, Kaplan M, Özderin Özın Y, Kılıç ZM, Demirbağ AE, Coşkun O, Aksoy A, Gangarapu V, Örmeci N, Kayaçetin E. The rate of mucosal healing by azathioprine therapy and prediction by artificial systems. *Turk J Gastroenterol* 2015; **26**: 315-321 [PMID: 26039001 DOI: 10.5152/tjg.2015.0199]
- 19 Peng JC, Ran ZH, Shen J. Seasonal variation in onset and relapse of IBD and a model to predict the frequency of onset, relapse, and severity of IBD based on artificial neural network. *Int J Colorectal Dis* 2015; **30**: 1267-1273 [PMID: 25976931 DOI: 10.1007/s00384-015-2250-6]
- 20 Ichimasa K, Kudo SE, Mori Y, Misawa M, Matsudaira S, Kouyama Y, Baba T, Hidaka E, Wakamura K, Hayashi T, Kudo T, Ishigaki T, Yagawa Y, Nakamura H, Takeda K, Haji A, Hamatani S, Mori K, Ishida F, Miyachi H. Artificial intelligence may help in predicting the need for additional surgery after endoscopic resection of T1 colorectal cancer. *Endoscopy* 2018; **50**: 230-240 [PMID: 29272905 DOI: 10.1055/s-0043-122385]
- 21 Yang HX, Feng W, Wei JC, Zeng TS, Li ZD, Zhang LJ, Lin P, Luo RZ, He JH, Fu JH. Support vector machine-based nomogram predicts postoperative distant metastasis for patients with oesophageal

- squamous cell carcinoma. *Br J Cancer* 2013; **109**: 1109-1116 [PMID: [23942069](#) DOI: [10.1038/bjc.2013.379](#)]
- 22 **Takiyama H**, Ozawa T, Ishihara S, Fujishiro M, Shichijo S, Nomura S, Miura M, Tada T. Automatic anatomical classification of esophagogastrroduodenoscopy images using deep convolutional neural networks. *Sci Rep* 2018; **8**: 7497 [PMID: [29760397](#) DOI: [10.1038/s41598-018-25842-6](#)]
 - 23 **van der Sommen F**, Zinger S, Curvers WL, Bisschops R, Pech O, Weusten BL, Bergman JJ, de With PH, Schoon EJ. Computer-aided detection of early neoplastic lesions in Barrett's esophagus. *Endoscopy* 2016; **48**: 617-624 [PMID: [27100718](#) DOI: [10.1055/s-0042-105284](#)]
 - 24 **Swager AF**, van der Sommen F, Klomp SR, Zinger S, Meijer SL, Schoon EJ, Bergman JJGHM, de With PH, Curvers WL. Computer-aided detection of early Barrett's neoplasia using volumetric laser endomicroscopy. *Gastrointest Endosc* 2017; **86**: 839-846 [PMID: [28322771](#) DOI: [10.1016/j.gie.2017.03.011](#)]
 - 25 **Kodashima S**, Fujishiro M, Takubo K, Kammori M, Nomura S, Kakushima N, Muraki Y, Goto O, Ono S, Kaminishi M, Omata M. Ex vivo pilot study using computed analysis of endo-cytoscopic images to differentiate normal and malignant squamous cell epithelia in the oesophagus. *Dig Liver Dis* 2007; **39**: 762-766 [PMID: [17611178](#) DOI: [10.1016/j.dld.2007.03.004](#)]
 - 26 **Shin D**, Protano MA, Polydorides AD, Dawsey SM, Pierce MC, Kim MK, Schwarz RA, Quang T, Parikh N, Bhutani MS, Zhang F, Wang G, Xue L, Wang X, Xu H, Anandasabapathy S, Richards-Kortum RR. Quantitative analysis of high-resolution microendoscopic images for diagnosis of esophageal squamous cell carcinoma. *Clin Gastroenterol Hepatol* 2015; **13**: 272-279.e2 [PMID: [25066838](#) DOI: [10.1016/j.cgh.2014.07.030](#)]
 - 27 **Quang T**, Schwarz RA, Dawsey SM, Tan MC, Patel K, Yu X, Wang G, Zhang F, Xu H, Anandasabapathy S, Richards-Kortum R. A tablet-interfaced high-resolution microendoscope with automated image interpretation for real-time evaluation of esophageal squamous cell neoplasia. *Gastrointest Endosc* 2016; **84**: 834-841 [PMID: [27036635](#) DOI: [10.1016/j.gie.2016.03.1472](#)]
 - 28 **Horie Y**, Yoshio T, Aoyama K, Yoshimizu S, Horiuchi Y, Ishiyama A, Hirasawa T, Tsuchida T, Ozawa T, Ishihara S, Kumagai Y, Fujishiro M, Maetani I, Fujisaki J, Tada T. Diagnostic outcomes of esophageal cancer by artificial intelligence using convolutional neural networks. *Gastrointest Endosc* 2019; **89**: 25-32 [PMID: [30120958](#) DOI: [10.1016/j.gie.2018.07.037](#)]
 - 29 **Huang CR**, Sheu BS, Chung PC, Yang HB. Computerized diagnosis of *Helicobacter pylori* infection and associated gastric inflammation from endoscopic images by refined feature selection using a neural network. *Endoscopy* 2004; **36**: 601-608 [PMID: [15243882](#) DOI: [10.1055/s-2004-814519](#)]
 - 30 **Shichijo S**, Nomura S, Aoyama K, Nishikawa Y, Miura M, Shinagawa T, Takiyama H, Tanimoto T, Ishihara S, Matsuo K, Tada T. Application of Convolutional Neural Networks in the Diagnosis of *Helicobacter pylori* Infection Based on Endoscopic Images. *EBioMedicine* 2017; **25**: 106-111 [PMID: [29056541](#) DOI: [10.1016/j.ebiom.2017.10.014](#)]
 - 31 **Itoh T**, Kawahira H, Nakashima H, Yata N. Deep learning analyzes *Helicobacter pylori* infection by upper gastrointestinal endoscopy images. *Endosc Int Open* 2018; **6**: E139-E144 [PMID: [29399610](#) DOI: [10.1055/s-0043-120830](#)]
 - 32 **Nakashima H**, Kawahira H, Kawachi H, Sakaki N. Artificial intelligence diagnosis of *Helicobacter pylori* infection using blue laser imaging-bright and linked color imaging: a single-center prospective study. *Ann Gastroenterol* 2018; **31**: 462-468 [PMID: [29991891](#) DOI: [10.20524/aog.2018.0269](#)]
 - 33 **Kubota K**, Kuroda J, Yoshida M, Ohta K, Kitajima M. Medical image analysis: computer-aided diagnosis of gastric cancer invasion on endoscopic images. *Surg Endosc* 2012; **26**: 1485-1489 [PMID: [22083334](#) DOI: [10.1007/s00464-011-2036-z](#)]
 - 34 **Hirasawa T**, Aoyama K, Tanimoto T, Ishihara S, Shichijo S, Ozawa T, Ohnishi T, Fujishiro M, Matsuo K, Fujisaki J, Tada T. Application of artificial intelligence using a convolutional neural network for detecting gastric cancer in endoscopic images. *Gastric Cancer* 2018; **21**: 653-660 [PMID: [29335825](#) DOI: [10.1007/s10120-018-0793-2](#)]
 - 35 **Zhu Y**, Wang QC, Xu MD, Zhang Z, Cheng J, Zhong YS, Zhang YQ, Chen WF, Yao LQ, Zhou PH, Li QL. Application of convolutional neural network in the diagnosis of the invasion depth of gastric cancer based on conventional endoscopy. *Gastrointest Endosc* 2019; **89**: 806-815.e1 [PMID: [30452913](#) DOI: [10.1016/j.gie.2018.11.011](#)]
 - 36 **Kanesaka T**, Lee TC, Uedo N, Lin KP, Chen HZ, Lee JY, Wang HP, Chang HT. Computer-aided diagnosis for identifying and delineating early gastric cancers in magnifying narrow-band imaging. *Gastrointest Endosc* 2018; **87**: 1339-1344 [PMID: [29225083](#) DOI: [10.1016/j.gie.2017.11.029](#)]
 - 37 **Gatos I**, Tsantis S, Spiliopoulos S, Karnabatidis D, Theotokas I, Zoumpoulis P, Loupas T, Hazle JD, Kagadis GC. A Machine-Learning Algorithm Toward Color Analysis for Chronic Liver Disease Classification, Employing Ultrasound Shear Wave Elastography. *Ultrasound Med Biol* 2017; **43**: 1797-1810 [PMID: [28634041](#) DOI: [10.1016/j.ultrasmedbio.2017.05.002](#)]
 - 38 **Kuppili V**, Biswas M, Sreekumar A, Suri HS, Saba L, Edla DR, Marinhoe RT, Sanches JM, Suri JS. Extreme Learning Machine Framework for Risk Stratification of Fatty Liver Disease Using Ultrasound Tissue Characterization. *J Med Syst* 2017; **41**: 152 [PMID: [28836045](#) DOI: [10.1007/s10916-017-0797-1](#)]
 - 39 **Liu X**, Song JL, Wang SH, Zhao JW, Chen YQ. Learning to Diagnose Cirrhosis with Liver Capsule Guided Ultrasound Image Classification. *Sensors (Basel)* 2017; **17** [PMID: [28098774](#) DOI: [10.3390/s17010149](#)]
 - 40 **Fernández-Esparrach G**, Bernal J, López-Cerón M, Córdova H, Sánchez-Montes C, Rodríguez de Miguel C, Sánchez FJ. Exploring the clinical potential of an automatic colonic polyp detection method based on the creation of energy maps. *Endoscopy* 2016; **48**: 837-842 [PMID: [27285900](#) DOI: [10.1055/s-0042-108434](#)]
 - 41 **Misawa M**, Kudo SE, Mori Y, Cho T, Kataoka S, Yamauchi A, Ogawa Y, Maeda Y, Takeda K, Ichimasa K, Nakamura H, Yagawa Y, Toyoshima N, Ogata N, Kudo T, Hisayuki T, Hayashi T, Wakamura K, Baba T, Ishida F, Itoh H, Roth H, Oda M, Mori K. Artificial Intelligence-Assisted Polyp Detection for Colonoscopy: Initial Experience. *Gastroenterology* 2018; **154**: 2027-2029.e3 [PMID: [29653147](#) DOI: [10.1053/j.gastro.2018.04.003](#)]
 - 42 **Urban G**, Tripathi P, Alkayali T, Mittal M, Jalali F, Karnes W, Baldi P. Deep Learning Localizes and Identifies Polyps in Real Time With 96% Accuracy in Screening Colonoscopy. *Gastroenterology* 2018; **155**: 1069-1078.e8 [PMID: [29928897](#) DOI: [10.1053/j.gastro.2018.06.037](#)]
 - 43 **Wang H**, Liang Z, Li LC, Han H, Song B, Pickhardt PJ, Barish MA, Lascarides CE. An adaptive paradigm for computer-aided detection of colonic polyps. *Phys Med Biol* 2015; **60**: 7207-7228 [PMID: [26348125](#) DOI: [10.1088/0031-9155/60/18/7207](#)]

- 44 **K G**, c R. Automatic Colorectal Polyp Detection in Colonoscopy Video Frames. *Asian Pac J Cancer Prev* 2016; **17**: 4869-4873 [PMID: 28030914 DOI: 10.22034/APJCP.2016.17.11.4869]
- 45 **Billah M**, Waheed S, Rahman MM. An Automatic Gastrointestinal Polyp Detection System in Video Endoscopy Using Fusion of Color Wavelet and Convolutional Neural Network Features. *Int J Biomed Imaging* 2017; **2017**: 9545920 [PMID: 28894460 DOI: 10.1155/2017/9545920]
- 46 **Klare P**, Sander C, Prinzen M, Haller B, Nowack S, Abdelhazef M, Poszler A, Brown H, Wilhelm D, Schmid RM, von Delius S, Wittenberg T. Automated polyp detection in the colorectum: a prospective study (with videos). *Gastrointest Endosc* 2019; **89**: 576-582.e1 [PMID: 30342029 DOI: 10.1016/j.gie.2018.09.042]
- 47 **Wang P**, Xiao X, Brown JR, Berzin TM, Tu M, Xiong F, Hu X, Liu P, Song Y, Zhang D, Yang X. Development and validation of a deep-learning algorithm for the detection of polyps during colonoscopy. *Nat Biomed Eng* 2018; **2**: 741 [DOI: 10.1038/s41551-018-0301-3]
- 48 **Tischendorf JJ**, Gross S, Winograd R, Hecker H, Auer R, Behrens A, Trautwein C, Aach T, Stehle T. Computer-aided classification of colorectal polyps based on vascular patterns: a pilot study. *Endoscopy* 2010; **42**: 203-207 [PMID: 20101564 DOI: 10.1055/s-0029-1243861]
- 49 **Gross S**, Trautwein C, Behrens A, Winograd R, Palm S, Lutz HH, Schirin-Sokhan R, Hecker H, Aach T, Tischendorf JJ. Computer-based classification of small colorectal polyps by using narrow-band imaging with optical magnification. *Gastrointest Endosc* 2011; **74**: 1354-1359 [PMID: 22000791 DOI: 10.1016/j.gie.2011.08.001]
- 50 **Takemura Y**, Yoshida S, Tanaka S, Onji K, Oka S, Tamaki T, Kaneda K, Yoshihara M, Chayama K. Quantitative analysis and development of a computer-aided system for identification of regular pit patterns of colorectal lesions. *Gastrointest Endosc* 2010; **72**: 1047-1051 [PMID: 21034905 DOI: 10.1016/j.gie.2010.07.037]
- 51 **Takemura Y**, Yoshida S, Tanaka S, Kawase R, Onji K, Oka S, Tamaki T, Raytchev B, Kaneda K, Yoshihara M, Chayama K. Computer-aided system for predicting the histology of colorectal tumors by using narrow-band imaging magnifying colonoscopy (with video). *Gastrointest Endosc* 2012; **75**: 179-185 [PMID: 22196816 DOI: 10.1016/j.gie.2011.08.051]
- 52 **Kominami Y**, Yoshida S, Tanaka S, Sanomura Y, Hirakawa T, Raytchev B, Tamaki T, Koide T, Kaneda K, Chayama K. Computer-aided diagnosis of colorectal polyp histology by using a real-time image recognition system and narrow-band imaging magnifying colonoscopy. *Gastrointest Endosc* 2016; **83**: 643-649 [PMID: 26264431 DOI: 10.1016/j.gie.2015.08.004]
- 53 **Byrne MF**, Chapados N, Soudan F, Oertel C, Linares Pérez M, Kelly R, Iqbal N, Chandelier F, Rex DK. Real-time differentiation of adenomatous and hyperplastic diminutive colorectal polyps during analysis of unaltered videos of standard colonoscopy using a deep learning model. *Gut* 2019; **68**: 94-100 [PMID: 29066576 DOI: 10.1136/gutjnl-2017-314547]
- 54 **Chen PJ**, Lin MC, Lai MJ, Lin JC, Lu HH, Tseng VS. Accurate Classification of Diminutive Colorectal Polyps Using Computer-Aided Analysis. *Gastroenterology* 2018; **154**: 568-575 [PMID: 29042219 DOI: 10.1053/j.gastro.2017.10.010]
- 55 **Komeda Y**, Handa H, Watanabe T, Nomura T, Kitahashi M, Sakurai T, Okamoto A, Minami T, Kono M, Arizumi T, Takenaka M, Hagiwara S, Matsui S, Nishida N, Kashida H, Kudo M. Computer-Aided Diagnosis Based on Convolutional Neural Network System for Colorectal Polyp Classification: Preliminary Experience. *Oncology* 2017; **93** Suppl 1: 30-34 [PMID: 29258081 DOI: 10.1159/000481227]
- 56 **Mori Y**, Kudo SE, Wakamura K, Misawa M, Ogawa Y, Kutsukawa M, Kudo T, Hayashi T, Miyachi H, Ishida F, Inoue H. Novel computer-aided diagnostic system for colorectal lesions by using endocytoscopy (with videos). *Gastrointest Endosc* 2015; **81**: 621-629 [PMID: 25440671 DOI: 10.1016/j.gie.2014.09.008]
- 57 **Mori Y**, Kudo SE, Chiu PW, Singh R, Misawa M, Wakamura K, Kudo T, Hayashi T, Katagiri A, Miyachi H, Ishida F, Maeda Y, Inoue H, Nimura Y, Oda M, Mori K. Impact of an automated system for endocytoscopic diagnosis of small colorectal lesions: an international web-based study. *Endoscopy* 2016; **48**: 1110-1118 [PMID: 27494455 DOI: 10.1055/s-0042-113609]
- 58 **Misawa M**, Kudo SE, Mori Y, Nakamura H, Kataoka S, Maeda Y, Kudo T, Hayashi T, Wakamura K, Miyachi H, Katagiri A, Baba T, Ishida F, Inoue H, Nimura Y, Mori K. Characterization of Colorectal Lesions Using a Computer-Aided Diagnostic System for Narrow-Band Imaging Endocytoscopy. *Gastroenterology* 2016; **150**: 1531-1532.e3 [PMID: 27072671 DOI: 10.1053/j.gastro.2016.04.004]
- 59 **Mori Y**, Kudo SE, Misawa M, Saito Y, Ikematsu H, Hotta K, Ohtsuka K, Urushibara F, Kataoka S, Ogawa Y, Maeda Y, Takeda K, Nakamura H, Ichimasa K, Kudo T, Hayashi T, Wakamura K, Ishida F, Inoue H, Itoh H, Oda M, Mori K. Real-Time Use of Artificial Intelligence in Identification of Diminutive Polyps During Colonoscopy: A Prospective Study. *Ann Intern Med* 2018; **169**: 357-366 [PMID: 30105375 DOI: 10.7326/M18-0249]
- 60 **Takeda K**, Kudo SE, Mori Y, Misawa M, Kudo T, Wakamura K, Katagiri A, Baba T, Hidaka E, Ishida F, Inoue H, Oda M, Mori K. Accuracy of diagnosing invasive colorectal cancer using computer-aided endocytoscopy. *Endoscopy* 2017; **49**: 798-802 [PMID: 28472832 DOI: 10.1055/s-0043-105486]
- 61 **Maeda Y**, Kudo SE, Mori Y, Misawa M, Ogata N, Sasanuma S, Wakamura K, Oda M, Mori K, Ohtsuka K. Fully automated diagnostic system with artificial intelligence using endocytoscopy to identify the presence of histologic inflammation associated with ulcerative colitis (with video). *Gastrointest Endosc* 2019; **89**: 408-415 [PMID: 30268542 DOI: 10.1016/j.gie.2018.09.024]
- 62 **Leenhardt R**, Vasseur P, Li C, Saurin JC, Rahmi G, Cholet F, Becq A, Marteau P, Histace A, Dray X; CAD-CAP Database Working Group. A neural network algorithm for detection of GI angiectasia during small-bowel capsule endoscopy. *Gastrointest Endosc* 2019; **89**: 189-194 [PMID: 30017868 DOI: 10.1016/j.gie.2018.06.036]
- 63 **Zhou T**, Han G, Li BN, Lin Z, Ciaccio EJ, Green PH, Qin J. Quantitative analysis of patients with celiac disease by video capsule endoscopy: A deep learning method. *Comput Biol Med* 2017; **85**: 1-6 [PMID: 28412572 DOI: 10.1016/j.compbiomed.2017.03.031]
- 64 **He JY**, Wu X, Jiang YG, Peng Q, Jain R. Hookworm Detection in Wireless Capsule Endoscopy Images With Deep Learning. *IEEE Trans Image Process* 2018; **27**: 2379-2392 [PMID: 29470172 DOI: 10.1109/TIP.2018.2801119]
- 65 **Seguí S**, Drozdal M, Pascual G, Radeva P, Malagelada C, Azpiroz F, Vitrià J. Generic feature learning for wireless capsule endoscopy analysis. *Comput Biol Med* 2016; **79**: 163-172 [PMID: 27810622 DOI: 10.1016/j.compbiomed.2016.10.011]
- 66 **England JR**, Cheng PM. Artificial Intelligence for Medical Image Analysis: A Guide for Authors and Reviewers. *AJR Am J Roentgenol* 2019; **212**: 513-519 [PMID: 30557049 DOI: 10.2214/AJR.18.20490]
- 67 **Park SH**, Han K. Methodologic Guide for Evaluating Clinical Performance and Effect of Artificial

- Intelligence Technology for Medical Diagnosis and Prediction. *Radiology* 2018; **286**: 800-809 [PMID: 29309734 DOI: 10.1148/radiol.2017171920]
- 68 **Park SH.** Artificial intelligence in medicine: beginner's guide. *J Korean Soc Radiol* 2018; **78**: 301-308 [DOI: 10.3348/jksr.2018.78.5.301]
- 69 **Bae HJ,** Kim CW, Kim N, Park B, Kim N, Seo JB, Lee SM. A Perlin Noise-Based Augmentation Strategy for Deep Learning with Small Data Samples of HRCT Images. *Sci Rep* 2018; **8**: 17687 [PMID: 30523268 DOI: 10.1038/s41598-018-36047-2]
- 70 **Tavanaei A,** Ghodrati M, Kheradpisheh SR, Masquelier T, Maida A. Deep learning in spiking neural networks. *Neural Netw* 2019; **111**: 47-63 [PMID: 30682710 DOI: 10.1016/j.neunet.2018.12.002]



Basic Study

Clinical significance of programmed death 1/programmed death ligand 1 pathway in gastric neuroendocrine carcinomas

Min-Wei Yang, Xue-Liang Fu, Yong-Sheng Jiang, Xiao-Jing Chen, Ling-Ye Tao, Jian-Yu Yang, Yan-Miao Huo, Wei Liu, Jun-Feng Zhang, Pei-Feng Liu, Qiang Liu, Rong Hua, Zhi-Gang Zhang, Yong-Wei Sun, De-Jun Liu

ORCID number: Min-Wei Yang (0000-0002-9902-2183); Xue-Liang Fu (0000-0002-2454-207X); Yong-Sheng Jiang (0000-0002-6073-284X); Xiao-Jing Chen (0000-0002-0241-1968); Ling-Ye Tao (0000-0001-8930-6302); Jian-Yu Yang (0000-0002-4868-1437); Yan-Miao Huo (0000-0003-4730-7184); Wei Liu (0000-0001-7064-3798); Jun-Feng Zhang (0000-0002-8630-3090); Pei-Feng Liu (0000-0003-1391-0727); Qiang Liu (0000-0002-8095-2049); Rong Hua (0000-0003-2477-3764); Zhi-Gang Zhang (0000-0001-8965-223X); Yong-Wei Sun (0000-0002-5937-634X); De-Jun Liu (0000-0001-5336-0809).

Author contributions: Liu DJ and Sun YW conceived and designed the experiments; Yang MW, Fu XL, Jiang YS, and Chen XJ performed the experiments and wrote the manuscript; Fu XL and Yang MW analyzed the data; Tao LY, Yang JY, Huo YM, Liu W, Zhang JF, Liu PF, and Liu Q contributed clinical samples and data; Liu DJ, Sun YW, Zhang ZG, and Hua R revised and edited the manuscript; all authors reviewed and approved the final manuscript.

Supported by Municipal Commission of Health and Family Planning of Shanghai, China (No. 20174Y0243 to Liu DJ, No. 20154Y0163 to Chen XJ), Cultivating Funds of Renji Hospital, School of Medicine, Shanghai Jiao Tong University, China (No. PYXJS 16-002 to Liu W).

Institutional review board statement: The research was

Min-Wei Yang, Xue-Liang Fu, Yong-Sheng Jiang, Ling-Ye Tao, Jian-Yu Yang, Yan-Miao Huo, Wei Liu, Jun-Feng Zhang, Rong Hua, Yong-Wei Sun, De-Jun Liu, Department of Biliary-Pancreatic Surgery, Ren Ji Hospital, School of Medicine, Shanghai Jiao Tong University, Shanghai 200127, China

Xiao-Jing Chen, Pei-Feng Liu, Central Laboratory, Ren Ji Hospital, School of Medicine, Shanghai Jiao Tong University, Shanghai 200127, China

Qiang Liu, Department of Pathology, Ren Ji Hospital, School of Medicine, Shanghai Jiao Tong University, Shanghai 200127, China

Zhi-Gang Zhang, State Key Laboratory of Oncogenes and Related Genes, Shanghai Cancer Institute, Shanghai Jiao Tong University, Shanghai 200240, China

Corresponding author: De-Jun Liu, MAMS, Doctor, Department of Biliary-Pancreatic Surgery, Ren Ji Hospital, School of Medicine, Shanghai Jiao Tong University, No 160, Pujian Road, Shanghai 200127, China. liudj1126@yeah.net

Telephone: +86-21-68383773

Fax: +86-21-68383699

Abstract

BACKGROUND

Recently, more and more studies have demonstrated the pivotal role of programmed death 1/programmed death ligand 1 (PD-1/PD-L1) pathway in the immune evasion of tumors from the host immune system. However, the role of PD-1/PD-L1 pathway in gastric neuroendocrine carcinomas (G-NECs) remains unknown.

AIM

To investigate the expression of PD-1/PD-L1 and role of PD-1/PD-L1 pathway in G-NECs, which occur rarely but are highly malignant and clinically defiant.

METHODS

We investigated the expression of PD-L1 on tumor cells and PD-1⁺, CD8⁺, and FOXP3⁺ T cell infiltration by immunohistochemistry in 43 resected G-NEC tissue specimens. The copy number alterations of PD-L1 were assessed by qRT-PCR.

RESULTS

Most of the G-NECs tumor cells exhibited a near-uniform expression pattern of PD-L1, while some showed a tumor-stromal interface enhanced pattern. Of the 43

approved by the Research Ethics Committee of Ren Ji Hospital.

Conflict-of-interest statement: No potential conflicts of interest are disclosed.

Open-Access: This article is an open-access article which was selected by an in-house editor and fully peer-reviewed by external reviewers. It is distributed in accordance with the Creative Commons Attribution Non Commercial (CC BY-NC 4.0) license, which permits others to distribute, remix, adapt, build upon this work non-commercially, and license their derivative works on different terms, provided the original work is properly cited and the use is non-commercial. See: <http://creativecommons.org/licenses/by-nc/4.0/>

Manuscript source: Unsolicited manuscript

Received: January 30, 2019

Peer-review started: January 31, 2019

First decision: February 26, 2019

Revised: March 5, 2019

Accepted: March 16, 2019

Article in press: March 16, 2019

Published online: April 14, 2019

P-Reviewer: Bramhall S, Cerwenka H, Okubo Y

S-Editor: Yan JP

L-Editor: Wang TQ

E-Editor: Song H



G-NECs, 21 (48.8%) were classified as a high PD-L1 expression group, and the high expression of PD-L1 was associated with poor overall survival (OS). The high expression of PD-L1 was correlated with abundant PD-1⁺ tumor infiltrating lymphocytes (TILs) instead of CD8⁺ TILs and FOXP3⁺ regulatory T cells (Tregs). Our analysis also suggested that the infiltration of CD8⁺ TILs tended to be a favorable factor for OS, although the difference did not reach the statistical significance ($P = 0.065$). Meanwhile, PD-L1 was significantly overexpressed in cases with copy number gain as compared with those without.

CONCLUSION

Our data demonstrated for the first time that high expression of PD-L1 in G-NECs is associated with a poor prognosis, while the high expression may be due to the copy number variation of PD-L1 gene or stimulation of TILs. These results provide a basis for the immunotherapy targeting PD-1/PD-L1 pathway in G-NECs.

Key words: Programmed death 1; Programmed death ligand 1; Gastric neuroendocrine carcinomas; Prognosis; Tumor infiltrating lymphocytes

©The Author(s) 2019. Published by Baishideng Publishing Group Inc. All rights reserved.

Core tip: This study for the first time demonstrated that programmed death ligand 1 (PD-L1) can be expressed by gastric neuroendocrine carcinoma (G-NEC) cancer cells and the high PD-L1 expression was associated with a poor prognosis. And the high expression of PD-L1 may be due to the copy number variation of PD-L1 gene or stimulation of tumor infiltrating lymphocytes. These findings provide important implications for the potential use of antibody therapies targeting the PD-1/PD-L1 signaling pathway in G-NECs.

Citation: Yang MW, Fu XL, Jiang YS, Chen XJ, Tao LY, Yang JY, Huo YM, Liu W, Zhang JF, Liu PF, Liu Q, Hua R, Zhang ZG, Sun YW, Liu DJ. Clinical significance of programmed death 1/programmed death ligand 1 pathway in gastric neuroendocrine carcinomas. *World J Gastroenterol* 2019; 25(14): 1684-1696

URL: <https://www.wjnet.com/1007-9327/full/v25/i14/1684.htm>

DOI: <https://dx.doi.org/10.3748/wjg.v25.i14.1684>

INTRODUCTION

Neuroendocrine neoplasms (NENs), which used to be called neuroendocrine tumors, are benign or high-grade malignant. Meanwhile, they are pathologically and clinically heterogeneous rare tumors. In the past several years, the incidence of NENs has gradually increased over time^[1,2], from 1.09/100000 in 1973 to 5.25/100000 in 2004 in the United States^[3]. However, there was no improvement in outcomes because of the limited awareness of this disease^[4,5]. As the most malignant subgroup, neuroendocrine carcinomas (NECs) are characterized by high-grade cytological atypia, apparent pleomorphism, extensive necrosis, and prominent mitotic activity^[6]. As one of the most common type of NECs, gastric NECs (G-NECs) are poorly differentiated and high-grade malignant and might be either small-cell carcinomas or large-cell NECs in histology. Since the limited knowledge of the epidemiological and clinical characters for G-NECs, this disease deserves more attention.

Programmed death 1 (PD-1), first discovered in 1992 when searching genes responsible for programmed cell death by Ishida *et al*^[7], is an immunoinhibitory receptor expressed by activated T cells, B cells, myeloid cells, and other antigen-presenting cells. Programmed death ligand 1 (PD-L1), a member of the B7 gene family, originally called B7H1 by Dong *et al*^[8], was reported in 2000 by Freeman *et al*^[9]. It is an immunomodulatory glycoprotein, which cannot be detected in normal liver parenchyma, breast, colon, kidney, uterus, muscle, pancreas, or gastric tissue^[10,11], but could be selectively expressed in various malignancies, such as esophageal cancer^[12], gastric cancer^[13], pancreatic cancer^[13], colorectal cancer^[14], breast cancer^[15], thymoma^[16], and thymic cancer^[17].

The host immune functions play an important role in inhibiting the development of malignant tumors. And the induction of anti-tumor immune responses needs the host

immune system to identify the tumor antigen efficiently and to activate various T cells. Binding of PD-1 and PD-L1 inhibits phosphatidylinositol 3-kinase/Akt, suppresses T-cell IL2 production, and then reduces T-cell proliferation and survival^[18]. Therefore, some malignant tumors can escape from immune-surveillance mechanisms by the expression of PD-L1^[18]. Then, the blockade of the PD-1/PD-L1 pathway has become an attractive target in cancer therapy. The success of immunotherapy in various malignancies such as advanced melanoma, non-small cell lung cancer, and renal cell carcinoma have suggested that immunotherapy can be a promising alternative by blocking PD-1/PD-L1 signaling^[19,20]. Until now, no study has evaluated the role of PD-1/PD-L1 in G-NECs.

CD8⁺ tumor infiltrating lymphocytes (TILs) are the key effector in antitumor immune response, and its presence has been reported to be a favorable prognostic factor in some malignancies, such as colorectal cancer^[21], esophageal cancer^[22,23], and breast cancer^[24]. Meanwhile, it has been reported that the upregulation of PD-L1 on tumour cells may be driven by the stimulation of CD8⁺ T cells in melanoma^[25,26]. FOXP3, as a forkhead-family transcription factor, controls regulatory T cell (Treg) development and function^[27]. Tregs are a subset of T lymphocytes possessing the immunoregulatory capacity to suppress the proliferation and cytokine secretion of effector T lymphocytes. And previous studies have reported that the infiltration of FOXP3⁺ Tregs is correlated with the upregulation of PD-L1 in gastric cancer^[28], breast cancer^[29], and colorectal cancer^[14].

In this study, we first detected PD-L1 expression in 43 G-NECs and analyzed the relationship between PD-L1 expression and patients' prognosis. Then, we investigated PD-1⁺ T cells, CD8⁺ T cells, and FOXP3⁺ Treg cells in NECs and their associations with clinicopathological parameters and PD-L1 expression. PD-L1 gene copy number alterations and its relationship to PD-L1 expression were also examined.

MATERIALS AND METHODS

Patients

This study examined 43 formalin-fixed, paraffin-embedded (FFPE) tissue samples from patients with G-NECs treated at Ren Ji Hospital, School of Medicine, Shanghai Jiao Tong University, from 2007 to 2014. We diagnosed, graded, and staged G-NECs by the 2010 WHO classification^[30]. Cases with mixed tumors were excluded. TNM staging was done according to the 7th Edition of the AJCC Cancer TNM Classification^[31]. None of these patients had received tumor-related treatment before. For all cases enrolled in this study, information on age, gender, tumor size, tumor location, T classification, lymph node metastasis, liver metastasis, pathological stage, pathology, treatment, and outcome was reviewed.

The overall survival (OS) time was calculated from the date of surgery to death, or August 30, 2016, the ultimate follow-up deadline. Research Ethics Committee of Ren Ji Hospital approved this study and all participants signed informed consent forms.

Immunohistochemistry

Deparaffinization and rehydration of G-NEC tissues were first performed with xylene and graded alcohol, respectively. Activity of endogenous peroxidase was quenched with 3% hydrogen peroxide at room temperature for 15 min. Antigen retrieval was achieved at high temperature and high pressure. Blocking was done with 10% bovine serum albumin for 30 min, then slides were incubated with antibodies against CD8 (1:200, 17335-1-AP, ProteinTech, United States), FOXP3 (1:200, 22228-1-AP, ProteinTech), PD-1 (1:25, ab140950, Abcam, United Kingdom), and PD-L1 (1:500, ab205921, Abcam) at 4 °C overnight. The next day, the slides were incubated with a corresponding peroxidase-labeled secondary antibody for 30 min at room temperature. Finally, positive staining was visualized with diaminobenzidine tetrahydrochloride (Maixin Biotech, China) and counterstained with hematoxylin.

The final score of PD-L1 expression was assessed according to the percent of positive cell score × staining intensity score as follows: 0, 0-5%; 1, 6%-35%; 2, 36%-70%; 3, 71%-100%; 0, no staining; 1, weak staining; 2, moderate staining; 3, strong staining. The tissues with a final score < 4 were defined as PD-L1 low expression and those with a final score ≥ 4 were classified as PD-L1 high expression. The densities of PD-1⁺, CD8⁺, and FOXP3⁺ cells were measured in four high power fields from each tumor by an experienced pathologist and the average density was calculated. Low infiltration of PD-1⁺, CD8⁺, and FOXP3⁺ cells was defined as less than the median value.

Copy number assay of PD-L1

Tissue DNA was extracted from FFPE tissue using QIAamp DNA FFPE Tissue Kit (QIAGEN, 56404, Germany). Copy number assay of PD-L1 was performed by qRT-PCR, CD274 TaqMan Copy Number Assays (Hs03704252_cn, Applied Biosystems, United States) was used to evaluate PD-L1 copy number while TaqMan Copy Number Reference Assay RNase P (Applied Biosystems 4403328, United States) was used to normalize the results. TaqMan Genotyping Master Mix (Applied Biosystems 4381656, United States) was used to perform the qRT-PCR on a 7500 real-time PCR system (Applied Biosystems, United States). Results were analyzed with CopyCaller Software (Applied Biosystems, United States).

Statistical analysis

Data are presented as the mean \pm SD. Statistical analyses and graphical representations were performed using SPSS 22.0 software (IBM Corp., Armonk, NY, United States) and GraphPad Prism 6 (San Diego, CA, United States) software, respectively. χ^2 test and Fisher's exact test were used to evaluate the correlation of PD-L1, PD-1, FOXP3, and CD8 with clinic-pathologic parameters in patients with G-NECs. Survival curves were evaluated using the Kaplan-Meier method and differences were analyzed by the log-rank test. Identification of factors that had a significant influence on survival was performed by univariate and multivariate Cox regression analyses. Comparison between two groups was performed by the student's *t*-test or Mann-Whitney *U* test. *P*-values (two-sided) < 0.05 were considered statistically significant.

RESULTS

Clinicopathologic features of G-NECs

A total of 43 patients diagnosed with G-NECs were enrolled in this study and the clinicopathologic features are described in detail in [Table 1](#). The cases included 35 males (81.4%) and 8 females (18.6%) with a median age of 62 years (range, 33-82 years). Nearly half of the tumors were located in cardia, while the others were distributed evenly in the corpus and the antrum of the stomach, with two cases located in the residual stomach anastomosis. The majority of patients were diagnosed with stage III disease (81.4%), two cases with stage II (4.65%), and six cases with stage IV (13.95%). For the patients with liver metastases, one of six received resection of both primary and metastatic tumors, while the others received palliative resection of primary tumor. None of the patients received neoadjuvant therapy prior to the surgical resection. The median OS was 31 mo (range, 1-90 mo).

Immunohistochemical characteristics of PD-L1, PD-1, CD8, and FOXP3 expression

PD-L1 was mainly expressed on both the membrane and cytoplasm of tumor cells ([Figure 1C](#) and [F](#)). Most of the G-NEC tissues demonstrated a near-uniform expression pattern of PD-L1 ([Figure 1E](#) and [F](#)), while five specimens showed a tumor-stromal interface enhanced pattern ([Figure 1B](#)). The expression score of PD-L1 was evaluated based on the product of ratio of positive cells (range, 0-3) and staining intensity (range, 0-3), as shown in [Figure 1](#). We predefined the expression score less than 4 as low expression group while the others were high expression group, and 21 (48.8%) of 43 cases were classified as high PD-L1 expression.

The expression of PD-1 was almost on the surface of immune cells in the stroma among tumor nests ([Figure 2A](#)), and the expression of CD8 and FOXP3 was mainly on both membrane and cytoplasm of immune cells in the stroma among tumor nests ([Figure 2B](#) and [C](#)). We defined the expression of PD-1, CD8, and FOXP3 by the number of positive immune cells. The median value of PD-1+ cells in a high power field was 12, and the median values of CD8+ and FOXP3+ cells were 22 and 102.

Association of immune marker staining and clinical parameters

[Table 2](#) shows the correlation between immune markers and clinicopathologic characteristics. We found that the FOXP3+ Treg cell infiltration was significantly associated with age ($P = 0.019$), gender ($P = 0.015$), and tumor location ($P = 0.018$). It demonstrated that female patients, patients with elder age, and patients with G-NECs at the corpus were more likely to have a high infiltration of Treg cells. Importantly, we also found that patients with high infiltration of PD-1 positive immune cells tended to have higher expression of PD-L1 ($P = 0.009$). The infiltration of CD8+ cells was not associated with any clinical parameters or other immune markers. And all the five specimens with a tumor-stromal interface enhanced pattern of PD-L1 had high CD8+ T cell infiltration.

Survival analysis of patients with G-NECs

Table 1 Clinical characteristics of 43 patients with gastric neuroendocrine carcinomas

Clinicopathological feature	n (%)
Age (yr)	
< 60/≥ 60	15 (34.88)/28 (65.12)
mean ± SD	62.26 ± 10.46
Gender	
Male/female	35 (81.40)/8 (18.60)
Tumor location	
Cardia	21 (48.84)
Corpus	10 (23.26)
Antrum	10 (23.26)
Residual stomach anastomosis	2 (4.65)
Tumor size (max diameter, cm)	
≤ 5/> 5	20 (46.51)/23 (53.49)
mean ± SD	5.47 ± 3.18
T classification	
T1/T2/T3/T4	0 (0)/4 (9.30)/0 (0)/39 (90.70)
Lymph node metastasis	
N0/N1	12 (27.91)/31 (72.09)
Liver metastasis	
Absent/present	37 (86.05)/6 (13.95)
Pathological stage	
I/II/III/IV	0 (0)/2 (4.65)/35 (81.40)/6 (13.95)
Pathology	
Small cell carcinomas	39 (90.70)
Large cell carcinomas	4 (9.30)
Operation	
Curative resection	38 (88.37)
Palliative resection	5 (11.63)
Neoadjuvant therapy	
No/present	100 (100)/0 (0)
Follow-up	
Median OS (mo)	31.0

Patients were staged in accordance with the 7th Edition of the AJCC Cancer TNM Classification. OS: Overall survival.

For Kaplan-Meier analysis, the OS of patients with high expression of PD-L1 was significantly shorter compared with patients with low PD-L1 expression ($P = 0.016$). We also found that patients with high CD8⁺ T cell infiltration may have a better clinical prognosis, however, due to the limited patient cohort, the P -value did not reach the statistical significance ($P = 0.065$). Univariate and multivariate analyses were performed to assess the impact of potential prognostic factors on OS. As shown in **Table 3**, corpus tumor [hazard ratio (HR) = 3.034, $P = 0.032$], liver metastasis (HR = 3.515, $P = 0.016$), and PD-L1 expression (HR = 2.846, $P = 0.021$) were significantly associated with OS in univariate analysis, while multivariate analysis demonstrated that only liver metastasis (HR = 4.045, $P = 0.031$) and PD-L1 expression (HR = 3.646, $P = 0.009$) were independent prognostic factors. Based on the theory that PD-L1 played a role in immune evasion by suppressing the function of PD-1 positive immune cells, we divided the patients into two groups depending on the infiltration of PD-1 positive cells and performed the Kaplan-Meier analysis to explore the influence of PD-L1 expression on patients' survival. The results suggested that in the low PD-1⁺ cell infiltration group, patients' survival was not associated with PD-L1 expression statistically (**Figure 3C**, $P = 0.242$); while in the high PD-1⁺ cells infiltration group, patients with high expression of PD-L1 had a significantly shorter survival (**Figure 3D**, $P = 0.013$).

Expression of PD-L1 is correlated with PD-L1 copy number in G-NECs

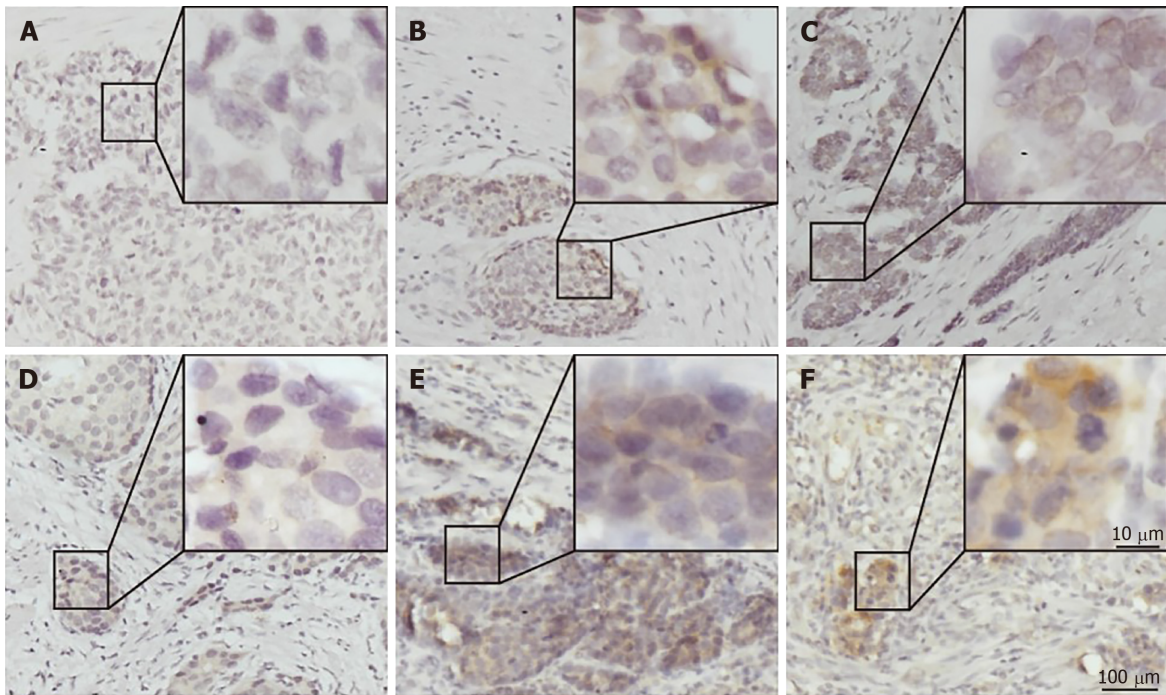


Figure 1 Immunohistochemical staining for programmed death ligand 1 in human gastric neuroendocrine carcinomas. A: Representative case of negative programmed death ligand 1 (PD-L1) expression; B: Tumor-stromal interface enhanced expression of PD-L1; C: Membrane expression of PD-L1; D: Weak staining; E: Moderate staining; F: Strong staining. PD-L1: Programmed death ligand 1.

The G-NEC tissues demonstrated broad PD-L1 expression. Given the near-uniform expression pattern, we considered that genetic alteration may contribute to the PD-L1 expression. To address this issue, we analyzed the copy number variation in the tissue of G-NEC patients. In a cohort of 19 G-NEC patients, we found that 6/19 demonstrated a copy number gain of PD-L1 compared to normal human tissue. Furthermore, we found that the copy number of PD-L1 was positively correlated with the expression of PD-L1 at the protein level (Figure 4). However, we found no correlation between copy number gain and OS of patients (data not shown).

DISCUSSION

In this study, our data showed that more than half of G-NECs were diagnosed at an advanced stage (regional lymph node metastasis 72.09%, and liver metastasis 13.95%). And the median OS was only 31 mo. Meanwhile, as a rare group of poorly differentiated tumors with high-grade malignancy, novel therapeutic approaches are lack because of its rarity, complexity, and heterogeneity. Now, cancer immunotherapy is considered to be a major treatment backbone in the following decade^[32]. Overexpression of PD-L1 and PD-1 in tumor and tumor stromal cells has been reported in various types of cancers, and antibodies targeting either PD-1 or PD-L1 have produced significant anti-tumor activity in several malignancies, such as non-small-cell lung cancer, melanoma, renal-cell cancer, bladder cancer, and head and neck cancer^[20,33,34]. Therefore, there is an urgent need to define the significance of PD-1/PD-L1 pathway in G-NECs, with the potential to provide a new promising therapeutic approach.

In a recent study, Kim *et al*^[35] evaluated the expression of PD-L1 in 32 metastatic GEP-NENs including one gastric NEN. Meanwhile, Cavalcanti *et al*^[36] detected the expression of PD-L1 in 57 GEP-NENs including ten gastric NENs. They found that the expression of PD-L1 was associated with higher WHO tumor grade (grade 3) and it can be used as a predictive and prognostic marker for survival. So far, these are the only reports about PD-1/PD-L1 in GEP-NENs, and there is no research about PD-1/PD-L1 in G-NECs.

In our study, we first investigated the expression of PD-L1 in 43 G-NECs and the relationship between PD-L1 expression and clinical data. We found that 21 (48.8%) of 43 patients can be classified as high PD-L1 expression, and these people had a significant worse prognosis. This result is consistent with many previous studies focusing on gastric cancer^[11], esophageal cancer^[12], pancreatic cancer^[13], and breast

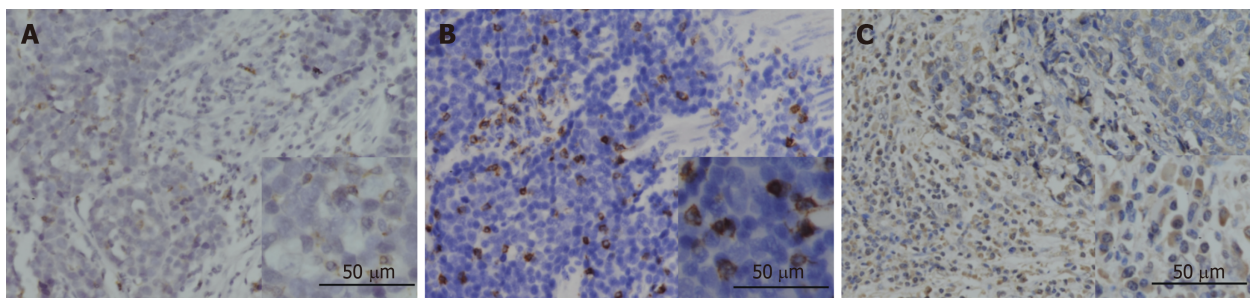


Figure 2 Immunohistochemical staining for programmed death 1, CD8, and FOXP3 in human gastric neuroendocrine carcinomas. A: The programmed death 1 positive infiltrating lymphocytes; B: CD8 positive lymphocytes; C: FOXP3 positive Treg cells.

cancer^[29]. And we also found that the expression of PD-L1 was an independent prognostic factor in G-NECs independent of tumor size and N classification.

PD-1, the ligand of PD-L1, expressed by activated T cells, B cells, myeloid cells, and other antigen-presenting cells, was also investigated in this research. According to previous studies, PD-1 expression in TILs is associated with PD-L1 expression in tumor cells^[17,37], and increased number of PD-1⁺ TILs was also reported to be a significant predictor of poor survival^[17,38,39]. In this study, we confirmed the positive association between PD-1⁺ TIL number and tumor cell PD-L1 expression. Then, the subgroup analysis indicated that PD-L1 had a role in predicting the prognosis only in PD-1⁺ group. These results supported that PD-L1 expressed by tumor cells interacts with PD-1⁺ TILs to suppress antitumor activity. However, in this study, we found no significant correlation between PD-1⁺ TILs and survival.

In our study, PD-L1 copy number analysis was performed to investigate the mechanisms underlying PD-L1 overexpression in G-NECs. We found that a large number of patients demonstrated a copy number alteration and PD-L1 expression was significantly higher in cases with PD-L1 copy number gain, implying that PD-L1 gene alteration is a mechanism of PD-L1 overexpression, similar to a study in thymic cancer^[17]. Meanwhile, we noticed that survival analyses based on PD-L1 expression were inconsistent. Some recent research indicated that PD-L1 expression was associated with favorable OS in several malignancies, such as colorectal cancer, thymic cancer, breast cancer, and non-small cell lung cancer^[14,17,40,41]. And in these studies, the authors detected a significant positive correlation between PD-L1 expression and increased TILs, especially CD8⁺ TILs, the key effector in antitumor immune response. Moreover, in melanoma, it was revealed that the up-regulation of immunosuppressive molecules PD-L1 and FOXP3⁺ Tregs is driven by CD8⁺ T cells^[25], which means that the upregulated expression of PD-L1, PD-1, and FOXP3 might be a negative feedback mechanism following CD8⁺ T cell infiltration, to against activation of host antitumor immunity. Although the discrepancy between PD-L1 expression and prognosis can be attributed to a difference in experiment method and tumor heterogeneity, we determined CD8⁺ TILs and FOXP3⁺ Tregs in G-NECs.

As a glycoprotein, CD8 plays an important role in cell-mediated immunity by binding to the major histocompatibility complex class I molecule together with the T-cell receptor to stimulate the cytotoxic effect of TILs on cancer cells^[42,43]. And it has been reported as a favorable prognostic factor in many malignancies^[21-24]. In accordance with the previous research, we found that patients with high CD8⁺ T cell infiltration may have a better clinical prognosis, although it did not reach the statistical significance ($P = 0.065$). We found no association between PD-L1 expression and CD8⁺ TILs, however, we noticed that five specimens with high CD8⁺ T cell infiltration exhibited a tumor-stromal interface enhanced expression pattern of PD-L1. And this might support the correlation between tumor cell PD-L1 expression and CD8⁺ T cell infiltration in the stroma. And there was also no correlation between FOXP3⁺ Tregs, CD8⁺ TILs infiltration, and PD-L1 expression.

Finally, as a retrospective study, there are selection bias and some other limitations in our results. The small sample size of this research might result in some bias in the multivariable prognosis analysis, so larger sample studies are needed. In this research, we used IHC to investigate the expression of PD-L1, and our data might be limited by the lack of standardization of IHC, for example specificity and reproducibility of antibodies, definition of optimal positivity cut-off, and interpretative subjectivity.

In conclusion, this study for the first time demonstrated that the high PD-L1 expression by tumor cells was associated with a poor prognosis in G-NECs, especially in the PD-1⁺ subgroup. Although we did not find a significant correlation between CD8⁺ TILs and PD-L1 expression, we partly demonstrated the role of CD8⁺ TILs as a

Table 2 Relationship between clinical characteristics and immune markers

	Low CD8 <i>n</i> (%)	High CD8 <i>n</i> (%)	<i>P</i> -value	Low FOXP3 <i>n</i> (%)	High FOXP3 <i>n</i> (%)	<i>P</i> -value	Low PD-1 <i>n</i> (%)	High PD-1 <i>n</i> (%)	<i>P</i> -value	Low PD- L1 <i>n</i> (%)	High PD-L1 <i>n</i> (%)	<i>P</i> -value
Age (yr)												
< 60	7	8	0.835	11	4	0.019	9	6	0.284	7	8	0.666
≥ 60	14	14		10	18		12	16		15	13	
Gender												
Male	17	18	0.942	14	21	0.015	16	19	0.391	19	16	0.391
Female	4	4		7	1		5	3		3	5	
Tumor location												
Cardia	9	12	0.492	11	10	0.018	10	11	0.999	11	10	0.489
Corpus	7	3		1	9		5	5		5	5	
Antrum	4	6		7	3		5	5		4	6	
Residual stomach anastom- osis	1	1		2	0		1	1		2	0	
Tumor size												
≤ 5 cm	12	8	0.172	11	9	0.451	11	9	0.451	10	10	0.887
> 5 cm	9	14		10	13		10	13		12	11	
T classification												
T1/2	3	1	0.272	2	2	0.961	2	2	0.961	1	3	0.272
T3/4	18	21		19	20		19	20		21	18	
Lymph node metastasis												
≤ 7	5	7	0.558	3	9	0.052	5	7	0.558	6	6	0.924
> 7	16	15		18	13		16	15		16	15	
Liver metastasis												
Absent	17	20	0.346	18	19	0.951	16	21	0.068	19	18	0.951
Present	4	2		3	3		5	1		3	3	
CD8												
High												
Low												
FOXP3												
Low	9	12	0.443									
High	12	10										
PD-1												
Low	13	8	0.094	12	9	0.287						
High	8	14		9	13							
PD-L1												
Low	9	13	0.287	12	10	0.443	15	7	0.009			
High	12	9		9	12		6	15				

PD-L1: Programmed death ligand 1; PD-1: Programmed death 1.

favorable prognostic biomarker for G-NEC patients. Due to the coinstantaneous impact of copy number variation and TILs' stimulation on the expression of PD-L1, the mechanism of high expression of PD-L1 in G-NECs remains complicated. Most importantly, our findings provide important implications for the potential use of antibody therapies targeting the PD-1/PD-L1 signaling pathway in G-NECs.

Table 3 Univariate and multivariate analyses of prognostic parameters for survival in the cohort patients with gastric neuroendocrine carcinomas

Prognostic parameter	Univariate			Multivariate		
	HR	95%CI	P-value	HR	95%CI	P-value
Age (yr)						
< 60	1.0 (Reference)					
≥ 60	2.718	0.921-8.023	0.07			
Gender						
Male	1.0 (Reference)					
Female	0.915	0.308-2.718	0.873			
Tumor location						
Cardia	1.0 (Reference)					
Corpus	3.034	1.100-8.374	0.032	2.878	0.971-8.529	0.057
Antrum	2.331	0.817-6.648	0.114	2.51	0.285-22.125	0.407
Residual stomach anastomosis	1.401	0.176-11.159	0.75	1.373	0.399-4.718	0.615
Tumor size						
≤ 5 cm	1.0 (Reference)					
> 5 cm	1.605	0.693-3.717	0.269			
T classification						
T1/2	1.0 (Reference)					
T3/4	0.76	0.407-1.420	0.39			
Lymph node metastasis						
Absent	1.0 (Reference)					
Present	1.976	0.731-5.342	0.179			
Liver metastasis						
Absent	1.0 (Reference)					
Present	3.515	1.269-9.731	0.016	4.045	1.140-14.351	0.031
CD8						
Low	1.0 (Reference)					
High	0.46	0.197-1.074	0.073			
FOXP3						
Low	1.0 (Reference)					
High	1.375	0.593-3.186	0.458			
PD-1						
Low	1.0 (Reference)					
High	0.954	0.420-2.167	0.91			
PD-L1						
Low	1.0 (Reference)					
High	2.846	1.170-6.922	0.021	3.646	1.372-9.688	0.009

PD-L1: Programmed death ligand 1; PD-1: Programmed death 1. HR: Hazard ratio; CI: Confidence interval.

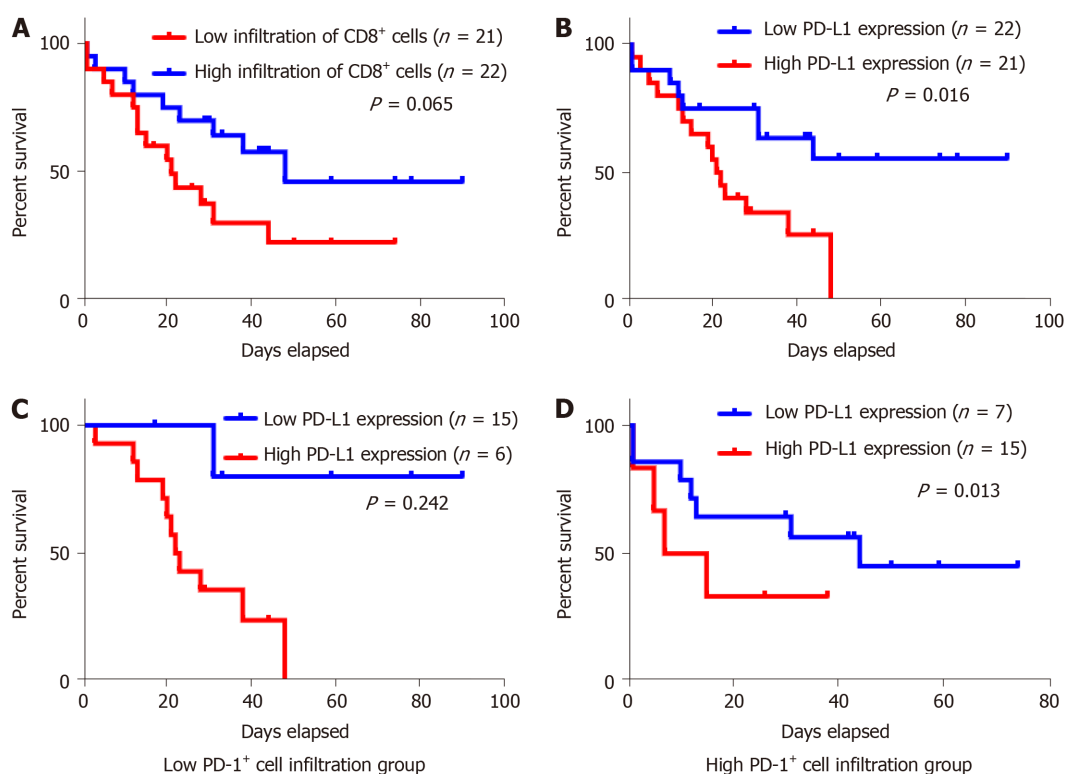


Figure 3 Kaplan-Meier survival analysis of the gastric neuroendocrine carcinomas patients. A: Patients with high infiltration of CD8⁺ lymphocytes tended to have a relative longer survival, but the difference was not statistically significant; B: Kaplan-Meier overall survival curves in patients with high and low expression of programmed death ligand 1 (PD-L1) in the whole population; C: Low PD-1⁺ cell infiltration group; D: High PD-1⁺ cell infiltration group. PD-L1: Programmed death ligand 1.

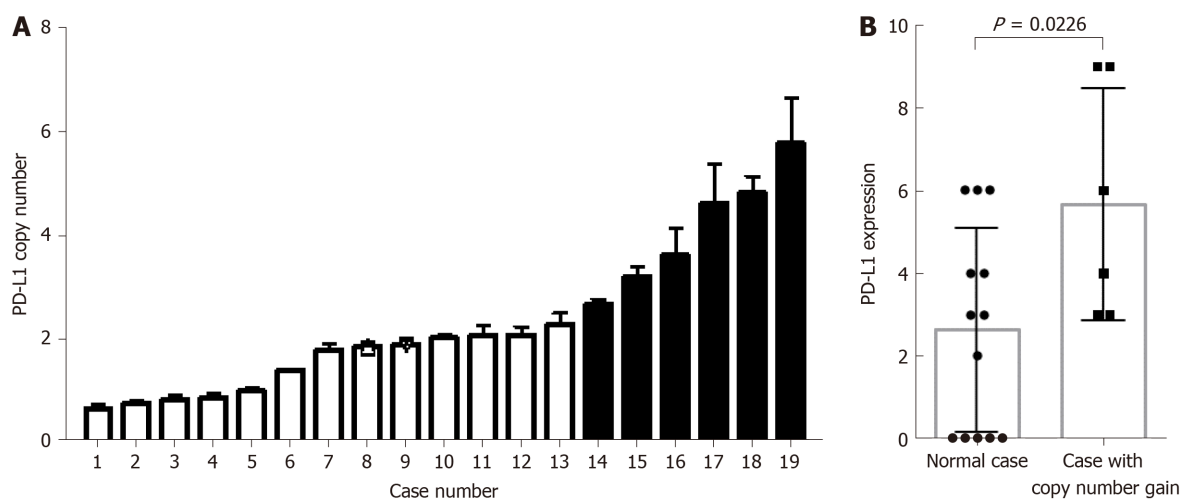


Figure 4 Programmed death ligand 1 copy number is associated with programmed death ligand 1 expression in gastric neuroendocrine carcinomas. A: Programmed death ligand 1 (PD-L1) copy number status varied in 19 gastric neuroendocrine carcinoma samples. The cases with copy number gain are shown in black; B: Cases with copy number gain showed significantly higher PD-L1 expression than those without. PD-L1: Programmed death ligand 1.

ARTICLE HIGHLIGHTS

Research background

Recently, more and more studies have demonstrated the pivotal role of programmed death 1/programmed death ligand 1 (PD-1/PD-L1) pathway in the immune evasion of tumors from the host immune system. However, the role of PD-1/PD-L1 pathway in gastric neuroendocrine carcinomas (G-NECs) remains unknown.

Research motivation

G-NECs are highly malignant, clinically defiant, and lack of effective treatment. Recent research

has proved the role of treatment targeting PD-1/PD-L1 pathway in several other advanced cancers. This study for the first time demonstrated that PD-L1 can be expressed by G-NEC cancer cells and the high PD-L1 expression was associated with a poor prognosis. These findings provide important implications for the potential use of antibody therapies targeting the PD-1/PD-L1 signaling pathway in G-NECs.

Research objectives

We performed this research to investigate the expression of PD-1/PD-L1 and role of PD-1/PD-L1 pathway in G-NECs.

Research methods

We investigated the expression of PD-L1 on tumor cells and PD-1⁺, CD8⁺, and FOXP3⁺ T cell infiltration by immunohistochemistry in 43 resected G-NECs tissue specimens, while the copy number alterations of PD-L1 were assessed by qRT-PCR. Statistical analyses and graphical representations were performed using SPSS 22.0 software and GraphPad Prism 6 software, respectively. χ^2 test and Fisher's exact test were used to evaluate the correlation of PD-L1, PD-1, FOXP3, and CD8 with clinicopathologic parameters in patients with G-NECs. Survival curves were evaluated using the Kaplan-Meier method and differences were analyzed by the log-rank test. Identification of factors that had a significant influence on survival was performed by univariate and multivariate Cox regression analyses. Comparison between two groups was performed by the Student's *t*-test or Mann-Whitney *U* test.

Research results

We found that most of the G-NECs tumor cells exhibited a near-uniform expression pattern of PD-L1, while some showed a tumor-stromal interface enhanced pattern. Of the 43 G-NECs, 21 (48.8%) were classified as a high PD-L1 expression group, and the high expression of PD-L1 was associated with poor overall survival (OS). The high expression of PD-L1 was correlated with abundant PD-1⁺ tumor infiltrating lymphocytes (TILs) instead of CD8⁺ TILs and FOXP3⁺ regulatory T cells (Tregs). Our analysis also suggested that the infiltration of CD8⁺ TILs tended to be a favorable factor for OS, although the difference did not reach the statistical significance (*P* = 0.065). Meanwhile, PD-L1 was significantly overexpressed in cases with copy number gain as compared with those without. However, as a retrospective study, the small sample size of this research might result in some bias in the multivariable prognosis analysis, so larger sample studies are needed.

Research conclusions

Our data demonstrated for the first time that the high expression of PD-L1 in G-NECs was associated with a poor prognosis, while the high expression may be due to the copy number variation of PD-L1 gene or stimulation of TILs. These results provide a basis for the immunotherapy targeting PD-1/PD-L1 pathway in G-NECs.

Research perspectives

By this study, we found that PD-1/PD-L1 pathway is involved in G-NECs. In the following, *in vitro* cell experiments and *in vivo* animal experiments are needed.

REFERENCES

- 1 Sorbye H, Welin S, Langer SW, Vestermark LW, Holt N, Osterlund P, Dueland S, Hofsl   E, Guren MG, Ohrling K, Birkemeyer E, Thiis-Evensen E, Biagini M, Gronbaek H, Soveri LM, Olsen IH, Federspiel B, Assmus J, Janson ET, Knigge U. Predictive and prognostic factors for treatment and survival in 305 patients with advanced gastrointestinal neuroendocrine carcinoma (WHO G3): The NORDIC NEC study. *Ann Oncol* 2013; **24**: 152-160 [PMID: 22967994 DOI: 10.1093/annonc/mds276]
- 2 Gastrointestinal Pathology Study Group of Korean Society of Pathologists; Cho MY, Kim JM, Sohn JH, Kim MJ, Kim KM, Kim WH, Kim H, Kook MC, Park DY, Lee JH, Chang H, Jung ES, Kim HK, Jin SY, Choi JH, Gu MJ, Kim S, Kang MS, Cho CH, Park MI, Kang YK, Kim YW, Yoon SO, Bae HI, Joo M, Moon WS, Kang DY, Chang SJ. Current Trends of the Incidence and Pathological Diagnosis of Gastroenteropancreatic Neuroendocrine Tumors (GEP-NETs) in Korea 2000-2009: Multicenter Study. *Cancer Res Treat* 2012; **44**: 157-165 [PMID: 23091441 DOI: 10.4143/crt.2012.44.3.157]
- 3 Yao JC, Hassan M, Phan A, Dagohoy C, Leary C, Mares JE, Abdalla EK, Fleming JB, Vauthey JN, Rashid A, Evans DB. One hundred years after "carcinoid": Epidemiology of and prognostic factors for neuroendocrine tumors in 35,825 cases in the United States. *J Clin Oncol* 2008; **26**: 3063-3072 [PMID: 18565894 DOI: 10.1200/JCO.2007.15.4377]
- 4 Lepage C, Rachet B, Coleman MP. Survival from malignant digestive endocrine tumors in England and Wales: A population-based study. *Gastroenterology* 2007; **132**: 899-904 [PMID: 17383419 DOI: 10.1053/j.gastro.2007.01.006]
- 5 Modlin IM, Oberg K, Chung DC, Jensen RT, de Herder WW, Thakker RV, Caplin M, Delle Fave G, Kaltsas GA, Krenning EP, Moss SF, Nilsson O, Rindi G, Salazar R, Ruszniewski P, Sundin A. Gastroenteropancreatic neuroendocrine tumours. *Lancet Oncol* 2008; **9**: 61-72 [PMID: 18177818 DOI: 10.1016/S1470-2045(07)70410-2]
- 6 Hijioka S, Hosoda W, Mizuno N, Hara K, Imaoka H, Bhatia V, Mekky MA, Tajika M, Tanaka T, Ishihara M, Yogi T, Tsutsumi H, Fujiyoshi T, Sato T, Hieda N, Yoshida T, Okuno N, Shimizu Y, Yatabe Y, Niwa Y, Yamao K. Does the WHO 2010 classification of pancreatic neuroendocrine neoplasms accurately characterize pancreatic neuroendocrine carcinomas? *J Gastroenterol* 2015; **50**: 564-572 [PMID: 25142799 DOI: 10.1007/s00535-014-0987-2]
- 7 Ishida Y, Agata Y, Shibahara K, Honjo T. Induced expression of PD-1, a novel member of the

- immunoglobulin gene superfamily, upon programmed cell death. *EMBO J* 1992; **11**: 3887-3895 [PMID: 1396582 DOI: 10.1002/j.1460-2075.1992.tb05481.x]
- 8 **Dong H**, Zhu G, Tamada K, Chen L. B7-H1, a third member of the B7 family, co-stimulates T-cell proliferation and interleukin-10 secretion. *Nat Med* 1999; **5**: 1365-1369 [PMID: 10581077 DOI: 10.1038/70932]
 - 9 **Freeman GJ**, Long AJ, Iwai Y, Bourque K, Chernova T, Nishimura H, Fitz LJ, Malenkovich N, Okazaki T, Byrne MC, Horton HF, Fouser L, Carter L, Ling V, Bowman MR, Carreno BM, Collins M, Wood CR, Honjo T. Engagement of the PD-1 immunoinhibitory receptor by a novel B7 family member leads to negative regulation of lymphocyte activation. *J Exp Med* 2000; **192**: 1027-1034 [PMID: 11015443 DOI: 10.1084/jem.192.7.1027]
 - 10 **Dong H**, Strome SE, Salomao DR, Tamura H, Hirano F, Flies DB, Roche PC, Lu J, Zhu G, Tamada K, Lennon VA, Celis E, Chen L. Tumor-associated B7-H1 promotes T-cell apoptosis: A potential mechanism of immune evasion. *Nat Med* 2002; **8**: 793-800 [PMID: 12091876 DOI: 10.1038/nm730]
 - 11 **Wu C**, Zhu Y, Jiang J, Zhao J, Zhang XG, Xu N. Immunohistochemical localization of programmed death-1 ligand-1 (PD-L1) in gastric carcinoma and its clinical significance. *Acta Histochem* 2006; **108**: 19-24 [PMID: 16530813 DOI: 10.1016/j.acthis.2006.01.003]
 - 12 **Ohgashi Y**, Sho M, Yamada Y, Tsurui Y, Hamada K, Ikeda N, Mizuno T, Yoriki R, Kashizuka H, Yane K, Tushima F, Otsuki N, Yagita H, Azuma M, Nakajima Y. Clinical significance of programmed death-1 ligand-1 and programmed death-1 ligand-2 expression in human esophageal cancer. *Clin Cancer Res* 2005; **11**: 2947-2953 [PMID: 15837746 DOI: 10.1158/1078-0432.ccr-04-1469]
 - 13 **Nomi T**, Sho M, Akahori T, Hamada K, Kubo A, Kanehiro H, Nakamura S, Enomoto K, Yagita H, Azuma M, Nakajima Y. Clinical significance and therapeutic potential of the programmed death-1 ligand/programmed death-1 pathway in human pancreatic cancer. *Clin Cancer Res* 2007; **13**: 2151-2157 [PMID: 17404099 DOI: 10.1158/1078-0432.ccr-06-2746]
 - 14 **Droeser RA**, Hirt C, Viehl CT, Frey DM, Nebiker C, Huber X, Zlobec I, Eppenberger-Castori S, Tzankov A, Rosso R, Zuber M, Muraro MG, Amicarella F, Cremonesi E, Heberer M, Iezzi G, Lugli A, Terracciano L, Sconocchia G, Oertli D, Spagnoli GC, Tornillo L. Clinical impact of programmed cell death ligand 1 expression in colorectal cancer. *Eur J Cancer* 2013; **49**: 2233-2242 [PMID: 23478000 DOI: 10.1016/j.ejca.2013.02.015]
 - 15 **Baptista MZ**, Sarian LO, Derchain SF, Pinto GA, Vassallo J. Prognostic significance of PD-L1 and PD-L2 in breast cancer. *Hum Pathol* 2016; **47**: 78-84 [PMID: 26541326 DOI: 10.1016/j.humpath.2015.09.006]
 - 16 **Yokoyama S**, Miyoshi H, Nishi T, Hashiguchi T, Mitsuoka M, Takamori S, Akagi Y, Kakuma T, Ohshima K. Clinicopathologic and Prognostic Implications of Programmed Death Ligand 1 Expression in Thymoma. *Ann Thorac Surg* 2016; **101**: 1361-1369 [PMID: 26794891 DOI: 10.1016/j.athoracsur.2015.10.044]
 - 17 **Yokoyama S**, Miyoshi H, Nakashima K, Shimono J, Hashiguchi T, Mitsuoka M, Takamori S, Akagi Y, Ohshima K. Prognostic Value of Programmed Death Ligand 1 and Programmed Death 1 Expression in Thymic Carcinoma. *Clin Cancer Res* 2016; **22**: 4727-4734 [PMID: 27166394 DOI: 10.1158/1078-0432.CCR-16-0434]
 - 18 **Pedoeem A**, Azoulay-Alfaguter I, Strazza M, Silverman GJ, Mor A. Programmed death-1 pathway in cancer and autoimmunity. *Clin Immunol* 2014; **153**: 145-152 [PMID: 24780173 DOI: 10.1016/j.clim.2014.04.010]
 - 19 **Hassel JC**. Ipilimumab plus nivolumab for advanced melanoma. *Lancet Oncol* 2016; **17**: 1471-1472 [PMID: 27617662 DOI: 10.1016/S1470-2045(16)30409-0]
 - 20 **Philips GK**, Atkins M. Therapeutic uses of anti-PD-1 and anti-PD-L1 antibodies. *Int Immunol* 2015; **27**: 39-46 [PMID: 25323844 DOI: 10.1093/intimm/ixu095]
 - 21 **Naito Y**, Saito K, Shiiba K, Ohuchi A, Saigenji K, Nagura H, Ohtani H. CD8+ T cells infiltrated within cancer cell nests as a prognostic factor in human colorectal cancer. *Cancer Res* 1998; **58**: 3491-3494 [PMID: 9721846 DOI: 10.1021/jp900525a]
 - 22 **Schumacher K**, Haensch W, Röefzaad C, Schlag PM. Prognostic significance of activated CD8(+) T cell infiltrations within esophageal carcinomas. *Cancer Res* 2001; **61**: 3932-3936 [PMID: 11358808]
 - 23 **Cho Y**, Miyamoto M, Kato K, Fukunaga A, Shichinohe T, Kawarada Y, Hida Y, Oshikiri T, Kurokawa T, Suzuoki M, Nakakubo Y, Hiraoka K, Murakami S, Shinohara T, Itoh T, Okushiba S, Kondo S, Katoh H. CD4+ and CD8+ T cells cooperate to improve prognosis of patients with esophageal squamous cell carcinoma. *Cancer Res* 2003; **63**: 1555-1559 [PMID: 12670904]
 - 24 **Huang Y**, Ma C, Zhang Q, Ye J, Wang F, Zhang Y, Hunborg P, Varvares MA, Hoft DF, Hsueh EC, Peng G. CD4+ and CD8+ T cells have opposing roles in breast cancer progression and outcome. *Oncotarget* 2015; **6**: 17462-17478 [PMID: 25968569 DOI: 10.18632/oncotarget.3958]
 - 25 **Spranger S**, Spaapen RM, Zha Y, Williams J, Meng Y, Ha TT, Gajewski TF. Up-regulation of PD-L1, IDO, and T(regs) in the melanoma tumor microenvironment is driven by CD8(+) T cells. *Sci Transl Med* 2013; **5**: 200ra116 [PMID: 23986400 DOI: 10.1126/scitranslmed.3006504]
 - 26 **Taube JM**, Young GD, McMiller TL, Chen S, Salas JT, Pritchard TS, Xu H, Meeker AK, Fan J, Cheadle C, Berger AE, Pardoll DM, Topalian SL. Differential Expression of Immune-Regulatory Genes Associated with PD-L1 Display in Melanoma: Implications for PD-1 Pathway Blockade. *Clin Cancer Res* 2015; **21**: 3969-3976 [PMID: 25944800 DOI: 10.1158/1078-0432.CCR-15-0244]
 - 27 **Kasprowicz DJ**, Smallwood PS, Tyznik AJ, Ziegler SF, Scurfin (FoxP3) controls T-dependent immune responses in vivo through regulation of CD4+ T cell effector function. *J Immunol* 2003; **171**: 1216-1223 [PMID: 12874208 DOI: 10.4049/jimmunol.171.3.1216]
 - 28 **Hou J**, Yu Z, Xiang R, Li C, Wang L, Chen S, Li Q, Chen M, Wang L. Correlation between infiltration of FOXP3+ regulatory T cells and expression of B7-H1 in the tumor tissues of gastric cancer. *Exp Mol Pathol* 2014; **96**: 284-291 [PMID: 24657498 DOI: 10.1016/j.yexmp.2014.03.005]
 - 29 **Li Z**, Dong P, Ren M, Song Y, Qian X, Yang Y, Li S, Zhang X, Liu F. PD-L1 Expression Is Associated with Tumor FOXP3(+) Regulatory T-Cell Infiltration of Breast Cancer and Poor Prognosis of Patient. *J Cancer* 2016; **7**: 784-793 [PMID: 27162536 DOI: 10.7150/jca.14549]
 - 30 **Bosman FT**, Carneiro F, Hruban RH, Theise ND. WHO classification of tumours of the digestive system. In: WHO classification of tumours. 4th ed. Lyon: IARC 2010; 417
 - 31 **Edge SB**, Compton CC. The American Joint Committee on Cancer: The 7th edition of the AJCC cancer staging manual and the future of TNM. *Ann Surg Oncol* 2010; **17**: 1471-1474 [PMID: 20180029 DOI: 10.1245/s10434-010-0985-4]
 - 32 **Teng MW**, Ngiew SF, Ribas A, Smyth MJ. Classifying Cancers Based on T-cell Infiltration and PD-L1. *Cancer Res* 2015; **75**: 2139-2145 [PMID: 25977340 DOI: 10.1158/0008-5472.CAN-15-0255]

- 33 **Topalian SL**, Hodi FS, Brahmer JR, Gettinger SN, Smith DC, McDermott DF, Powderly JD, Carvajal RD, Sosman JA, Atkins MB, Leming PD, Spigel DR, Antonia SJ, Horn L, Drake CG, Pardoll DM, Chen L, Sharfman WH, Anders RA, Taube JM, McMiller TL, Xu H, Korman AJ, Jure-Kunkel M, Agrawal S, McDonald D, Kollia GD, Gupta A, Wigginton JM, Sznol M. Safety, activity, and immune correlates of anti-PD-1 antibody in cancer. *N Engl J Med* 2012; **366**: 2443-2454 [PMID: [22658127](#) DOI: [10.1056/NEJMoa1200690](#)]
- 34 **Topalian SL**, Sznol M, McDermott DF, Kluger HM, Carvajal RD, Sharfman WH, Brahmer JR, Lawrence DP, Atkins MB, Powderly JD, Leming PD, Lipson EJ, Puzanov I, Smith DC, Taube JM, Wigginton JM, Kollia GD, Gupta A, Pardoll DM, Sosman JA, Hodi FS. Survival, durable tumor remission, and long-term safety in patients with advanced melanoma receiving nivolumab. *J Clin Oncol* 2014; **32**: 1020-1030 [PMID: [24590637](#) DOI: [10.1200/JCO.2013.53.0105](#)]
- 35 **Kim ST**, Ha SY, Lee S, Ahn S, Lee J, Park SH, Park JO, Lim HY, Kang WK, Kim KM, Park YS. The Impact of PD-L1 Expression in Patients with Metastatic GEP-NETs. *J Cancer* 2016; **7**: 484-489 [PMID: [26958083](#) DOI: [10.7150/jca.13711](#)]
- 36 **Cavalcanti E**, Armentano R, Valentini AM, Chieppa M, Caruso ML. Role of PD-L1 expression as a biomarker for GEP neuroendocrine neoplasm grading. *Cell Death Dis* 2017; **8**: e3004 [PMID: [28837143](#) DOI: [10.1038/cddis.2017.401](#)]
- 37 **Fan Y**, Ma K, Wang C, Ning J, Hu Y, Dong D, Dong X, Geng Q, Li E, Wu Y. Prognostic value of PD-L1 and PD-1 expression in pulmonary neuroendocrine tumors. *Oncotargets Ther* 2016; **9**: 6075-6082 [PMID: [27785054](#) DOI: [10.2147/ott.s115054](#)]
- 38 **Muenst S**, Soysal SD, Gao F, Obermann EC, Oertli D, Gillanders WE. The presence of programmed death 1 (PD-1)-positive tumor-infiltrating lymphocytes is associated with poor prognosis in human breast cancer. *Breast Cancer Res Treat* 2013; **139**: 667-676 [PMID: [23756627](#) DOI: [10.1007/s10549-013-2581-3](#)]
- 39 **Thompson RH**, Dong H, Lohse CM, Leibovich BC, Blute ML, Cheville JC, Kwon ED. PD-1 is expressed by tumor-infiltrating immune cells and is associated with poor outcome for patients with renal cell carcinoma. *Clin Cancer Res* 2007; **13**: 1757-1761 [PMID: [17363529](#) DOI: [10.1158/1078-0432.ccr-06-2599](#)]
- 40 **Schalper KA**, Velcheti V, Carvajal D, Wimberly H, Brown J, Pusztai L, Rimm DL. In situ tumor PD-L1 mRNA expression is associated with increased TILs and better outcome in breast carcinomas. *Clin Cancer Res* 2014; **20**: 2773-2782 [PMID: [24647569](#) DOI: [10.1158/1078-0432.CCR-13-2702](#)]
- 41 **Schmidt LH**, Kümmel A, Görlich D, Mohr M, Bröckling S, Mikesch JH, Grünewald I, Marra A, Schultheis AM, Wardelmann E, Müller-Tidow C, Spieker T, Schliemann C, Berdel WE, Wiewrodt R, Hartmann W. PD-1 and PD-L1 Expression in NSCLC Indicate a Favorable Prognosis in Defined Subgroups. *PLoS One* 2015; **10**: e0136023 [PMID: [26313362](#) DOI: [10.1371/journal.pone.0136023](#)]
- 42 **Fridman WH**, Pagès F, Sautès-Fridman C, Galon J. The immune contexture in human tumours: Impact on clinical outcome. *Nat Rev Cancer* 2012; **12**: 298-306 [PMID: [22419253](#) DOI: [10.1038/nrc3245](#)]
- 43 **Diana A**, Wang LM, D'Costa Z, Allen P, Azad A, Silva MA, Soonawalla Z, Liu S, McKenna WG, Muschel RJ, Fokas E. Prognostic value, localization and correlation of PD-1/PD-L1, CD8 and FOXP3 with the desmoplastic stroma in pancreatic ductal adenocarcinoma. *Oncotarget* 2016; **7**: 40992-41004 [PMID: [27329602](#) DOI: [10.18632/oncotarget.10038](#)]



Basic Study

Functional role of long non-coding RNA CASC19/miR-140-5p/CEMIP axis in colorectal cancer progression *in vitro*

Xiao-Dong Wang, Jian Lu, Yun-Shou Lin, Chao Gao, Feng Qi

ORCID number: Xiao-Dong Wang (0000-0003-4463-5852); Jian Lu (0000-0001-9656-2769); Yun-Shou Lin (0000-0003-4018-7503); Chao Gao (0000-0001-9083-6706); Feng Qi (0000-0001-5490-0985).

Author contributions: Qi F designed and coordinated the research; Wang XD performed the majority of experiments, analyzed the data, and wrote the paper; Lu J, Lin YS, and Gao C contributed new reagents or analytic tools.

Supported by the National Natural Science Foundation of China, No. 81570375.

Institutional review board statement: This study was approved by the Medical Ethics Committee of Tianjin Medical University General Hospital (Ethical No. IRB2015-YX-018) and was conducted in strict compliance with the Declaration of Helsinki.

Conflict-of-interest statement: The authors report no conflicts of interest in this work.

Data sharing statement: No additional unpublished data are available.

Open-Access: This article is an open-access article which was selected by an in-house editor and fully peer-reviewed by external reviewers. It is distributed in accordance with the Creative Commons Attribution Non Commercial (CC BY-NC 4.0) license, which permits others to distribute, remix, adapt, build upon this work non-commercially, and license their derivative works

Xiao-Dong Wang, Jian Lu, Yun-Shou Lin, Chao Gao, Feng Qi, Department of General Surgery, Tianjin Medical University General Hospital, Tianjin 300052, China

Corresponding author: Feng Qi, FRCS (Gen Surg), MD, PhD, Academic Research, Chief Doctor, Director, Doctor, Full Professor, Professor, Research Scientist, Senior Researcher, Senior Scientist, Surgeon, Surgical Oncologist, Teacher, Department of General Surgery, Tianjin Medical University General Hospital, No. 154, Anshan Road, Heping District, Tianjin 300052, China. qf@medmail.com.cn

Telephone: +86-13752115987

Fax: +86-22-60363901

Abstract

BACKGROUND

Long non-coding RNAs (lncRNAs) are widely involved in tumor regulation. Nevertheless, the role of the lncRNA cancer susceptibility 19 (CASC19) in colorectal cancer (CRC) has yet to be fully clarified.

AIM

To explore the effect of CASC19 on proliferation and metastasizing ability of CRC cells.

METHODS

CASC19 expression in human CRC tissues, pair-matched adjacent normal colon tissues, and CRC cells was detected using quantitative real-time PCR (qRT-PCR). CASC19 expression, as well as its relation to overall survival, was extrapolated by Kaplan-Meier survival analysis together with multivariable Cox regression assay. *In vitro* experiments were performed to confirm whether CASC19 regulates CRC cell invasion, migration, proliferation, and apoptosis.

RESULTS

CASC19 expression was markedly upregulated in CRC tissues and CRC cell lines ($P < 0.05$). qRT-PCR revealed that CASC19 expression was higher in 25 tissue samples from patients with aggressive CRC compared with the 27 tissue samples from patients with nonaggressive CRC ($P < 0.05$). Higher CASC19 expression was associated with poorer patient prognoses. Furthermore, *in vitro* experiments demonstrated that CASC19 overexpression enhanced CRC cell invasion, migration, and proliferation. CASC19 overexpression enhanced the expression of cell migration inducing hyaluronidase 1 (CEMIP) and epithelial-mesenchymal transition markers. MiR-140-5p was found to be able to bind directly to CASC19 and CEMIP. Overexpression of miR-140-5p reversed the effect of CASC19 on cell

on different terms, provided the original work is properly cited and the use is non-commercial. See: <http://creativecommons.org/licenses/by-nc/4.0/>

Manuscript source: Unsolicited manuscript

Received: January 13, 2019

Peer-review started: January 14, 2019

First decision: February 21, 2019

Revised: March 6, 2019

Accepted: March 15, 2019

Article in press: March 16, 2019

Published online: April 14, 2019

P-Reviewer: Leon J, Linnebacher M, Serafino A

S-Editor: Ma RY

L-Editor: Wang TQ

E-Editor: Song H



proliferation and tumor migration, as well as suppressed CASC19-induced CEMIP expression.

CONCLUSION

CASC19 positively regulates CEMIP expression through targeting miR-140-5p. CASC19 may possess an oncogenic function in CRC progression, highlighting its potential as an essential biomarker in CRC diagnosis and therapy.

Key words: Colorectal cancer; Long non-coding RNA; MicroRNA; Proliferation; Metastasis

©The Author(s) 2019. Published by Baishideng Publishing Group Inc. All rights reserved.

Core tip: The long non-coding RNA cancer susceptibility 19 is highly expressed in colorectal cancer tissues. *In vitro* studies have shown that the long non-coding RNA cancer susceptibility 19 may regulate the proliferation, epithelial-mesenchymal transition, and metastasizing ability of colorectal cancer cells by regulating microRNA-140-5p, as well as cell migration by inducing hyaluronidase 1.

Citation: Wang XD, Lu J, Lin YS, Gao C, Qi F. Functional role of long non-coding RNA CASC19/miR-140-5p/CEMIP axis in colorectal cancer progression *in vitro*. *World J Gastroenterol* 2019; 25(14): 1697-1714

URL: <https://www.wjgnet.com/1007-9327/full/v25/i14/1697.htm>

DOI: <https://dx.doi.org/10.3748/wjg.v25.i14.1697>

INTRODUCTION

Colorectal cancer (CRC) is a tumor that is increasingly common in the modern world^[1]. Tumor metastasis is one of the most important causes of poor prognosis for patients with CRC. At the time of diagnosis, approximately 20%-25% of patients with CRC are found to have liver metastasis. At the same time, liver metastasis occurs in up to 40%-50% of patients after resection of primary CRC^[2]. Although current methods for the diagnosis and therapy of CRC have achieved remarkable progress, tumor metastasis remains an important factor affecting the survival of patients^[3]. In recent years, gene therapy has become an intense focus of research. Transporting tumor suppressor genes or non-coding RNAs via nanocarriers may be a new option for cancer therapeutics^[4]. Therefore, a thorough understanding of the molecular pathophysiological pathways underlying CRC is crucial to developing an effective therapeutic strategy.

Non-coding RNAs include microRNAs (miRNAs) and long non-coding RNAs (lncRNAs). MiRNAs bind to the 3'-untranslated regions (3'-UTR) of the message RNA (mRNA) of the target genes, resulting in mRNA degradation and inhibition of the translation process. LncRNAs are RNAs that are longer than 200 nucleotides. The existing literature primarily investigates the regulatory roles of lncRNAs in several biological processes^[5,6]. Dysregulation of lncRNAs is observed in various types of cancers, including breast cancer^[7], oesophageal cancer^[8], hepatocellular carcinoma^[9-11], lung cancer^[12], gastric cancer^[13], and CRC^[14-18]. LncRNA dysregulation has been discovered to be closely related to cancer progression. For example, overexpression of the lncRNA n335586 contributes to cell migration and invasion in hepatocellular carcinoma^[19], while the lncRNA CASP5 facilitates the migration and invasion of human glioblastoma cells^[20]. The regulatory mechanism of lncRNAs is still not clearly understood, and its possible role in cancer has been hypothesized to be as a competing endogenous RNA (ceRNA) for sponge miRNAs. For instance, the lncRNA UCA1 may adsorb microRNA (miRNA/miR)-182, thereby affecting the expression of its downstream target gene PFKFB2 and promoting glioma metastasis^[21]. The lncRNA PVT1 enhances colon cancer metastasis by altering the miR-30d-5p/RUNX2 axis^[22]. CRC progression has recently been discovered to be associated with endogenous lncRNA sponges. The cancer susceptibility 19 (CASC19) is a 324 bp lncRNA that is located on chromosome 8q24.21. Several lines of evidence suggest that the expression of CASC19 is overregulated in CRC, and this may play an oncogenic role in CRC progression^[23-25]. However, the mechanism by which CASC19 regulates CRC

progression is not fully understood.

The cell migration inducing hyaluronidase 1 (CEMIP) gene is located on chromosome 15q25 and encodes a 150 kDa protein. CEMIP is originally described as an inner ear protein and its mutation leads to hearing loss^[26]. CEMIP has traditionally been linked to hyaluronic acid depolymerization^[27]. Recent findings indicate that CEMIP may be involved in tumor development and may promote tumor cell proliferation and metastasis. For instance, the high expression of CEMIP is associated with a poor prognosis of prostate cancer^[28], gastric cancer^[29], and CRC^[28,30-34]. These reports suggest that CEMIP contributes to cancer heterogeneity and may be a potential therapeutic target.

Our present study demonstrated that CRC possesses a characteristic alteration in CASC19 expression profile that is related to CRC progression. Overexpression of CASC19 promotes CRC progression. In addition, mechanism analysis showed that CASC19 positively regulates CEMIP expression via sponge miR-140-5p, thereby exerting a carcinogenic effect in CRC progression. Future therapies targeting the CASC19/miR-140-5p/CEMIP axis may be beneficial in CRC.

MATERIALS AND METHODS

Patients and tissue specimens

This study included 52 patients who were pathologically diagnosed as having CRC and received surgical treatment between January 2015 and December 2016 at Tianjin Medical University General Hospital. Dissected tumor and adjacent normal colonic mucosal tissues (as samples taken from areas well close to the section margin) were immediately frozen in liquid nitrogen and stored at -80 °C. All the patients did not receive neoadjuvant therapy. All patients provided written informed consent. This study was approved by the Medical Ethics Committee of Tianjin Medical University General Hospital (Ethical No. IRB2015-YX-018) and was conducted in strict compliance with the Declaration of Helsinki.

Cell culture and transfection

Healthy colon epithelial cell line (FHC) and CRC cell lines (HCT-116, SW480, Lovo, and SW620) were purchased from the Chinese Academy of Sciences (Shanghai, China). All cells were maintained in DMEM medium supplemented with 10% FBS in a controlled environment of 5% CO₂ at 37 °C. Cell medium was replaced every 2 d. Before transfection, a total of 2.5×10^4 cells per well were seeded onto 6-well plates and incubated for 24 h, then the culture medium was discarded and 100 nmol/L of CASC19 overexpressing plasmid (CASC19-p; Genechem, Shanghai, China), 200 nmol/L of siRNA mixture, 100 nmol/L of miR-140-5p mimic (Ribobio, Guangzhou, China), or 200 nmol/L of miR-140-5p inhibitor (Ribobio, Guangzhou, China) was used for cell transfection. The pcDNA 3.1 negative control (CASC19-p NC), pcNDA3.1-CASC19 (CASC19-p), CASC19 siRNAs (siCASC19), CEMIP siRNAs (siCEMIP), and pcNDA3.1-CEMIP (CEMIP-p) were purchased from Genechem (Shanghai, China). MiR-140-5p mimic, miR-140-5p inhibitor, mimic NC, and inhibitor NC were obtained from Ribobio (Guangzhou, China).

Luciferase reporter system

The luciferase reporter system was constructed by Genechem (Shanghai, China) as previously described^[35]. Briefly, site-directed mutations were introduced into the CASC19 or CEMIP binding site of miR-140-5p (QuikChange Lightning Site-Directed Mutagenesis Kit, Stratagene, United States). The 3'-UTR fragment of wild-type (Wt) and mutant (Mut) CASC19 or CEMIP was then sub-cloned into the pGL3 luciferase vector (Promega, United States) by PCR, respectively. The miR-140-5p mimic was co-transfected with the vector into 293T cell lines for 12 h in 96-well plates using an enhanced infection solution (containing 5 µg/mL polybrene) (Genechem, Shanghai, China). The 293T cells were then cultured for 24 h and lysed to analyze the luciferase activity. Renilla (Promega, United States) activity was used as the internal control.

Cell cycle assay

A flow cytometric technique was used to perform cell cycle analysis as detailed in a prior study^[36]. In brief, HCT-116 and SW480 cells were harvested after transfection, and cell fixation was done with 70% pre-cooled ethanol at -20 °C overnight. Subsequently, cell staining was carried out using propidium iodide (PI, 50 µg/mL; Solarbio, Tianjin, China) and RNase A (0.1 mg/mL, Sigma, United States) at room temperature for 30 min. Then, the cells were analyzed with a flow cytometer (BD FACSCanto II Flow Cytometer, BD Biosciences, Franklin Lakes, United States). All data pertaining to cell cycle studies are described in terms of the percentage of cell

distributions in different phases (G0/G1, S, and G2/M).

Cell proliferation assay

The cell counting kit-8 (CCK-8) assay was used to assess the ability of SW480 and HCT-116 cells to proliferate. Cells (2×10^3) were added to each well of a 96-well plate with 100 μ L of culture medium. CCK-8 solution (10 μ L; Dojindo Laboratories, Japan) was applied into each well from day 0 to day 5. The cells were left to incubate for 3 h at 37 °C. A microplate luminometer (Bio-Rad Laboratories, United States) was then used to quantify absorbance values at 450 nm.

Wound-healing and transwell assays

The abilities of cells to migrate and invade were assessed by wound-healing assay and Transwell assay with Matrigel (BD Bioscience, United States). Briefly, for the wound-healing assay, transfected cells were allowed to proliferate in 6-well plates until a confluent monolayer was achieved. The cell layer was gently scratched with a 200 μ L pipette tip to inflict a wound. PBS was used to rinse the cells to remove debris and wound healing was allowed to take place for the next 24 h. The area of open wound covered by cells was described in terms of “percent wound closure (%)” [(Scratch distance_{0h} - Scratch distance_{24h})/Scratch distance_{0h} \times 100%, the distances were measured with Image J]. For the transwell assay, 200 μ L of medium without serum containing 1×10^5 cells was applied onto the upper chamber, while 600 μ L of medium with 10% fetal bovine serum (FBS) was added to the bottom chamber. The cells were left to incubate for 24 h at 37 °C. The membranes were then removed and cells were fixed with 4% paraformaldehyde before undergoing a 10-min staining period with 0.1% crystal violet. An inverted microscope was used to count the total cell number.

Apoptosis assay

For the apoptosis assay, 200 μ L of PBS was used to suspend cells. PI and fluorescein isothiocyanate (FITC) conjugated Annexin V (BD Biosciences, Franklin Lakes, NJ, United States) were then added into the suspension and left to incubate for 20 minutes at room temperature. A flow cytometer (FACSVerse, BD Biosciences, San Diego, CA, United States) was used to analyze cells.

RNA extraction and quantitative real-time PCR (qRT-PCR)

Total RNA was extracted with an RNA extraction kit (QIAGEN, Shanghai, China) and 1 μ g of total RNA was added to a 20 μ L system. The GoScript Reverse Transcription system (Promega, United States) was used for reverse transcription of CASC19 and CEMIP, and miR-140-5p was reverse transcribed by the stem-loop method (QIAGEN, Shanghai, China). GAPDH and U6 served as internal controls. The primer sequences are as follows: forward, 5'-GAGGAAGGCAGCACAATGATG-3' and reverse, 5'-CTTGCCAGTGTCTTCTCCTGA-3' for CASC19; forward, 5'-GCTCTGGGATTAAAGCAGC-3' and reverse, 5'-ATTGGAGCCATGGACTGTGA-3' for CEMIP; forward, 5'-CAGTGGTTTTACCTATGGTAG-3' and universal primer, 5'-TGGTGTCTCGTGA GTCG-3' for miR-140-5p; forward, 5'-TGCACCACTGCTTAGC-3' and reverse 5'-GGCATGGACTGTGGTCATGAG-3' for GAPDH; forward, 5'-CTCGCTTCGGCAGCACA-3' and reverse, 5'-AACGCTTCACGAATTTGCGT-3' for U6. All PCR reactions lasted 40 cycles, and the relative fold change of gene expression was derived using the $2^{-\Delta\Delta Ct}$ method.

Subcellular fractionation

Cellular localization of CASC19 was determined by subcellular fractionation using the PARIS Kit (Thermo Fisher Scientific, United States). Briefly, cytoplasmic and nuclear RNA were first extracted. The expression of CASC19 in the cytoplasmic and nuclear fractions was determined by qRT-PCR. GAPDH and U6 served as the cytoplasmic and nuclear controls, respectively.

RNA immunoprecipitation (RIP) assay

RIP assay (Magna RIP™ RNA Binding Protein Immunoprecipitation Kit, Millipore, United States) was utilized to verify the binding association between miR-140-5p and endogenous CASC19 in CRC cells. Briefly, harvested HCT-116 and SW480 cells were resuspended in cell RIP lysis buffer and kept on ice for 20 min. The RIP lysate was then centrifuged and 100 μ L of the supernatant was removed and added to each bead-antibody [anti-Argonaute 2 (Ago2) or negative control IgG] complex in RIP immunoprecipitation buffer. All tubes were left to incubate overnight in a rotator at 4 °C. The next day, immunoprecipitation tubes were centrifuged briefly and placed on a magnetic separator to collect the bead-antibody-RNA complexes. Protein K was used to purify the RNA. Purified RNA was then analyzed by RT-PCR.

Western blot analysis

Specimens and CRC cells were lysed in RIPA to obtain total protein, and 10% sodium dodecyl sulfate-polyacrylamide gel electrophoresis (SDS-PAGE) was used to separate 40 µg of each protein sample with the proteins subsequently reappplied to polyvinylidene fluoride membranes (Millipore, United States). These membranes containing blotted proteins were exposed to 0.5% bovine serum albumin to block endogenous reactions, followed by overnight probing at 4 °C with anti-CEMIP (1:1500, Novus, United States), anti-Vimentin (1:1500, CST, United States), anti-N-cadherin (1:1500, CST, United States), anti-E-cadherin [1:1500, Cell Signaling Technology (CST), United States], anti-poly AD-ribose polymerase (PARP) (1:2000, CST, United States), anti-caspase 3 (1:2000, CST, United States), anti-caspase 7 (1:2000, CST, United States), and anti-β-actin (1:3000, CST, United States) antibodies. The next day, membranes were rinsed and subjected to 2-h room temperature incubation with diluted secondary horseradish peroxidase (HRP)-marked antibodies (1:2500, CST, United States). An enhanced chemiluminescence detection kit (Millipore, United States) was used to detect immunoreactive protein bands. Images were acquired with a G-Box system (Syngene, United States) and analyzed with Image J (National Institute of Mental Health, United States).

Immunohistochemistry assay

Immunohistochemistry assay was used to determine CEMIP expression in CRC tissues and adjacent normal colonic mucosal tissues as described in our previous study^[37]. Briefly, tissue samples were fixed in 4% paraformaldehyde, embedded in paraffin, and sliced into 4 µm sections. Dehydration was carried out with xylene and a gradient of ethanol solution before endogenous peroxidase blocking was carried out with a 3% H₂O₂ solution. Antigen retrieval was performed with heated sodium citrate solution (92 °C-95 °C, 10 nmol/L, pH 6.0) for 5 min and 1% goat serum was added to the sections at room temperature for 2 min to block the sections. Rabbit anti-human CEMIP antibody (1:150; CST, United States) was applied onto the sections and left overnight to incubate at 4 °C. After incubation with the secondary antibody for 1 h at RT, freshly prepared diaminobenzidine was then added to the sections that were then stained with hematoxylin. A light microscope (Leica Microsystems, Wetzlar, Germany) was used to visualize slides and brown particles in the cytoplasm or cytomembranes were taken to indicate positive staining.

Statistical analysis

All data are expressed in terms of the mean ± SD. Continuous data were analyzed using the *t*-test or the one-way analysis of variance (ANOVA). The relationship between CASC19 expression and clinicopathological features was determined by one-way analysis of variance, the Chi-squared test, or the Fisher's exact test. The prognostic value of CASC19 in CRC patients was explored by Cox regression analysis. Kaplan-Meier methods and log-rank tests were used to carry out survival analyses. The correlations between CASC19, miR-140-5p, and CEMIP were analyzed using Spearman or Pearson correlation analysis. All statistical analyses were carried out with the use of GraphPad Prism (GraphPad Software, Version 5.0, United States) and SigmaPlot software (SPSS 22.0, United States). *P*-values < 0.05 were considered statistically significant. All results are representative of three repeated experiments.

RESULTS

CASC19 is upregulated in CRC tissues and CRC cell lines, and high expression of CASC19 indicates a poor prognosis

CASC19 expression was analyzed in 52 pairs of CRC tissues and adjacent normal colonic mucosal tissues using qRT-PCR. CASC19 exhibited significantly increased expression in CRC tissues in contrast to adjacent healthy colonic mucosal tissues (*P* < 0.05) (Figure 1A). Consistently, the CASC19 expression in CRC cell lines was markedly elevated in comparison to FHC cells (*P* < 0.05) (Figure 1B). For further *in vitro* studies, HCT-116 and SW480 cell lines were used.

We also focused on determining the association between expression of CASC19 and clinical phenotypes of patients with CRC. Participants were stratified into an aggressive tumor group (*n* = 25) and a non-aggressive tumor group (*n* = 27) based on whether the patient had or not lymph node or liver metastasis. Results showed that aggressive CRC tumors had higher CASC19 expression (*P* < 0.05) (Figure 1C). Next, we calculated the average of relative CASC19 expression levels in tumor tissues, and the average value (2.9310) was determined to be the cutoff point between "High CASC19" and "Low CASC19". Results showed that 22 samples were included in the

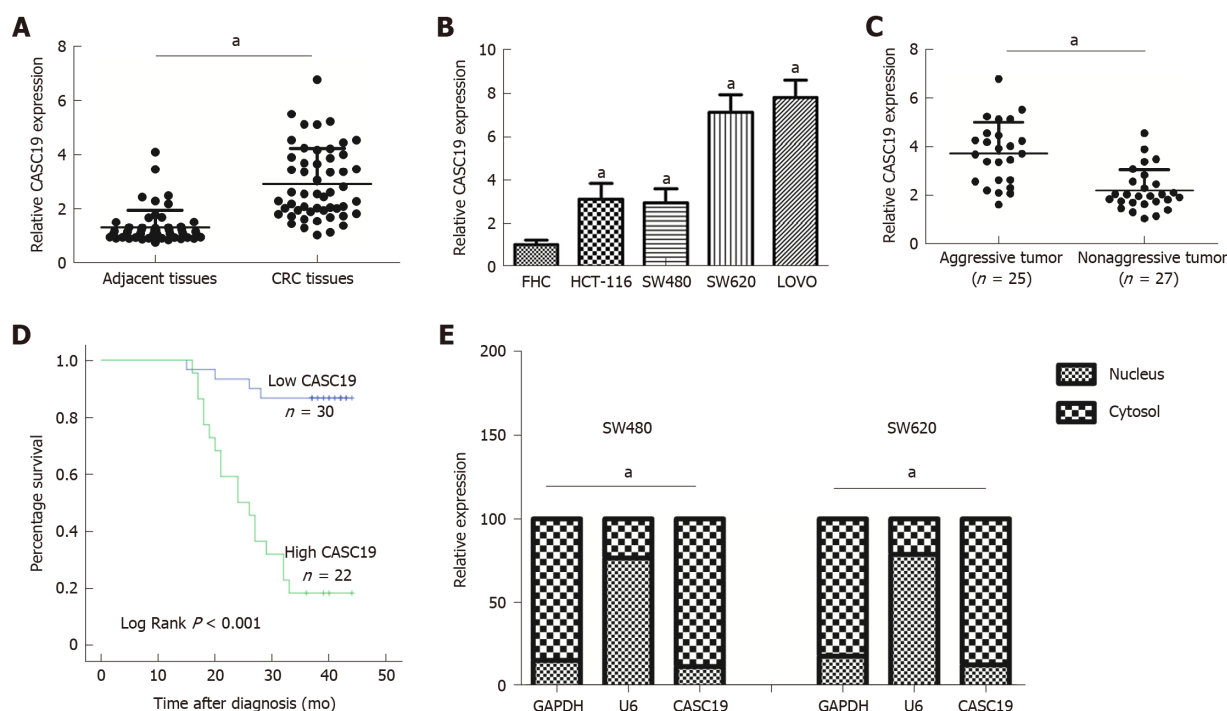


Figure 1 Differential expression of cancer susceptibility 19 in colorectal cancer tissues and cell lines. A: Differential cancer susceptibility 19 (CASC19) expression in CRC tissues and adjacent normal colon mucosa tissues. B: Differential CASC19 expression in colorectal cancer (CRC) cell lines and FHC cells. C: Differential CASC19 expression in aggressive tumor tissue samples and nonaggressive tumor tissue samples. D: Kaplan-Meier analyses of the correlations between CASC19 and overall survival of 52 patients with CRC. E: Cellular localization of CASC19 in CRC cells. Data are reported as the mean \pm SD. ^aP < 0.05. CASC19: Cancer susceptibility 19; CRC: Colorectal cancer.

high CASC19 group while another 30 were included in the low CASC19 group. Subsequent correlation analysis revealed that CASC19 expression was associated with liver metastasis ($P < 0.01$), lymphatic metastasis ($P < 0.01$), and TNM stage ($P < 0.05$) (Table 1) (Supplementary Figure 1). Significant associations were not present between CASC19 expression and other clinical parameters such as tumor size, local invasion, age, and gender ($P > 0.05$) (Table 1). Kaplan-Meier survival curves demonstrated that patients who possessed raised expression of CASC19 experienced shorter survival durations in contrast to those who had lower CASC19 expression (log-rank $P < 0.001$) (Figure 1D). We then carried out multivariable Cox regression analysis to further determine the impact of clinicopathological features and expression of CASC19 on the overall survival times of patients with CRC. The findings indicated that CASC19 expression [the exponent of B (Exp (B) = 8.893, 95% confidence interval (CI): 2.596-30.464, $P = 0.001$)] was an independent prognostic factor for CRC (Table 2).

Moreover, the results of subcellular fractionation confirmed that CASC19 was predominantly localized in the cell plasma (Figure 1E). Taken together, our findings demonstrated that CASC19 was a highly expressed lncRNA in CRC and is highly involved in CRC metastasis.

CASC19 promotes proliferation and inhibits apoptosis of CRC cells in vitro

To explore the role of CASC19 in CRC cells, SW480 and HCT-116 cells were transfected with CASC19-p or siCASC19. CASC19 was increased significantly in the CASC19-p group (CASC19 overexpression) in contrast to the control group ($P < 0.05$) and was substantially attenuated in the siCASC19 group (CASC19 knockdown) ($P < 0.05$) (Figure 2A). CASC19-p NC or siCASC19 NC did not alter CASC19 expression in CRC cells (Figure 2A).

Additionally, the CCK-8 assay was used to assess the impact of CASC19 on the proliferation of SW480 and HCT-116 cells. Figure 2B demonstrates that HCT-116 and SW480 cells experienced augmented proliferation in the presence of CASC19 overexpression ($P < 0.05$). Conversely, knockdown of CASC19 inhibited HCT-116 and SW480 cell proliferation ($P < 0.05$).

Interestingly, high CASC19 expression in CRC cells led to markedly decreased caspase-3, caspase-7, and PARP ($P < 0.05$ for all) (Figure 2C). Overexpression of CASC19 decreased the apoptotic rate of CRC cells ($P < 0.05$) (Figure 2D), while CASC19 knockdown enhanced caspase-7, caspase-3, and PARP protein levels. Furthermore, CASC19 knockdown markedly elevated the percentage of apoptotic

Table 1 Associations of cancer susceptibility 19 expression with clinicopathologic features of patients with colorectal cancer

Feature	Total (n = 52)	CASC19 expression		P-value
		High	Low	
Gender				
Male	25	10	15	0.483
Female	27	12	15	
Age, yr				
≤ 60	13	5	8	0.503
> 60	39	17	22	
Tumor size				
≤ 5 cm	22	9	13	0.379
> 5 cm	30	13	17	
TNM stage				
I-II	23	6	17	0.019 ^a
III-IV	29	16	13	
Local invasion				
T1 + T2	9	4	5	0.585
T3 + T4	43	18	25	
Lymphatic metastasis				
Yes	22	14	8	0.008 ^b
No	30	8	22	
Liver metastasis				
Yes	18	13	5	0.002 ^b
No	34	9	25	

^aP < 0.05.^bP < 0.01.

CASC19: Cancer susceptibility 19; CRC: Colorectal cancer.

cells ($P < 0.05$ for all) (Figure 2D). Cell cycle assay revealed that CASC19 overexpression led to a higher proportion of SW480 and HCT-116 cells that were in the S phase. This proportion was significantly reduced in cells that had suppressed CASC19 levels. It can be concluded that CASC19 promoted CRC cell growth, while knockdown of CASC19 expression could impede CRC cell growth.

CASC19 promotes CRC cell migration and invasion in vitro

The wound-healing and transwell assays were used to determine the impact of CASC19 expression on CRC cell migration and invasion, respectively. Cells transfected with CASC19-p completed wound healing at a faster rate in comparison to cells that were transfected with CASC19-p NC ($P < 0.05$) (Figure 3A). HCT-116 and SW480 cells that were induced to overexpress CASC19 were observed to undergo higher invasion rates (Figure 3B). Whereas, the migration and invasion abilities were inhibited in cells that had CASC19 knockdown (Figure 3A and B) ($P < 0.05$).

Given the crucial function of epithelial-mesenchymal transition (EMT) in the malignant transformation and invasive properties of cancer cells, we sought to clarify the impact of CASC19 on EMT marker expression in CRC cell lines. E-cadherin was downregulated ($P < 0.05$), while Vimentin and N-cadherin were upregulated ($P < 0.05$ for all) in HCT-116 and SW480 cell lines that had upregulated CASC19 (Figure 3C). In contrast, E-cadherin expression was increased ($P < 0.05$), and the expression of Vimentin and N-cadherin was decreased ($P < 0.05$ for all) in HCT-16 and SW480 cells that had suppressed CASC19 levels (Figure 3C). Together, these data indicate that CASC19 promotes CRC cell metastasis.

CASC19 promotes CEMIP expression by targeting miR-140-5p

To understand how CASC19 affects the CRC cell migration and proliferation, a ceRNA network analysis was carried out using starBase v 2.0 (<http://starbase.sysu.edu.cn/index.php>)^[38,39]. Interestingly, CASC19 was positively correlated with CEMIP expression. We examined the protein and mRNA levels of CEMIP in CRC cell lines and tissues. CEMIP expression was augmented in CRC

Table 2 Univariate and multivariate analyses of variables influencing survival of 52 patients with colorectal cancer

Variable	Univariate analysis	Multivariate analysis		
	P-value	Exp(B)	95%CI	P-value
CASC19	< 0.001 ^b	8.893	2.596-30.464	0.001 ^a
Age, yr	0.202	-	-	-
Gender	0.719	-	-	-
Tumor size	0.376	-	-	-
TNM stage	0.025 ^a	-	-	0.407
Local invasion	0.011 ^a	-	-	0.322
Lymphatic metastasis	< 0.001 ^b	11.395	3.201-40.565	< 0.001 ^b
Local invasion and liver metastasis	< 0.001 ^b	7.274	2.382-22.211	< 0.001 ^b

^a $P < 0.05$.^b $P < 0.01$.

CASC19: Cancer susceptibility 19; CRC: Colorectal cancer; Exp(B): The exponent of B; CI: Confidence interval.

tissues in contrast to healthy normal colonic mucosa at both the mRNA and protein levels ($P < 0.05$ for all) (Figure 4A and B). Similarly, the mRNA levels of CEMIP in CRC cells lines was upregulated in contrast to levels found in FHC cells ($P < 0.05$) (Figure 4C). Furthermore, Spearman's correlation analysis revealed CASC19 expression was positively correlated CEMIP mRNA expression in CRC tissues (Pearson $r = 0.809$, $P < 0.001$) (Figure 4D). Additionally, we examined the effect of CASC19 on CEMIP expression in SW480 and HCT-116 cell lines. The mRNA and protein levels of CEMIP were upregulated after CASC19 overexpression in both cell lines, while suppression of CASC19 expression decreased CEMIP protein and mRNA levels in the two cell lines ($P < 0.05$ for all).

It has been demonstrated that lncRNAs are able to bind directly to miRNA and function as ceRNAs^[40]. We next predicted miR-140-5p to be a potential target of CASC19 by using starBase v 2.0 program (<http://starbase.sysu.edu.cn/index.php>)^[38,39] (Figure 4F). We went on to examine the expression of miR-140-5p in CRC cell lines and tissues. CRC tissue samples were found to possess a much lower miR-140-5p level in contrast to adjacent healthy colonic mucosal tissues ($P < 0.05$) (Figure 4G).

Besides, miR-140-5p was suppressed in CRC cell lines in contrast to FHC cells ($P < 0.05$) (Figure 4G). CASC19 and miR-140-5p expression appeared to negatively correlate in CRC tissues, based on Spearman's correlation analysis (Pearson $r = -0.660$, $P < 0.001$) (Figure 4H). The anti-Ago2 RIP assay was performed to verify the presence of direct binding between CASC19 and miR-140-5p. Endogenous CASC19 was specifically enriched in miR-140-5p mimic transfected CRC cells in contrast to the NC mimic group ($P < 0.05$) (Figure 4I). A luciferase reporter assay was carried out to determine if CASC19 could directly target miR-140-5p. The luciferase activity was reduced in wild-type CASC19 3'-UTR and miR-140-5p mimic co-transfected 293T cells in comparison to wild-type CASC19 3'-UTR and miR-140-5p mimic NC co-transfected 293T cells ($P < 0.05$) (Figure 4J).

Interestingly, CEMIP is a potential target gene of miR-140-5p [predicted by TargetScan (http://www.targetscan.org/vert_71/) and miRBase (<http://www.mirbase.org/>)] (Figure 4K). Spearman's correlation analysis showed that CEMIP correlated negatively with miR-140-5p in CRC tissues (Pearson $r = -0.657$, $P < 0.001$) (Figure 4L). CEMIP is a direct target of miR-140-5p, as revealed by luciferase reporter assays (Figure 4M).

Furthermore, it was suggested that the CEMIP protein expression was downregulated in siCASC19 and NC inhibitor co-transfected CRC cells, a phenomenon which could be reversed with the addition of miR-140-5p inhibitor ($P < 0.05$) (Figure 4N). CEMIP expression was markedly raised after transfecting CRC cells with CASC19-p and NC mimic. Moreover, the effects of CASC19 were reversed by the addition of miR-140-5p mimic to CRC cell lines ($P < 0.05$) (Figure 4O). Collectively, these finding indicate that CASC19 is able to function as a ceRNA and indirectly regulate CEMIP expression by sponging miR-140-5p.

MiR-140-5p reverses the promoting effect of CASC19 on the proliferation and metastasizing ability of CRC cells

To confirm whether CASC19 exerts its function through sponging miR-140-5p in CRC

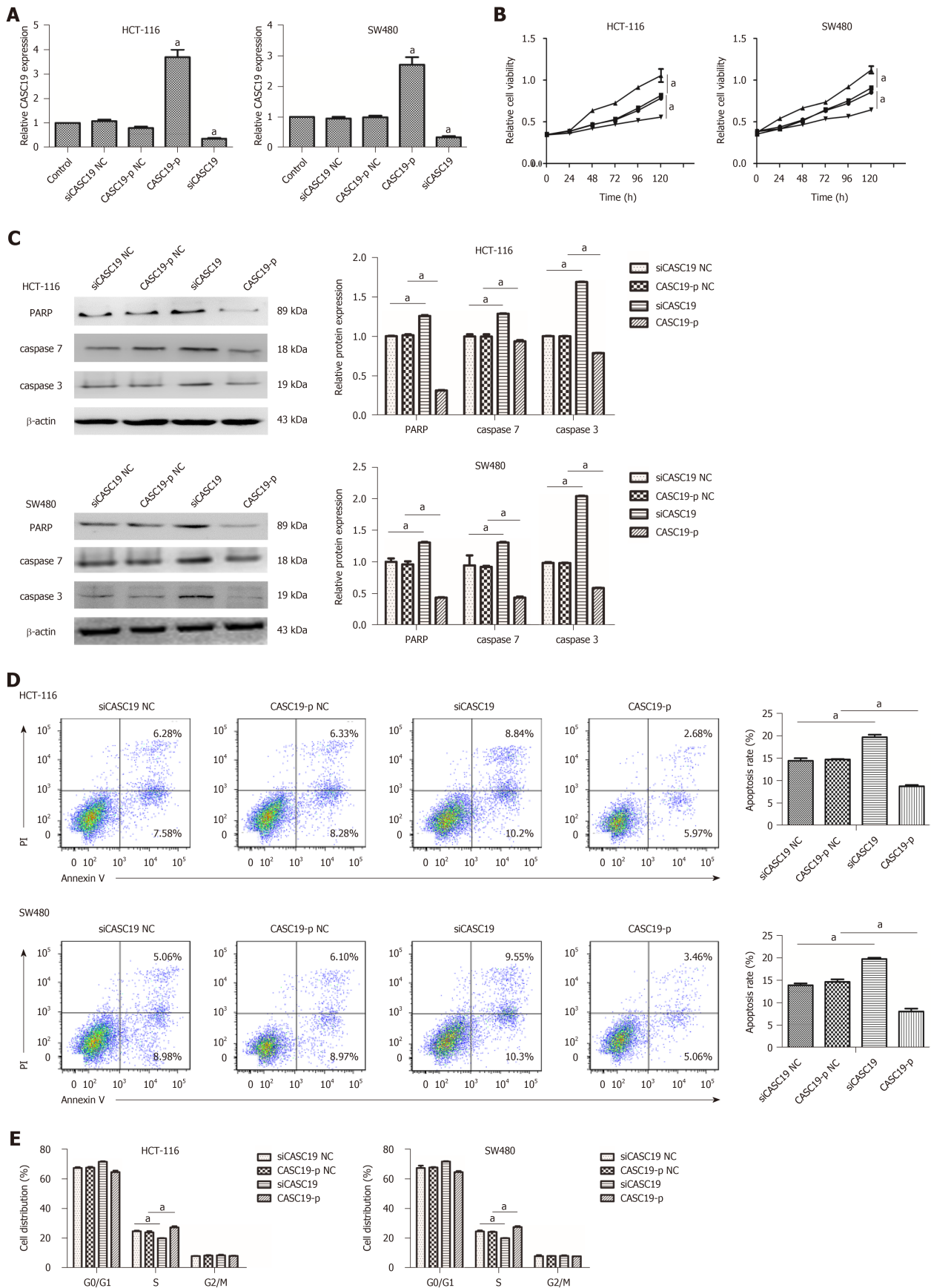


Figure 2 Role of cancer susceptibility 19 in the proliferation and migration of colorectal cancer cells. A: Expression of cancer susceptibility 19 (CASC19) in colorectal cancer (CRC) cells transfected with siCASC19 or CASC19-p and their NCs was quantified by quantitative real-time PCR. B: Growth curves of HCT-116 and SW480 cell lines that were transfected with CASC19-p or siCASC19 were analyzed using the Cell Counting Kit-8 assay. C: Western blot was used to determine the expression of caspase 3, caspase 7, and PARP in HCT-116 and SW480 cells that were transfected with either CASC19-p or siCASC19. The grayscale value of proteins was measured with Image J. D: Cell apoptosis rate was detected by flow cytometry after transfection with CASC19-p or siCASC19. E: The proportion of cells in each cell cycle phase was detected using flow cytometry after cells were transfected with CASC19-p or siCASC19. Data are reported as the mean \pm SD. $^aP < 0.05$.

CASC19: Cancer susceptibility 19; CRC: Colorectal cancer.

tissues, CCK-8 and transwell assays were performed. Results demonstrated that knockdown of CASC19 or CEMIP expression significantly inhibited the proliferation and invasion of HCT-116 and SW480 cells ($P < 0.05$) (Figure 5A-D). The addition of miR-140-5p inhibitor reversed this effect. Moreover, miR-140-5p inhibitor was able to promote the proliferation and invasion abilities of cells. Conversely, overexpression of CASC19 or CEMIP in the cell lines promoted the proliferative and invasive capacities of HCT-116 and SW480 cells, with this effect reversed by miR-140-5p mimic. Furthermore, miR-140-5p alone significantly inhibited the proliferative and invasive capacities of both cell lines ($P < 0.05$) (Figure 5A-D). Lastly, the expression of E-cadherin and vimentin in transfected CRC cells was analyzed. Consistent with the previous results, the effect of knockdown or overexpression of CASC19 on the expression of the markers was reversed by miR-140-5p inhibitor or miR-140-5p mimic (Figure 5E and F). These data suggested that miR-140-5p is able to counteract the effect of CASC19 on the growth and metastasizing abilities of CRC cells *in vitro*.

DISCUSSION

Studies have confirmed that dysregulation of lncRNAs is closely related to the occurrence and development of various tumors. lncRNAs may become potential targets for the development of future chemotherapeutic medications^[41,42]. Therefore, studying the clinical significance and function of lncRNA along with its possible mechanisms of action may contribute towards the gene therapy in cancer. Recently, researchers have demonstrated that lncRNAs are involved in the progression of CRC. For instance, the lncRNA SUMO1P3 drives CRC growth and metastasis^[16,43,44]. Lymph node metastasis and poor CRC prognosis have been linked to the upregulation of the lncRNA BANC1^[43]. The lncRNA HAND2-AS1 sponging miR-1275 suppresses CRC progression by upregulating KLF14^[44]. Previous studies demonstrate that the lncRNA CASC19 may promote the progression of several cancers, and it has been suggested that CASC19 may function as a biomarker for CRC poor prognosis^[24,45]. Therefore, it is necessary to study the function of CASC19 in CRC. In our study, it was observed that the expression of CASC19 was greatly raised in both CRC cell lines and tissue samples. This result is consistent with previous results, which suggests that CASC19 may be an important lncRNA that regulates CRC heterogeneity. Given that the cellular location of CASC19 was related to lncRNA function, we examined the subcellular distribution of CASC19 using cellular fractionation. Cellular localization showed that CASC19 was mostly located in the cellular plasma, indicating that CASC19 may function to sponge miRNA.

Heterogeneity is a key property that is responsible for malignant processes such as initiation, migration, and metastasis of cancer. One example is the lncRNA HOTAIR that may promote the progression of a variety of cancers by affecting the proliferation, migration, and invasion of various cancer cells^[46]. Knockdown of the lncRNA LCPAT1 inhibits autophagy in lung cancer^[47]. The lncRNA PVT1 may promote ovarian cancer progression^[48]. These data suggest that lncRNAs are emerging as crucial cancer regulators. Correlation analysis showed that high expression of CASC19 was associated with CRC metastasis. Thus, we speculated that CASC19 may be correlated with CRC progression. As we expected, *in vitro* experiments showed that CASC19 promoted CRC progression.

It has been demonstrated that lncRNAs may function as ceRNAs by sponging miRNAs^[49]. For example, HOTAIR promotes renal cell carcinoma progression via absorbing miR-138^[50]. The lncRNA SNHG7 sponges miR-216b to upregulate GALNT1, leading ultimately to the promotion of CRC cell proliferation and liver metastasis^[51]. Previously, miR-140-5p was observed to be expressed abnormally in several malignancies including CRC^[52], breast cancer^[53], ovarian cancer^[54], glioma^[55], and gastric cancer^[56]. Similar to previous studies, our study revealed that CASC19 may promote CRC by targeting miR-140-5p. The current investigations revealed that CASC19 directly targets miR-140-5p. Importantly, there was an endogenous interaction between these two molecules in CRC cells. Moreover, inhibiting proliferation and invasion and promoting apoptosis of cancer cells are known to involve miR-140-5p^[55,57]. These studies suggest that miR-140-5p may play a tumor suppressive role in different tumors. However, literature is scarce regarding its role in CRC. Our results demonstrated that miR-140-5p was markedly reduced in CRC cell lines and tissue samples. In addition, miR-140-5p reversed the function of CASC19 in

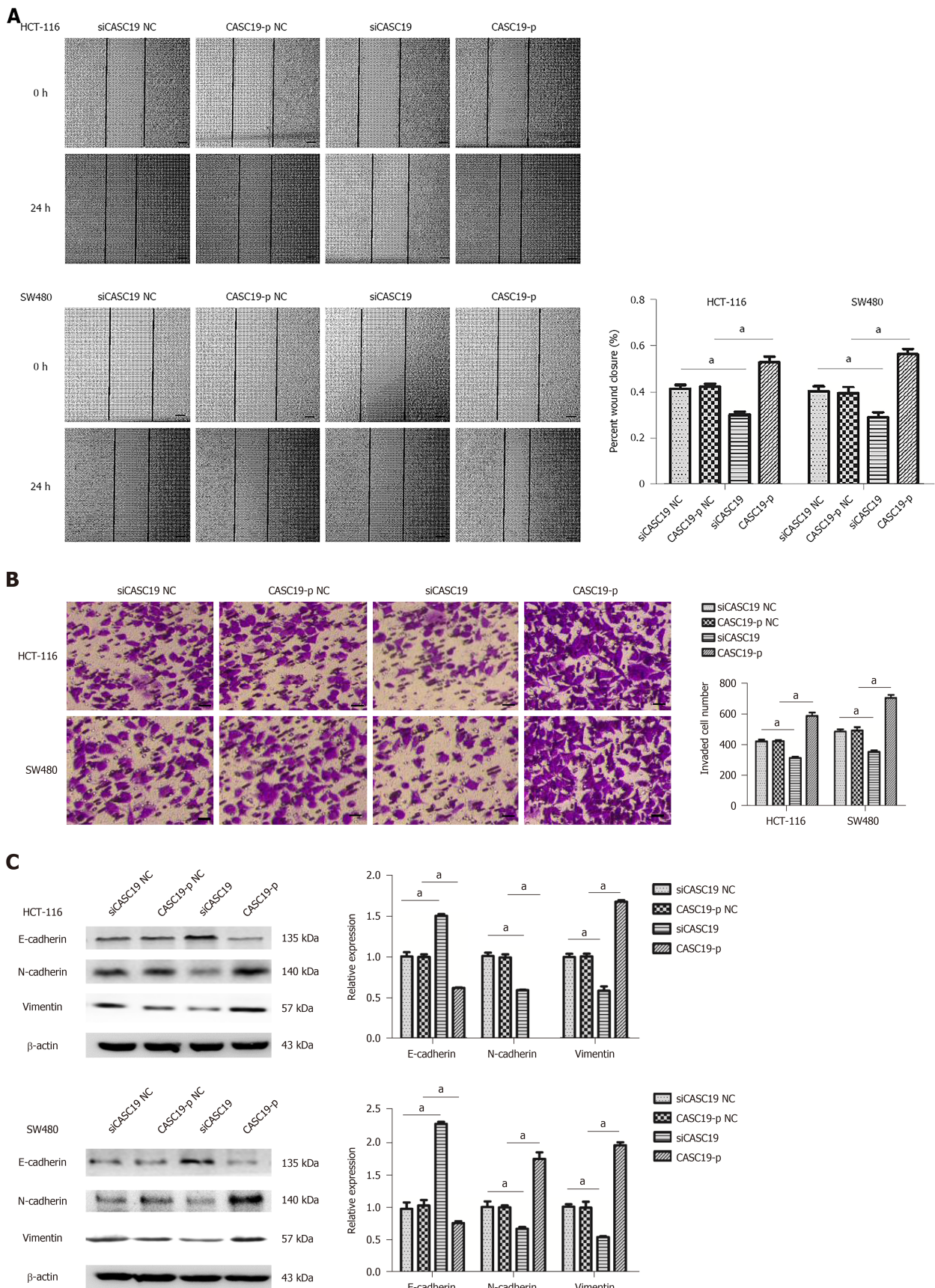


Figure 3 Role of cancer susceptibility 19 in the cell migration, invasion, and epithelial-mesenchymal transition in colorectal cancer cells. A: The migration abilities of SW480 and HCT-116 cells were analyzed by wound-healing assay after the cells were transfected with CASC19-p or siCASC19. Scale bars = 100 μ m. B: The invasion abilities of SW480 and HCT-116 were determined by transwell assay after the cells were transfected with CASC19-p or siCASC19. Scale bars = 20 μ m. C: The expression of vimentin, N-cadherin, and E-cadherin in HCT-116 and SW480 cells was detected by Western blot after transfection with CASC19-p or siCASC19. The grayscale value of protein was measured with Image J. Data are reported as the mean \pm SD. * P < 0.05. CASC19: Cancer susceptibility 19.

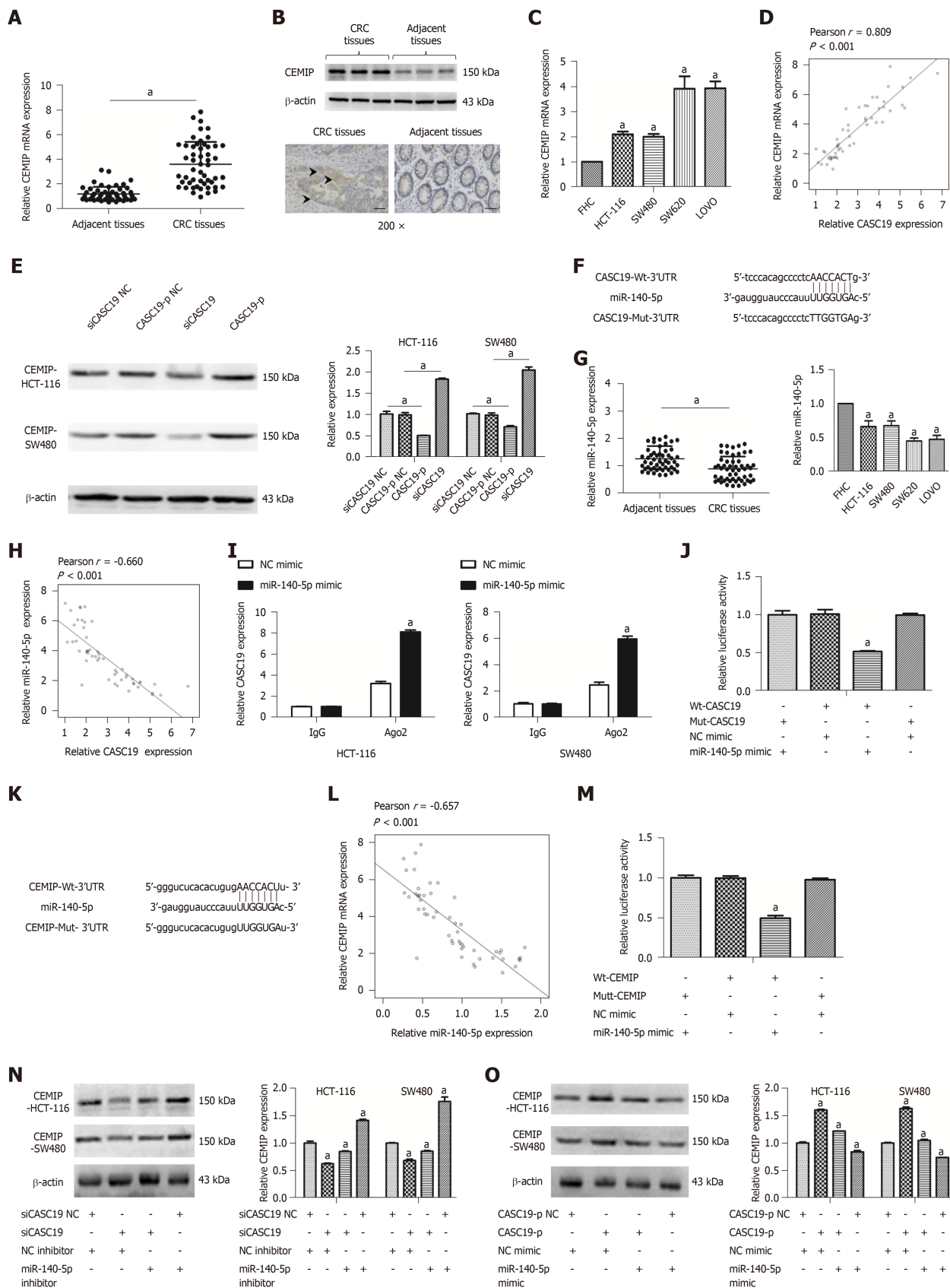


Figure 4 Cancer susceptibility 19 acts as a competing endogenous RNA by sponging miR-140-5p to regulate cell migration inducing hyaluronidase 1 expression. A: Differential mRNA expression of cell migration inducing hyaluronidase 1 (CEMIP) in colorectal cancer (CRC) tissues and adjacent healthy colonic mucosa tissues was determined by quantitative real-time PCR (qRT-PCR). B: Differential protein expression of CEMIP in CRC tissues and adjacent healthy colonic mucosa tissues was analyzed using Western blot and immunohistochemistry. C: Differential mRNA expression of CEMIP in CRC cell lines and FHC cells was determined by qRT-PCR. D: Cancer susceptibility 19 (CASC19) and CEMIP correlated positively in CRC tissues, based on Pearson's correlation curve. E: Protein expression of CEMIP in SW480 and HCT-116 cells was determined by Western blot after transfection with CASC19-p or siCASC19. The grayscale value of protein was measured with Image J. F: Predicted binding sites of miR-140-5p in the CASC19 sequence. G: Differential expression of miR-140-5p in CRC tissues and adjacent healthy

colonic mucosa tissues, CRC cell lines, and FHC cells was determined by qRT-PCR. H: CASC19 and miR-140-5p correlated negatively in CRC tissues, as determined by Pearson's correlation curve. I: RNA-IP was performed in SW480 and HCT-116 cells and CASC19 expression was determined by qRT-PCR. J: Luciferase reporter assay verified miR-140-5p to be a direct target of CASC19. K: Predicted binding sites of miR-140-5p in the CEMIP mRNA sequence. L: CEMIP and miR-140-5p correlated negatively in CRC tissues, based on Pearson's correlation curve. M: Luciferase reporter assay verified CEMIP to be a direct target of miR-140-5p. N: CEMIP expression in SW480 and HCT-116 cells transfected with miR-140-5p mimic or siCASC19 was determined by Western blot and qRT-PCR. O: The expression of CEMIP in SW480 and HCT-116 cells transfected with miR-140-5p inhibitor or CASC19-p was determined by Western blot and qRT-PCR. Data are reported as the mean \pm SD. ^a $P < 0.05$. CASC19: Cancer susceptibility 19; CRC: Colorectal cancer; CEMIP: Cell migration inducing hyaluronidase 1.

CRC cell lines. These results suggest that CASC19 sponging of miR-140-5p may be a mechanism regulating the heterogeneity of CRC. Given that miRNAs are known to simultaneously control the expression of a broad range of genes, our working hypothesis was that miR-140-5p may target different genes in different cell lines, resulting in varying phenotypes. Therefore, we examined the target genes predicted and found out that CEMIP may be a target gene of miR-140-5p in CRC.

Tumor malignancy is driven by its almost limitless capability for proliferation and metastasis. CEMIP was initially known as an enzyme to depolymerize hyaluronic acid. Further studies reveal CEMIP overexpression to be a common phenomenon in several tumors. For instance, CEMIP drives breast cancer progression and predicts poor prognosis in pancreatic ductal adenocarcinoma^[31,32]. In CRC, tumor metastasis and invasion are able to be suppressed through the miR-216a-mediated attenuation of CEMIP^[58]. CEMIP therefore may be associated with the progression of CRC. Previous studies have demonstrated that CEMIP may interact with the glycogen phosphorylase kinase β -subunit (PHKB) to promote cancer cell survival by breakdown of glycogen^[59]. In CRC tissues, the tumor cells are exposed to a nutrient deprivation and hypoxia environment^[60]. Energy deprivation is one of the main courses of cell death. It has been demonstrated that glycogen accumulation contributes to cell survival when cancer cells expose to hypoxia^[61-63]. At the same time, glycogen lysis is an important process for cell survival. CEMIP overexpressing tumor cells have relatively low glycogen content, while the survival rate of these cells is relatively high. CEMIP may play a vital role in CRC survival and metastasis. Many differing miR-140-5p targets, such as YES1^[56], Wnt1^[64], and VEGFA^[65], have been documented to be associated with cell invasion and migration. In our study, we observed that CASC19 functions as a ceRNA, controlling the availability of miR-140-5p that can be acted on by the CEMIP gene. The current investigations focused on CEMIP, which was found to have strong associations with CASC19 and cancer cell survival. Our results strongly suggest that CASC19 may regulate CEMIP expression via sponging of miR-140-5p.

In conclusion, CASC19 overexpression augmented CRC cell proliferation and metastasizing abilities *in vitro*. Our study is the first to report a novel mechanism for CASC19 in CRC. CASC19 exerted its effects partially through the CASC19/miR-140-5p/CEMIP axis. Investigation of this CASC19/miR-140-5p/CEMIP pathway allows a deeper understanding of the pathogenesis of CRC, with the members of this pathway serving as useful targets for future preventive and therapeutic innovations in the management of CRC.

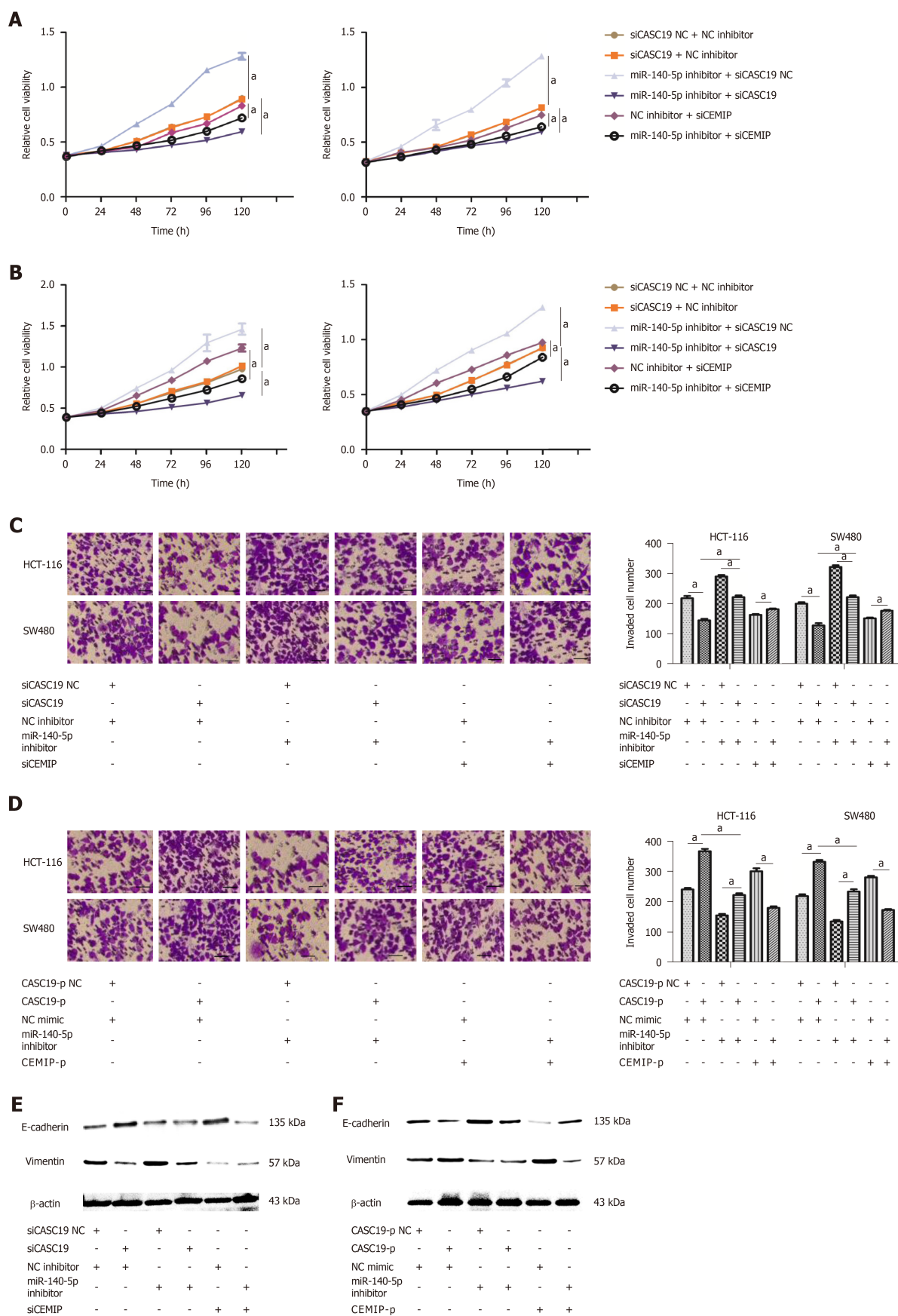


Figure 5 MiR-140-5p suppresses cancer susceptibility 19-induced enhancement of colorectal cancer cell proliferation and metastasis. A: Growth curves of SW480 and HCT-116 cell lines after being transfected by either miR-140-5p inhibitor or siCASC19 were determined by the Cell Counting Kit-8 (CCK-8) assay. B: Growth curves of SW480 and HCT-116 cell lines after being transfected by either miR-140-5p mimic or CASC19-p were analyzed by the CCK-8 assay. C: The number of invading HCT-116 and SW480 cells was determined by transwell assay after being transfected by either miR-140-5p inhibitor or siCASC19. Scale bars = 20 μ m. D: The number of invading HCT-116 and SW480 cells was determined by transwell assay after being transfected with either miR-140-5p mimic or CASC19-p. Scale bars = 20 μ m. E: The expression of E-cadherin and vimentin in CRC cells was determined by Western blot after being transfected by either miR-140-5p inhibitor or

siCASC19. F: The expression of E-cadherin and vimentin in CRC cells was determined by Western blot after being transfected with either miR-140-5p mimic or CASC19-p. Data are reported as the mean \pm SD. * $P < 0.05$. CASC19: Cancer susceptibility; CRC: Colorectal cancer; CEMIP: Cell migration inducing hyaluronidase 1.

ARTICLE HIGHLIGHTS

Research background

There is increasing evidence that long non-coding RNAs (lncRNAs) play an important role in tumor progression. The lncRNA cancer susceptibility 19 (CASC19) is highly expressed in colorectal cancer (CRC) tissues, and may be associated with colon cancer progression. However, there has been no experimental evidence regarding the function of CASC19 in CRC.

Research motivation

Investigation of the functions of the lncRNA CASC19 may suggest potential molecular mechanisms of CRC carcinogenesis and progression, and may further offer the potential for future preventive and therapeutic innovations in the management of CRC.

Research objectives

We measured the lncRNA CASC19 expression in CRC tissues and pair-matched adjacent non-tumor tissues, and investigated biological functions and the possible molecular mechanisms of CASC19 in CRC.

Research methods

We detected CASC19 expression in CRC tissues and pair-matched adjacent non-tumor tissues using quantitative real-time PCR. The biological behavior of CASC19 *in vitro* was then assessed by overexpression and knockdown of the expression of CASC19. In further molecular mechanism studies, we confirmed the possible molecular mechanisms by which CASC19 plays a role by overexpression and knockdown of the expression of downstream molecules of CASC19.

Research results

The lncRNA CASC19 was upregulated in CRC tissue, which was related to tumor stage and metastasis. The lncRNA CASC19 had a role of promoting proliferation, metastasizing ability, and epithelial-mesenchymal transition, and inhibiting apoptosis by regulating microRNA 140-5p/cell migration inducing hyaluronidase 1 (miR-140-5p/CEMIP) expression in CRC cells.

Research conclusions

The lncRNA CASC 19 is overexpressed in CRC tissues and cell lines, which could promote CRC progression through regulating miR-140-5p/CEMIP.

Research perspectives

Members of the CASC19/miR-140-5p/CEMIP axis may serve as useful targets for future preventive and therapeutic innovations in the management of CRC.

REFERENCES

- 1 Siegel RL, Miller KD, Jemal A. Cancer statistics, 2018. *CA Cancer J Clin* 2018; **68**: 7-30 [PMID: 29313949 DOI: 10.3322/caac.21442]
- 2 Garden OJ, Rees M, Poston GJ, Mirza D, Saunders M, Ledermann J, Primrose JN, Parks RW. Guidelines for resection of colorectal cancer liver metastases. *Gut* 2006; **55** Suppl 3: iii1-iii8 [PMID: 16835351 DOI: 10.1136/gut.2006.098053]
- 3 Gallagher DJ, Kemeny N. Metastatic colorectal cancer: from improved survival to potential cure. *Oncology* 2010; **78**: 237-248 [PMID: 20523084 DOI: 10.1159/000315730]
- 4 Liang C, Sun W, He H, Zhang B, Ling C, Wang B, Huang T, Hou B, Guo Y. Antitumor effect of a new nano-vector with miRNA-135a on malignant glioma. *Int J Nanomedicine* 2017; **13**: 209-220 [PMID: 29343959 DOI: 10.2147/IJN.S148142]
- 5 Gomez JA, Wapinski OL, Yang YW, Bureau JF, Gopinath S, Monack DM, Chang HY, Brahic M, Kirkegaard K. The NeST long ncRNA controls microbial susceptibility and epigenetic activation of the interferon- γ locus. *Cell* 2013; **152**: 743-754 [PMID: 23415224 DOI: 10.1016/j.cell.2013.01.015]
- 6 Lee JT. Epigenetic regulation by long noncoding RNAs. *Science* 2012; **338**: 1435-1439 [PMID: 23239728 DOI: 10.1126/science.1231776]
- 7 Li S, Wang Q, Qiang Q, Shan H, Shi M, Chen B, Zhao S, Yuan L. Sp1-mediated transcriptional regulation of MALAT1 plays a critical role in tumor. *J Cancer Res Clin Oncol* 2015; **141**: 1909-1920 [PMID: 25773124 DOI: 10.1007/s00432-015-1951-0]
- 8 Xue WH, Fan ZR, Li LF, Lu JL, Ma BJ, Kan QC, Zhao J. Construction of an oesophageal cancer-specific ceRNA network based on miRNA, lncRNA, and mRNA expression data. *World J Gastroenterol* 2018; **24**: 23-34 [PMID: 29358879 DOI: 10.3748/wjg.v24.i1.23]
- 9 Ma J, Li T, Han X, Yuan H. Knockdown of lncRNA ANRIL suppresses cell proliferation, metastasis, and invasion via regulating miR-122-5p expression in hepatocellular carcinoma. *J Cancer Res Clin Oncol* 2018; **144**: 205-214 [PMID: 29127494 DOI: 10.1007/s00432-017-2543-y]
- 10 Xiao JN, Yan TH, Yu RM, Gao Y, Zeng WL, Lu SW, Que HX, Liu ZP, Jiang JH. Long non-coding RNA UCA1 regulates the expression of Snail2 by miR-203 to promote hepatocellular carcinoma progression. *J Cancer Res Clin Oncol* 2017; **143**: 981-990 [PMID: 28271214 DOI: 10.1007/s00432-017-2370-1]

- 11 **Wang BG**, Xu Q, Lv Z, Fang XX, Ding HX, Wen J, Yuan Y. Association of twelve polymorphisms in three onco-lncRNA genes with hepatocellular cancer risk and prognosis: A case-control study. *World J Gastroenterol* 2018; **24**: 2482-2490 [PMID: 29930469 DOI: 10.3748/wjg.v24.i23.2482]
- 12 **Zheng S**, Zheng D, Dong C, Jiang J, Xie J, Sun Y, Chen H. Development of a novel prognostic signature of long non-coding RNAs in lung adenocarcinoma. *J Cancer Res Clin Oncol* 2017; **143**: 1649-1657 [PMID: 28409273 DOI: 10.1007/s00432-017-2411-9]
- 13 **Pan L**, Liang W, Fu M, Huang ZH, Li X, Zhang W, Zhang P, Qian H, Jiang PC, Xu WR, Zhang X. Exosomes-mediated transfer of long noncoding RNA ZFAS1 promotes gastric cancer progression. *J Cancer Res Clin Oncol* 2017; **143**: 991-1004 [PMID: 28285404 DOI: 10.1007/s00432-017-2361-2]
- 14 **Lu M**, Liu Z, Li B, Wang G, Li D, Zhu Y. The high expression of long non-coding RNA PANDAR indicates a poor prognosis for colorectal cancer and promotes metastasis by EMT pathway. *J Cancer Res Clin Oncol* 2017; **143**: 71-81 [PMID: 27629879 DOI: 10.1007/s00432-016-2252-y]
- 15 **Ping G**, Xiong W, Zhang L, Li Y, Zhang Y, Zhao Y. Silencing long noncoding RNA PVT1 inhibits tumorigenesis and cisplatin resistance of colorectal cancer. *Am J Transl Res* 2018; **10**: 138-149 [PMID: 29423000]
- 16 **Zhang LM**, Wang P, Liu XM, Zhang YJ. LncRNA SUMO1P3 drives colon cancer growth, metastasis and angiogenesis. *Am J Transl Res* 2017; **9**: 5461-5472 [PMID: 29312498]
- 17 **Yang S**, Sun Z, Zhou Q, Wang W, Wang G, Song J, Li Z, Zhang Z, Chang Y, Xia K, Liu J, Yuan W. MicroRNAs, long noncoding RNAs, and circular RNAs: potential tumor biomarkers and targets for colorectal cancer. *Cancer Manag Res* 2018; **10**: 2249-2257 [PMID: 30100756 DOI: 10.2147/CMAR.S166308]
- 18 **Liang Y**, Zhang C, Ma MH, Dai DQ. Identification and prediction of novel non-coding and coding RNA-associated competing endogenous RNA networks in colorectal cancer. *World J Gastroenterol* 2018; **24**: 5259-5270 [PMID: 30581274 DOI: 10.3748/wjg.v24.i46.5259]
- 19 **Fan H**, Lv P, Mu T, Zhao X, Liu Y, Feng Y, Lv J, Liu M, Tang H. LncRNA n335586/miR-924/CKMT1A axis contributes to cell migration and invasion in hepatocellular carcinoma cells. *Cancer Lett* 2018; **429**: 89-99 [PMID: 29753758 DOI: 10.1016/j.canlet.2018.05.010]
- 20 **Zhou Y**, Dai W, Wang H, Pan H, Wang Q. Long non-coding RNA CASP5 promotes the malignant phenotypes of human glioblastoma multiforme. *Biochem Biophys Res Commun* 2018; **500**: 966-972 [PMID: 29715460 DOI: 10.1016/j.bbrc.2018.04.217]
- 21 **He Z**, You C, Zhao D. Long non-coding RNA UCA1/miR-182/PFKFB2 axis modulates glioblastoma-associated stromal cells-mediated glycolysis and invasion of glioma cells. *Biochem Biophys Res Commun* 2018; **500**: 569-576 [PMID: 29655792 DOI: 10.1016/j.bbrc.2018.04.091]
- 22 **Yu X**, Zhao J, He Y. Long non-coding RNA PVT1 functions as an oncogene in human colon cancer through miR-30d-5p/RUNX2 axis. *J BUON* 2018; **23**: 48-54 [PMID: 29552759]
- 23 **Wang JJ**, Li XM, He L, Zhong SZ, Peng YX, Ji N. Expression and Function of Long Non-coding RNA CASC19 in Colorectal Cancer. *Zhongguo Yi Xue Ke Xue Yuan Xue Bao* 2017; **39**: 756-761 [PMID: 29338818 DOI: 10.3881/j.issn.1000-503X.2017.06.004]
- 24 **Ozawa T**, Matsuyama T, Toiyama Y, Takahashi N, Ishikawa T, Uetake H, Yamada Y, Kusunoki M, Calin G, Goel A. CCAT1 and CCAT2 long noncoding RNAs, located within the 8q.24.21 'gene desert', serve as important prognostic biomarkers in colorectal cancer. *Ann Oncol* 2017; **28**: 1882-1888 [PMID: 28838211 DOI: 10.1093/annonc/mdx248]
- 25 **Yamada A**, Yu P, Lin W, Okugawa Y, Boland CR, Goel A. A RNA-Sequencing approach for the identification of novel long non-coding RNA biomarkers in colorectal cancer. *Sci Rep* 2018; **8**: 575 [PMID: 29330370 DOI: 10.1038/s41598-017-18407-6]
- 26 **Abe S**, Usami S, Nakamura Y. Mutations in the gene encoding KIAA1199 protein, an inner-ear protein expressed in Deiters' cells and the fibrocytes, as the cause of nonsyndromic hearing loss. *J Hum Genet* 2003; **48**: 564-570 [PMID: 14577002 DOI: 10.1007/s10038-003-0079-2]
- 27 **Yoshida H**, Nagaoka A, Kusaka-Kikushima A, Tobiishi M, Kawabata K, Sayo T, Sakai S, Sugiyama Y, Enomoto H, Okada Y, Inoue S. KIAA1199, a deafness gene of unknown function, is a new hyaluronan binding protein involved in hyaluronan depolymerization. *Proc Natl Acad Sci USA* 2013; **110**: 5612-5617 [PMID: 23509262 DOI: 10.1073/pnas.1215432110]
- 28 **Zhang P**, Song Y, Sun Y, Li X, Chen L, Yang L, Xing Y. AMPK/GSK3 β / β -catenin cascade-triggered overexpression of CEMIP promotes migration and invasion in anoikis-resistant prostate cancer cells by enhancing metabolic reprogramming. *FASEB J* 2018; **32**: 3924-3935 [PMID: 29505302 DOI: 10.1096/fj.201701078R]
- 29 **Matsuzaki S**, Tanaka F, Mimori K, Tahara K, Inoue H, Mori M. Clinicopathologic significance of KIAA1199 overexpression in human gastric cancer. *Ann Surg Oncol* 2009; **16**: 2042-2051 [PMID: 19434458 DOI: 10.1245/s10434-009-0469-6]
- 30 **Fink SP**, Myeroff LL, Kariv R, Platzer P, Xin B, Mikkola D, Lawrence E, Morris N, Nosrati A, Willson JK, Willis J, Veigl M, Barnholtz-Sloan JS, Wang Z, Markowitz SD. Induction of KIAA1199/CEMIP is associated with colon cancer phenotype and poor patient survival. *Oncotarget* 2015; **6**: 30500-30515 [PMID: 26437221 DOI: 10.18632/oncotarget.5921]
- 31 **Koga A**, Sato N, Kohi S, Yabuki K, Cheng XB, Hisaoka M, Hirata K. KIAA1199/CEMIP/HYBID overexpression predicts poor prognosis in pancreatic ductal adenocarcinoma. *Pancreatol* 2017; **17**: 115-122 [PMID: 28012880 DOI: 10.1016/j.pan.2016.12.007]
- 32 **Shostak K**, Zhang X, Hubert P, Göktuna SI, Jiang Z, Klevernic I, Hildebrand J, Roncarati P, Hennuy B, Ladang A, Somja J, Gothot A, Close P, Delvenne P, Chariot A. NF- κ B-induced KIAA1199 promotes survival through EGFR signalling. *Nat Commun* 2014; **5**: 5232 [PMID: 25366117 DOI: 10.1038/ncomms6232]
- 33 **Evensen NA**, Kusec C, Nguyen HL, Zarrabi K, Dufour A, Kadam P, Hu YJ, Pulkoski-Gross A, Bahou WF, Zucker S, Cao J. Unraveling the role of KIAA1199, a novel endoplasmic reticulum protein, in cancer cell migration. *J Natl Cancer Inst* 2013; **105**: 1402-1416 [PMID: 23990668 DOI: 10.1093/jnci/djt224]
- 34 **Liang G**, Fang X, Yang Y, Song Y. Knockdown of CEMIP suppresses proliferation and induces apoptosis in colorectal cancer cells: downregulation of GRP78 and attenuation of unfolded protein response. *Biochem Cell Biol* 2018; **96**: 332-341 [PMID: 29024602 DOI: 10.1139/bcb-2017-0151]
- 35 **Ding M**, Bowman L, Castranova V. Luciferase reporter system for studying the effect of nanoparticles on gene expression. *Methods Mol Biol* 2012; **906**: 403-414 [PMID: 22791452 DOI: 10.1007/978-1-61779-953-2_33]
- 36 **Mattheolabakis G**, Wang R, Rigas B, Mackenzie GG. Phospho-valproic acid inhibits pancreatic cancer growth in mice: enhanced efficacy by its formulation in poly-(L)-lactic acid-poly(ethylene glycol)

- nanoparticles. *Int J Oncol* 2017; **51**: 1035-1044 [PMID: 28849098 DOI: 10.3892/ijo.2017.4103]
- 37 **Wang X**, Lu J, Cao J, Ma B, Gao C, Qi F. MicroRNA-18a promotes hepatocellular carcinoma proliferation, migration, and invasion by targeting Bcl2L10. *Onco Targets Ther* 2018; **11**: 7919-7934 [PMID: 30519035 DOI: 10.2147/OTT.S180971]
- 38 **Li JH**, Liu S, Zhou H, Qu LH, Yang JH. starBase v2.0: decoding miRNA-ceRNA, miRNA-ncRNA and protein-RNA interaction networks from large-scale CLIP-Seq data. *Nucleic Acids Res* 2014; **42**: D92-D97 [PMID: 24297251 DOI: 10.1093/nar/gkt1248]
- 39 **Yang JH**, Li JH, Shao P, Zhou H, Chen YQ, Qu LH. starBase: a database for exploring microRNA-mRNA interaction maps from Argonaute CLIP-Seq and Degradome-Seq data. *Nucleic Acids Res* 2011; **39**: D202-D209 [PMID: 21037263 DOI: 10.1093/nar/gkq1056]
- 40 **Zhou X**, Gao Q, Wang J, Zhang X, Liu K, Duan Z. Linc-RNA-RoR acts as a "sponge" against mediation of the differentiation of endometrial cancer stem cells by microRNA-145. *Gynecol Oncol* 2014; **133**: 333-339 [PMID: 24589415 DOI: 10.1016/j.ygyno.2014.02.033]
- 41 **Li Y**, Duo Y, Bi J, Zeng X, Mei L, Bao S, He L, Shan A, Zhang Y, Yu X. Targeted delivery of anti-miR-155 by functionalized mesoporous silica nanoparticles for colorectal cancer therapy. *Int J Nanomedicine* 2018; **13**: 1241-1256 [PMID: 29535520 DOI: 10.2147/IJN.S158290]
- 42 **Küçüktürkmen B**, Bozkır A. Development and characterization of cationic solid lipid nanoparticles for co-delivery of pemetrexed and miR-21 antisense oligonucleotide to glioblastoma cells. *Drug Dev Ind Pharm* 2018; **44**: 306-315 [PMID: 29023168 DOI: 10.1080/03639045.2017.1391835]
- 43 **Shen X**, Bai Y, Luo B, Zhou X. Upregulation of lncRNA BANCRC associated with the lymph node metastasis and poor prognosis in colorectal cancer. *Biol Res* 2017; **50**: 32 [PMID: 28969673 DOI: 10.1186/s40659-017-0136-5]
- 44 **Zhou J**, Lin J, Zhang H, Zhu F, Xie R. LncRNA HAND2-AS1 sponging miR-1275 suppresses colorectal cancer progression by upregulating KLF14. *Biochem Biophys Res Commun* 2018; **503**: 1848-1853 [PMID: 30078677 DOI: 10.1016/j.bbrc.2018.07.125]
- 45 **Teerlink CC**, Leongamornlert D, Dadaev T, Thomas A, Farnham J, Stephenson RA, Riska S, McDonnell SK, Schaid DJ, Catalona WJ, Zheng SL, Cooney KA, Ray AM, Zuhlke KA, Lange EM, Giles GG, Southey MC, Fitzgerald LM, Rinckleb A, Luedeke M, Maier C, Stanford JL, Ostrander EA, Kaikkonen EM, Sipeky C, Tammela T, Schleutker J, Wiley KE, Isaacs SD, Walsh PC, Isaacs WB, Xu J, Cancel-Tassin G, Cussenot O, Mandal D, Laurie C, Laurie C, Thibodeau SN, Eeles RA, Kote-Jarai Z, Cannon-Albright L; PRACTICAL consortium; International Consortium for Prostate Cancer Genetics. Genome-wide association of familial prostate cancer cases identifies evidence for a rare segregating haplotype at 8q24.21. *Hum Genet* 2016; **135**: 923-938 [PMID: 27262462 DOI: 10.1007/s00439-016-1690-6]
- 46 **Hajjari M**, Salavaty A. HOTAIR: an oncogenic long non-coding RNA in different cancers. *Cancer Biol Med* 2015; **12**: 1-9 [PMID: 25859406 DOI: 10.7497/j.issn.2095-3941.2015.0006]
- 47 **Yu X**, Ye X, Lin H, Feng N, Gao S, Zhang X, Wang Y, Yu H, Deng X, Qian B. Knockdown of long non-coding RNA *LCPAT1* inhibits autophagy in lung cancer. *Cancer Biol Med* 2018; **15**: 228-237 [PMID: 30197790 DOI: 10.20892/j.issn.2095-3941.2017.0150]
- 48 **Chen Y**, Du H, Bao L, Liu W. LncRNA PVT1 promotes ovarian cancer progression by silencing miR-214. *Cancer Biol Med* 2018; **15**: 238-250 [PMID: 30197791 DOI: 10.20892/j.issn.2095-3941.2017.0174]
- 49 **Salmena L**, Poliseno L, Tay Y, Kats L, Pandolfi PP. A ceRNA hypothesis: the Rosetta Stone of a hidden RNA language? *Cell* 2011; **146**: 353-358 [PMID: 21802130 DOI: 10.1016/j.cell.2011.07.014]
- 50 **Ding J**, Yeh CR, Sun Y, Lin C, Chou J, Ou Z, Chang C, Qi J, Yeh S. Estrogen receptor β promotes renal cell carcinoma progression via regulating lncRNA HOTAIR-miR-138/200c/204/217 associated CeRNA network. *Oncogene* 2018; **37**: 5037-5053 [PMID: 29789714 DOI: 10.1038/s41388-018-0175-6]
- 51 **Shan Y**, Ma J, Pan Y, Hu J, Liu B, Jia L. LncRNA SNHG7 sponges miR-216b to promote proliferation and liver metastasis of colorectal cancer through upregulating GALNT1. *Cell Death Dis* 2018; **9**: 722 [PMID: 29915311 DOI: 10.1038/s41419-018-0759-7]
- 52 **Zhai H**, Fesler A, Ba Y, Wu S, Ju J. Inhibition of colorectal cancer stem cell survival and invasive potential by hsa-miR-140-5p mediated suppression of Smad2 and autophagy. *Oncotarget* 2015; **6**: 19735-19746 [PMID: 25980495 DOI: 10.18632/oncotarget.3771]
- 53 **Güllü G**, Peker I, Haholu A, Eren F, Küçükodaci Z, Güleç B, Baloglu H, Erzik C, Özer A, Akkiprik M. Clinical significance of miR-140-5p and miR-193b expression in patients with breast cancer and relationship to IGFBP5. *Genet Mol Biol* 2015; **38**: 21-29 [PMID: 25983620 DOI: 10.1590/S1415-475738120140167]
- 54 **Lan H**, Chen W, He G, Yang S. miR-140-5p inhibits ovarian cancer growth partially by repression of PDGFRA. *Biomed Pharmacother* 2015; **75**: 117-122 [PMID: 26297547 DOI: 10.1016/j.biopha.2015.07.035]
- 55 **Cui Y**, Yi L, Zhang MM, Zhou Y, Tan ZG, Huang T, Jiang YG. WITHDRAWN: Knockdown of lncRNA HOXA11 Antisense Promotes Glioma Cell Apoptosis Via Sponging MiR-140-5p. *Oncol Res* 2017 [PMID: 28653605 DOI: 10.3727/096504017X14972669062547]
- 56 **Fang Z**, Yin S, Sun R, Zhang S, Fu M, Wu Y, Zhang T, Khaliq J, Li Y. miR-140-5p suppresses the proliferation, migration and invasion of gastric cancer by regulating YES1. *Mol Cancer* 2017; **16**: 139 [PMID: 28818100 DOI: 10.1186/s12943-017-0708-6]
- 57 **Sun Y**, Qin B. Long noncoding RNA MALAT1 regulates HDAC4-mediated proliferation and apoptosis via decoying of miR-140-5p in osteosarcoma cells. *Cancer Med* 2018; **7**: 4584-4597 [PMID: 30094957 DOI: 10.1002/cam4.1677]
- 58 **Zhang D**, Zhao L, Shen Q, Lv Q, Jin M, Ma H, Nie X, Zheng X, Huang S, Zhou P, Wu G, Zhang T. Down-regulation of KIAA1199/CEMP by miR-216a suppresses tumor invasion and metastasis in colorectal cancer. *Int J Cancer* 2017; **140**: 2298-2309 [PMID: 28213952 DOI: 10.1002/ijc.30656]
- 59 **Terashima M**, Fujita Y, Togashi Y, Sakai K, De Velasco MA, Tomida S, Nishio K. KIAA1199 interacts with glycogen phosphorylase kinase β -subunit (PHKB) to promote glycogen breakdown and cancer cell survival. *Oncotarget* 2014; **5**: 7040-7050 [PMID: 25051373 DOI: 10.18632/oncotarget.2220]
- 60 **Hirayama A**, Kami K, Sugimoto M, Sugawara M, Toki N, Onozuka H, Kinoshita T, Saito N, Ochiai A, Tomita M, Esumi H, Soga T. Quantitative metabolome profiling of colon and stomach cancer microenvironment by capillary electrophoresis time-of-flight mass spectrometry. *Cancer Res* 2009; **69**: 4918-4925 [PMID: 19458066 DOI: 10.1158/0008-5472.CAN-08-4806]
- 61 **Pelletier J**, Bellot G, Gounon P, Lacas-Gervais S, Pouyssegur J, Mazure NM. Glycogen Synthesis is Induced in Hypoxia by the Hypoxia-Inducible Factor and Promotes Cancer Cell Survival. *Front Oncol* 2012; **2**: 18 [PMID: 22649778 DOI: 10.3389/fonc.2012.00018]
- 62 **Pescador N**, Villar D, Cifuentes D, Garcia-Rocha M, Ortiz-Barahona A, Vazquez S, Ordoñez A, Cuevas

- Y, Saez-Morales D, Garcia-Bermejo ML, Landazuri MO, Guinovart J, del Peso L. Hypoxia promotes glycogen accumulation through hypoxia inducible factor (HIF)-mediated induction of glycogen synthase 1. *PLoS One* 2010; **5**: e9644 [PMID: [20300197](#) DOI: [10.1371/journal.pone.0009644](#)]
- 63 **Shen GM**, Zhang FL, Liu XL, Zhang JW. Hypoxia-inducible factor 1-mediated regulation of PPP1R3C promotes glycogen accumulation in human MCF-7 cells under hypoxia. *FEBS Lett* 2010; **584**: 4366-4372 [PMID: [20888814](#) DOI: [10.1016/j.febslet.2010.09.040](#)]
- 64 **Wu D**, Zhang J, Lu Y, Bo S, Li L, Wang L, Zhang Q, Mao J. miR-140-5p inhibits the proliferation and enhances the efficacy of doxorubicin to breast cancer stem cells by targeting Wnt1. *Cancer Gene Ther* 2018 [PMID: [30032164](#) DOI: [10.1038/s41417-018-0035-0](#)]
- 65 **Zhang W**, Zou C, Pan L, Xu Y, Qi W, Ma G, Hou Y, Jiang P. MicroRNA-140-5p inhibits the progression of colorectal cancer by targeting VEGFA. *Cell Physiol Biochem* 2015; **37**: 1123-1133 [PMID: [26402430](#) DOI: [10.1159/000430237](#)]



Basic Study

Seven-senescence-associated gene signature predicts overall survival for Asian patients with hepatocellular carcinoma

Xiao-Hong Xiang, Li Yang, Xing Zhang, Xiao-Hua Ma, Run-Chen Miao, Jing-Xian Gu, Yu-Nong Fu, Qing Yao, Jing-Yao Zhang, Chang Liu, Ting Lin, Kai Qu

ORCID number: Xiao-Hong Xiang (0000-0002-9020-9187); Li Yang (0000-0002-8325-8335); Xing Zhang (0000-0001-9568-8124); Xiao-Hua Ma (0000-0002-5546-8458); Run-Chen Miao (0000-0003-1651-3970); Jing-Xian Gu (0000-0002-6183-4004); Yu-Nong Fu (0000-0001-8324-0613); Qing Yao (0000-0002-4904-9214); Jing-Yao Zhang (0000-0002-1177-0401); Chang Liu (0000-0003-1892-3957); Ting Lin (0000-0003-3825-6178); Kai Qu (0000-0002-1138-3727).

Author contributions: Qu K, Lin T, Liu C, and Xiang XH designed the research; Yang L, Zhang X, Ma XH, Miao RC, and Gu JX collected and analyzed the data; Qu K, Xiang XH, Fu YN, and Yao Q prepared the figures; Zhang JY, Lin T, Qu K, and Liu C drafted and revised the manuscript.

Supported by the National Natural Science Foundation of China, No. 81773128 and No. 81871998; the Natural Science Basic Research Plan in Shaanxi Province of China, No. 2018JM7013 and No. 2017JM8039; the Research Fund for Young Star of Science and Technology in Shaanxi Province, No. 2018KJXX-022; and China Postdoctoral Science Foundation, No. 2018M641000.

Institutional review board

statement: The study was reviewed and approved by the First Affiliated Hospital of Xi'an Jiaotong University Institutional Review Board.

Conflict-of-interest statement:

Xiao-Hong Xiang, Xing Zhang, Xiao-Hua Ma, Run-Chen Miao, Jing-Xian Gu, Yu-Nong Fu, Qing Yao, Jing-Yao Zhang, Chang Liu, Ting Lin, Kai Qu, Department of Hepatobiliary Surgery, the First Affiliated Hospital of Xi'an Jiaotong University, Xi'an 710061, Shaanxi Province, China

Li Yang, Department of Clinical Laboratory, Liaocheng People's Hospital, Taishan Medical College, Liaocheng 252000, Shandong Province, China

Corresponding author: Kai Qu, MD, PhD, Professor, Research Assistant Professor, Department of Hepatobiliary Surgery, the First Affiliated Hospital of Xi'an Jiaotong University, 277 West Yanta Road, Xi'an 710061, Shaanxi Province, China. qukai@xjtu.edu.cn

Telephone: +86-29-85323900

Fax: +86-29-85324695

Abstract

BACKGROUND

Cellular senescence is a recognized barrier for progression of chronic liver diseases to hepatocellular carcinoma (HCC). The expression of a cluster of genes is altered in response to environmental factors during senescence. However, it is questionable whether these genes could serve as biomarkers for HCC patients.

AIM

To develop a signature of senescence-associated genes (SAGs) that predicts patients' overall survival (OS) to improve prognosis prediction of HCC.

METHODS

SAGs were identified using two senescent cell models. Univariate COX regression analysis was performed to screen the candidate genes significantly associated with OS of HCC in a discovery cohort (GSE14520) for the least absolute shrinkage and selection operator modelling. Prognostic value of this seven-gene signature was evaluated using two independent cohorts retrieved from the GEO (GSE14520) and the Cancer Genome Atlas datasets, respectively. Time-dependent receiver operating characteristic (ROC) curve analysis was conducted to compare the predictive accuracy of the seven-SAG signature and serum α -fetoprotein (AFP).

RESULTS

A total of 42 SAGs were screened and seven of them, including *KIF18B*, *CEP55*, *CIT*, *MCM7*, *CDC45*, *EZH2*, and *MCM5*, were used to construct a prognostic formula. All seven genes were significantly downregulated in senescent cells and

None.

Open-Access: This article is an open-access article which was selected by an in-house editor and fully peer-reviewed by external reviewers. It is distributed in accordance with the Creative Commons Attribution Non Commercial (CC BY-NC 4.0) license, which permits others to distribute, remix, adapt, build upon this work non-commercially, and license their derivative works on different terms, provided the original work is properly cited and the use is non-commercial. See: <http://creativecommons.org/licenses/by-nc/4.0/>

Manuscript source: Unsolicited manuscript

Received: January 6, 2019

Peer-review started: January 7, 2019

First decision: February 13, 2019

Revised: March 6, 2019

Accepted: March 15, 2019

Article in press: March 16, 2019

Published online: April 14, 2019

P-Reviewer: El Eneen Khattab MA, Kamimura K, Toriguchi K

S-Editor: Yan JP

L-Editor: Wang TQ

E-Editor: Song H



upregulated in HCC tissues. Survival analysis indicated that our seven-SAG signature was strongly associated with OS, especially in Asian populations, both in discovery and validation cohorts. Moreover, time-dependent ROC curve analysis suggested the seven-gene signature had a better predictive accuracy than serum AFP in predicting HCC patients' 1-, 3-, and 5-year OS.

CONCLUSION

We developed a seven-SAG signature, which could predict OS of Asian HCC patients. This risk model provides new clinical evidence for the accurate diagnosis and targeted treatment of HCC.

Key words: Senescence-associated genes; Hepatocellular carcinoma; Overall survival; Risk model; Asian patients

©The Author(s) 2019. Published by Baishideng Publishing Group Inc. All rights reserved.

Core tip: In the present study, we identified a total of 42 senescence-associated genes (SAGs) and found seven of them were significantly downregulated in senescent cells and upregulated in HCC tissues. By using the least absolute shrinkage and selection operator, we constructed a seven-SAG signature that could predict the overall survival (OS) of hepatocellular carcinoma. This seven-SAG signature was further validated and developed in another independent dataset from The Cancer Genome Atlas project. Moreover, our risk score system showed better utility in predicting the OS than classic serum biomarker α -fetoprotein.

Citation: Xiang XH, Yang L, Zhang X, Ma XH, Miao RC, Gu JX, Fu YN, Yao Q, Zhang JY, Liu C, Lin T, Qu K. Seven-senescence-associated gene signature predicts overall survival for Asian patients with hepatocellular carcinoma. *World J Gastroenterol* 2019; 25(14): 1715-1728

URL: <https://www.wjgnet.com/1007-9327/full/v25/i14/1715.htm>

DOI: <https://dx.doi.org/10.3748/wjg.v25.i14.1715>

INTRODUCTION

Hepatocellular carcinoma (HCC) becomes the third leading cause of cancer deaths worldwide, with approximately 80% of mortalities occurring within 5 years^[1,2]. During the past decades, great effects have been made to improve the management of HCC. As more and more HCCs are diagnosed at an early stage, treatment efficacy is greatly improved^[3]. Whereas, deaths caused by HCC always occur when patients undergo treatment and the clinical outcome of HCC patients is still poor^[4]. Moreover, HCC is an extremely heterogeneous disease, which must be monitored for high-risk patients with poor clinical outcomes and adopt effective treatments to improve patient survival^[5]. Traditional serum markers, especially alpha-fetoprotein (AFP), have been the most common prognostic indicators in clinic. However, they significantly depend on tumor burden, which limits their value in diagnosing early stage tumors. Therefore, identifying novel prognostic biomarkers contributes to early diagnosis and reducing HCC mortality.

Cellular senescence is considered to be a response of a proliferating somatic cell to stress and damage derived from both exogenous and endogenous sources, and persistent DNA damage is the most common cause^[6]. It is characterized as a permanent cell cycle arrest^[7]. Cellular senescence has been deemed as a mechanism of limited cell division due to progressive telomere shortening^[8]. In cancer cells, there exists telomere-independent senescence due to their activation of telomerase. For instance, numerous studies found that RAS activation could induce cellular senescence in many cancer cell types. Both telomere-dependent and -independent pathways induced senescence by inducing a DNA damage response. Recently, it has been demonstrated that hepatocytes escaping from senescence played a key role in hepatic carcinogenesis and HCC progression^[9,10]. During the senescence process, a large number of genes are expressed differentially. Hence, it is reliable to focus on senescence associated genes (SAGs) as a novel approach in cancer diagnosis and monitor.

Bearing this in mind, we first identified the SAGs by analyzing the genome profiling data derived from two types of senescent cells, replicative senescence (RS) and oncogene-induced senescence (OIS). Next, we investigated the prognostic value of several candidate SAGs in predicting survival of HCC by multistep comparisons. Finally, we validated that the candidate SAGs were superior to classic serum biomarker AFP in predicting the OS in HCC cohort retrieved from the Cancer Genome Atlas (TCGA). As far as we know, the study is the first to investigate the expression patterns of SAGs between senescence and HCC and their association with clinical prognosis of Asian patients with HCC.

MATERIALS AND METHODS

Data sources and processing

Two genomic profiling datasets of RS cells (GSE19018 and GSE36640), three datasets of OIS cells (GSE19864, GSE40349, and GSE60652), and one HCC dataset (GSE14520) were obtained from the Gene Expression Omnibus (GEO) database (<http://www.ncbi.nlm.nih.gov/geo/>). RMA algorithm was performed to normalize and transform all the selected data from GEO to expression values in the R environment (v3.5.1). Among them, GSE14520 (based on GPL3921 platform) enrolled 209 HCC patients with survival data. An independent HCC cohort derived from TCGA database (TCGA-LIHC) was used as a validation group. The level 3 RNAseqv2 data and clinical data were derived from the TCGA data portal. A total of 370 HCC samples were included.

Differential gene expression analysis

Differentially expressed genes (DEGs) were calculated in RS and OIS cell models, respectively. Only fold change (FC) ≥ 1.5 and q -value < 0.05 were considered statistically significant. Then, we picked up the overlapped significantly expressed genes in the two senescent models. Venn diagram was carried out using Venny 2.1.0. Moreover, the expression levels of candidate genes were plotted and analyzed by the t -test in GSE14520 and TCGA-LIHC cohorts.

Prognostic model development

A prognostic model was created by the seven-SAG signature according to least absolute shrinkage and selection operator (LASSO) analysis. LASSO is one of the most popular approaches for sparse linear regression^[11]. "Almnet" package was carried out based on a series of λ in the R environment (v3.5.1)^[12] and the coefficients of each gene in the risk score system were generated. We got a risk score for every patient based on their own expression levels of the seven genes after the LASSO regression analysis.

Survival analysis

Univariate and multivariate survival analyses were carried out and further multivariate COX regression analysis only included variables with $P < 0.05$. All tests were carried out using SPSS (version 24.0; Chicago, United States). Kaplan-Meier curves were generated using GraphPad Prism 7.0. Comparisons between different subgroups were performed by the Log-Rank test. Patients are divided into high- and low- risk groups by the median.

Time-dependent receiver operating characteristic curve (ROC) analysis

ROC curve is extended to evaluate biomarker's accuracy of discriminating binary outcomes^[13]. Individuals with a high risk of developing the disease later may be disease-free in earlier life and their markers' value may change from baseline during follow-up. Therefore, time-dependent ROC curve analysis is more appropriate and outperforms the conventional method adopted for handling censored biomarker data. In this study, the time-dependent ROC curve analysis was performed with "survival ROC" package (R version 3.5.1). The prognostic performance was evaluated at 1, 3, and 5 years to compare the predictive accuracy and sensitivity of different prognostic models.

Statistical analysis

The chi-square test was carried out to discover the relationship between gene expression and clinical parameters. Unpaired student's t -test was used to analyze the difference of gene expression in HCC patients of different features. $P < 0.05$ was considered statistically different. Statistical analyses were performed using IBM SPSS Statistics software program version 24.0 (IBM Corp, NY, United States).

RESULTS

Identification of SAGs using different senescent models

The overall workflow of the data processing is presented in **Figure 1A**. To identify SAGs, we first integrated five different microarray profiles (GSE19018, GSE36640, GSE19864, GSE40349, and GSE60652). All datasets used in the present study were normalized before analysis. The relative expression of all samples pre- and post-normalization is shown in **Figure 1B**. Next, we screened the DEGs, which were identified as $FC \geq 1.5$ and $q\text{-value} < 0.05$ (senescent *vs* proliferating cells), in RS and OIS models, respectively. A total of 781 up-regulated and 739 down-regulated genes were selected in the RS model, and 103 up-regulated and 288 down-regulated genes in the OIS model (**Figure 2A**). By overlapping the two DEG lists, 42 common differentially expressed genes (35 downregulated and only 7 upregulated genes) were selected as SAGs (**Figure 2B**) and the expression levels of these genes in RS and OIS models are presented as a heat map in **Figure 2C**.

Construction of a risk score system

To obtain a prognostic SAG signature for HCC survival prediction, we first performed univariate COX regression analysis to evaluate the prognostic value of each candidate gene. And we found that all seven genes (*CEP55*, *MCM7*, *CDC45*, *MCM5*, *KIF18B*, *CIT*, and *EZH2*) were proved to be risk factors for HCC patients. Next, we screened the expression pattern of the above 7 candidate genes in HCC cohorts. Intriguingly, seven downregulated genes in senescent cells, were significantly upregulated in HCC tissues in both discovery and validation groups, with a $P\text{-value} < 0.0001$ (**Figure 3**). We then developed a risk score formula based on these seven SAGs using the LASSO method: Risk score = $(0.243 \times \text{relative expression value of } KIF18B) + (0.274 \times \text{relative expression value of } CEP55) + (0.282 \times \text{relative expression value of } CIT) + (0.266 \times \text{relative expression value of } MCM7) + (0.678 \times \text{relative expression value of } CDC45) + (0.175 \times \text{relative expression value of } EZH2) + (0.536 \times \text{relative expression value of } MCM5)$. In this risk score system, the contribution of every gene to the risk score model was weighted by absolute value of coefficients. Every patient would get a risk score based on the expression of the seven SAGs of themselves.

Validation of the seven-SAG signature for prognosis

To confirm the potentiality of the seven-SAG prognostic model, Kaplan-Meier curve was carried out to evaluate the association between the overall survival (OS) and our gene signature in discovery (GSE14520) and validation (TCGA-LIHC) cohorts. The whole group was divided into the high- and low-risk subgroups according to the median of all patients' risk scores. In the discovery cohort, with the increase in the risk score, the expression of all the seven genes was increasing, and the death events accumulated (**Figure 4A**). The patients in the high-risk subgroup had a 1.92-fold higher death risk than the low subgroup [hazard ratio (HR), 95% confidence interval (CI) = 1.92, 1.16-3.19; log-rank P value = 0.011] (**Figure 4B**). We then tempted to test these findings in the validation cohort (TCGA-LIHC) (**Figure 4C**). Similar to the findings obtained from the discovery cohort, patients in the high-risk group [median survival time (MST) = 46.6 m] had significantly shorter OS time than patients with a low-risk score (MST = 70.5 m) [HR (95%CI) = 1.80 (1.27-2.54), log-rank P value = 0.001] (**Figure 4D**). Interestingly, when we analyzed the data in the Asian population, we observed a highly significant association between the seven-SAG signature and OS. The majority of death events occurred in the high-risk group (**Figure 4E**). Asian HCC patients with a high-risk score were shown to have a > 5-fold increased death risk than low-risk patients [HR (95%CI) = 5.81 (3.20-10.54), log-rank P value < 0.0001]. The MST of the high-risk subgroup was only 60% of that of the low-risk group (MST = 21.6 m *vs* 91.7 m) (**Figure 4F**). In order to investigate the prognostic value of the risk score system in different patient groups with different characteristics, we performed univariate/multivariate Cox regression analysis of clinicopathologic factors associated with OS in the discovery and validation cohorts. From the Cox regression results, both the seven-SAG signature and serum AFP level were confirmed to be independent risk factors of OS in the two cohorts (**Table 1**).

Comparison of the seven-SAG signature and serum AFP in predicting OS

To assess the prognostic accuracy of the seven-SAG signature, we performed time-dependent ROC analysis of 1-, 3-, and 5-year OS of the validation cohort. The area under the curve (AUC) of the seven-SAG signature model indicated an acceptable predictive accuracy, which is superior to AFP, a widely used traditional serum marker, at 1 year (our seven-gene model AUC = 0.708, serum AFP level AUC = 0.606) (**Figure 5A**), 3 years (our seven-gene model AUC = 0.699, serum AFP level AUC = 0.568) (**Figure 5B**) as well as 5 years (our seven-gene model AUC = 0.678, serum AFP

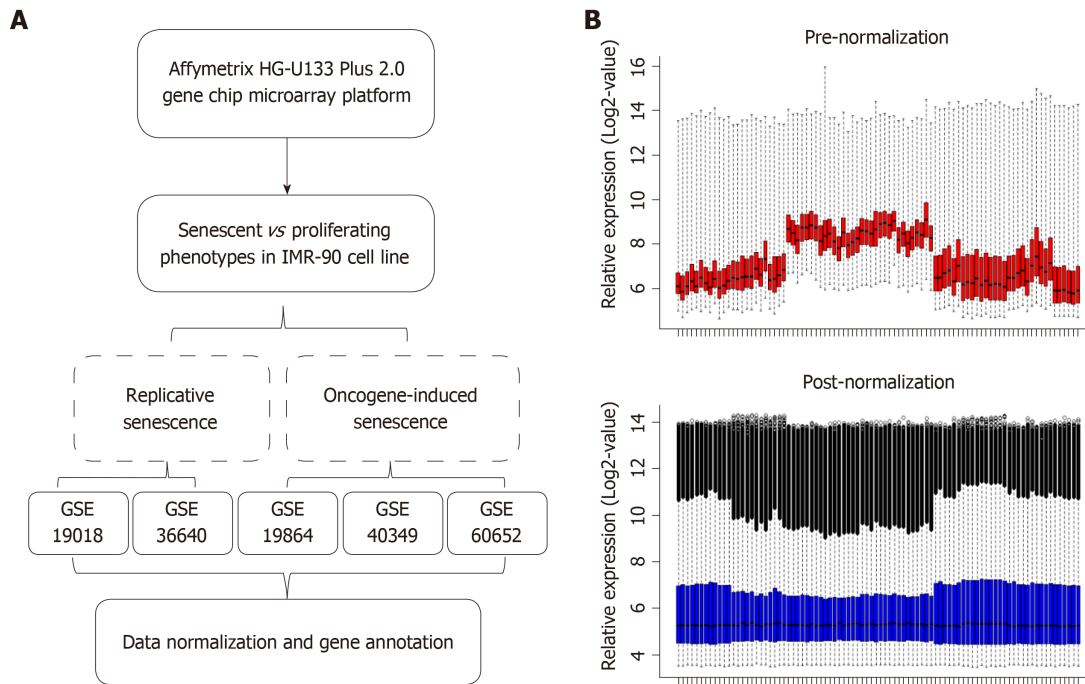


Figure 1 Data sources and processing. A: Flowchart describing the process used to generate differentially expressed senescence-associated genes; B: The relative expression in all samples pre- and post-normalization.

level AUC = 0.604) (Figure 5C). These results indicated the validation of the prognostic signature.

Stratified analysis of the seven-SAG signature for prognosis prediction

Stratified analyses based on the clinical characteristics were carried out to identify the suitable Asian patient groups for the seven-SAG signature (Table 2). In the elderly population, patients with a high-risk score had a more than 3-fold increased risk of death than the low-risk group (Figure 6A-C). These results suggested that our seven-SAG signature was more applicable to the HCC patients with older age in predicting OS.

DISCUSSION

In this study, we first identified 42 overlapped DEGs using the RS and OIS models. Among them, seven downregulated genes in senescent cells, *KIF18B*, *CEP55*, *CIT*, *MCM7*, *CDC45*, *EZH2*, and *MCM5*, were shown to be upregulated in HCC tissues and selected to construct a prognostic model. The seven-SAG signature was shown to be associated with OS in both discovery and validation cohorts. Stratified analysis showed that our seven-SAG signature was significantly associated with OS in elderly Asian patients. Moreover, time-dependent ROC analysis showed a favorable prognostic value of our seven-SAG signature when compared with serum AFP.

The cellular senescence is considered an aging hallmark. With the increase in age, the number of senescent cells is increasing. Cellular senescence is widely considered to be an anti-tumor mechanism. Studies have shown that a source of stress that triggers liver senescence is chronic inflammation, which causes damage to liver cell regeneration. Importantly, abrogation of senescence leads to aggressive HCC development^[14]. In the present study, we found that the HCC patients carrying high expression of seven SAGs had a shorter OS time. Stratified results further suggested the seven-SAG signature was more applicable to the elderly HCC patients. The potential explanation might be that due to the increasing number of senescent cells, the expression of the seven-SAG signature is decreased, while its high expression indicates a higher proliferation rate and poorer OS.

It has been widely accepted that senescence pathways are collectively at the level of activation of CDKs, which play pivotal roles in regulating the cell cycle progression. Of the seven genes, *KIF18B*, a member of the kinesin-8 subfamily, is involved in cell cycle process^[15] and acts as an oncogene in cervical cancer^[16]. *CEP55*, also known as c10orf3 and FLJ10540, promotes tumorigenesis and regulates stemness in various

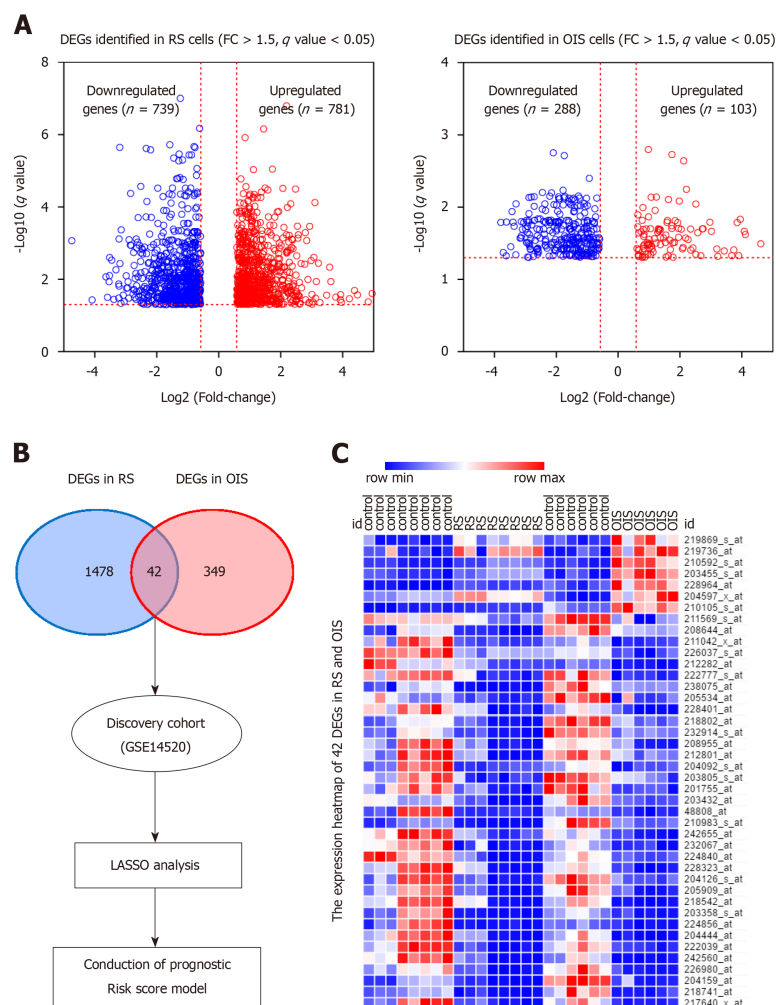


Figure 2 Expression of differentially expressed genes in senescent cells. A: The differentially expressed genes were identified in replicative senescence (RS) and oncogene-induced senescence (OIS) models. There were 781 up-regulated and 739 down-regulated genes selected using the RS model, and 103 up-regulated and 288 down-regulated genes selected using the OIS model; B: Overlapping the two lists, 42 common differentially expressed genes were selected as senescence associated genes; C: The expression levels of 42 genes are presented as a heat map in RS and OIS models. DEGs: Differentially expressed genes; RS: Replicative senescence; OIS: Oncogene-induced senescence; SAGs: Senescence associated genes; FC: Fold change; LASSO: Least absolute shrinkage and selection operator.

cancers, such as lung adenocarcinoma^[17-19]. *CIT* (Serine/threonine kinase 21) encoding a serine/threonine protein kinase, is a downstream effector of Rho family GTPases and participates in cell cycle regulation. Liu *et al*^[20] and Xu *et al*^[21] have demonstrated that *CIT* is up-regulated in HCC and regulates the G2/M transition in rat hepatocytes. EZH2 is a subunit of polycomb repressive complex 2 (PRC2), a protein complex that induces epigenetically silencing of genes^[22]. And it has been reported that several lncRNAs are able to regulate gene transcription by binding to PRC2^[23,24].

In most eukaryotes, the MCM complex consists of six highly conserved MCM proteins, namely MCM2-7, which functions as a replicative DNA helicase to unwind the DNA duplex template during DNA replication^[25]. Recent evidence has demonstrated that several MCM proteins are tightly associated with tumorigenesis^[26-28]. The MCM2-7 hexamer complexes with CDC45 and the heterotetrameric GINS complex, the Cdc45-Mcm2-7-GINS (CMG) complex, function as a potential target for cancer treatment and CDC45 interacts with MCM2^[29]. Furthermore, our previous study showed that MCM7 promotes cancer progression through cyclin D1-dependent signaling in HCC^[30]. Three members of CMG complex, MCM5, MCM7, and CDC45, were included in the risk formula. This evidence indicated that more attention should be focused on the pro-oncogenic mechanisms of senescence escape of HCC cells.

Our study showed that AFP was an independent risk factor for HCC patients. AFP is often expressed at high levels in most HCC patients and is considered a reliable clinical tumor biomarker. As a classic serum biomarker, AFP was found to be

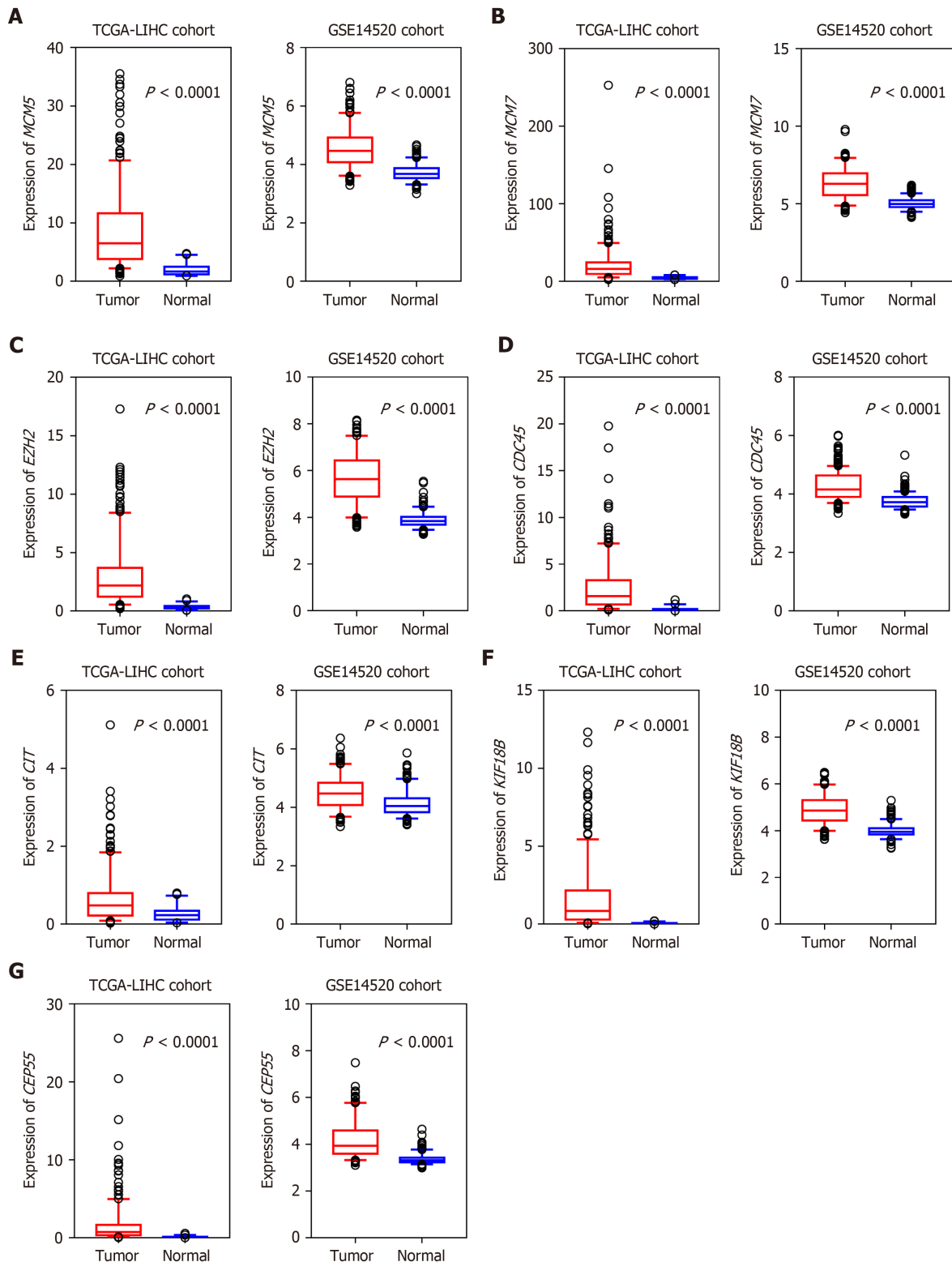


Figure 3 Expression of the seven candidate genes in hepatocellular carcinoma and normal liver tissues. A: *MCM5*; B: *MCM7*; C: *EZH2*; D: *CDC45*; E: *CIT*; F: *KIF18B*; G: *CEP55*. Seven senescence associated genes, which were downregulated in senescent cells, were shown to be upregulated in hepatocellular carcinoma tissues in both discovery and validation cohorts. $P < 0.0001$ for all.

associated with prognosis in HCC patients^[31,32]. Park *et al.*^[33] reported that AFP combined with PIVKA-II were useful in predicting survival in the radiological treatment of locally advanced HCC. Jiang *et al.*^[34] also found that preoperative AFP and fibrinogen showed a predictive power for recurrence of HCC after liver transplantation. Here, our study demonstrated that the seven-SAG signature model was superior to serum AFP level and more applicable in predicting OS of HCC patients with older age. The above findings suggested a potential clinical application

Table 1 Univariate/multivariate Cox regression analysis of clinicopathologic factors associated with overall survival in GSE14520 and The Cancer Genome Atlas cohorts

Variable	Discovery cohort				Validation cohort-Asian only			
	Univariate analysis		Multivariate analysis		Univariate analysis		Multivariate analysis	
	HR (95%CI)	P-value	HR (95%CI)	P-value	HR (95%CI)	P-value	HR (95%CI)	P-value
Gender (male/female)	1.36 (0.55-3.40)	0.507	-	-	0.89 (0.43-1.86)	0.755	-	-
Age (> 60/≤ 60 yr)	1.06 (0.57-2.00)	0.851	-	-	1.21 (0.66-2.24)	0.541	-	-
Cirrhosis (yes/no)	3.09 (0.76-12.65)	0.117	-	-	2.44 (1.56-3.85)	< 0.001 ^a	1.67 (1.04-2.70)	0.034 ^a
AFP (> 300/≤ 300 ng/mL)	2.30 (1.37-3.86)	0.002 ^a	2.26 (1.38-3.69)	0.001 ^a	3.70 (2.13-6.25)	< 0.001 ^a	2.13 (1.30-3.57)	0.003 ^a
Risk score (high/low)	1.93 (1.15-3.23)	0.012 ^a	1.99 (1.19-3.34)	0.009 ^a	5.91 (2.74-12.76)	< 0.001 ^a	4.22 (1.89-9.41)	< 0.001 ^a

^aStatistically significant. HR: Hazard ratio; CI: Confidence interval; AFP: Alpha-fetoprotein.

of the seven-SAG signature in HCC patients.

However, there are some limitations in our study. First, the samples for screening SAG were small, which might cause false positive results. Second, we constructed the risk score system merely based on the gene expression levels, rather than the other genetic events that probably have an effect on the initiation and progression of cancer. Third, patients in the discovery cohort were from Asia, thus, the risk score system was established based on an Asian background. And further stratified analysis in the validation cohort also showed that this model was more suitable for Asian patients. Hence, our HCC prognostic signature still needs to be validated in a larger group of patients from various populations.

In conclusion, we constructed and confirmed a prognostic risk score system comprised of seven SAGs. The seven-SAG signature could be a potential predictor for OS, particularly in elderly Asian HCC patients. Our data provide new promising evidence on prediction biomarkers and targeted therapy for HCC.

Table 2 Stratified analysis of overall survival in GSE14520 and The Cancer Genome Atlas cohorts

Variable	Discovery cohort			Validation cohort-Asian only		
	High-risk/low-risk	HR (95%CI)	P-value	High-risk/low-risk	HR (95%CI)	P-value
Overall	76/75	1.92 (1.16-3.19)	0.011 ^a	79/78	5.81 (3.20-10.54)	< 0.001 ^a
Gender						
Male	69/67	2.15 (1.27-3.64)	0.004 ^a	62/61	5.18 (2.66-10.10)	< 0.001 ^a
Female	7/8	0.60 (0.10-3.47)	0.569	17/17	9.63 (2.59-35.77)	0.009 ^a
Age (yr)						
≤ 60	64/60	1.70 (0.97-2.98)	0.064	53/52	5.22 (2.49-10.97)	< 0.001 ^a
> 60	12/15	3.19 (1.00-10.20)	0.045 ^a	26/26	6.47 (2.38-17.59)	< 0.001 ^a
Cirrhosis						
Yes	70/69	1.93 (1.15-3.22)	0.012 ^a	17/24	3.50 (0.66-18.47)	0.122
No	6/6	1.73 (0.10-30.65)	0.695	11/28	0.98 (0.19-5.00)	0.979
AFP (ng/mL)						
≤ 300	40/39	1.73 (0.77-3.87)	0.179	34/55	2.94 (1.01-8.57)	0.036 ^a
> 300	34/34	2.11 (1.09-4.08)	0.025 ^a	16/16	2.65 (0.60-11.66)	0.226

^aStatistically significant. HR: Hazard ratio; CI: Confidence interval; AFP: Alpha-fetoprotein.

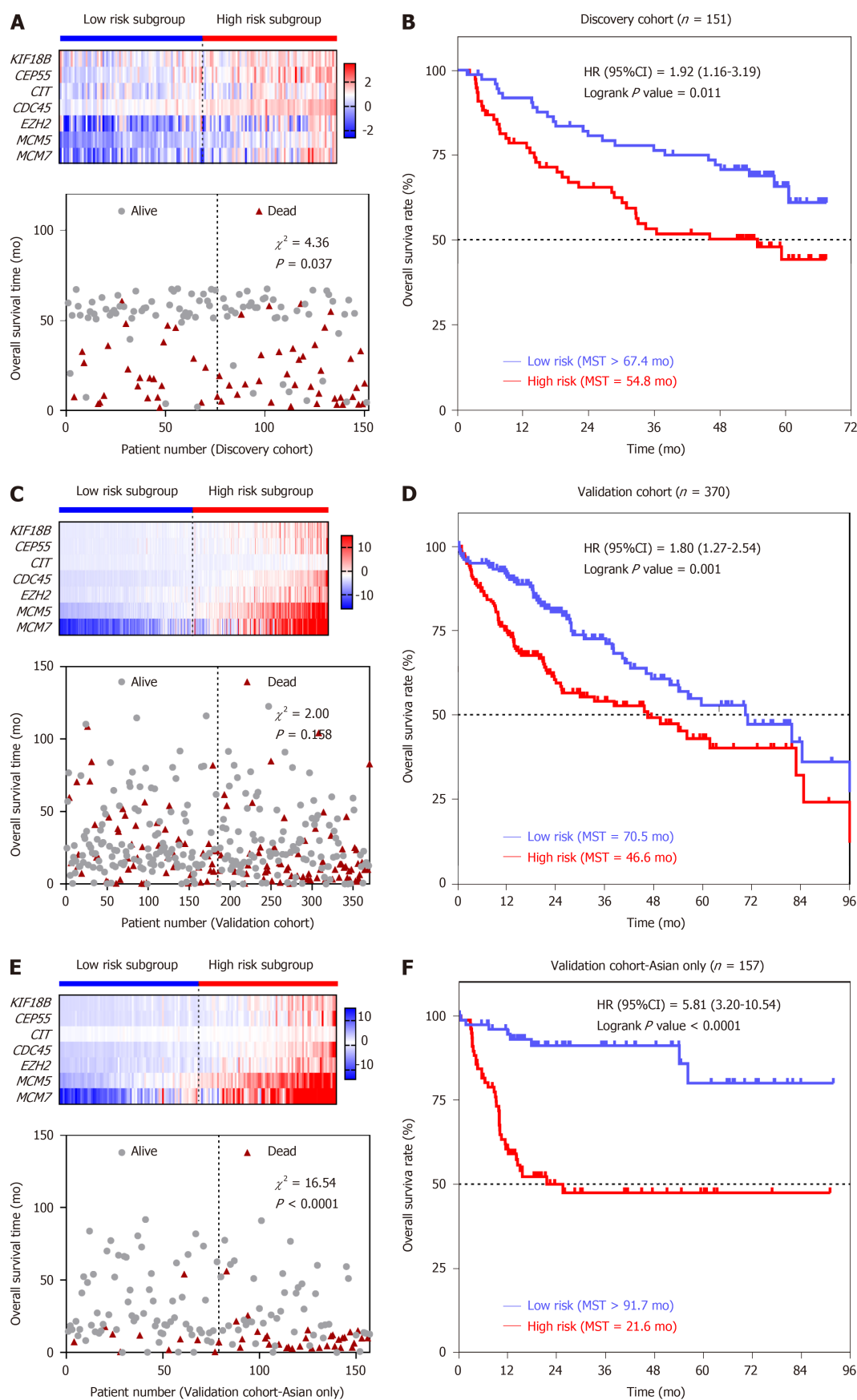


Figure 4 The seven-senescence associated gene signature is associated with overall survival in the discovery and validation cohorts. A: The heat map of the expression of seven genes and patients' death status in the discovery cohort; B: Kaplan-Meier survival curves plotted to estimate the overall survival probabilities for the low-risk vs high-risk group in the discovery cohort; C: The heat map of the expression of seven genes and patients' death status in the validation cohort; D: Kaplan-Meier survival curves plotted to estimate the overall survival probabilities for the low-risk vs high-risk group in the validation cohort; E: The heat map of the expression of seven genes and patients' death status in the validation cohort-Asian only subgroup; F: Kaplan-Meier survival curves plotted to estimate the overall survival probabilities for the low-risk vs high-risk group in the validation cohort-Asian only subgroup. HR: Hazard ratio; CI: Confidence interval.

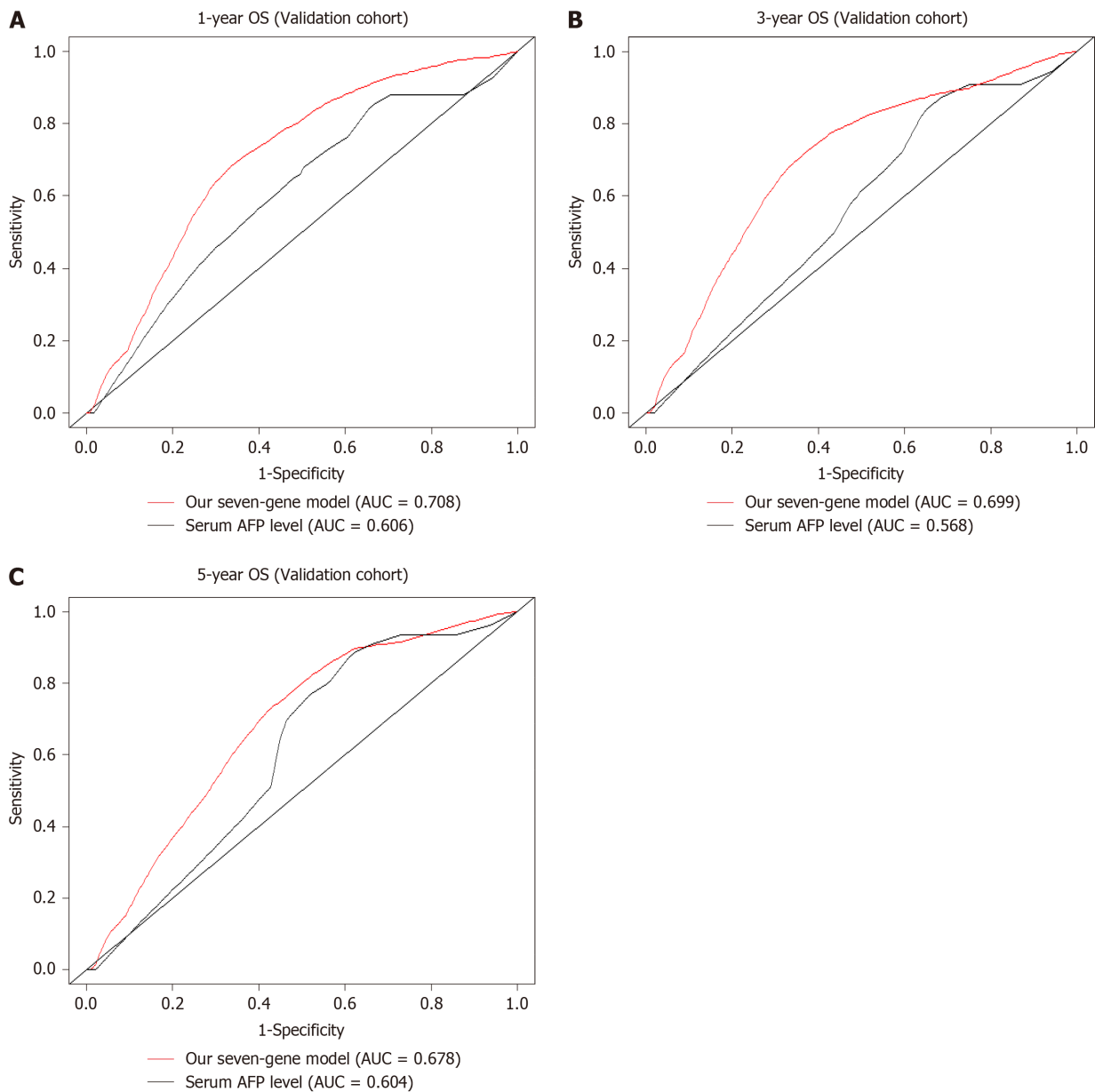


Figure 5 Comparison of the seven-senescence associated gene signature and α -fetoprotein in predicting overall survival of hepatocellular carcinoma patients. To assess the prognostic accuracy of the seven-senescence associated gene signature and serum- α -fetoprotein level, time-dependent receiver operating characteristic curve analysis was conducted for 1-, 3-, and 5-year overall survival (OS). A: 1-year OS; B: 3-year OS; C: 5-year OS. AUC: Area under the curve; AFP: Alpha-fetoprotein; OS: Overall survival.

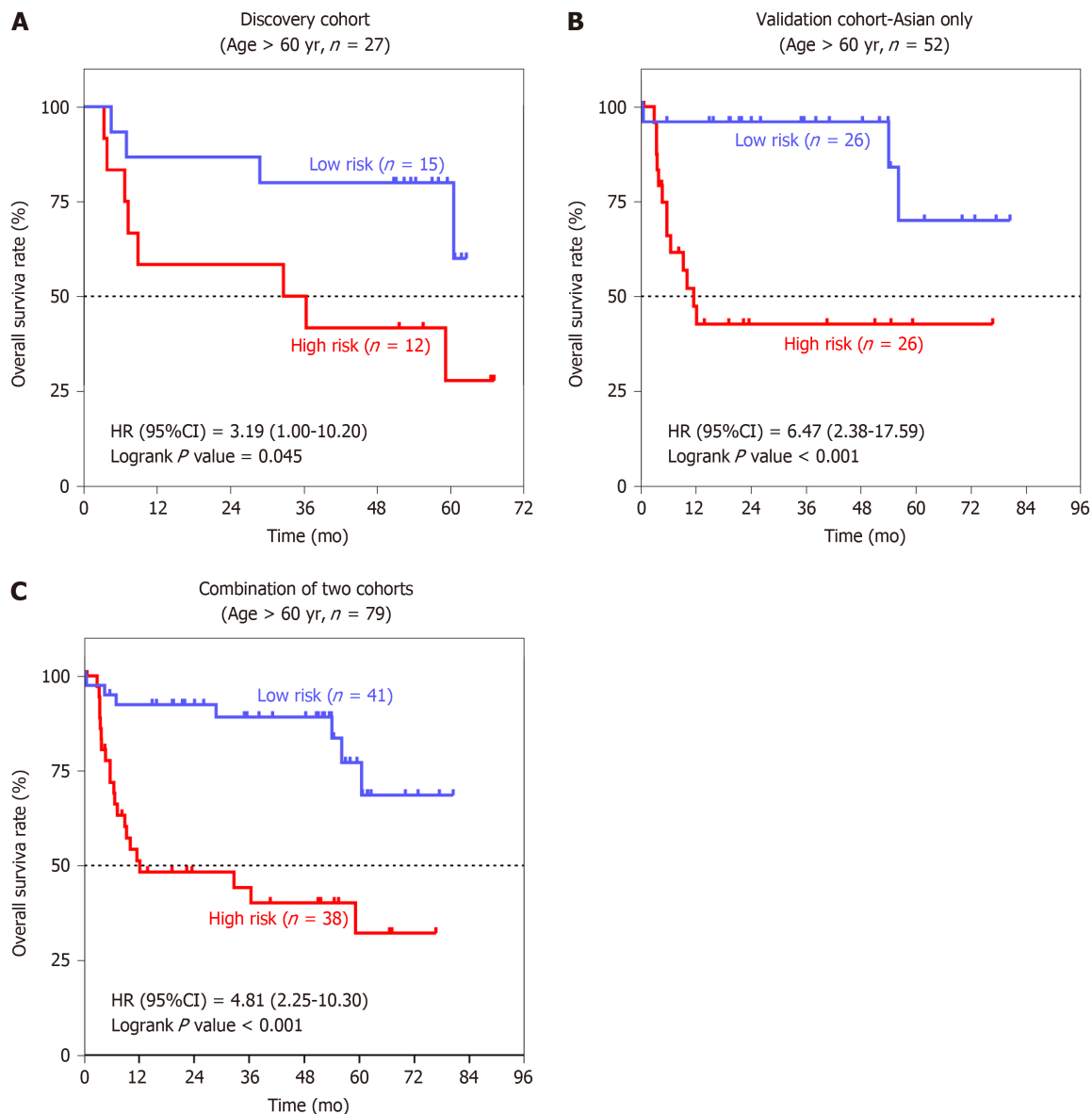


Figure 6 Association between the seven-senescence associated gene signature and overall survival in the elderly age subgroup. Kaplan-Meier survival curves were plotted to estimate the overall survival probabilities for the low-risk vs high-risk group. A: Discovery group; B: Validation group; C: Combination of discovery group and validation group. HR: Hazard ratio; CI: Confidence interval.

ARTICLE HIGHLIGHTS

Research background

Hepatocellular carcinoma (HCC) is a common malignancy that remains a serious cause of death worldwide. Recently, molecular markers and prognostic models have been used to improve the diagnosis and treatment of HCC, but few can be applied clinically. Currently, bioinformatics technology has been used for data mining in large public databases. The abundant sample size in the public database can make up for the shortcomings of small samples in real hospitals and help to seek for a more accurate and applicable prognostic model for HCC.

Research motivation

Researchers have been making efforts to find molecular markers or prognostic models that can effectively predict the prognosis of HCC. Senescence is a cell cycle arrest caused by stress in cells, but the cells are still alive. Studies have shown that the proportion of senescent cells in tissues of patients with cirrhosis increases, but a considerable number of patients with cirrhosis can develop liver cancer, and its specific molecular mechanism has rarely been reported.

Research objectives

By analyzing the database of two cellular senescence models from Gene Expression Omnibus, we screened for senescence-associated genes and validated these genes in the liver cancer databases (GSE14520 and TCGA-LIHC). Then, we constructed an HCC prognostic model and

evaluate its prognostic accuracy.

Research methods

Senescence-associated genes (SAGs) were identified using R package "limma". The latest statistical algorithm-the least absolute shrinkage and selection operator (LASSO) was applied to create our prognostic model. Time-dependent receiver operating characteristic (ROC) curves were used to compare the prognostic accuracy between the seven-SAG signature and serum α -fetoprotein.

Research results

The prognostic model for predicting the overall survival (OS) of HCC was constructed by LASSO, consisting of the seven senescence-associated genes (SAGs) (*KIF18B*, *CEP55*, *CIT*, *MCM7*, *CDC45*, *EZH2*, and *MCM5*). All seven SAGs were highly expressed in HCC and proliferating cells, while lowly expressed in normal tissues and senescent cells. Survival analysis showed that our seven-SAG characteristics are closely related to OS, especially in Asian populations, both in the discovery and validation cohorts. In addition, the time-dependent ROC curve analysis indicated that the seven-gene marker is better than serum alpha-fetoprotein in predicting 1-, 3-, and 5-year OS of HCC patients.

Research conclusions

The seven-SAG signature was more applicable to evaluate OS of Asian HCC patients, which may provide new clinical evidence for the diagnosis and treatment of HCC transformed from cirrhosis.

Research perspectives

The current study provides clues that the expression changes of senescence-associated gene are the molecular basis for the progression of cirrhosis to liver cancer. Finding effective senescence-associated molecular biomarkers and predictive features of HCC prognosis is necessary.

REFERENCES

- Chen W, Zheng R, Baade PD, Zhang S, Zeng H, Bray F, Jemal A, Yu XQ, He J. Cancer statistics in China, 2015. *CA Cancer J Clin* 2016; **66**: 115-132 [PMID: 26808342 DOI: 10.3322/caac.21338]
- Reddy SK, Steel JL, Chen HW, DeMateo DJ, Cardinal J, Behari J, Humar A, Marsh JW, Geller DA, Tsung A. Outcomes of curative treatment for hepatocellular cancer in nonalcoholic steatohepatitis versus hepatitis C and alcoholic liver disease. *Hepatology* 2012; **55**: 1809-1819 [PMID: 22183968 DOI: 10.1002/hep.25536]
- Bruix J, Gores GJ, Mazzaferro V. Hepatocellular carcinoma: Clinical frontiers and perspectives. *Gut* 2014; **63**: 844-855 [PMID: 24531850 DOI: 10.1136/gutjnl-2013-306627]
- Dutkowski P, Linecker M, DeOliveira ML, Müllhaupt B, Clavien PA. Challenges to liver transplantation and strategies to improve outcomes. *Gastroenterology* 2015; **148**: 307-323 [PMID: 25224524 DOI: 10.1053/j.gastro.2014.08.045]
- Llovet JM, Villanueva A, Lachenmayer A, Finn RS. Advances in targeted therapies for hepatocellular carcinoma in the genomic era. *Nat Rev Clin Oncol* 2015; **12**: 408-424 [PMID: 26054909 DOI: 10.1038/nrclinonc.2015.103]
- Kuilman T, Michaloglou C, Mooi WJ, Peeper DS. The essence of senescence. *Genes Dev* 2010; **24**: 2463-2479 [PMID: 21078816 DOI: 10.1101/gad.1971610]
- Demidenko ZN, Korotchikina LG, Gudkov AV, Blagosklonny MV. Paradoxical suppression of cellular senescence by p53. *Proc Natl Acad Sci U S A* 2010; **107**: 9660-9664 [PMID: 20457898 DOI: 10.1073/pnas.1002298107]
- Wiemann SU, Satyanarayana A, Tsahuridu M, Tillmann HL, Zender L, Klempnauer J, Flemming P, Franco S, Blasco MA, Manns MP, Rudolph KL. Hepatocyte telomere shortening and senescence are general markers of human liver cirrhosis. *FASEB J* 2002; **16**: 935-942 [PMID: 12087054 DOI: 10.1096/fj.01-0977com]
- Wei W, Ji S. Cellular senescence: Molecular mechanisms and pathogenicity. *J Cell Physiol* 2018; **233**: 9121-9135 [PMID: 30078211 DOI: 10.1002/jcp.26956]
- Guo M. Cellular senescence and liver disease: Mechanisms and therapeutic strategies. *Biomed Pharmacother* 2017; **96**: 1527-1537 [PMID: 29174037 DOI: 10.1016/j.biopha.2017.11.075]
- Arbet J, McGue M, Chatterjee S, Basu S. Resampling-based tests for Lasso in genome-wide association studies. *BMC Genet* 2017; **18**: 70 [PMID: 28738830 DOI: 10.1186/s12863-017-0533-3]
- Friedman J, Hastie T, Tibshirani R. Regularization Paths for Generalized Linear Models via Coordinate Descent. *J Stat Softw* 2010; **33**: 1-22 [PMID: 20808728 DOI: 10.1163/ej.9789004178922.i-328.7]
- Kim Y, Kong L. Time-dependent ROC analysis for censored biomarker data due to limit of detection. *J Biopharm Stat* 2018; **28**: 612-621 [PMID: 28862526 DOI: 10.1080/10543406.2017.1372768]
- Zeng S, Shen WH, Liu L. Senescence and Cancer. *Cancer Transl Med* 2018; **4**: 70-74 [PMID: 30766922 DOI: 10.4103/ctm.ctm_22_18]
- Lee YM, Kim E, Park M, Moon E, Ahn SM, Kim W, Hwang KB, Kim YK, Choi W, Kim W. Cell cycle-regulated expression and subcellular localization of a kinesin-8 member human KIF18B. *Gene* 2010; **466**: 16-25 [PMID: 20600703 DOI: 10.1016/j.gene.2010.06.007]
- Wu Y, Wang A, Zhu B, Huang J, Lu E, Xu H, Xia W, Dong G, Jiang F, Xu L. KIF18B promotes tumor progression through activating the Wnt/ β -catenin pathway in cervical cancer. *Oncotargets Ther* 2018; **11**: 1707-1720 [PMID: 29636620 DOI: 10.2147/OTT.S157440]
- Tao J, Zhi X, Tian Y, Li Z, Zhu Y, Wang W, Xie K, Tang J, Zhang X, Wang L, Xu Z. CEP55 contributes to human gastric carcinoma by regulating cell proliferation. *Tumour Biol* 2014; **35**: 4389-4399 [PMID: 24390615 DOI: 10.1007/s13277-013-1578-1]
- Chen CH, Lu PJ, Chen YC, Fu SL, Wu KJ, Tsou AP, Lee YC, Lin TC, Hsu SL, Lin WJ, Huang CY, Chou

- CK. FLJ10540-elicited cell transformation is through the activation of PI3-kinase/AKT pathway. *Oncogene* 2007; **26**: 4272-4283 [PMID: [17237822](#) DOI: [10.1038/sj.onc.1210207](#)]
- 19 **Martinez-Garay I**, Rustom A, Gerdes HH, Kutsche K. The novel centrosomal associated protein CEP55 is present in the spindle midzone and the midbody. *Genomics* 2006; **87**: 243-253 [PMID: [16406728](#) DOI: [10.1016/j.ygeno.2005.11.006](#)]
- 20 **Liu H**, Di Cunto F, Imarisio S, Reid LM. Citron kinase is a cell cycle-dependent, nuclear protein required for G2/M transition of hepatocytes. *J Biol Chem* 2003; **278**: 2541-2548 [PMID: [12411428](#) DOI: [10.1074/jbc.M210391200](#)]
- 21 **Xu XR**, Huang J, Xu ZG, Qian BZ, Zhu ZD, Yan Q, Cai T, Zhang X, Xiao HS, Qu J, Liu F, Huang QH, Cheng ZH, Li NG, Du JJ, Hu W, Shen KT, Lu G, Fu G, Zhong M, Xu SH, Gu WY, Huang W, Zhao XT, Hu GX, Gu JR, Chen Z, Han ZG. Insight into hepatocellular carcinogenesis at transcriptome level by comparing gene expression profiles of hepatocellular carcinoma with those of corresponding noncancerous liver. *Proc Natl Acad Sci U S A* 2001; **98**: 15089-15094 [PMID: [11752456](#) DOI: [10.1073/pnas.241522398](#)]
- 22 **Kim KH**, Roberts CW. Targeting EZH2 in cancer. *Nat Med* 2016; **22**: 128-134 [PMID: [26845405](#) DOI: [10.1038/nm.4036](#)]
- 23 **Su M**, Xiao Y, Tang J, Wu J, Ma J, Tian B, Zhou Y, Wang H, Yang D, Liao QJ, Wang W. Role of lncRNA and EZH2 Interaction/Regulatory Network in Lung Cancer. *J Cancer* 2018; **9**: 4156-4165 [PMID: [30519315](#) DOI: [10.7150/jca.27098](#)]
- 24 **Dong P**, Xiong Y, Yue J, Hanley SJB, Kobayashi N, Todo Y, Watari H. Long Non-coding RNA NEAT1: A Novel Target for Diagnosis and Therapy in Human Tumors. *Front Genet* 2018; **9**: 471 [PMID: [30374364](#) DOI: [10.3389/fgene.2018.00471](#)]
- 25 **Ishimi Y**. Regulation of MCM2-7 function. *Genes Genet Syst* 2018; **93**: 125-133 [PMID: [30369561](#) DOI: [10.1266/ggs.18-00026](#)]
- 26 **Zhou YM**, Zhang XF, Cao L, Li B, Sui CJ, Li YM, Yin ZF. MCM7 expression predicts post-operative prognosis for hepatocellular carcinoma. *Liver Int* 2012; **32**: 1505-1509 [PMID: [22784096](#) DOI: [10.1111/j.1478-3231.2012.02846.x](#)]
- 27 **Toyokawa G**, Masuda K, Daigo Y, Cho HS, Yoshimatsu M, Takawa M, Hayami S, Maejima K, Chino M, Field HI, Neal DE, Tsuchiya E, Ponder BA, Maehara Y, Nakamura Y, Hamamoto R. Minichromosome Maintenance Protein 7 is a potential therapeutic target in human cancer and a novel prognostic marker of non-small cell lung cancer. *Mol Cancer* 2011; **10**: 65 [PMID: [21619671](#) DOI: [10.1186/1476-4598-10-65](#)]
- 28 **You Z**, Ishimi Y, Masai H, Hanaoka F. Roles of Mcm7 and Mcm4 subunits in the DNA helicase activity of the mouse Mcm4/6/7 complex. *J Biol Chem* 2002; **277**: 42471-42479 [PMID: [12207017](#) DOI: [10.1074/jbc.M205769200](#)]
- 29 **Abid Ali F**, Renault L, Gannon J, Gahlon HL, Kotecha A, Zhou JC, Rueda D, Costa A. Cryo-EM structures of the eukaryotic replicative helicase bound to a translocation substrate. *Nat Commun* 2016; **7**: 10708 [PMID: [26888060](#) DOI: [10.1038/ncomms10708](#)]
- 30 **Qu K**, Wang Z, Fan H, Li J, Liu J, Li P, Liang Z, An H, Jiang Y, Lin Q, Dong X, Liu P, Liu C. MCM7 promotes cancer progression through cyclin D1-dependent signaling and serves as a prognostic marker for patients with hepatocellular carcinoma. *Cell Death Dis* 2017; **8**: e2603 [PMID: [28182015](#) DOI: [10.1038/cddis.2016.352](#)]
- 31 **Lee SH**, Lee JS, Na GH, You YK, Kim DG. Immunohistochemical markers for hepatocellular carcinoma prognosis after liver resection and liver transplantation. *Clin Transplant* 2017; **31** [PMID: [27653235](#) DOI: [10.1111/ctr.12852](#)]
- 32 **Liu G**, Wang K, Li J, Xia Y, Lu L, Wan X, Yan Z, Shi L, Lau WY, Wu M, Shen F. Changes in serum alpha fetoprotein in patients with recurrent hepatocellular carcinoma following hepatectomy. *J Gastroenterol Hepatol* 2015; **30**: 1405-1411 [PMID: [25801981](#) DOI: [10.1111/jgh.12953](#)]
- 33 **Park H**, Kim SU, Park JY, Kim DY, Ahn SH, Chon CY, Han KH, Seong J. Clinical usefulness of double biomarkers AFP and PIVKA-II for subdividing prognostic groups in locally advanced hepatocellular carcinoma. *Liver Int* 2014; **34**: 313-321 [PMID: [23895043](#) DOI: [10.1111/liv.12274](#)]
- 34 **Jiang N**, Zeng KN, Dou KF, Lv Y, Zhou J, Li HB, Tang JX, Li JJ, Wang GY, Yi SH, Yi HM, Li H, Chen GH, Yang Y. Preoperative Alfa-Fetoprotein and Fibrinogen Predict Hepatocellular Carcinoma Recurrence After Liver Transplantation Regardless of the Milan Criteria: Model Development with External Validation. *Cell Physiol Biochem* 2018; **48**: 317-327 [PMID: [30016765](#) DOI: [10.1159/000491731](#)]



Case Control Study

Chronic functional constipation is strongly linked to vitamin D deficiency

Alba Panarese, Francesco Pesce, Piero Porcelli, Giuseppe Riezzo, Palma Aurelia Iacovazzi, Carla Maria Leone, Massimo De Carne, Caterina Mammone Rinaldi, Endrit Shahini

ORCID number: Alba Panarese (0000-0002-4909-043); Francesco Pesce (0000-0002-2882-4226); Piero Porcelli (0000-0002-2263-8051); Giuseppe Riezzo (0000-0002-1800-4830); Palma Aurelia Iacovazzi (0000-0003-3590-4125); Carla Maria Leone (0000-0003-0465-3781); Massimo De Carne (0000-0001-8753-5486); Caterina Mammone Rinaldi (0000-0003-0223-6976); Endrit Shahini (0000-0002-4909-0436).

Author contributions: Panarese A has conceived the protocol; Shahini E and Panarese A drafted the initial and final manuscript; Panarese A enrolled patients; Panarese A, and Leone CM collected in a database the baseline and on-treatment information; Shahini E, Pesce F and Porcelli P systematically reviewed the data entries for completeness and consistency, checked for completeness of information and performed the statistical analysis; all the authors reviewed and approved the final draft.

Institutional review board

statement: National Institute of Gastroenterology "S. De Bellis" Research Hospital (0807/16) and by the Research Ethics Committee of the National Oncological Institute of Bari (CAAE:147/16) (Trial registration number: NCT03096704).

Informed consent statement: All study participants or their legal guardian provided informed written consent about personal and

Alba Panarese, Massimo De Carne, Endrit Shahini, Department of Gastroenterology and Digestive Endoscopy, Scientific Institute for Digestive Disease "Saverio de Bellis" Hospital, Castellana Grotte (Bari) 70013, Italy

Francesco Pesce, Nephrology section, Department of Emergency and Organ Transplantation, University of Bari, Bari 70013, Italy

Piero Porcelli, Department of Psychological, Health, and Territorial Sciences, D'Annunzio University of Chieti-Pescara, Chieti 70013, Italy

Giuseppe Riezzo, Palma Aurelia Iacovazzi, Carla Maria Leone, Department of Clinical Pathology, Scientific Institute for Digestive Disease "Saverio de Bellis" Hospital, Castellana Grotte (Bari) 70013, Italy

Caterina Mammone Rinaldi, Department of Radiology, Scientific Institute for Digestive Disease "Saverio de Bellis" Hospital, Castellana Grotte (Bari) 70013, Italy

Endrit Shahini, Department of Emergency and Organ Transplantation, University of Bari, Bari 70124, Italy

Corresponding author: Alba Panarese, MD, Doctor, Department of Gastroenterology and Digestive Endoscopy, Scientific Institute for Digestive Disease "Saverio de Bellis" Hospital, Turi Street n. 27, Castellana Grotte (Bari) 70013, Italy. alba.panarese@ircsdebis.it

Telephone: +39-3471401487; +39-0804994251

Fax: +39-0804994250

Abstract

BACKGROUND

Few studies have examined intestinal motility disorders, which are disabling conditions associated with chronic functional constipation, whose pathogenesis is actually not well-defined.

AIM

To investigate the relationship between serum 25-hydroxyvitamin D levels and functional chronic constipation associated to intestinal motility disorders.

METHODS

We performed a prospective case-control study, from May-June to November 2017. Glucose/lactulose breath tests, radiopaque markers (multiple capsule techniques) and wireless motility capsule analysis were used to assess colonic

medical data collection prior to study enrolment.

Conflict-of-interest statement: All authors declare no conflict of interest related to this publication.

STROBE statement: The guidelines of the STROBE Statement have been adopted.

Open-Access: This article is an open-access article which was selected by an in-house editor and fully peer-reviewed by external reviewers. It is distributed in accordance with the Creative Commons Attribution Non Commercial (CC BY-NC 4.0) license, which permits others to distribute, remix, adapt, build upon this work non-commercially, and license their derivative works on different terms, provided the original work is properly cited and the use is non-commercial. See: <http://creativecommons.org/licenses/by-nc/4.0/>

Manuscript source: Invited manuscript

Received: February 16, 2019

Peer-review started: February 18, 2019

First decision: February 26, 2019

Revised: March 11, 2019

Accepted: March 24, 2019

Article in press: March 25, 2019

Published online: April 14, 2019

P-Reviewer: Feretis M, Luthin DR, Negreanu L

S-Editor: Yan JP

L-Editor: A

E-Editor: Song H



and oro-cecal transit time, after excluding small-intestinal bacterial overgrowth condition. Then, we measured 25-hydroxyvitamin D levels in patients with intestinal motility disorders and we further evaluated the influence of intestinal motility disorders on psychological symptoms/quality of life using validated questionnaires, the Irritable Bowel Syndrome Quality of life (IBS-QOL), the Short Form Health Survey 12, and the Hospital Anxiety and Depression Scale 14 (HADS-14 A and HADS-14 D).

RESULTS

We enrolled 86 patients with chronic functional constipation associated to intestinal motility disorders and 86 matched healthy subjects. Patients with intestinal motility disorders had lower 25-hydroxyvitamin D levels ($P < 0.001$), and they showed a significant impairment of all health-related quality of life and psychological tests (IBS-QOL, Short Form Health Survey 12-Physical Component Summary, Short Form Health Survey 12-Mental Component Summary, HADS-14 A and HADS-14 D), as compared to the control group ($P < 0.001$), which significantly correlated with low vitamin D levels ($r = -0.57$, $P < 0.001$; $r = 0.21$, $P = 0.01$; $r = -0.48$, $P < 0.001$; $r = -0.57$, $P < 0.001$; $r = -0.29$, $P < 0.001$, respectively). At multivariate analysis vitamin D low levels remained a significant independent risk factor for the occurrence of intestinal motility disorder (odds ratio = 1.19; 95% confidence interval: 1.14-1.26, $P < 0.001$).

CONCLUSION

Vitamin D deficiency, anxiety and depression symptoms are commonly associated with chronic functional constipation induced by intestinal motility disorders. Vitamin D serum levels should be routinely measured in these patients.

Key words: Chronic constipation; Intestinal motility; Vitamin D; Quality of life; Anxiety; Depression

©The Author(s) 2019. Published by Baishideng Publishing Group Inc. All rights reserved.

Core tip: Intestinal motility disorders, which are disabling conditions associated with chronic constipation, have been examined in only a few studies. Patients with intestinal motility disorders are frequently affected by vitamin D deficiency, which is strongly associated to anxiety, depression symptoms and to severe impairment of quality of life. These data suggest that vitamin D serum levels should be routinely measured, and its supplementation should be evaluated in patients with intestinal motility disorders.

Citation: Panarese A, Pesce F, Porcelli P, Riezzo G, Iacovazzi PA, Leone CM, De Carne M, Rinaldi CM, Shahini E. Chronic functional constipation is strongly linked to vitamin D deficiency. *World J Gastroenterol* 2019; 25(14): 1729-1740

URL: <https://www.wjgnet.com/1007-9327/full/v25/i14/1729.htm>

DOI: <https://dx.doi.org/10.3748/wjg.v25.i14.1729>

INTRODUCTION

The term “Constipation” has a broad definition both for physicians and patients^[1]. The most common form is functional chronic constipation, which is a gastrointestinal disorder defined by symptom criteria, after the exclusion of secondary causes^[2-4]. This clinical condition usually affects women, older subjects, particularly those of lower socioeconomic status^[5], and has a prevalence ranging between 2% and 27% in western countries with a high burden on global health-care system^[2,6,7]. The main symptoms of functional chronic constipation are difficulty with evacuation, bloating, abdominal pain, discomfort or hard stools that significantly impair health-related quality of life^[2,8]. Since depression has been commonly observed in patients with the constipation variant of irritable bowel syndrome (IBS), specific questionnaires have been endorsed to evaluate some aspects of the quality of life of these patients, especially the IBS Quality of life (IBS-QOL), the Short Form Health Survey 12 (SF-12),

and the Hospital Anxiety and Depression Scale 14 (HADS-14-A/D)^[9-12]. Moreover, previous studies showed a possible role of vitamin D deficiency in the pathophysiology of IBS and depression, and also beneficial effects of vitamin D supplementation in alleviating depression and certain gastrointestinal symptoms in a population of study prevalently affected by diarrhea or by alternating subtype, and the minority by constipation symptoms^[13-20]. Normal transit constipation is probably the most common form, and it frequently overlaps with the constipation variant of IBS^[9].

Among patients with functional chronic constipation, intestinal motility disorders have been reported. Although the overall prevalence of intestinal motility disorders is not currently well-defined^[2], it involves more commonly patients affected by slow transit constipation (STC)^[2], and rarely subjects with delayed oro-cecal transit time^[21]. In addition, defecation disorders significantly overlap with normal and STC^[9,22]. While STC is characterized by an altered colonic motor activity, and reduced reaction after a meal and when waking up, decreased “high amplitude propagated contractions”, which have been associated to altered regulation of enteric nervous system, reduction of neurons and axons in the myenteric plexus^[2,22-24], delayed oro-cecal transit time could be partially associated with an underlying small-intestinal bacterial overgrowth (SIBO)^[25].

Moreover, the most severe form of intestinal motility disorder may be considered chronic intestinal pseudo-obstruction, which is a symptomatic and disabling disease, related to a visceral myopathy or/and neuropathy^[26]. Hence, colonic transit time could be objectively measured by radiopaque markers (single or multiple capsule techniques), and this diagnostic tool is also used to rule out dyssynergia defecation^[2,23]. Radiopaque markers studies are useful, inexpensive and widely available^[2,23]. In addition, even if not definitively recommended by guidelines, lactulose breath test (LBT) and glucose breath test (GBT), are commonly used in clinical practice to evaluate the presence of SIBO as well as small-bowel motility by estimating oral-cecal transit time^[25,27]. Other expensive tests such as colonic scintigraphy and wireless ingestible motility capsule, measure more accurately overall transit time^[23,27], whereas advanced physiologic tests identify anorectal dysfunctions in patients not responding to initial therapy^[2,27]. In this paper we hypothesized that serum vitamin D deficiency could be associated with chronic functional constipation secondary to delayed intestinal transit time and consequently we investigated this relationship and the related psychological aspects.

MATERIALS AND METHODS

Study design

This case-control study was performed from May-June to November 2017, in the Outpatients Clinic of our Institution, in Apulia, a Mediterranean region located in southeast of Italy. As shown in **Figure 1**, we enrolled 86 subjects from a population of 152 consecutive constipated patients affected by intestinal motility disorders.

Inclusion criteria were the following: Caucasian subjects ≥ 18 years old, body mass index (BMI) ≥ 18.5 kg/m², affected by functional chronic constipation associated to delayed intestinal transit time, supported by Roma IV criteria^[8,26,28]. Exclusion criteria were the following: Subjects > 75 years old, IBS, pregnancy, significant comorbidities such as cardiac, respiratory, chronic renal insufficiency, anorectal and pelvic floor dysfunctions, metabolic/endocrine (diabetes mellitus, hypothyroidism, hypercalcaemia, panhypopituitarism), medications (opiates, antihypertensive agents, iron preparations, anti-epileptic drugs, tricyclic antidepressants, anticholinergics or dopaminergics), organic (extra-intestinal mass, colorectal cancer, ischaemic or surgical stenosis, anal fissure, anal strictures, inflammatory bowel disease, intestinal malabsorption and diverticular diseases), neurological (Parkinson disease, multiple sclerosis, paraplegia, autonomic neuropathy, chronic intestinal pseudo-obstruction, gastroparesis, Hirschsprung disease and stroke), past psychiatric disease, and myogenic (scleroderma, amyloidosis and myotonic dystrophy dermatomyositis)^[2,21,26]. In addition, we also assessed a control group of 86 healthy subjects (sex, age and BMI matched), recruited from a population-based cohort study of 150 healthy subjects, which underwent routine clinical exams in our Institute to check their healthy status, after excluding the presence of a functional chronic constipation during the clinical interview.

Our research was carried out in compliance with the Helsinki Declaration and procedures received approval by the Institutional review board of the National Institute of Gastroenterology “S. De Bellis” Research Hospital (0807/16) and by the Research Ethics Committee of the National Oncological Institute of Bari (CAAE:147/16) (Trial registration number: NCT03096704). Informed consent was

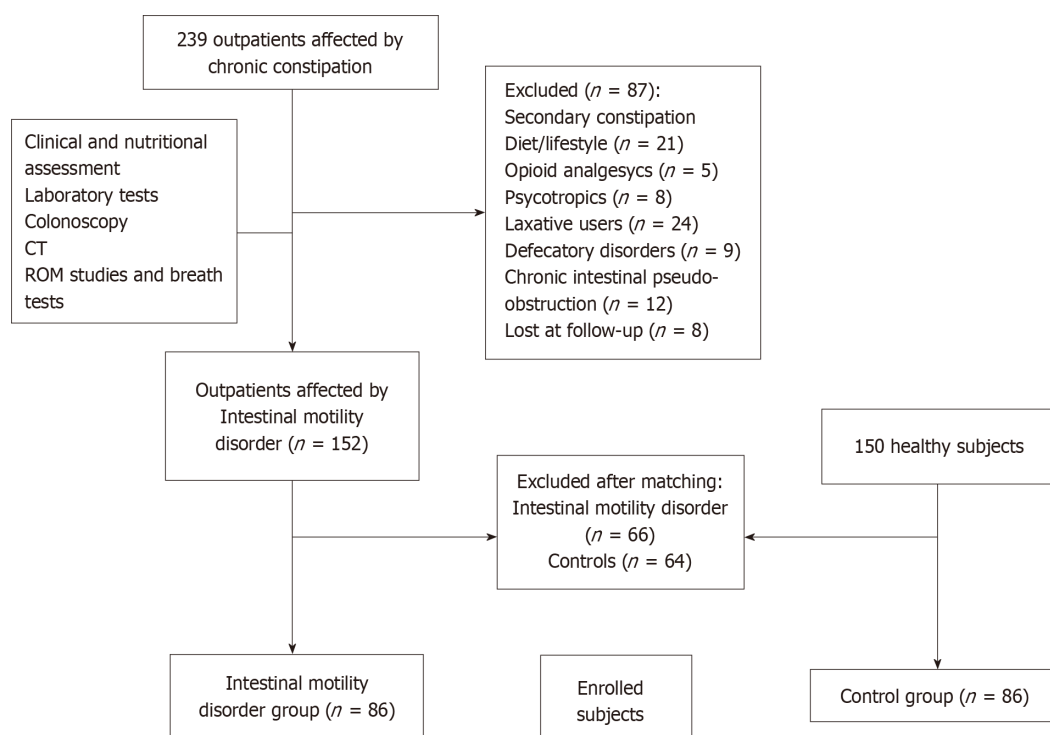


Figure 1 Flow diagram describing the process of patients' selection. CT: Computerized tomography; ROM: Radiopaque markers.

obtained from all participants of the study. The statistical review of the study was performed by a biomedical statistician.

Definition of functional chronic constipation

All selected patients were inquired, before, for any possible secondary causes of functional chronic constipation, including alarm features, lifestyle factors and medical treatments and we also identified the response (or lack of) to previous treatment about constipation symptoms, by interviewing patients. Then, they were considered affected by functional chronic constipation only when they showed a frequency of evacuation less than twice a week with increased stool consistency^[8,26,28]. All the selected patients underwent blood tests, colonoscopy, nutritional assessment (with daily food frequency questionnaires), stool frequency diary, LBT, GBT, wireless motility testing, radiopaque markers studies, and when required, tests for pelvic floor dysfunction, and psychological tests exploring patient's quality of life.

Accordingly, when not eligible, patients were excluded (Figure 1): 152 consecutive subjects affected by functional chronic constipation with intestinal motility disorders met the eligibility criteria, along with 150 healthy subjects. Patients and controls in each group were first randomly sampled from the pool of available individuals (152 with intestinal motility disorders and 150 controls) and, then matched for age, sex and BMI, using MatchIt^[29]. This analysis resulted in 86 patients and 86 matched controls that were enrolled for the study. Our patients did not receive any pharmacological treatment before all evaluations.

Colonic transit time, breath tests and wireless motility analysis

The colon transit time was measured with radiopaque markers, using multiple capsule techniques (P and A Mauch CH-4142 Munchenstein). The patient ingested 1 capsule a day (at 9.00 am, during breakfast) for 3 consecutive days and each capsule with 24 different shaped radio-opaque polyurethane markers, and then performed abdominal x-rays (100KV) on day 7, at 9.00 am, to reconstruct the colon activity during the last week^[30,31]. Normal transit time was considered about 30-40 h, whereas the upper limit, above 70 h. Markers scattered about the colon was due most likely to STC, whereas markers gathered in the recto-sigmoid tract was considered a defecatory disorder^[5,27] (Supplementary material).

Moreover, LBT and GBT were used for measuring oro-cecal transit time. A rise in hydrogen of ≥ 20 ppm by 90 min was considered the cut-off value used to exclude SIBO for both tests^[25]. Time to the second peak and rise of 5-10 ppm of hydrogen, or a level of positivity for methane ≥ 10 ppm on a breath test, were considered useful in estimating oro-cecal transit time^[25,27,32] (Supplementary material). Wireless motility

analysis was also used to quantify oro-cecal transit time (Smartpill, Medtronic, Sunnyvale, California, United States), in order to define the presence of a delayed small intestinal transit time. Normal small-bowel transit should be 6 hours or less^[25] (Supplementary material). Finally, STC and/or delayed oro-cecal transit time were definitively endorsed when radiopaque markers and/or breath tests with wireless motility analysis identified a specific intestinal motility disorder^[27].

Questionnaires for the evaluation of quality of life in patients with intestinal motility disorders

The IBS-QOL questionnaire is a 34-item tool validated to quantify quality of life in non-subtyped IBS patients, but also used to assess the severity of IBS-like symptoms, and psychological factors^[10]. The SF-12 includes a subset of 12 items, used to assess the physical and mental health domain in many diseases. All these scores are converted into a standardized 0-100 score. Higher scores indicate a better self-reported health status^[11]. Furthermore, the HADS-14 represents a global measure of psychological distress and includes 14 items, 7 of them evaluate anxiety symptoms, and 7 depressive ones. Each item is coded from 0 to 3. The total scores for anxiety and depression can range between 0-21, based on symptoms characteristics^[12].

Vitamin D and parathyroid hormone levels measurement

Serum 25-hydroxyvitamin D [25-(OH)-D] (Supplementary material) and parathyroid hormone (PTH) levels were measured in patients and healthy controls within 1 hour from blood draw. Overall subjects were enrolled in the interval time of the year with major sunlight exposition, when 25-(OH)-D values are usually higher^[13]. The 25-(OH)-D levels status was categorized as usually proposed by experts in literature: using a standardized cut-off (deficiency less than 20 ng/mL, insufficiency from 20 to 29 ng/mL and sufficient when equal or higher than 30 ng/mL)^[13].

Statistical analysis

Screened patients and controls in each group were matched for age, sex and BMI using the nearest neighbor matching algorithm implemented in MatchIt^[29]. Normal distribution of continuous variables was assessed with the Shapiro-Wilk test and data were expressed as mean and standard deviation and compared using Student's *t*-test. Categorical variables were reported as percentages and compared using the Chi-squared test or Fisher's exact test, when needed.

Spearman's test was performed to evaluate possible correlations of vitamin D values with quality of life scores and psychological functions (IBS-QOL, SF12-PCS, SF12-MCS, HADS-14 A and HADS-14 D). The impact of the vitamin D levels on patient's risk to have intestinal motility disorders was analysed using univariate and multivariate logistic regression analyses. The association between each explanatory variable and the outcome (intestinal motility disorders occurrence) was tested using the likelihood ratio test. We included in the multivariate model all explanatory variables showing a $P < 0.05$ at univariate analysis. For each variable included in the multivariate model, we calculated both unadjusted and adjusted odds ratios (OR), with their 95% confidence intervals (CI), and the level of significance (using the likelihood ratio test). Statistical significance was set at $P < 0.05$. All statistical analyses were performed using SPSS 23.0 software (SPSS, Chicago, IL, United States) and R version 3.4.3 (<http://www.R-project.org/>).

RESULTS

Characteristics of patients with intestinal motility disorders

As shown in **Figure 1**, 86 patients along with 86 healthy matched subjects, were finally enrolled. The characteristics of patients are shown in **Table 1**. About 85% of patients suffering from intestinal motility disorders were female, and mean age was 49.9 ± 17.4 years. Patients with intestinal motility disorders had significantly lower intermediate and bachelor schooling degree, as compared to the control group ($P = 0.001$ and $P < 0.001$, respectively).

The proportion of patients with intestinal motility disorders was more affected by constipation, abdominal pain, swelling, anxiety and depression symptoms as well as by quality of life alterations, as compared to healthy subjects ($P < 0.001$). The results of the various questionnaires compiled by patients (IBS-QOL, HADS-14 A, HADS-14 D, SF12-PCS and SF12-MCS) showed a significant impairment in all health-related domains ($P < 0.001$) (**Table 1**). Patients with intestinal motility disorders had lower vitamin D serum levels, as compared to the control group ($P < 0.001$). Moreover, the poor results of psychological tests (IBS-QOL, SF12-PCS, SF12-MCS, HADS-14 A and

Table 1 Characteristics of patients with functional chronic constipation with intestinal motility disorders and of controls

Variables	Intestinal motility disorders (n = 86)	Controls (n = 86)
Age, mean \pm SD, yr	49.9 (17.4)	50 (17.1)
Sex, n (%)		
Male	13 (15.1)	13 (15.1)
Female	73 (84.9)	73 (84.9)
BMI, mean \pm SD, kg/m ²	23.7 (2.8)	24.6 (3.4)
Education, n (%)		
Primary	5 (5.8)	5 (5.8)
Intermediate	33 (38.4) ^a	14 (16.3) ^a
High school	38 (44.2)	37 (43)
Bachelor degree	10 (11.6) ^a	28 (32.6) ^a
No data	0	2 (2.3)
Marital status		
Single	30 (34.9)	22 (25.6)
Married	53 (61.6)	58 (67.4)
Widower	3 (3.5)	4 (4.7)
Divorced	0	1 (1.2)
No data	0	1 (1.2)
Symptoms		
Constipation	78 (90.1) ^a	3 (3.5) ^a
Abdominal pain	73 (84.9) ^a	2 (2.3) ^a
Swelling	79 (91.9) ^a	14 (16) ^a
IBS-QOL (total score)	108.4 (23.7) ^a	39.8 (7.7) ^a
Dysphoria	24.1 (7.7) ^a	8.7 (1.5) ^a
Interference	15.9 (5.5) ^a	8 (1.6) ^a
Body image	15 (2.1) ^a	4.8 (1.4) ^a
Anxiety health	13.5 (1.8) ^a	3.7 (1.4) ^a
Food avoidance	13.6 (1.6) ^a	3.7 (1.4) ^a
Social reaction	10.8 (3.2) ^a	5 (1.1) ^a
Interpersonal relationships	6.3 (3.3) ^a	3.3 (0.6) ^a
Sexuality	4.6 (2.2) ^a	2 (0.1) ^a
HADS-14 A	14.6 (4.3) ^a	2.4 (1.8) ^a
HADS-14 D	14.6 (3.1) ^a	4.5 (2.6) ^a
SF12-PCS	37.3 (9.8) ^a	47.2 (7.6) ^a
SF12-MCS	29.1 (7.4) ^a	56 (7.1) ^a
PTH, mean \pm SD, 10-70 pg/mL	51.1 (12.1)	-
Vitamin D, mean \pm SD, IU/mL	14.6 (7.7) ^a	28.4 (8.8) ^a

^a $P < 0.01$ vs controls by t , F or χ^2 . Values are absolute numbers and percentages (in parentheses) or average numbers and standard deviation (in parentheses). BMI: Body mass index; IBS-QOL: Irritable Bowel Syndrome Quality of life; HADS-14 A: Hospital Anxiety and Depression Scale-14 for Anxiety; HADS-14 D: Hospital Anxiety and Depression Scale-14 for Depression; SF12-PCS: Short Form Health Survey12-Physical Component Summary; SF12-MCS: Short Form Health Survey12-Mental Component Summary; PTH: Parathyroid hormone.

HADS-14 D) significantly correlated with low vitamin D levels ($r = -0.57$, $P < 0.001$; $r = 0.21$, $P = 0.01$; $r = -0.48$, $P < 0.001$; $r = -0.57$, $P < 0.001$; $r = -0.29$, $P < 0.001$, respectively). Other parameters, such as the age, sex and marital status did not differ between the two groups (Table 1).

In the groups with intestinal motility disorders, 32, 28 and 26 patients, after completing all diagnostic tests, received a diagnosis of delayed oro-cecal transit time (37.2%), STC (32.6%) or delayed oro-cecal transit time with STC (30.2%), respectively. In the group with delayed oro-cecal transit time and with STC, the proportion of patients who suffered constipation, swelling, abdominal pain and vitamin D deficiency (< 20 ng/mL) was higher than groups with delayed oro-cecal transit time or with STC ($P = 0.03$, $P = 0.02$, $P = 0.03$ and $P = 0.04$ respectively) (Figure 2). When we

considered the three groups: subjects with delayed transit time in both intestinal tracts (26), to patients with delayed transit time in only one tract (60) and to controls (86), the quality of life showed worsening functions. Moreover, vitamin D and BMI were significantly reduced with decreasing values as following for the variables: delayed oro-cecal transit time with STC group less than delayed oro-cecal transit time or STC group, less than controls ($P < 0.001$, respectively) (Supplementary material).

Patients with delayed transit time of both intestinal tracts, as compared to patients with delayed transit time involving only one tract, showed significantly reduced levels of vitamin D and higher PTH levels (for both $P < 0.001$), and showed worsening quality of life ($P < 0.001$) (Supplementary material). Patients with delayed transit time in both intestinal tracts showed significantly reduced serum levels of vitamin D and higher PTH serum levels (for both $P < 0.001$), and showed worsening quality of life ($P < 0.001$) than patients with delayed transit time in only one tract (Supplementary material).

Risk factors associated to intestinal motility disorders

Results from linear regression analysis are shown in Table 2. At univariate and multivariate analysis adjusted for BMI, vitamin D levels remained a significant independent risk factor for intestinal motility disorders occurrence (OR = 1.19; 95% CI: 1.14-1.26, $P < 0.001$).

DISCUSSION

In this study, we demonstrated for the first time that serum vitamin D deficiency could be associated to functional chronic constipation induced by intestinal motility disorders. Furthermore, patients showing the latter clinical condition are frequently affected by anxiety and depression symptoms which severely impair their quality of life.

About 1 billion people have vitamin D insufficiency or deficiency^[13]. Nowadays, this phenomenon is associated with significant disability and healthcare costs^[14,15]. Several studies showed that hypovitaminosis D may be a risk factor for many chronic diseases and for mortality^[16,33-36]. Notably, vitamin D deficiency has been involved in the pathophysiology of inflammatory bowel disease, IBS and also depression^[13-17,19].

Some multicentric studies, reported a higher prevalence of hypovitaminosis D in the southern Europe^[37,38]. Interestingly, Italian elderly subjects showed the lowest levels of vitamin D in Europe in the winter season^[37,38]. In our study, we found low serum levels of vitamin D, mainly checked during the summer season, among patients affected by intestinal motility disorders during an interval time when vitamin D values are usually high, due to beta-ultraviolet rays exposition^[13,36]. Moreover, our patients were prevalently female (84.9%) and relatively younger, although, vitamin D deficiency has not been limited to the elderly age^[35-38]. While low levels of vitamin D have been also observed in winter in 33% of pre-menopausal women, especially if obese^[39], in our study the majority of patients with intestinal motility disorders had normal BMI.

How vitamin D deficiency and intestinal motility disorders are linked remains an open question. One intriguing hypothesis may be that STC and/or delayed small intestinal transit time could negatively modify the gut microbiota^[36], or conversely altered microbiome could primarily affect mucosal barrier and gut motility due to microbial-derived metabolites^[40]. In addition, some studies suggested that vitamin D deficiency could predispose to gastrointestinal infections^[16], which could be responsible of the “leaky gut” alteration and of loss of immune homeostasis^[40,41]. However, in our patients we also performed LBT and GBT, to exclude SIBO. When the clinical suspicion of the latter condition remained, we treated them “*ex juvantibus*”, and we further excluded SIBO as the main cause of bowel symptoms, especially when they did not disappear after a gut-targeted antibiotic therapeutic cycle.

Anyway, the presence of vitamin D receptor on gut epithelial cells, macrophages and lymphocytes surface, has suggested a possible link between vitamin D deficiency, the dysfunction of its receptor and gut microbiota composition, leading to the onset of autoimmune diseases^[40,42,43]. Finally, the influence of vitamin D deficiency on human immune system is also supported by its involvement in the development of multiple sclerosis^[44]. As concerning this aspect, an interesting study supported a role of autoantibodies against enteric nervous system targets in B cell-deficient mice with experimental autoimmune encephalomyelitis model of multiple sclerosis, showing that serum immunoreactivity (idiopathically or secondary to another autoimmune disease), could be implicated in the induction of autoimmune gastrointestinal

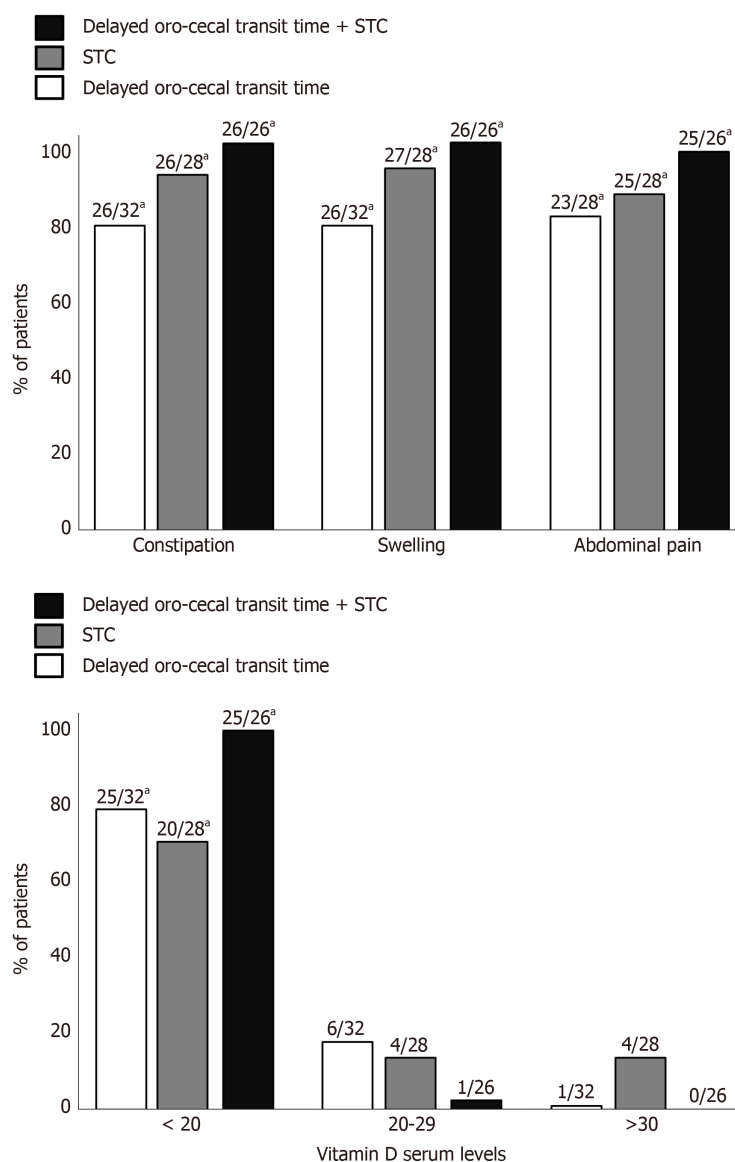


Figure 2 Proportion of patients who suffered constipation, swelling, abdominal pain and vitamin D serum levels, in delayed small intestinal transit time, slow transit constipation, and delayed small intestinal transit time (with) slow transit constipation groups. STC: Slow transit constipation. Significantly different by ^a $P < 0.05$.

dysmotility^[45]. In fact, in humans with multiple sclerosis, whose pathogenesis has been linked to vitamin D deficiency, a slow colonic motility in the proximal tract as well as autonomic rectal dysfunction has been observed^[44-48].

We may suppose that the intestinal motility disorder could be the “primum movens” of an underlying autoimmune process in a specific genetic background and unmasked by chronic vitamin D deficiency, which could exert metabolic/immunologic damage on epithelial and neuromuscular structures of the gut. The latter alterations could include gut hyper-permeability and bacterial translocation, whose degree of injury and extension could be influenced by the severity of vitamin D deficiency^[22,45]. This hypothesis may be supported by our results, which showed that levels of vitamin D were independently associated with intestinal motility disorders and by the fact that the prevalence of symptoms associated to functional chronic constipation grew up in concordance with the worsening of vitamin D levels, especially in patients involving more extensively the bowel tract. Furthermore, patients with intestinal motility disorders had high levels of psychological distress with impaired quality of life, and hypovitaminosis D significantly correlated with the worsening of the psychological functions. In our study, a potential bias could derive from disease misclassification, which could be a negligible factor since intestinal motility disorder was diagnosed following standardized criteria, and from the small sample size of our population. Moreover, we did not check fecal microbiota composition.

Table 2 Probability of intestinal motility disorder occurrence at the univariate and multivariate analysis

Variable	Univariate analysis		Multivariate analysis	
	OR (95%CI)	P value	OR ¹ (95%CI)	P value
Age, yr	1.0 (0.98-1.01)	0.76	-	-
BMI, kg/m ²	0.91 (0.82-1.0)	0.04	0.98 (0.86-1.11)	0.72
Vitamin D, IU/mL	0.82 (0.78-0.87)	< 0.001	0.83 (0.78-0.87)	< 0.001

¹Adjusted for all variables in the multivariate model. BMI: Body mass index. OR: Odds ratio; CI: Confidence interval.

In conclusion, we demonstrated that vitamin D deficiency could be strongly related to intestinal motility disorders. Moreover, patients with intestinal motility disorders are very commonly affected by anxiety and depression symptoms which severely influence their quality of life. If the latter two psychiatric symptoms are caused by intestinal factors, it will be confirmed only through a cross-sectional study. Therefore, we suggest that vitamin D serum levels should be routinely measured and vitamin D supplementation should be considered, to better evaluate its effects on intestinal motility and quality of life of patients with intestinal motility disorders.

ARTICLE HIGHLIGHTS

Research background

Functional chronic constipation is a gastrointestinal disorder that affects more commonly women and older subjects, with a deep impact on global health-care system. Nowadays, only few studies have examined intestinal motility disorders, which are severe clinical conditions associated with chronic functional constipation, whose pathogenesis and prevalence are actually partially known. In this subgroup are included patients with slow transit constipation, as well as with slow oro-cecal transit time, whereas their extreme clinical form, could be considered chronic intestinal pseudo-obstruction, which has been related to the structural damage of neural and smooth muscle cells of gut.

Research motivation

Although some studies have shown a possible link between vitamin D deficiency and irritable bowel syndrome (IBS), as well as with depression (and with several other diseases), the same link has never been detected before in patients affected by intestinal motility disorders, and the indications to look for vitamin D in these patients relied only of opinions of experts in the field. Therefore we investigated this relationship and the psychological aspects in this subgroup of patients.

Research objectives

To investigate the relationship between serum 25-hydroxyvitamin D levels and functional chronic constipation linked to intestinal motility disorders.

Research methods

Herein, we applied rigorous statistical methods to elucidate this relationship. We performed a prospective case-control study, from May-June to November 2017. We used Glucose/lactulose breath tests, radiopaque markers (multiple capsule techniques) and wireless motility capsule analysis to estimate both oro-cecal and colonic transit time. After receiving a diagnosis of intestinal motility disorders, patients underwent to blood sampling, for checking 25-hydroxyvitamin D levels. Furthermore, we evaluated for these patients the influence on psychological features and on their quality of life, which were estimated by using validated questionnaires, the IBS Quality of life (IBS-QOL), the Short Form Health Survey 12 (SF-12), and the Hospital Anxiety and Depression Scale 14 (HADS-14 A and HADS-14 D).

Research results

Our cohort included 86 patients with chronic functional constipation associated to intestinal motility disorders and 86 age, sex, body mass index (BMI)-matched healthy subjects. Patients with intestinal motility disorders had lower 25-hydroxyvitamin D levels ($P < 0.001$), and they showed a significant impairment of all health-related quality of life domains and psychological tests (IBS-QOL, SF12-PCS, SF12-MCS, HADS-14 A and HADS-14 D), as compared to the control group ($P < 0.001$). Moreover, the latter tests significantly correlated with reduced vitamin D levels ($r = -0.57$, $P < 0.001$; $r = 0.21$, $P = 0.01$; $r = -0.48$, $P < 0.001$; $r = -0.57$, $P < 0.001$; $r = -0.29$, $P < 0.001$, respectively). In multivariate analysis, vitamin D low levels remained significantly associated with the occurrence of intestinal motility disorder, after adjusting for BMI (odds ratio = 1.19; 95% confidence interval: 1.14-1.26, $P < 0.001$).

Research conclusions

We demonstrated for the first time a strong association between vitamin D deficiency and intestinal motility disorders. Moreover, these patients are very commonly affected by anxiety and depression symptoms which deeply impact on their quality of life. These findings suggest that vitamin D serum levels should be routinely measured in this category of patients and consequently vitamin D supplementation could represent a further therapeutic aid for this clinical condition.

Research perspectives

Our findings may confirm how vitamin D deficiency could exert a wide spectrum of action in many gastrointestinal (or not) diseases, being highly associated with intestinal motility disorders and with certain neuropsychiatric symptoms, but remains unclear if it could have a causative role in this process, and for this reason, future cross-sectional studies are needed, also to investigate if anxiety and depression symptoms are caused by intestinal factors.

ACKNOWLEDGEMENTS

We thank to Vanessa Terenzio and Domenico Flavio Terenzio, native English speakers, for the language revision of this manuscript.

REFERENCES

- 1 Pare P, Ferrazzi S, Thompson WG, Irvine EJ, Rance L. An epidemiological survey of constipation in Canada: Definitions, rates, demographics, and predictors of health care seeking. *Am J Gastroenterol* 2001; **96**: 3130-3137 [PMID: 11721760 DOI: 10.1111/j.1572-0241.2001.05259.x]
- 2 Tack J, Müller-Lissner S, Stanghellini V, Boeckxstaens G, Kamm MA, Simren M, Galmiche JP, Fried M. Diagnosis and treatment of chronic constipation—a European perspective. *Neurogastroenterol Motil* 2011; **23**: 697-710 [PMID: 21605282 DOI: 10.1111/j.1365-2982.2011.01709.x]
- 3 Palsson OS, Baggish JS, Turner MJ, Whitehead WE. IBS patients show frequent fluctuations between loose/watery and hard/lumpy stools: Implications for treatment. *Am J Gastroenterol* 2012; **107**: 286-295 [PMID: 22068664 DOI: 10.1038/ajg.2011.358]
- 4 Palsson OS, Baggish J, Whitehead WE. Episodic nature of symptoms in irritable bowel syndrome. *Am J Gastroenterol* 2014; **109**: 1450-1460 [PMID: 24980882 DOI: 10.1038/ajg.2014.181]
- 5 Wald A, Scarpignato C, Kamm MA, Mueller-Lissner S, Helfrich I, Schuijt C, Bubeck J, Limoni C, Petrini O. The burden of constipation on quality of life: Results of a multinational survey. *Aliment Pharmacol Ther* 2007; **26**: 227-236 [PMID: 17593068 DOI: 10.1111/j.1365-2036.2007.03376.x]
- 6 Suares NC, Ford AC. Prevalence of, and risk factors for, chronic idiopathic constipation in the community: Systematic review and meta-analysis. *Am J Gastroenterol* 2011; **106**: 1582-1591; quiz 1581, 1592 [PMID: 21606976 DOI: 10.1038/ajg.2011.164]
- 7 Cottone C, Tosetti C, Disclafani G, Ubaldi E, Cogliandro R, Stanghellini V. Clinical features of constipation in general practice in Italy. *United European Gastroenterol J* 2014; **2**: 232-238 [PMID: 25360307 DOI: 10.1177/2050640614527283]
- 8 Belsey J, Greenfield S, Candy D, Geraint M. Systematic review: Impact of constipation on quality of life in adults and children. *Aliment Pharmacol Ther* 2010; **31**: 938-949 [PMID: 20180788 DOI: 10.1111/j.1365-2036.2010.04273.x]
- 9 Shekhar C, Monaghan PJ, Morris J, Issa B, Whorwell PJ, Keevil B, Houghton LA. Rome III functional constipation and irritable bowel syndrome with constipation are similar disorders within a spectrum of sensitization, regulated by serotonin. *Gastroenterology* 2013; **145**: 749-757; quiz e13-4 [PMID: 23872499 DOI: 10.1053/j.gastro.2013.07.014]
- 10 Drossman DA, Patrick DL, Whitehead WE, Toner BB, Diamant NE, Hu Y, Jia H, Bangdiwala SI. Further validation of the IBS-QOL: A disease-specific quality-of-life questionnaire. *Am J Gastroenterol* 2000; **95**: 999-1007 [PMID: 10763950 DOI: 10.1111/j.1572-0241.2000.01941.x]
- 11 Gondek B, Ware JE, Aaronson NK, Apolone G, Bjorner JB, Brazier JE, Bullinger M, Kaasa S, Leplege A, Prieto L, Sullivan M. Cross-validation of item selection and scoring for the SF-12 Health Survey in nine countries: Results from the IQOLA Project. International Quality of Life Assessment. *J Clin Epidemiol* 1998; **51**: 1171-1178 [PMID: 9817135 DOI: 10.1155/2016/9282087]
- 12 Pallant JF, Tennant A. An introduction to the Rasch measurement model: an example using the Hospital Anxiety and Depression Scale (HADS). *Br J Clin Psychol* 2007; **46**: 1-18 [PMID: 17472198 DOI: 10.1348/014466506X96931]
- 13 Holick MF. Vitamin D deficiency. *N Engl J Med* 2007; **357**: 266-281 [PMID: 17634462 DOI: 10.1056/NEJMr070553]
- 14 Lopez AD, Mathers CD, Ezzati M, Jamison DT, Murray CJ. Global and regional burden of disease and risk factors, 2001: Systematic analysis of population health data. *Lancet* 2006; **367**: 1747-1757 [PMID: 16731270 DOI: 10.1016/S0140-6736(06)68770-9]
- 15 Plum LA, DeLuca HF. Vitamin D, disease and therapeutic opportunities. *Nat Rev Drug Discov* 2010; **9**: 941-955 [PMID: 21119732 DOI: 10.1038/nrd3318]
- 16 Autier P, Mullie P, Macacu A, Dragomir M, Boniol M, Coppens K, Pizot C, Boniol M. Effect of vitamin D supplementation on non-skeletal disorders: A systematic review of meta-analyses and randomised trials. *Lancet Diabetes Endocrinol* 2017; **5**: 986-1004 [PMID: 29102433 DOI: 10.1016/S2213-8587(17)30357-1]
- 17 Tazzyman S, Richards N, Trueman AR, Evans AL, Grant VA, Garaiova I, Plummer SF, Williams EA, Corfe BM. Vitamin D associates with improved quality of life in participants with irritable bowel syndrome: Outcomes from a pilot trial. *BMJ Open Gastroenterol* 2015; **2**: e000052 [PMID: 26719813 DOI: 10.1136/bmjgast-2015-000052]
- 18 Abbasnezhad A, Amani R, Hajiani E, Alavinejad P, Cheraghian B, Ghadiri A. Effect of vitamin D on gastrointestinal symptoms and health-related quality of life in irritable bowel syndrome patients: A

- randomized double-blind clinical trial. *Neurogastroenterol Motil* 2016; **28**: 1533-1544 [PMID: 27154424 DOI: 10.1111/nmo.12851]
- 19 **Anglin RE**, Samaan Z, Walter SD, McDonald SD. Vitamin D deficiency and depression in adults: Systematic review and meta-analysis. *Br J Psychiatry* 2013; **202**: 100-107 [PMID: 23377209 DOI: 10.1192/bjp.bp.111.106666]
 - 20 **Li G**, Mbuagbaw L, Samaan Z, Falavigna M, Zhang S, Adachi JD, Cheng J, Papaioannou A, Thabane L. Efficacy of vitamin D supplementation in depression in adults: A systematic review. *J Clin Endocrinol Metab* 2014; **99**: 757-767 [PMID: 24423304 DOI: 10.1210/jc.2013-3450]
 - 21 **Rao SS**, Rattanakovit K, Patcharatrakul T. Diagnosis and management of chronic constipation in adults. *Nat Rev Gastroenterol Hepatol* 2016; **13**: 295-305 [PMID: 27033126 DOI: 10.1038/nrgastro.2016.53]
 - 22 **De Giorgio R**, Camilleri M. Human enteric neuropathies: Morphology and molecular pathology. *Neurogastroenterol Motil* 2004; **16**: 515-531 [PMID: 15500508 DOI: 10.1111/j.1365-2982.2004.00538.x]
 - 23 **Rao SS**, Kuo B, McCallum RW, Chey WD, DiBaise JK, Hasler WL, Koch KL, Lackner JM, Miller C, Saad R, Semler JR, Sitrin MD, Wilding GE, Parkman HP. Investigation of colonic and whole-gut transit with wireless motility capsule and radiopaque markers in constipation. *Clin Gastroenterol Hepatol* 2009; **7**: 537-544 [PMID: 19418602 DOI: 10.1016/j.cgh.2009.01.017]
 - 24 **Parthasarathy G**, Chen J, Chen X, Chia N, O'Connor HM, Wolf PG, Gaskins HR, Bharucha AE. Relationship Between Microbiota of the Colonic Mucosa vs Feces and Symptoms, Colonic Transit, and Methane Production in Female Patients With Chronic Constipation. *Gastroenterology* 2016; **150**: 367-379.e1 [PMID: 26460205 DOI: 10.1053/j.gastro.2015.10.005]
 - 25 **Rezaie A**, Buresi M, Lembo A, Lin H, McCallum R, Rao S, Schmulson M, Valdovinos M, Zakko S, Pimentel M. Hydrogen and Methane-Based Breath Testing in Gastrointestinal Disorders: The North American Consensus. *Am J Gastroenterol* 2017; **112**: 775-784 [PMID: 28323273 DOI: 10.1038/ajg.2017.46]
 - 26 **Di Nardo G**, Karunaratne TB, Frediani S, De Giorgio R. Chronic intestinal pseudo-obstruction: Progress in management? *Neurogastroenterol Motil* 2017; **29** [PMID: 29143474 DOI: 10.1111/nmo.13231]
 - 27 **Rao SS**, Camilleri M, Hasler WL, Maurer AH, Parkman HP, Saad R, Scott MS, Simren M, Soffer E, Szarka L. Evaluation of gastrointestinal transit in clinical practice: Position paper of the American and European Neurogastroenterology and Motility Societies. *Neurogastroenterol Motil* 2011; **23**: 8-23 [PMID: 21138500 DOI: 10.1111/j.1365-2982.2010.01612.x]
 - 28 **Mearin F**, Lacy BE, Chang L, Chey WD, Lembo AJ, Simren M, Spiller R. Bowel Disorders. *Gastroenterology* 2016; pii: S0016-5085(16)00222-5 [PMID: 27144627 DOI: 10.1053/j.gastro.2016.02.031]
 - 29 **Ho DE**, Imai K, King G, Stuart EA. MatchIt: Nonparametric reprocessing for parametric causal inference. *J Stat Softw* 2011; **42**: 1-28 [DOI: 10.18637/jss.v042.i08]
 - 30 **Metcalf AM**, Phillips SF, Zinsmeister AR, MacCarty RL, Beart RW, Wolff BG. Simplified assessment of segmental colonic transit. *Gastroenterology* 1987; **92**: 40-47 [PMID: 3023168 DOI: 10.1016/0016-5085(87)90837-7]
 - 31 **Chaussade S**, Roche H, Khyari A, Couturier D, Guerre J. Measurement of colonic transit time: Description and validation of a new method. *Gastroenterol Clin Biol* 1986; **10**: 385-389 [PMID: 3732742]
 - 32 **Ghoshal UC**. How to interpret hydrogen breath tests. *J Neurogastroenterol Motil* 2011; **17**: 312-317 [PMID: 21860825 DOI: 10.5056/jnm.2011.17.3.312]
 - 33 **Hess AF**, Unger LJ. The cure of infantile rickets by sunlight. *JAMA* 1921; **77**: 39-41 [DOI: 10.1001/jama.1921.02630270037013]
 - 34 **Stamp TC**. Sources of vitamin D nutrition. *Lancet* 1980; **1**: 316 [PMID: 6101773 DOI: 10.1016/S0140-6736(80)90814-4]
 - 35 **van der Wielen RP**, Löwik MR, van den Berg H, de Groot LC, Haller J, Moreiras O, van Staveren WA. Serum vitamin D concentrations among elderly people in Europe. *Lancet* 1995; **346**: 207-210 [PMID: 7616799 DOI: 10.1016/S0140-6736(95)91266-5]
 - 36 **Vaes AMM**, Brouwer-Brolsma EM, van der Zwaluw NL, van Wijngaarden JP, Berendsen AAM, van Schoor N, van der Velde N, Uitterlinden A, Lips P, Dhonukshe-Rutten RAM, de Groot LCPGM. Food sources of vitamin D and their association with 25-hydroxyvitamin D status in Dutch older adults. *J Steroid Biochem Mol Biol* 2017; **173**: 228-234 [PMID: 27777183 DOI: 10.1016/j.jsbmb.2016.10.004]
 - 37 **Cashman KD**, Dowling KG, Škrabáková Z, Gonzalez-Gross M, Valtueña J, De Henauw S, Moreno L, Damsgaard CT, Michaelsen KF, Mølgaard C, Jorde R, Grimnes G, Moschonis G, Mavrogianni C, Manios Y, Thamm M, Mensink GB, Rabenberg M, Busch MA, Cox L, Meadows S, Goldberg G, Prentice A, Dekker JM, Nijpels G, Pilz S, Swart KM, van Schoor NM, Lips P, Eiriksdottir G, Gudnason V, Cotch MF, Koskinen S, Lamberg-Allardt C, Durazo-Arvizu RA, Sempos CT, Kiely M. Vitamin D deficiency in Europe: Pandemic? *Am J Clin Nutr* 2016; **103**: 1033-1044 [PMID: 26864360 DOI: 10.3945/ajcn.115.120873]
 - 38 **Carnevale V**, Modoni S, Pileri M, Di Giorgio A, Chiodini I, Minisola S, Vieth R, Scillitani A. Longitudinal evaluation of vitamin D status in healthy subjects from southern Italy: Seasonal and gender differences. *Osteoporos Int* 2001; **12**: 1026-1030 [PMID: 11846328 DOI: 10.1007/s001980170012]
 - 39 **Adami S**, Bertoldo F, Braga V, Fracassi E, Gatti D, Gandolini G, Minisola S, Battista Rini G. 25-hydroxy vitamin D levels in healthy premenopausal women: Association with bone turnover markers and bone mineral density. *Bone* 2009; **45**: 423-426 [PMID: 19465168 DOI: 10.1016/j.bone.2009.05.012]
 - 40 **Clark A**, Mach N. Role of Vitamin D in the Hygiene Hypothesis: The Interplay between Vitamin D, Vitamin D Receptors, Gut Microbiota, and Immune Response. *Front Immunol* 2016; **7**: 627 [PMID: 28066436 DOI: 10.3389/fimmu.2016.00627]
 - 41 **Ge X**, Zhao W, Ding C, Tian H, Xu L, Wang H, Ni L, Jiang J, Gong J, Zhu W, Zhu M, Li N. Potential role of fecal microbiota from patients with slow transit constipation in the regulation of gastrointestinal motility. *Sci Rep* 2017; **7**: 441 [PMID: 28348415 DOI: 10.1038/s41598-017-00612-y]
 - 42 **He L**, Liu T, Shi Y, Tian F, Hu H, Deb DK, Chen Y, Bissonnette M, Li YC. Gut Epithelial Vitamin D Receptor Regulates Microbiota-Dependent Mucosal Inflammation by Suppressing Intestinal Epithelial Cell Apoptosis. *Endocrinology* 2018; **159**: 967-979 [PMID: 29228157 DOI: 10.1210/en.2017-00748]
 - 43 **Shahini E**, Iannone A, Romagno D, Armandi A, Carparelli S, Principi M, Viggiani MT, Ierardi E, Di Leo A, Barone M. Clinical relevance of serum non-organ-specific antibodies in patients with HCV infection receiving direct-acting antiviral therapy. *Aliment Pharmacol Ther* 2018; **48**: 1138-1145 [PMID: 30375693 DOI: 10.1111/apt.14999]
 - 44 **Thompson AJ**, Baranzini SE, Geurts J, Hemmer B, Ciccarelli O. Multiple sclerosis. *Lancet* 2018; **391**: 1622-1636 [PMID: 29576504 DOI: 10.1016/S0140-6736(18)30481-1]

- 45 **Spear ET**, Holt EA, Joyce EJ, Haag MM, Mawe SM, Hennig GW, Lavoie B, Applebee AM, Teuscher C, Mawe GM. Altered gastrointestinal motility involving autoantibodies in the experimental autoimmune encephalomyelitis model of multiple sclerosis. *Neurogastroenterol Motil* 2018; **30**: e13349 [PMID: 29644797 DOI: 10.1111/nmo.13349]
- 46 **Chia YW**, Gill KP, Jameson JS, Forti AD, Henry MM, Swash M, Shorvon PJ. Paradoxical puborectalis contraction is a feature of constipation in patients with multiple sclerosis. *J Neurol Neurosurg Psychiatry* 1996; **60**: 31-35 [PMID: 8558147 DOI: 10.1136/jnnp.60.1.31]
- 47 **Li Q**, Michel K, Annahazi A, Demir IE, Ceyhan GO, Zeller F, Komorowski L, Stöcker W, Beyak MJ, Grundy D, Farrugia G, De Giorgio R, Schemann M. Anti-Hu antibodies activate enteric and sensory neurons. *Sci Rep* 2016; **6**: 38216 [PMID: 27905561 DOI: 10.1038/srep38216]
- 48 **De Giorgio R**, Bovara M, Barbara G, Canossa M, Sarnelli G, De Ponti F, Stanghellini V, Tonini M, Cappello S, Pagnotta E, Nobile-Orazio E, Corinaldesi R. Anti-HuD-induced neuronal apoptosis underlying paraneoplastic gut dysmotility. *Gastroenterology* 2003; **125**: 70-79 [PMID: 12851872 DOI: 10.1016/s0016-5085(03)00664-4]



Retrospective Study

Clinical characteristics of non-alcoholic fatty liver disease in Chinese adult hypopituitary patients

Xian-Xian Yuan, Hui-Juan Zhu, Hui Pan, Shi Chen, Ze-Yu Liu, Yue Li, Lin-Jie Wang, Lin Lu, Hong-Bo Yang, Feng-Ying Gong

ORCID number: Xian-Xian Yuan (0000-0001-8762-8471); Hui-Juan Zhu (0000-0001-5172-6870); Hui Pan (0000-0003-2413-0646); Shi Chen (0000-0002-6473-5511); Ze-Yu Liu (0000-0001-7318-9340); Yue Li (0000-0001-6799-1812); Lin-Jie Wang (0000-0002-9548-0398); Lin Lu (0000-0003-3379-8277); Hong-Bo Yang (0000-0003-2985-8265); Feng-Ying Gong (0000-0002-6361-3811).

Author contributions: All authors helped to perform the research; Zhu HJ conceived and designed the project; Pan H, Gong FY, and Zhu HJ contributed to the project management; Chen S, Wang LJ, Lu L, and Yang HB took part in the collection of clinical samples; Yuan XX and Liu ZY took part in the statistical analysis; Yuan XX and Zhu HJ wrote the manuscript; and Li Y took part in the revision of the manuscript.

Supported by the National Key Program of Clinical Science, No. WBYZ 2011-873; the Chinese Academy of Medical Sciences Innovation Fund for Medical Sciences, No. 2016YFC0901500; and the Special Research Fund for Central Universities, Peking Union Medical College, No. 2017PT31004.

Institutional review board

statement: This study was reviewed and approved by the Ethics Committee of the Peking Union Medical College Hospital (No. JS1233).

Informed consent statement:

Patients were not required to give informed consent to the study

Xian-Xian Yuan, Hui-Juan Zhu, Hui Pan, Shi Chen, Lin-Jie Wang, Lin Lu, Hong-Bo Yang, Feng-Ying Gong, Department of Endocrinology, Key Laboratory of Endocrinology of National Health Commission of the People's Republic of China, The Translational Medicine Center of Peking Union Medical College Hospital, Peking Union Medical College Hospital, Chinese Academy of Medical Sciences and Peking Union Medical College, Beijing 100730, China

Ze-Yu Liu, Department of Radiology, Peking Union Medical College Hospital, Chinese Academy of Medical Sciences and Peking Union Medical College, Beijing 100730, China

Yue Li, Department of Gastroenterology, Peking Union Medical College Hospital, Chinese Academy of Medical Sciences and Peking Union Medical College, Beijing 100730, China

Corresponding author: Hui-Juan Zhu, MD, Professor, Department of Endocrinology, Key Laboratory of Endocrinology of National Health Commission of the People's Republic of China, The Translational Medicine Center of Peking Union Medical College Hospital, Peking Union Medical College Hospital, Chinese Academy of Medical Sciences and Peking Union Medical College, No. 1, Shuaifuyuan, Dongcheng District, Beijing 100730, China.
shengxin2004@163.com

Telephone: +86-10-69155073

Fax: +86-10-69155073

Abstract

BACKGROUND

Patients with hypothalamic-pituitary disease have the feature of central obesity, insulin resistance, and dyslipidemia, and there is increased prevalence of liver dysfunction consistent with non-alcoholic fatty liver disease (NAFLD) in this population. The causes of hypopituitarism in the reported studies varied and combined pituitary hormone deficiency including central diabetes insipidus is much common in this population. This retrospective cross-sectional study was performed to analyze the clinical characteristics and related factors with NAFLD and cirrhosis in Chinese adult hypopituitary/panhypopituitary patients.

AIM

To analyze the clinical characteristics of and related risk factors for NAFLD in Chinese adult hypopituitary patients.

METHODS

Adult Chinese patients with hypopituitarism and/or panhypopituitarism were enrolled at the Pituitary Center of Peking Union Medical College Hospital

because the analysis used anonymous clinical data that were obtained from the Electronic Medical Record of Peking Union Medical College Hospital.

Conflict-of-interest statement:

There is no conflict of interest regarding the work presented in this manuscript.

Open-Access: This article is an open-access article which was selected by an in-house editor and fully peer-reviewed by external reviewers. It is distributed in accordance with the Creative Commons Attribution Non Commercial (CC BY-NC 4.0) license, which permits others to distribute, remix, adapt, build upon this work non-commercially, and license their derivative works on different terms, provided the original work is properly cited and the use is non-commercial. See: <http://creativecommons.org/licenses/by-nc/4.0/>

Manuscript source: Unsolicited manuscript

Received: January 13, 2019

Peer-review started: January 14, 2019

First decision: February 13, 2019

Revised: March 13, 2019

Accepted: March 15, 2019

Article in press: March 16, 2019

Published online: April 14, 2019

P-Reviewer: Sitkin S, Gatselis NK

S-Editor: Ma RY

L-Editor: Wang TQ

E-Editor: Song H



between August 2012 and April 2018. According to abdominal ultrasonography, these patients were divided into an NAFLD (-) group and an NAFLD (+) group, and the latter was further divided into an NAFLD group and a cirrhotic group. The data, such as patient characteristics, diagnosis, and treatment, were extracted from medical records, and statistical analysis was performed.

RESULTS

A total of 36 male and 14 female adult Chinese patients with hypopituitarism were included in this retrospective study; 43 (87.0%) of these patients exhibited growth hormone (GH) deficiency, and 39 (78.3%) had diabetes insipidus. A total of 27 (54.0%) patients were diagnosed with NAFLD, while seven patients were cirrhotic. No significant differences were noted in serum GH or insulin-like growth factor 1 among patients with cirrhosis, subjects with NAFLD, and those without NAFLD. However, plasma osmolality and serum sodium concentration of the cirrhotic patients were 314.9 mOsm/kgH₂O and 151.0 mmol/L, respectively, which were significantly higher than those of the NAFLD patients ($P = 0.036$ and 0.042 , respectively). Overweight/obesity and insulin resistance were common metabolic disorders in this population. The body mass index (BMI) and homeostasis model assessment of insulin resistance parameters of the cirrhotic patients were 27.7 kg/m² and 9.57, respectively, which were significantly higher than those of the patients without NAFLD ($P = 0.011$ and 0.044 , respectively). A correlation analysis was performed, and fasting insulin concentration was positively associated with plasma osmolality in patients with NAFLD, after adjusting for gender, age, and BMI ($r = 0.540$, $P = 0.046$), but no correlation was noted in patients without NAFLD.

CONCLUSION

NAFLD is common in patients with hypopituitarism. Plasma osmolality and serum sodium levels of hypopituitary patients with cirrhosis are higher than those of subjects with NAFLD, and fasting insulin concentration is positively associated with plasma osmolality in patients with NAFLD, which suggests that hyperosmolality might be a contributor to the worsening of NAFLD in hypopituitary patients.

Key words: Hypopituitarism; Non-alcoholic fatty liver disease; Cirrhosis; Diabetes insipidus; Plasma osmolality

©The Author(s) 2019. Published by Baishideng Publishing Group Inc. All rights reserved.

Core tip: Fifty-four percent of hypopituitary patients in this retrospective study were diagnosed with non-alcoholic fatty liver disease (NAFLD), which was significantly higher than that of the general adult population in China. Growth hormone (GH) deficiency has been considered an important contributing factor to NAFLD in those patients. However, no significant differences were noted in GH or insulin-like growth factor 1 among patients with cirrhosis, subjects with NAFLD, and those without NAFLD in this study. Interestingly, we found that plasma osmolality and serum sodium concentration of the cirrhotic patients were significantly higher than those of the NAFLD patients. In addition, fasting insulin concentration was positively associated with plasma osmolality in patients with NAFLD. Additional studies are required to confirm that hyperosmolality may be a significant contributor to the worsening of NAFLD in hypopituitary patients.

Citation: Yuan XX, Zhu HJ, Pan H, Chen S, Liu ZY, Li Y, Wang LJ, Lu L, Yang HB, Gong FY. Clinical characteristics of non-alcoholic fatty liver disease in Chinese adult hypopituitary patients. *World J Gastroenterol* 2019; 25(14): 1741-1752

URL: <https://www.wjgnet.com/1007-9327/full/v25/i14/1741.htm>

DOI: <https://dx.doi.org/10.3748/wjg.v25.i14.1741>

INTRODUCTION

Primary non-alcoholic fatty liver disease (NAFLD) is caused by an excess of fat in the liver (steatosis) that is not the result of excessive alcohol consumption or other secondary causes^[1,2]. The disease can be presented in the form of hepatic steatosis, inflammatory non-alcoholic steatohepatitis (NASH), fibrosis and/or cirrhosis^[1,2]. Approximately 2%-3% of NAFLD patients develop NASH, which carries a 20% potential risk of evolving further and causing cirrhosis^[1,3]. Furthermore, NAFLD patients are five times more likely to develop hepatocellular carcinoma in the absence of cirrhosis compared with hepatitis C patients^[4,5]. However, the pathogenesis of NAFLD and its progression are a complex process, and the “multiple-hit” hypothesis proposed by Buzzetti *et al*^[6] in 2016 suggested that simple steatosis and NASH not only exhibited different risks of progression but might also reflect different disease entities in terms of pathogenesis. Multiple insults, including insulin resistance, obesity, and gut microbiota, contribute to the development of steatosis and liver inflammation^[6].

Patients with hypothalamic-pituitary disease present with central obesity, insulin resistance, and dyslipidemia, whereas liver dysfunction and NAFLD are common symptoms in this subpopulation^[7-10]. Hong *et al*^[8] reported that the frequency of fatty liver on abdominal ultrasonography in male subjects with hypopituitarism was significantly higher compared with that of control subjects (70.6% *vs* 32.5%). Growth hormone (GH) deficiency (GHD) has been considered an important contributing factor to these metabolic changes in hypopituitary patients^[11-13]. However, the causes of hypopituitarism in the reported studies varied, and combined pituitary hormone deficiency, including central diabetes insipidus, was more common in this subpopulation. To the best of our knowledge, the imbalance of central diabetes insipidus and concomitant serum electrolyte concentration has not been investigated with regard to the pathophysiology of NAFLD in patients with hypopituitarism. The aim of this retrospective cross-sectional study was to compare Chinese adult hypopituitary patients with NAFLD and those without NAFLD in terms of their clinical manifestations, endocrine function, metabolic parameters, and serum electrolyte parameters and to analyze the associated factors with NAFLD and cirrhosis.

MATERIALS AND METHODS

The present study is a retrospective cross-sectional observational study. The study protocol was approved by the Ethics Committee of the Peking Union Medical College Hospital (PUMCH; No. JS1233).

Subjects

A total of 36 male and 14 female adult Chinese patients with hypopituitarism and/or panhypopituitarism were consecutively enrolled at the Pituitary Center of PUMCH between August 2012 and April 2018. According to abdominal ultrasonography, these patients were divided into an NAFLD (-) group and an NAFLD (+) group, and the latter was further divided into an NAFLD group and a cirrhotic group according to the histological and/or clinical diagnostic criteria of cirrhosis.

Hypopituitarism/panhypopituitarism was diagnosed clinically based on clinical manifestations, basal evaluation of pituitary function, and provocative tests. Hypopituitarism/panhypopituitarism was confirmed as follows: GHD was diagnosed as a peak serum GH level lower than 3 µg/L in both insulin tolerance tests (ITTs) and L-arginine tests^[14]. Hypogonadotropic hypogonadism (HH) was defined by a reduction in the levels of luteinizing hormone (LH) and follicle stimulating hormone (FSH) for premenopausal women with a low serum estradiol concentration, and for adult men with a morning serum total testosterone concentration lower than 10.4 nmol/L^[15]. HH was diagnosed via gonadotropin releasing hormone analogue (triptorelin) stimulation tests as follows: LH_{60min} was lower than 4 IU/L (indispensable tests for delayed or absent puberty)^[16]. Secondary hypocortisolism was diagnosed based on a peak serum cortisol response lower than 18 µg/dL (497.5 nmol/L) in ITTs^[14]. Secondary hypothyroidism was diagnosed from a serum free thyroxine (FT4) level below the laboratory reference range in conjunction with a low, normal, or mildly elevated thyroid stimulating hormone (TSH) level in the setting of pituitary disease^[17]. Central diabetes insipidus was considered when serum osmolality was higher than 295 mOsm/kg, while the corresponding urine osmolality was lower than 300 mOsm/kg in fluid deprivation tests, and a subsequent response to arginine vasopressin (AVP) was observed^[18].

Diagnosis of NAFLD was confirmed by fatty infiltration of the liver on abdominal ultrasonography in association with or without abnormal liver enzymes. The patients

were diagnosed as cirrhotic by the development of clinically evident complications of liver diseases (such as esophageal varices, ascites, jaundice, hepatic encephalopathy, portal hypertension, hypersplenism, and hepatocellular carcinoma) or by liver biopsy.

The exclusion criteria were as follows: (1) patients with isolated pituitary hormone deficiencies; (2) patients with primary and secondary autoimmune hypophysitis treated with glucocorticoids; (3) patients with hypopituitarism secondary to functional pituitary adenomas, including somatotrophin, lactotrophin, thyrotrophin, corticotrophin, gonadotrophin, and plurihormonal and double adenomas; (4) patients with positive hepatitis B or C serology or with evidence of inherited, autoimmune, cholestatic, drug-induced, or metabolic liver disease using standard clinical, laboratory, imaging, and histologic criteria; (5) patients with weekly alcohol intake of more than 21 units for men or 14 units for women; (6) patients with liver dysfunction of a specific etiology other than hypopituitarism and NAFLD; and (7) children and adolescents.

Data extraction and management

The data were extracted from medical records, which included patient characteristics, such as age, gender, race, anthropometric parameters including height, weight, body mass index (BMI), waist circumference (WC), and blood pressure, diagnosis of the cause of hypopituitarism/panhypopituitarism, laboratory results, abdominal ultrasonography results, complications and comorbidities, treatments, and hormone replacements. The time of diagnosis of hypopituitarism/panhypopituitarism was obtained from the date of symptoms and signs if applicable, or the time of clinical diagnosis. The time of diagnosis of NAFLD was considered to be the date of abdominal ultrasonography that was indicative of primary NAFLD. Hormone replacement therapy refers to regular and dose titration replacement for at least 3 months. Biochemical and hormone levels were measured within three days after admission. Homeostasis model assessment of insulin resistance (HOMA-IR) was obtained according to the formula: (fasting plasma glucose \times fasting serum insulin)/22.5.

Statistical analysis

The statistical package for the social science (SPSS, version 22.0; SPSS Inc., Chicago, IL, United States) was used for data and statistical analyses. Continuous data conforming to a normal distribution are expressed as the mean \pm standard deviation, while continuous data of partial distribution are represented by the median values [interquartile range (IQR)]. Frequency data are expressed as the number (proportion) of patients with a condition. The Student's *t*-test and Wilcoxon Signed-Rank test were used for continuous variables, and the chi-square or Fisher's exact test was used for categorical variables. A *P*-value less than 0.05 was considered significant.

RESULTS

Clinical characteristics of studied subjects

A total of 36 male and 14 female patients with hypopituitarism and/or panhypopituitarism were included in the present study. Their mean age was 26.9 years (range from 18.0 to 41.5 years). The frequency of fatty liver on abdominal ultrasonography was 54.0%. A total of two patients were diagnosed as cirrhotic by liver biopsy, while five patients were diagnosed as cirrhotic by the development of clinically evident complications of liver disease as indicated in the Materials and Methods section. Three cirrhotic patients were decompensated, one of whom had upper gastrointestinal bleeding, another two had hypersplenism, ascites, esophageal and gastric varices, and hepatopulmonary syndrome. The clinical characteristics of hypopituitary patients with NAFLD and without NAFLD are shown in Table 1, and a comparative analysis was completed. No significant differences were noted in the gender ratio among patients with cirrhosis, those with NAFLD, and those without NAFLD. Cirrhotic patients were younger than NAFLD patients ($P = 0.009$), with no significant difference in the course of hypopituitarism. The course of hypopituitarism of cirrhotic patients was significantly longer than that of patients without NAFLD (median course 13.0 years and 3.0 years, respectively, $P = 0.023$), although there was no significant difference in the age between the two groups.

Etiology of hypopituitarism

The underlying etiology of hypopituitarism is illustrated in Table 2. The profile of the causes of hypopituitarism in the cirrhotic group was similar to those of the NAFLD (-) and the NAFLD groups ($P = 0.431$ and 0.466 , respectively). Intracranial germ cell tumors were the most common cause of hypopituitarism in patients without NAFLD

Table 1 Clinical characteristics of hypopituitary patients with or without non-alcoholic fatty liver disease

	NAFLD (-) (n = 23)	NAFLD (+)	
		NAFLD (n = 20)	Cirrhosis (n = 7)
Male n (%)	17 (73.9)	13 (65.0)	6 (85.7)
Age (yr)	22.8 (19.6-30.4)	30.8 (24.5-34.6)	21.0 (19.0-25.2)
Duration (yr)	3.0 (1.0-13.0) ^a	8.5 (1.1-19.0)	13.0 (11.0-18.0)
BMI (kg/m ²)	22.2 (19.3-25.3) ^a	27.9 (25.4-31.7)	27.7 (24.2-32.1)
WC (cm)	73.0 (81.5-96.3) ^a	102.0 (92.5-109.8)	110.5 (91.5-128.8)
SBP (mmHg)	108.7 ± 15.3	122.0 ± 13.4	108.4 ± 15.5
DBP (mmHg)	70.0 ± 12.5	77.1 ± 11.1	64.4 ± 8.1
GH (ng/mL)	0.10 (0.05-0.30)	0.10 (0.08-0.10)	0.10 (0.05-0.25)
IGF1 (ng/mL)	66.0 (28.0-113.0)	107.0 (43.0-141.0)	92.5 (25.0-205.3)
FT ₃ (pg/mL)	2.61 (2.24-3.15)	2.43 (2.25-3.08)	2.53 (2.15-2.72)
FT ₄ (ng/dL)	0.86 (0.66-1.01)	0.88 (0.70-1.11)	0.97 (0.46-1.14)
TSH (μIU/mL)	1.907 (0.151-2.968)	2.098 (0.806-2.557)	3.083 (0.091-4.945)
GLU (mmol/L)	5.0 (4.6-5.3)	4.9 (4.5-5.3)	5.3 (4.7-8.9)
HOMA-IR	2.60 (1.60-3.71) ^a	3.92 (2.62-6.02)	9.57 (2.23-10.94)
HbA1C (%)	5.2 (4.7-5.5)	5.5 (5.3-5.9)	6.7 (4.7-8.8)
TC (mmol/L)	4.98 (4.18-5.74)	5.07 (4.70-7.03)	5.31 (4.55-6.16)
TG (mmol/L)	1.29 (0.98-1.78)	1.89 (1.06-2.48)	2.15 (1.16-2.89)
HDL-C (mmol/L)	1.17 (0.97-1.44)	0.99 (0.89-1.49)	0.93 (0.70-1.41)
LDL-C (mmol/L)	2.91 ± 0.97	3.29 ± 1.08	3.34 ± 0.72
UA (μmol/L)	418.91 ± 88.25	457.42 ± 111.01	493.14 ± 212.83
hsCRP (mg/L)	2.07 (1.14-5.24)	3.43 (2.27-6.68)	2.28 (1.50-13.71)
Posm (mOsm/kgH ₂ O)	305.2 (298.8-314.6)	299.3 (293.7-305.5) ^b	314.9 (296.0-336.1)
Na (mmol/L)	146.0 (143.0-150.0)	143.0 (140.0-146.5) ^b	151.0 (141.0-162.0)
Cl (mmol/L)	109.0 (108.0-114.0)	106.0 (104.3-110.8) ^b	118.0 (108.0-130.0)
K (mmol/L)	4.20 ± 0.30	4.10 ± 0.30	4.10 ± 0.20
Cr (μmol/L)	66.8 ± 15.2	70.2 ± 16.9	64.4 ± 17.0

^aP < 0.05 vs the cirrhosis group.^bP < 0.05 vs the cirrhosis group.

NAFLD: Non-alcoholic fatty liver disease; BMI: Body mass index; WC: Waist circumference; SBP: Systolic blood pressure; DBP: Diastolic blood pressure; GH: Growth hormone; IGF1: Insulin like growth factor 1; FT₃: Free triiodothyronine; FT₄: Free thyroxine; TSH: Thyroid stimulating hormone; GLU: Glucose; HOMA-IR: Homeostasis model assessment of insulin resistance; HbA1C: Glycated hemoglobin A1C; TC: Total cholesterol; TG: Triglyceride; HDL-C: High density lipoprotein cholesterol; LDL-C: Low density lipoprotein cholesterol; UA: Uric acid; hsCRP: Hypersensitive C reactive protein; Posm: Plasma osmolality; Na: Serum sodium; K: Serum potassium; Cl: Serum chlorine; Cr: Serum creatinine.

(43.5%), while congenital hypopituitarism was the most common cause in NAFLD and cirrhotic patients (45.0% and 42.9%, respectively), followed by craniopharyngioma and other causes.

Distribution of anterior pituitary deficiencies and hormone replacement

The distribution of deficiency in anterior pituitary hormones is shown in Table 2, and all patients exhibited gonadotropin deficiency. The subjects who were on hormone replacement were evaluated clinically and biochemically at regular intervals, according to standard clinical practice, to ensure the physiological replacement of the deficient hormones. Although four (57.1%) cirrhotic patients were panhypopituitary, no significant differences were noted with regard to the distribution of deficiency in anterior pituitary hormones and to the proportion of patients who received physiological hormone replacement. No patient received GH therapy in the present study. No significant difference was noted in serum GH or insulin-like growth factor 1 (IGF1). Serum thyroid hormone levels were similar in cirrhotic, NAFLD, and NAFLD (-) patients, as shown in Table 1. In addition, there was no difference in the proportion of patients with hypothalamic dysfunction in cirrhotic, NAFLD, and NAFLD (-) patients.

Table 2 Etiology of hypopituitarism and distribution of pituitary deficiencies in our patients *n* (%)

			NAFLD (+)	
NAFLD (-) (<i>n</i> = 23)			NAFLD (<i>n</i> = 20)	Cirrhosis (<i>n</i> = 7)
Etiology	Congenital hypopituitarism	7 (30.4)	9 (45.0)	3 (42.9)
	Intracranial germ cell tumor	10 (43.5)	4 (20.0)	3 (42.9)
	Craniopharyngioma	1 (4.3)	2 (10.0)	1 (14.3)
	Others	5 (21.7)	5 (25.0)	0 (0.0)
Distribution of pituitary deficiencies	Gonadotrophins	23 (100)	20 (100)	7 (100.0)
	Growth hormone	20 (87.0)	19 (95.0)	7 (100.0)
	Thyroid	18 (78.3)	12 (60.0)	7 (100.0)
	Adrenal	14 (60.9)	13 (65.0)	6 (85.7)
	Diabetes insipidus	18 (78.3)	13 (65.0)	5 (71.4)
Number of pituitary axis deficiencies	1	0 (0.0)	0 (0.0)	0 (0.0)
	2	2 (8.7)	3 (15.0)	0 (0.0)
	3	6 (26.1)	4 (20.0)	0 (0.0)
	4	4 (17.4)	6 (30.0)	3 (42.9)
	5	11 (47.8)	7 (35.0)	4 (57.1)

NAFLD: Non-alcoholic fatty liver disease.

Diabetes insipidus and electrolytic imbalance

No patients were taking medications, such as diuretics, that could affect plasma osmolality and serum sodium for the treatment of cirrhotic conditions. A total of 36 (72%) patients also had diabetes insipidus; however, 21 of them (58.3%) did not receive treatment with desmopressin. No significant differences were noted in the proportion of patients with diabetes insipidus or in the proportion of patients who received desmopressin treatment, between patients with and without NAFLD. In addition, no significant differences were observed between the NAFLD and the cirrhotic groups, as shown in Table 2. However, plasma osmolality of patients with cirrhosis was significantly higher than that of NAFLD patients (median plasma osmolality = 314.9 mOsm/kgH₂O and 299.3 mOsm/kgH₂O, respectively, $P = 0.036$). Similar differences were observed in the concentrations of serum sodium and chlorine, as shown in Table 1, but no significant differences were noted between patients with cirrhosis and those without NAFLD.

Association with metabolic syndrome

The comparison of the clinical characteristics demonstrated that no significant differences were noted in systolic blood pressure (SBP) or diastolic blood pressure (DBP) between patients with and without NAFLD. SBP and DBP of cirrhotic patients were lower than those of the NAFLD patients, although no statistically significant differences were observed (P adjusted for age = 0.116 and 0.050, respectively). The median BMI and WC in cirrhotic patients were 27.7 kg/m² and 110.5 cm, respectively. These values were significantly higher than those of patients without NAFLD (22.2 kg/m² and 73.0 cm, $P = 0.011$ and 0.040, respectively) but similar to those of the NAFLD patients (BMI = 27.9 kg/m² and WC = 102.0 cm, $P = 0.912$ and 0.396, respectively). The HOMA-IR of cirrhotic patients was significantly higher than that of patients without NAFLD ($P = 0.045$), although no significant difference was noted between the cirrhotic patients and NAFLD patients. A correlation analysis was performed, and it showed that fasting insulin concentration was positively associated with plasma osmolality in patients with NAFLD after adjusting for gender, age, and BMI ($r = 0.540$, $P = 0.046$), but no correlation was noted in total hypopituitary patients or in patients without NAFLD. There was no correlation between HOMA-IR and plasma osmolality. In contrast to previous studies^[7-9], no significant difference was noted in the levels of fasting plasma glucose, glycated hemoglobin A1c (HbA1c), total cholesterol (TC), low density lipoprotein cholesterol (LDL-C), high density lipoprotein cholesterol (HDL-C), or triglycerides (TG), as shown in Table 1.

Abnormal liver function

Serum aminotransferase and bilirubin levels were considered elevated if they were above the normal laboratory reference range. No significant differences were noted among cirrhotic, NAFLD, and NAFLD (-) patients with regard to serum aminotrans-

ferase and bilirubin levels, as shown in Table 3. The median levels of γ -glutamyl-transferase (GGT) in cirrhotic patients were higher than those in patients without NAFLD (52.0 U/L and 23.0 U/L, respectively, $P = 0.046$), although no significant difference was noted between NAFLD patients and cirrhotic patients ($P = 0.862$). The comparison of the tests for hepatic synthetic function, including serum albumin, prothrombin time (PT), and international normalized ratio (INR), demonstrated that the average PT and INR in cirrhotic patients were significantly higher than those in the NAFLD patients and NAFLD (-) patients (as shown in Table 3), although no significant difference was noted between patients with and without NAFLD. The cirrhotic patients frequently exhibited a number of hematological abnormalities, including varying degrees of cytopenia. Thrombocytopenia was the most common type of hematological abnormality, while leukopenia and anemia developed later in the disease course. As shown in Table 3, white blood counts and blood platelet counts were lower in cirrhotic patients than in NAFLD and NAFLD (-) patients, although no significant differences were noted between patients with and without NAFLD.

Changes in biochemical indicators following hormone replacement in cirrhotic patients

The biochemical indicators of the seven cirrhotic patients were retested following regular hormone replacement, as shown in Figure 1. Liver function was generally stable, which was reflected by serum aminotransferase levels, white blood count, and blood platelet count. TG was significantly lower than that before hormone replacement ($P = 0.043$). The fasting serum insulin and HOMA-IR levels were decreased following regular hormone replacement, although no significant differences were obtained ($P = 0.593$ and 0.593 , respectively). Serum sodium was decreased from 152.9 mmol/L to 143.6 mmol/L after hormone replacement ($P = 0.046$); however, no significant difference was noted in plasma osmolality (319.6 mOsm/kgH₂O and 300.1 mOsm/kgH₂O, $P = 0.080$).

DISCUSSION

NAFLD is the most common cause of chronic liver dysfunction and a major global health problem over the past decades, whereas hypopituitarism/panhypopituitarism is a rare cause of NAFLD, which is easily misdiagnosed by endocrinologists and gastroenterologists. The data reported in the present study showed that the frequency of fatty liver in hypopituitary patients based on abdominal ultrasonography was 54.0%, which is significantly higher than that of the general adult population in China (approximately 15%), reported in 2013^[19]. The incidence of cirrhosis in the present study population (patients with hypopituitarism and NAFLD) was 28%, which was significantly higher than that in the general NAFLD population but similar to that reported in a longitudinal cohort study (29%)^[10,20].

Disturbances in endocrine hypothalamic-pituitary axes have been associated with NAFLD, including GHD, hypothyroidism, and hypogonadism^[21]. GHD has been considered an important contributing factor to the metabolic change encountered in hypopituitary patients. The majority of the patients in the present study had GHD, and the average IGF1 level was considerably low in this patient group. Comparative analysis demonstrated no significant differences in serum growth hormone or IGF1 levels between hypopituitary patients with NAFLD and those without. Moreover, no significant differences were noted in the distribution of anterior pituitary deficiencies or hormone replacement in current hypopituitary patients with and without NAFLD. The causes of hypopituitarism varied, and combined pituitary hormone deficiency, including central diabetes insipidus, was more common in this population. Therefore, we speculated that this condition would be the result of multihormonal deficiency and that additional aggravating factors would be responsible for the pathophysiology of NAFLD in hypopituitary patients.

Congenital hypopituitarism, intracranial germ cell tumor, and craniopharyngioma were common causes of hypopituitarism in the present study. The latter two disorders usually affect the secretion of AVP. Combined deficits in AVP secretion and thirst sensation can result in life-threatening hyperosmolality and hypernatremia. In the current study, 72% of patients with hypopituitarism presented with central diabetes insipidus. Thus, hypernatremia manifested in these hypopituitary patients. Plasma osmolality levels of cirrhotic patients were significantly higher than those of NAFLD patients, and similar differences were noted with regard to serum sodium and serum chlorine levels. Homeostasis of electrolytes and the normal concentration of plasma osmolality are essential for the maintenance of normal cellular function. Cell volume changes are triggered by osmotic substances, thereby activating signals

Table 3 Liver function including liver enzymes, routine blood tests, and coagulation function tests in our patients

Index		NAFLD (-) (n = 23)	NAFLD (+)	
			NAFLD (n = 20)	Cirrhosis (n = 7)
Liver enzymes	ALT (U/L)	26.0 (20.0-41.0)	35.0 (27.3-81.8)	23.0 (19.0-59.0)
	ALB (g/L)	46.8 ± 3.5 ^a	47.7 ± 3.0 ^a	49.6 ± 4.6
	TBil (μmol/L)	8.7 (6.9-14.4) ^b	12.3 (8.0-17.1) ^a	13.2 (9.9-15.9)
	DBil (μmol/L)	2.6 (2.2-4.4)	3.4 (2.6-5.5)	4.4 (3.2-5.1)
	GGT (U/L)	23.0 (16.0-33.0) ^a	52.0 (29.0-77.0)	52.0 (23.0-141.0)
	ALP (U/L)	77.0 (60.5-122.5)	82.0 (69.0-92.0)	71.0 (62.0-117.0)
	AST (U/L)	28.0 (22.5-38.5)	36.0 (26.0-55.0)	26.0 (20.0-59.0)
	TBA (μmol/L)	2.90 (1.35-3.25)	3.60 (2.30-7.00)	3.60 (1.30-9.10)
	LD (U/L)	233.9 ± 54.8	227.6 ± 41.4	215.3 ± 60.8
Routine blood tests	WBC (×10 ⁹ /L)	6.53 ± 2.61 ^a	6.32 ± 1.71 ^a	4.02 ± 1.14
	NEUT# (×10 ⁹ /L)	3.65 ± 1.90 ^b	3.44 ± 1.24 ^a	1.75 ± 0.30
	PLT (×10 ⁹ /L)	250.5 ± 81.1 ^c	273.0 ± 90.1 ^c	91.1 ± 53.3
Coagulation function tests	PT (s)	12.11 ± 1.06 ^c	11.87 ± 1.01 ^c	15.43 ± 2.24
	PT% (%)	87.3 ± 8.8 ^c	94.3 ± 14.9 ^c	62.6 ± 12.1
	INR	1.05 ± 0.08 ^c	1.01 ± 0.10 ^c	1.33 ± 0.17
	FgB (g/L)	2.97 ± 0.78 ^b	3.09 ± 0.81 ^b	1.89 ± 0.59
	APTT (s)	31.35 (25.70-35.15)	28.45 (25.30-38.33)	33.50 (30.48-41.58)
	TT (s)	18.34 ± 0.97 ^b	17.82 ± 0.94 ^c	19.75 ± 1.08

^a*P* < 0.05 *vs* the cirrhosis group.^b*P* < 0.01 *vs* the cirrhosis group.^c*P* < 0.001 *vs* the cirrhosis group.

NAFLD: Non-alcoholic fatty liver disease; ALT: Alanine aminotransferase; ALB: Albumin; TBil: Total bilirubin; DBil: Direct bilirubin; GGT: γ-glutamyltransferase; ALP: Alkaline phosphatase; AST: Aspartate aminotransferase; TBA: Total bile acid; LD: Lactic dehydrogenase; WBC: White blood cells; NEUT: Neutrophil granulocyte; PLT: Blood platelet; PT: Prothrombin time; INR: International normalized ratio; FgB: Fibrinogen; APTT: Activated partial thromboplastin time; TT: Thrombin time.

that contribute to the control and regulation of metabolism and gene expression. Following the induction of hyperosmolality, cells shrink and may undergo apoptosis^[22-24]. Moreover, some components of insulin signaling, such as the enzyme protein kinase B, are sensitive to hyperosmolality^[22-24]. Hyperosmolality can inhibit insulin-induced glucose uptake, glycogen synthesis, and lipogenesis in 3T3-L1 adipocytes^[25,26]. Therefore, the dehydration of hepatocytes, which is triggered by hyperosmolality, can also induce insulin and cytokine resistance and promote the progression of NAFLD^[27,28].

The pathogenesis of NAFLD has not been fully elucidated, and multiple etiologies have been proposed. The most prevalent hypothesis includes insulin resistance as the key mechanism leading to hepatic steatosis and possibly to steatohepatitis and liver fibrosis^[6,29]. The data reported in the present study indicated that the metabolic changes accompanied by hypopituitarism/panhypopituitarism notably caused an increase in the weight and obesity parameters, insulin resistance, and hyperlipidemia, which is consistent with the findings reported previously^[7-10]. HOMA-IR in patients with hypopituitarism and cirrhosis was significantly higher than that in patients without NAFLD. Moreover, fasting insulin concentration was positively associated with plasma osmolality in patients with NAFLD, although no correlation was noted between HOMA-IR and plasma osmolality. However, peripheral IR, pancreatic β-cell dysfunction, and even diabetes mellitus may occur in cirrhotic patients^[30,31]. Therefore, the effect of the hyperosmolar state on the progression of NAFLD in hypopituitary patients requires further studies.

The sensitivity of ultrasound has been reported to range from 53% to 100% and its specificity from 77% to 98%^[32]. Higher diagnostic sensitivities and specificities are achieved during the evaluation of moderate to severe hepatic steatosis cases, whereas lower values are noted during all grades of hepatic steatosis^[32]. The accurate diagnosis of NASH and cirrhosis can be conducted by liver biopsy. Adams *et al*^[10] reported that in ten patients with hypothalamic and pituitary dysfunction whose NAFLD symptoms were confirmed by liver biopsy, six were cirrhotic (29% of the total cohort), two exhibited NASH with fibrosis (10.5% of the total cohort), and two presented with simple steatosis. In the present study, two of our patients underwent liver biopsy,

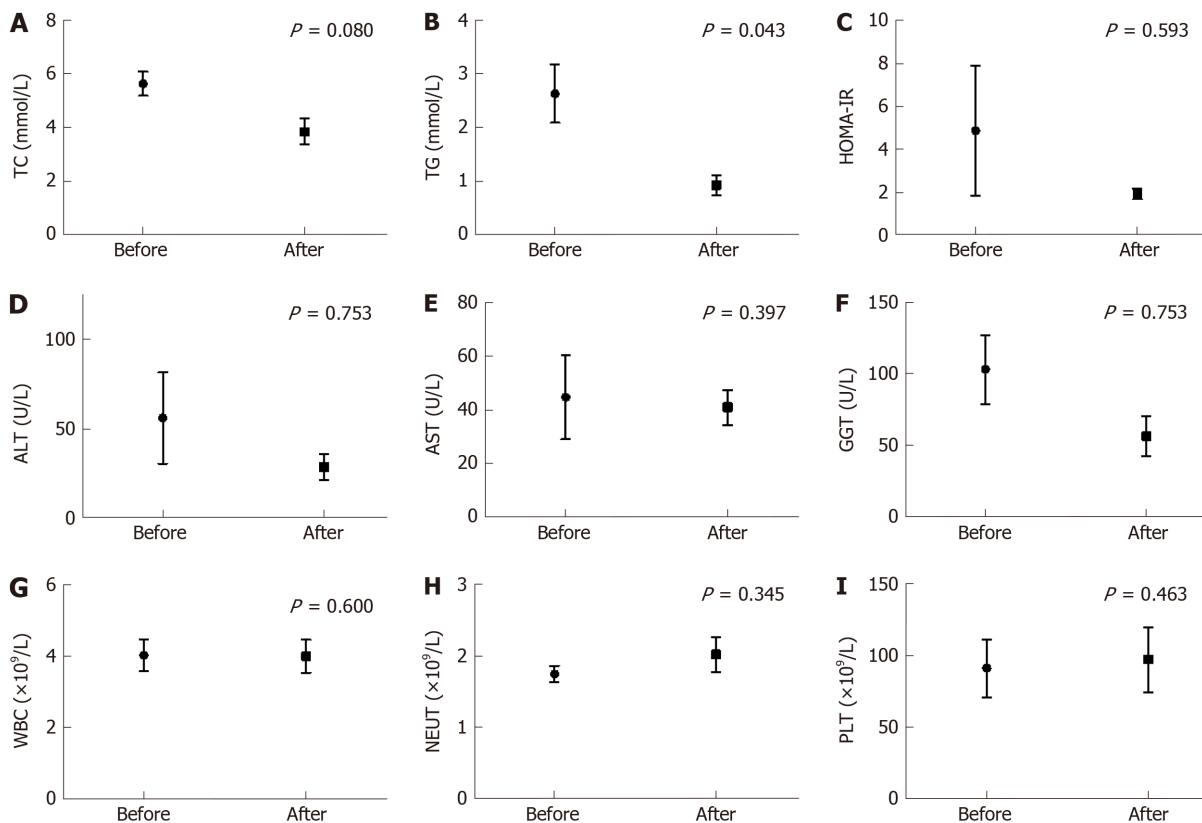


Figure 1 Measurement of biochemical indicators after hormone replacement in cirrhotic patients. The *P*-values were compared before and after hormone replacement. A-C: Changes of total cholesterol (A), triglyceride (B), and homeostasis model assessment of insulin resistance (C). D-F: Changes of serum aminotransferase alanine aminotransferase (D), aspartate aminotransferase (E), and γ -glutamyltransferase (F). G-I: Changes of white blood count (G), neutrophil count (H), and blood platelet count (I). Significant differences were defined by a *P*-value being lower than 0.05. ALT: Alanine aminotransferase; AST: Aspartate aminotransferase; GGT: γ -glutamyltransferase; WBC: White blood cells; NEUT: Neutrophil granulocyte; PLT: Blood platelet; TC: Total cholesterol; TG: Triglyceride; HOMA-IR: Homeostasis model assessment of insulin resistance.

which indicated the lack of differential diagnosis between simple steatosis and NASH from NAFLD. Consequently, the incidence of NASH and fibrosis in our cohort was not clear. Only two of the seven cirrhotic patients received regular hormone replacement, while three of them received this therapy until they developed symptoms of decompensated cirrhosis, such as upper gastrointestinal bleeding and hypersplenism. Comparative analysis of our patients indicated that the variables of hepatic synthetic function, white blood count, and blood platelet count of cirrhotic patients were significantly lower than those of patients with hypopituitarism without NAFLD. However, no significant differences were noted in the level of serum aminotransferase or bilirubin. Following a period of regular hormone replacement, the biochemical indicators of the seven cirrhotic patients exhibited no further deterioration and were reflected by serum aminotransferase levels, white blood count, and blood platelet count, although it was unknown whether the pathological indicators of liver cirrhosis had improved. Therefore, routine liver blood tests could not be used to assess the progression of liver fibrosis and cirrhosis in NAFLD subjects, and liver biopsy was performed if necessary^[1,2].

In conclusion, our data demonstrated a high prevalence of NAFLD and cirrhosis in patients with hypopituitarism. Notably, hypopituitary patients with cirrhosis exhibited significantly higher BMI and HOMA-IR compared with those without NAFLD. In addition, fasting insulin concentration was positively associated with plasma osmolality in patients with NAFLD, following adjustment for gender, age, and BMI. We reported for the first time that plasma osmolality and serum sodium levels of hypopituitary patients with cirrhosis were significantly higher than those of hypopituitary patients with NAFLD. Additional studies are required to confirm that hyperosmolality may be a significant contributor to the deterioration of NAFLD in hypopituitary patients. Routine liver blood tests could not be used to assess the progression of liver fibrosis and cirrhosis in subjects with NAFLD.

The present study was limited by insufficient sample size, as hypopituitarism is a rare condition. We did not use corrections for multiple comparisons because the findings from this analysis were general associations rather than affirmative findings.

Thus, prospective, multicenter, cohort studies and animal experiments are required in the future to facilitate further understanding of the NAFLD pathophysiology in hypopituitary patients.

ARTICLE HIGHLIGHTS

Research background

Non-alcoholic fatty liver disease (NAFLD) is a major global health problem with a substantial rise in prevalence over the last decades. Patients with hypothalamic-pituitary disease have the features of central obesity, insulin resistance, and dyslipidemia, and there is an increased prevalence of liver dysfunction consistent with NAFLD in this population. Growth hormone deficiency (GHD) has been considered as an important contributing factor to these metabolic changes in hypopituitary patients. However, the causes of hypopituitarism in the reported studies varied, and combined pituitary hormone deficiency, including central diabetes insipidus, was more common in this population. This retrospective cross-sectional study was performed to analyze clinical characteristics of NAFLD in Chinese adult hypopituitary/panhypopituitary patients, and to explore the risk factors that lead to rapid progression to cirrhosis.

Research motivation

The research motivation of the present study was to identify possible risk factors related to NAFLD in patients with hypopituitarism by summarizing the characteristics of NAFLD in this patient population, in order to prevent and delay the occurrence and progression of NAFLD in patients with hypopituitarism in future.

Research objectives

The main objectives of the present study were to analyze clinical characteristics of NAFLD in Chinese adult hypopituitary/panhypopituitary patients, and to explore the risk factors that lead to rapid progression to cirrhosis. Additional studies are required to research the mechanism of rapid progression of NAFLD to cirrhosis in hypopituitary patients.

Research methods

The present study is a retrospective cross-sectional observational study. A total of 50 adult Chinese patients with hypopituitarism and/or panhypopituitarism were enrolled. The data were extracted from the medical records, including patients' characteristics, diagnosis and treatment, biochemical and hormonal tests, and abdominal ultrasound. And then statistical analysis was performed.

Research results

Fifty-four percent of hypopituitary patients in this study were diagnosed with NAFLD, and seven patients were cirrhotic, which was significantly higher than that of the general population. Body mass index (BMI) and homeostasis model assessment of insulin resistance (HOMA-IR) of the cirrhotic patients were significantly higher than those of the patients without NAFLD. Moreover, plasma osmolality and serum sodium concentration of the cirrhotic patients were significantly higher than those of the NAFLD patients, and fasting insulin concentration was positively associated with plasma osmolality in patients with NAFLD, following adjustment for gender, age, and BMI.

Research conclusions

The present study demonstrated a high prevalence of NAFLD and cirrhosis in patients with hypopituitarism. Hypopituitary patients with cirrhosis exhibited significantly higher BMI and HOMA-IR compared with those without NAFLD. In addition, fasting insulin concentration was positively associated with plasma osmolality in patients with NAFLD, following adjustment for gender, age, and BMI. Moreover, we report for the first time that plasma osmolality and serum sodium levels of hypopituitary patients with cirrhosis were significantly higher than those of hypopituitary patients with NAFLD. Additional studies are required to confirm that hyperosmolality may be a significant contributor to the rapid progression of NAFLD in hypopituitary patients.

Research perspectives

There is a high prevalence of NAFLD and cirrhosis in patients with hypopituitarism, but the factors that lead to rapid progression to cirrhosis are not clear. Further studies are needed to determine whether hyperosmolality contributes to the deterioration of NAFLD in hypopituitary patients.

ACKNOWLEDGEMENTS

We are grateful to Yue-Lun Zhang for his recommendations on the statistical analysis.

REFERENCES

- 1 **National Guideline Centre (UK).** 2016 [PMID: [27441333](#)]
- 2 **Chalasani N, Younossi Z, Lavine JE, Charlton M, Cusi K, Rinella M, Harrison SA, Brunt EM, Sanyal AJ.** The diagnosis and management of nonalcoholic fatty liver disease: Practice guidance from the American Association for the Study of Liver Diseases. *Hepatology* 2018; **67**: 328-357 [PMID: [28714183](#) DOI: [10.1002/hep.29367](#)]
- 3 **Reccia I, Kumar J, Akladios C, Virdis F, Pai M, Habib N, Spalding D.** Non-alcoholic fatty liver disease: A sign of systemic disease. *Metabolism* 2017; **72**: 94-108 [PMID: [28641788](#) DOI: [10.1016/j.metabol.2017.04.011](#)]
- 4 **Mittal S, El-Serag HB, Sada YH, Kanwal F, Duan Z, Temple S, May SB, Kramer JR, Richardson PA, Davila JA.** Hepatocellular Carcinoma in the Absence of Cirrhosis in United States Veterans is Associated With Nonalcoholic Fatty Liver Disease. *Clin Gastroenterol Hepatol* 2016; **14**: 124-131.e1 [PMID: [26196445](#) DOI: [10.1016/j.cgh.2015.07.019](#)]
- 5 **Singal AG, El-Serag HB.** Hepatocellular Carcinoma From Epidemiology to Prevention: Translating Knowledge into Practice. *Clin Gastroenterol Hepatol* 2015; **13**: 2140-2151 [PMID: [26284591](#) DOI: [10.1016/j.cgh.2015.08.014](#)]
- 6 **Buzzetti E, Pinzani M, Tsochatzis EA.** The multiple-hit pathogenesis of non-alcoholic fatty liver disease (NAFLD). *Metabolism* 2016; **65**: 1038-1048 [PMID: [26823198](#) DOI: [10.1016/j.metabol.2015.12.012](#)]
- 7 **Gardner CJ, Irwin AJ, Daousi C, McFarlane IA, Joseph F, Bell JD, Thomas EL, Adams VL, Kemp GJ, Cuthbertson DJ.** Hepatic steatosis, GH deficiency and the effects of GH replacement: a Liverpool magnetic resonance spectroscopy study. *Eur J Endocrinol* 2012; **166**: 993-1002 [PMID: [22433286](#) DOI: [10.1530/EJE-12-0002](#)]
- 8 **Hong JW, Kim JY, Kim YE, Lee EJ.** Metabolic parameters and nonalcoholic fatty liver disease in hypopituitary men. *Horm Metab Res* 2011; **43**: 48-54 [PMID: [20865648](#) DOI: [10.1055/s-0030-1265217](#)]
- 9 **Irie M, Itoh Y, Miyashita Y, Tsushima T, Shirai K.** Complications in adults with growth hormone deficiency—a survey study in Japan. *Endocr J* 2004; **51**: 479-485 [PMID: [15516782](#)]
- 10 **Adams LA, Feldstein A, Lindor KD, Angulo P.** Nonalcoholic fatty liver disease among patients with hypothalamic and pituitary dysfunction. *Hepatology* 2004; **39**: 909-914 [PMID: [15057893](#) DOI: [10.1002/hep.20140](#)]
- 11 **Matsumoto R, Fukuoka H, Iguchi G, Nishizawa H, Bando H, Suda K, Takahashi M, Takahashi Y.** Long-term effects of growth hormone replacement therapy on liver function in adult patients with growth hormone deficiency. *Growth Horm IGF Res* 2014; **24**: 174-179 [PMID: [25116471](#) DOI: [10.1016/j.ghir.2014.07.002](#)]
- 12 **Nakajima K, Hashimoto E, Kaneda H, Tokushige K, Shiratori K, Hizuka N, Takano K.** Pediatric nonalcoholic steatohepatitis associated with hypopituitarism. *J Gastroenterol* 2005; **40**: 312-315 [PMID: [15830293](#) DOI: [10.1007/s00535-004-1541-4](#)]
- 13 **Jonas MM, Krawczuk LE, Kim HB, Lillehei C, Perez-Atayde A.** Rapid recurrence of nonalcoholic fatty liver disease after transplantation in a child with hypopituitarism and hepatopulmonary syndrome. *Liver Transpl* 2005; **11**: 108-110 [PMID: [15690545](#) DOI: [10.1002/lt.20332](#)]
- 14 **Ursula Kaiser KKYH, Melmed S, Polonsky KS, Larsen PR, Kronenberg HM.** Pituitary Physiology and Diagnostic Evaluation. Melmed S, Polonsky KS, Larsen PR, Kronenberg HM. *Williams Textbook Of Endocrinology, 13th ed.* Canada: Patricia Tannian 2015; 182-214
- 15 **Bhasin S, Cunningham GR, Hayes FJ, Matsumoto AM, Snyder PJ, Swerdloff RS, Montori VM; Task Force, Endocrine Society.** Testosterone therapy in men with androgen deficiency syndromes: an Endocrine Society clinical practice guideline. *J Clin Endocrinol Metab* 2010; **95**: 2536-2559 [PMID: [20525905](#) DOI: [10.1210/jc.2009-2354](#)]
- 16 **Mao JF, Xu HL, Duan J, Chen RR, Li L, Li B, Nie M, Min L, Zhang HB, Wu XY.** Reversal of idiopathic hypogonadotropic hypogonadism: a cohort study in Chinese patients. *Asian J Androl* 2015; **17**: 497-502 [PMID: [25578938](#) DOI: [10.4103/1008-682X.145072](#)]
- 17 **Sherlock M, Reulen RC, Alonso AA, Ayuk J, Clayton RN, Sheppard MC, Hawkins MM, Bates AS, Stewart PM.** ACTH deficiency, higher doses of hydrocortisone replacement, and radiotherapy are independent predictors of mortality in patients with acromegaly. *J Clin Endocrinol Metab* 2009; **94**: 4216-4223 [PMID: [19808848](#) DOI: [10.1210/jc.2009-1097](#)]
- 18 **Alan G, Robinson JGV.** Posterior Pituitary. In: Melmed S, Polonsky KS, Larsen PR, Kronenberg HM, editor. *Williams Textbook of Endocrinology*. 13th ed. Canada: Patricia Tannian 2015; 300-313
- 19 **Fan JG.** Epidemiology of alcoholic and nonalcoholic fatty liver disease in China. *J Gastroenterol Hepatol* 2013; **28** Suppl 1: 11-17 [PMID: [23855290](#) DOI: [10.1111/jgh.12036](#)]
- 20 **Kabbany MN, Conjeevaram Selvakumar PK, Watt K, Lopez R, Akkas Z, Zein N, Carey W, Alkhoury N.** Prevalence of Nonalcoholic Steatohepatitis-Associated Cirrhosis in the United States: An Analysis of National Health and Nutrition Examination Survey Data. *Am J Gastroenterol* 2017; **112**: 581-587 [PMID: [28195177](#) DOI: [10.1038/ajg.2017.5](#)]
- 21 **Hoffmann A, Müller HL.** RETRACTION Novel perspectives on hypothalamic-pituitary dysfunction as a risk factor for non-alcoholic fatty liver disease. *Minerva Endocrinol* 2017; **42**: 132-144 [PMID: [27405476](#) DOI: [10.23736/S0391-1977.16.02500-1](#)]
- 22 **Schliess F, Häussinger D.** Osmosensing and signaling in the regulation of liver function. *Contrib Nephrol* 2006; **152**: 198-209 [PMID: [17065813](#) DOI: [10.1159/000096324](#)]
- 23 **Reinehr R, Becker S, Höngen A, Häussinger D.** The Src family kinase Yes triggers hyperosmotic activation of the epidermal growth factor receptor and CD95. *J Biol Chem* 2004; **279**: 23977-23987 [PMID: [15039424](#) DOI: [10.1074/jbc.M401519200](#)]
- 24 **Reinehr R, Schliess F, Häussinger D.** Hyperosmolarity and CD95L trigger CD95/EGF receptor association and tyrosine phosphorylation of CD95 as prerequisites for CD95 membrane trafficking and DISC formation. *FASEB J* 2003; **17**: 731-733 [PMID: [12586732](#) DOI: [10.1096/fj.02-0915fje](#)]
- 25 **Meier R, Thelen M, Hemmings BA.** Inactivation and dephosphorylation of protein kinase Balpha (PKBalpha) promoted by hyperosmotic stress. *EMBO J* 1998; **17**: 7294-7303 [PMID: [9857186](#) DOI: [10.1093/emboj/17.24.7294](#)]
- 26 **Chen D, Elmendorf JS, Olson AL, Li X, Earp HS, Pessin JE.** Osmotic shock stimulates GLUT4 translocation in 3T3L1 adipocytes by a novel tyrosine kinase pathway. *J Biol Chem* 1997; **272**: 27401-27410 [PMID: [9341192](#)]
- 27 **Randhawa VK, Thong FS, Lim DY, Li D, Garg RR, Rudge R, Galli T, Rudich A, Klip A.** Insulin and hypertonicity recruit GLUT4 to the plasma membrane of muscle cells by using N-ethylmaleimide-sensitive factor-dependent SNARE mechanisms but different v-SNAREs: role of TI-VAMP. *Mol Biol Cell* 2004; **15**: 5565-5573 [PMID: [15469990](#) DOI: [10.1091/mbc.e04-03-0266](#)]

- 28 **Gual P**, Gonzalez T, Grémeaux T, Barres R, Le Marchand-Brustel Y, Tanti JF. Hyperosmotic stress inhibits insulin receptor substrate-1 function by distinct mechanisms in 3T3-L1 adipocytes. *J Biol Chem* 2003; **278**: 26550-26557 [PMID: [12730242](#) DOI: [10.1074/jbc.M212273200](#)]
- 29 **Ercin CN**, Dogru T, Genc H, Celebi G, Aslan F, Gurel H, Kara M, Sertoglu E, Tapan S, Bagci S, Rizzo M, Sonmez A. Insulin Resistance but Not Visceral Adiposity Index Is Associated with Liver Fibrosis in Nondiabetic Subjects with Nonalcoholic Fatty Liver Disease. *Metab Syndr Relat Disord* 2015; **13**: 319-325 [PMID: [26011302](#) DOI: [10.1089/met.2015.0018](#)]
- 30 **Kumar R**. Hepatogenous Diabetes: An Underestimated Problem of Liver Cirrhosis. *Indian J Endocrinol Metab* 2018; **22**: 552-559 [PMID: [30148106](#) DOI: [10.4103/ijem.IJEM_79_18](#)]
- 31 **Orsi E**, Grancini V, Menini S, Aghemo A, Pugliese G. Hepatogenous diabetes: Is it time to separate it from type 2 diabetes? *Liver Int* 2017; **37**: 950-962 [PMID: [27943508](#) DOI: [10.1111/liv.13337](#)]
- 32 **Esterson YB**, Grimaldi GM. Radiologic Imaging in Nonalcoholic Fatty Liver Disease and Nonalcoholic Steatohepatitis. *Clin Liver Dis* 2018; **22**: 93-108 [PMID: [29128063](#) DOI: [10.1016/j.cld.2017.08.005](#)]



Observational Study

Measurement of prostaglandin metabolites is useful in diagnosis of small bowel ulcerations

Yuichi Matsuno, Junji Umeno, Motohiro Esaki, Yoichiro Hirakawa, Yuta Fuyuno, Yasuharu Okamoto, Atsushi Hirano, Shigeyoshi Yasukawa, Fumihito Hirai, Toshiyuki Matsui, Shuhei Hosomi, Kenji Watanabe, Naoki Hosoe, Haruhiko Ogata, Tadakazu Hisamatsu, Shunichi Yanai, Shuji Kochi, Koichi Kurahara, Tsuneyoshi Yao, Takehiro Torisu, Takanari Kitazono, Takayuki Matsumoto

ORCID number: Yuichi Matsuno (0000-0002-1973-2573); Junji Umeno (0000-0002-5253-5600); Motohiro Esaki (0000-0002-1195-0074); Yoichiro Hirakawa (0000-0002-4405-4399); Yuta Fuyuno (0000-0003-3527-5648); Yasuharu Okamoto (0000-0001-5693-8565); Atsushi Hirano (0000-0002-4791-4550); Shigeyoshi Yasukawa (0000-0002-7421-2706); Fumihito Hirai (0000-0002-5493-5675); Toshiyuki Matsui (0000-0002-1817-8064); Shuhei Hosomi (0000-0002-8808-5672); Kenji Watanabe (0000-0002-3781-4724); Naoki Hosoe (0000-0002-4516-5648); Haruhiko Ogata (0000-0002-3304-3635); Tadakazu Hisamatsu (0000-0002-1178-3536); Shunichi Yanai (0000-0003-1871-2412); Shuji Kochi (0000-0002-1783-9545); Koichi Kurahara (0000-0002-6115-341X); Tsuneyoshi Yao (0000-0002-7381-4641); Takehiro Torisu (0000-0001-8256-2549); Takanari Kitazono (0000-0002-9006-5937); Takayuki Matsumoto (0000-0001-9786-3854).

Author contributions: All authors helped to perform the research; Umeno J, Esaki M and Matsumoto T conceived the study; Matsuno Y and Hirakawa Y contributed to statistical analysis and data interpretation; Matsuno Y, Umeno J, Torisu T and Esaki M drafted the manuscript; Matsuno Y, Umeno J, Esaki M, Fuyuno Y, Okamoto Y, Hirano A, Yasukawa S, Hirai F,

Yuichi Matsuno, Junji Umeno, Yoichiro Hirakawa, Yuta Fuyuno, Yasuharu Okamoto, Atsushi Hirano, Takehiro Torisu, Takanari Kitazono, Department of Medicine and Clinical Science, Graduate School of Medical Sciences, Kyushu University, Fukuoka 812-8582, Japan

Motohiro Esaki, Department of Endoscopic Diagnostics and Therapeutic, Saga University Hospital, Saga 849-8501, Japan

Yoichiro Hirakawa, Department of Epidemiology and Public Health, Graduate School of Medical Sciences, Kyushu University, Fukuoka 812-8582, Japan

Shigeyoshi Yasukawa, Fumihito Hirai, Toshiyuki Matsui, Department of Gastroenterology, Fukuoka University Chikushi Hospital, Chikushino 818-8502, Japan

Shuhei Hosomi, Department of Gastroenterology, Osaka City University Graduate School of Medicine, Osaka 545-8586, Japan

Kenji Watanabe, Department of Intestinal Inflammation Research, Hyogo College of Medicine, Nishinomiya 663-8501, Japan

Naoki Hosoe, Haruhiko Ogata, Center for Diagnostic and Therapeutic Endoscopy, School of Medicine, Keio University, Tokyo 160-0016, Japan

Tadakazu Hisamatsu, the Third Department of Internal Medicine, Kyorin University School of Medicine, Mitaka 181-8611, Japan

Shunichi Yanai, Takayuki Matsumoto, Division of Gastroenterology, Department of Internal Medicine, Iwate Medical University, Morioka 020-8505, Japan

Shuji Kochi, Koichi Kurahara, Division of Gastroenterology, Matsuyama Red Cross Hospital, Matsuyama 790-8524, Japan

Tsuneyoshi Yao, Department of Gastroenterology, Sada Hospital, Fukuoka 810-0004, Japan

Corresponding author: Takayuki Matsumoto, MD, PhD, Professor, Division of Gastroenterology, Department of Internal Medicine, Iwate Medical University, 19-1 Uchimaru, Morioka 020-8505, Japan. tmatsuno@iwate-med.ac.jp

Telephone: +81-196515111 (ext. 2314)

Fax: +81-196526664

Matsui T, Hosomi S, Watanabe K, Hosoe N, Ogata H, Hisamatsu T, Yanai S, Kochi S, Kurahara K, Yao T, and Torisu T were responsible for recruitment and phenotyping of the patients; Kitazono T and Matsumoto T revised the manuscript; all authors approved the final version of the manuscript.

Supported by the Practical Research Project for Rare/Intractable Diseases from the Japan Agency for Medical Research and Development (AMED), No. 15ek0109053h0002 to Matsumoto T, and by grants from the Japan Society for the Promotion of Science (JSPS) KAKENHI, No. 25460953, to Umeno J, Esaki M, and Matsumoto T.

Institutional review board

statement: This study was approved by the institutional review board at each collecting site in accordance with the Declaration of Helsinki Principles.

Informed consent statement: All urine and blood samples were collected after obtaining written informed consent.

Conflict-of-interest statement: All authors declare no conflicts-of-interest related to this article.

Data sharing statement: No additional data are available.

STROBE statement: The authors have read the STROBE Statement checklist of items, and the manuscript was prepared according to the STROBE Statement-checklist of items.

Open-Access: This article is an open-access article which was selected by an in-house editor and fully peer-reviewed by external reviewers. It is distributed in accordance with the Creative Commons Attribution Non Commercial (CC BY-NC 4.0) license, which permits others to distribute, remix, adapt, build upon this work non-commercially, and license their derivative works on different terms, provided the original work is properly cited and the use is non-commercial. See: <http://creativecommons.org/licenses/by-nc/4.0/>

Manuscript source: Unsolicited manuscript

Received: February 3, 2019

Peer-review started: February 6, 2019

First decision: February 21, 2019

Revised: February 27, 2019

Accepted: March 11, 2019

Article in press: March 12, 2019

Abstract

BACKGROUND

We recently reported on a hereditary enteropathy associated with a gene encoding a prostaglandin transporter and referred to as chronic enteropathy associated with *SLCO2A1* gene (CEAS). Crohn's disease (CD) is a major differential diagnosis of CEAS, because these diseases share some clinical features. Therefore, there is a need to develop a convenient screening test to distinguish CEAS from CD.

AIM

To examine whether prostaglandin E major urinary metabolites (PGE-MUM) can serve as a biomarker to distinguish CEAS from CD.

METHODS

This was a transactional study of 20 patients with CEAS and 98 patients with CD. CEAS was diagnosed by the confirmation of homozygous or compound heterozygous mutation of *SLCO2A1*. We measured the concentration of PGE-MUM in spot urine by radioimmunoassay, and the concentration was compared between the two groups of patients. We also determined the optimal cut-off value of PGE-MUM to distinguish CEAS from CD by receiver operating characteristic (ROC) curve analysis.

RESULTS

Twenty Japanese patients with CEAS and 98 patients with CD were enrolled. PGE-MUM concentration in patients with CEAS was significantly higher than that in patients with CD (median 102.7 vs 27.9 $\mu\text{g/g} \times \text{Cre}$, $P < 0.0001$). One log unit increase in PGE-MUM contributed to 7.3 increase in the likelihood for the diagnosis of CEAS [95% confidence interval (CI) 3.2-16.7]. A logistic regression analysis revealed that the association was significant even after adjusting confounding factors (adjusted odds ratio 29.6, 95%CI 4.7-185.7). ROC curve analysis revealed the optimal PGE-MUM cut-off value for the distinction of CEAS from CD to be 48.9 $\mu\text{g/g} \times \text{Cre}$ with 95.0% sensitivity and 79.6% specificity.

CONCLUSION

PGE-MUM measurement is a convenient, non-invasive and useful test for the distinction of CEAS from CD.

Key words: Chronic enteropathy associated with *SLCO2A1* gene; Prostaglandin E major urinary metabolites; Chronic nonspecific multiple ulcers of the small intestine; Crohn's disease; Small intestine

©The Author(s) 2019. Published by Baishideng Publishing Group Inc. All rights reserved.

Core tip: Chronic enteropathy associated with *SLCO2A1* gene (CEAS) is a rare hereditary enteropathy associated with a gene encoding a prostaglandin transporter. It is sometimes difficult to distinguish CEAS from Crohn's disease (CD), because these diseases share some clinical features. We report the usefulness of prostaglandin E-major urinary metabolites (PGE-MUM) to differentiate CEAS from CD. PGE-MUM concentration was significantly higher in CEAS than in CD, and optimal cut-off value for the distinction of CEAS from CD to be 48.9 $\mu\text{g/g} \times \text{Cre}$ with sensitivity of 95.0% and specificity of 79.6%. In clinical practice, PGE-MUM measurement might be useful as a screening test for CEAS.

Citation: Matsuno Y, Umeno J, Esaki M, Hirakawa Y, Fuyuno Y, Okamoto Y, Hirano A, Yasukawa S, Hirai F, Matsui T, Hosomi S, Watanabe K, Hosoe N, Ogata H, Hisamatsu T, Yanai S, Kochi S, Kurahara K, Yao T, Torisu T, Kitazono T, Matsumoto T. Measurement of prostaglandin metabolites is useful in diagnosis of small bowel ulcerations. *World J Gastroenterol* 2019; 25(14): 1753-1763

URL: <https://www.wjgnet.com/1007-9327/full/v25/i14/1753.htm>

DOI: <https://dx.doi.org/10.3748/wjg.v25.i14.1753>

Published online: April 14, 2019

P-Reviewer: Caboclo JF, Slomiany BL, Tsoulfas G
S-Editor: Yan JP
L-Editor: A
E-Editor: Song H



INTRODUCTION

The use of capsule endoscopy and balloon-assisted endoscopy has enabled the precise observation of small bowel mucosal lesions in gastrointestinal disease pathology, such as Crohn's disease (CD), intestinal tuberculosis, and nonsteroidal anti-inflammatory drug (NSAID)-induced enteropathy^[1-5]. While characteristic endoscopic findings of small bowel inflammation have been reported, it is sometimes difficult to correctly diagnose patients by endoscopic findings alone in cases lacking characteristic features of the disease.

We previously reported an independent disease entity termed chronic nonspecific multiple ulcers of the small intestine (CNSU) characterized by multiple small intestinal ulcers of nonspecific histology^[6-9]. In addition, we recently found that CNSU is caused by recessive inheritance of the *SLCO2A1* gene and proposed a new nomenclature for this disease: Chronic enteropathy associated with *SLCO2A1* gene (CEAS)^[10]. Therefore, it is now possible to diagnose CEAS based on a combination of clinical features and genetic analysis. However, it is sometimes difficult to differentiate CEAS from CD because these diseases share clinical features such as persistent anemia and hypoproteinemia, susceptible age in puberty, and a predominance of ileal involvement. The differentiation between CEAS and CD is clinically essential to avoid ineffective therapies because patients with CEAS do not respond to treatment with corticosteroids or biologics^[7,9]. Moreover, since the patients with CEAS usually show low inflammatory markers in blood test^[11], it is a particularly important problem to distinguish CEAS from CD with low disease activity. In clinical practice, however, it is unrealistic to perform genetic screening for all patients suspected as CD or CEAS.

The *SLCO2A1* gene encodes a prostaglandin transporter that mediates the cellular uptake of prostaglandins. *SLCO2A1* is also the causative gene of primary hypertrophic osteoarthropathy (PHO)^[12-14]. An increase in urinary levels of prostaglandin E2 (PGE2) and prostaglandin E metabolites in *SLCO2A1*-deficient PHO individuals has been confirmed^[14]. PGE2 is known to have the protective effect on the mucosal injury, however it is difficult to directly measure PGE2 level in local tissues or in the blood because of its extremely rapid metabolism^[15]. Prostaglandin E-major urinary metabolite (PGE-MUM) is known to be stable and we have also previously demonstrated an increase in the urinary levels of prostaglandin E metabolites in CEAS patients^[10]. Therefore, this study investigated whether PGE-MUM are useful for differentiating CEAS from CD.

MATERIALS AND METHODS

Subjects

Among the participants of our previous studies^[10,16,17] and the patients diagnosed as CEAS or CD at Kyushu University hospital, we enrolled 20 Japanese patients with CEAS and 98 patients with CD for the present investigation. A diagnosis of CEAS was confirmed based on published clinical criteria^[18,19] with genetic analysis (Supplementary Table 1). The diagnosis of CD was based on the Japanese diagnostic criteria for CD^[20]. No patients were administered prostaglandin analogues or NSAIDs at the time of urine sample collection. All urine and blood samples were collected after obtaining written informed consent. This study was approved by the institutional review board at each collecting site in accordance with the Declaration of Helsinki Principles.

Clinical characteristics

Clinical information including age, gender, history of surgery, concomitant drugs, serum C reactive protein (CRP) levels, disease location, and disease duration was collected from each participating institution. Because the PGE2 metabolite concentration was reported to increase in cases of thiazide-induced hyponatremia^[21] and laxative sennoside administration^[22], we collected information about the use of these medications. Because the PGE-MUM concentration was reported to be influenced by age, gender, smoking habit, and pulmonary inflammatory conditions including chronic fibrosing interstitial pneumonia^[15,23], we also collected information about smoking habit and pulmonary disease. Age was determined at the time of urine sample collection. Smoking habit was defined as never, current (> 6 mo on a daily basis), and former (cessation of smoking > 6 mo). Pulmonary diseases included chronic respiratory disease, diffuse lung disease, and any other lung or airway disease. History of surgery was defined as a history of intestinal resection at the time of study enrolment. The site of involvement was determined by radiographic and/or

Table 1 Clinical characteristics of the study subjects

	CEAS (n = 20)	CD (n = 98)	P value ¹
Age, yr	56 (41-63)	44 (38-54)	0.098
Gender			
Male	5 (25)	66 (67)	0.0008
Female	15 (75)	32 (33)	
Smoking			
Never smoker	16 (80)	68 (69)	0.42
Current smoker	1 (5)	13 (13)	
Former smoker	3 (15)	17 (18)	
Pulmonary disease	1 (5)	5 (5)	1
History of surgery	13 (65)	59 (60)	0.8
CRP, g/dL	0.30 (0.11-0.53)	0.13 (0.03-0.58)	0.26
Disease location			
L1, ileal		34 (35)	
L2, colonic		14 (14)	
L3, ileocolonic		50 (51)	
Disease duration, yr	33 (19-42)	20 (13-29)	0.0055

¹Mann-Whitney *U*-test or Fisher's exact test. Data are the number (%) or median (interquartile range). Significant *P* values are indicated in bold. CEAS: Chronic enteropathy associated with *SLCO2A1* gene; CD: Crohn disease; CRP: C reactive protein.

endoscopic findings, and these patients were categorized according to the Montreal classification^[24]. Disease duration was defined as the period from the onset of symptoms until study enrolment.

Genetic analysis

We used genomic DNA samples extracted from peripheral blood in our previous studies^[10,16,17,25]. In advance, we checked and confirmed that none of the patients with CD had homozygous or compound heterozygous *SLCO2A1* mutations with regards to the major six sites in our previous report^[10], including c.421G>T, c.664G>A, c.940+1G>A, c.1372G>T, c.1461+1G>C, and c.1807C>T. The diagnosis of CEAS was confirmed with 90.2% sensitivity by genotyping these 6 mutations on the basis of our previous investigation.

Measurement of prostaglandin E major urinary metabolite concentrations

All PGE-MUM concentrations were measured at SRL Inc. (Tokyo, Japan) by using a bicyclic PGE-MUM radioimmunoassay kit (Institute of Isotopes Co., Ltd. Budapest, Hungary). PGE-MUM, 7 α -hydroxy-5, 11-diketotetranorprosta-1, 16-dioic acid derived from PGE1 and PGE2 can be transformed to bicyclic PGE-MUM by alkali treatment. Each urine sample was collected and submitted individually according to the manufacturer's protocol described by Fujiwara *et al*^[22]. The urine samples were frozen and stored at -20 °C until the assay. PGE-MUM concentrations were corrected by the urinary creatinine concentration.

Statistical analyses

Categorical variables were expressed as the number (%) and continuous variables were expressed as the median (interquartile range). Comparison of the variables between CEAS and CD were performed using the chi-squared test, Fisher's exact probability test, or the Mann-Whitney *U*-test, where appropriate. The associations between clinical factors and the PGE-MUM concentration were estimated using univariable linear regression analyses. Because of the skewed distribution of the PGE-MUM concentration, values were log-transformed and used for regression analysis.

For the analysis of the clinical significance of PGE-MUM concentration to differentiate CEAS from CD, the logistic regression model was used to estimate the odds ratios (ORs) with 95% confidence intervals (CIs). The diagnostic accuracy of PGE-MUM concentration was evaluated using the area under the curve (AUC) with the receiver operating characteristic (ROC). The optimal cut-off value of PGE-MUM concentration for the diagnosis of CEAS was determined based on the maximum Youden Index (sensitivity + specificity - 1). In addition, sensitivity and specificity were compared using several cut-off values to confirm the diagnostic accuracy of this

cut-off value. Statistical analyses were performed using JMP version 13.0 (SAS Institute, Cary, NC, United States). A *P* value of 0.05 or smaller was considered statistically significant.

RESULTS

Baseline patient characteristics

The enrolled subjects consisted of 20 patients with CEAS (CEAS group) and 98 patients with CD (CD group). The clinical characteristics of the patients are shown in [Table 1](#). In the CEAS group, female patients were more frequent compared with the CD group. The disease duration was significantly longer in the CEAS group than in the CD group (median 33 *vs* 20 years, *P* = 0.0055). There was no significant difference in smoking status or medical history of pulmonary disease. Because most patients with CD were in clinical remission at the time of urine sample collection, the CRP levels remained low in the CD group.

PGE-MUM concentrations

Overall, 118 urinary samples were obtained from CEAS and CD patients. The PGE-MUM concentration ranged from 7.7 to 402.0 (median 34.1) $\mu\text{g/g} \times \text{Cre}$. [Table 2](#) shows the result of univariable linear regression analysis. A positive history of pulmonary disease and history of surgery were significantly associated with a higher PGE-MUM concentration (*P* < 0.0001 and *P* = 0.029, respectively). Serum CRP value was marginally associated with PGE-MUM concentration (*P* = 0.078). Factors with a *P* value < 0.1 were included in the multivariate analysis considering the possibility of confounding factors.

The PGE-MUM concentration was significantly higher in the CEAS group than in the CD group [median interquartile range (IQR): 102.7 (62.0-155.0) $\mu\text{g/g} \times \text{Cre}$ *vs* 27.9 (19.6-40.0) $\mu\text{g/g} \times \text{Cre}$, *P* < 0.0001, [Figure 1](#)]. Crude OR of 1 log unit increase in the PGE-MUM concentration for the distinction between CEAS and CD was 7.3 (95%CI 3.2-16.7, [Table 3](#)). This prediction model showed good differentiating ability between CEAS and CD, with an AUC of 0.90 (95%CI 0.82-0.95). This association was significant even after adjusting for possible confounding factors including age, gender, medical history of pulmonary disease, history of surgery, disease duration, and serum CRP value (model 3). The multivariate-adjusted OR was 29.6 (95%CI 4.7-185.7), with an AUC of 0.95 (95%CI 0.86-0.98).

Correlation between PGE-MUM and CD phenotype

The PGE-MUM concentration in the colonic CD group (L2) was significantly lower than in the other groups (median: 16.5 $\mu\text{g/g} \times \text{Cre}$ *vs* 29.5 $\mu\text{g/g} \times \text{Cre}$, *P* = 0.036), and the PGE-MUM concentration of the ileal CD group (L1) was significantly higher than in the colonic CD group (median: 32.9 $\mu\text{g/g} \times \text{Cre}$ *vs* 16.5 $\mu\text{g/g} \times \text{Cre}$, *P* = 0.017). When we confined the subjects to those with ileal CD, the PGE-MUM concentration in the CEAS group was still significantly higher than that in the ileal CD group (median 102.7 $\mu\text{g/g} \times \text{Cre}$ *vs* 32.9 $\mu\text{g/g} \times \text{Cre}$, *P* < 0.0001).

PGE-MUM cut-off level

[Figure 2](#) shows the ROC curve of the PGE-MUM concentration to differentiate CEAS from CD. Based on the ROC analysis, the optimal cut-off value was identified as 48.9 $\mu\text{g/g} \times \text{Cre}$, which differentiated CEAS from CD with 95.0% sensitivity and 79.6% specificity ([Supplementary Table 2](#)). The AUC was 0.90 (95%CI, 0.82-0.95).

Genetic screening in CD patients with a high PGE-MUM concentration

Among the CD group, six patients had particularly high PGE-MUM concentrations (> 100 $\mu\text{g/g} \times \text{Cre}$). Although we confirmed that they did not harbor the six major mutations in the *SLCO2A1* gene, we screened all 14 coding exons and intron-exon boundaries of the *SLCO2A1* gene using Sanger sequencing to exclude a possible misdiagnosis of CEAS. No homozygous or compound heterozygous *SLCO2A1* mutations were found in the six CD patients.

DISCUSSION

CEAS was initially reported as a novel disease entity referred to as "C" in the Japanese literature in the 1960s^[26]. We recently reported it is an autosomal recessive inherited disease^[8] caused by loss-of-function mutations in the *SLCO2A1* gene^[10]. Small bowel lesions in CEAS are characterized by multiple shallow ulcers with a circular or

Table 2 Factors associated with prostaglandin E major urinary metabolite concentrations

	Univariable linear regression (<i>P</i> value)
Age	<i>P</i> = 0.47 (0.067)
Gender (1, female; 0, male)	<i>P</i> = 0.26 (0.10)
Smoking (1, Current or former smoker; 0, Never smoker)	<i>P</i> = 0.17 (-0.13)
Pulmonary disease	<i>P</i> < 0.0001 (0.36)
History of surgery	<i>P</i> = 0.029 (0.20)
CRP	<i>P</i> = 0.078 (0.16)
Disease duration	<i>P</i> = 0.0040 (0.26)

The values of prostaglandin E major urinary metabolite were log-transformed. Significant *P* values are indicated in bold. CRP: C reactive protein.

eccentric oblique configuration^[18]. In contrast, CD typically develops longitudinal ulcers and cobblestoning, and ulcerations are predominantly located on the mesenteric side. However, both CEAS and CD involve the ileum with occasional ileal stenoses, and the clinical features of CEAS and CD are similar; therefore, it is not easy to differentiate CEAS from CD based on clinical manifestations alone^[11]. Although immunohistochemical staining for SLCO2A1 protein in biopsy specimens from the GI tract was reported to be useful to distinguish CEAS from CD^[27,28], a more convenient and non-invasive screening test is required.

PGE-MUM, a major urinary metabolite derived from PGE2, is clinically used to assess the severity of inflammatory conditions such as interstitial pneumonia^[23], cystic fibrosis^[29], and ulcerative colitis^[30,31]. Similarly, urinary PGE2 metabolite concentrations in patients with CD are higher than those in patients with colorectal neoplasms and healthy controls^[32]. Indeed, PGE-MUM concentrations in patients with CD (median 27.9, IQR 19.6-40.0 µg/g × Cre) in the present study were higher than those in Japanese healthy controls (median 13.1, IQR 10.3-17.2 µg/g × Cre) as reported in previous studies^[15,23]. Nevertheless, the PGE-MUM concentration, a surrogate marker of physiological PGE2 levels^[30], in patients with CEAS was significantly higher than in patients with CD. This difference was still significant even after the adjustment for confounding factors. In addition, we demonstrated that the provisional cut-off value (48.9 µg/g × Cre) of PGE-MUM had a differentiating ability with 95.0% sensitivity and 79.6% specificity (AUC 0.90). Therefore, PGE-MUM is useful to distinguish CEAS from CD.

Although prostaglandins are mediators of active inflammation, many experimental studies have indicated that they play pivotal roles in maintaining mucosal homeostasis^[33] and mucosal repair^[34] of the intestine. PGE2 is mainly derived from arachidonic acid by cyclooxygenase and PGE synthase and PGE2 acts through four different receptor subtypes (EP1, EP2, EP3 and EP4), which partly determines the various physiological effects of PGE2 including the regulation of acid secretion, bicarbonate secretion, mucus production, and mucosal blood flow^[35]. In particular, dimethyl PGE2 (dmPGE2), a stable derivative of PGE2, was reported to exert a potent inhibitory effect against indomethacin-induced intestinal injuries in a rat model *via* activation of EP3 and EP4 receptors^[36]. It was also shown that the deleterious effect of indomethacin on the healing of intestinal ulcers was induced by an EP4 antagonist and suppressed by the co-administration of PGE2 as well as an EP4 agonist^[34]. These results indicate that the protective effect of PGE2 on mucosal injury of the intestine is caused by EP3 and EP4 activation.

PHO, which develops skin and bone disorders caused by impaired prostaglandin metabolism, is classified into two types: PHOAR2 caused by the *SLCO2A1* gene^[12], and PHOAR1 caused by the *HPGD* gene^[37]. Prostaglandin-signaling is terminated by the cellular uptake of prostaglandins *via* the prostaglandin transporter, followed by intracellular oxidation by 15-ketoprostaglandin dehydrogenase (15-PGDH) encoded by the *HPGD* gene^[38]. Thus, cellular uptake of prostaglandins is the first critical step in inactivating prostaglandins. The *SLCO2A1* gene mediates the degradation of prostaglandins *via* their intracellular uptake^[39,40]. The *HPGD* gene is also related to the degradation of prostaglandins by encoding intracellular oxidation enzymes of 15-PGDH. In both conditions, significantly elevated plasma PGE2 levels have been observed^[13,37]. Because PGE2 promotes the proliferation of osteoblasts in bone tissue *via* the expression of vascular endothelial growth factor^[41,42], various clinical manifestations of PHO such as digital clubbing, periostosis, acroosteolysis, painful joint enlargement, and thickened skin, are suggested to be the consequence of an

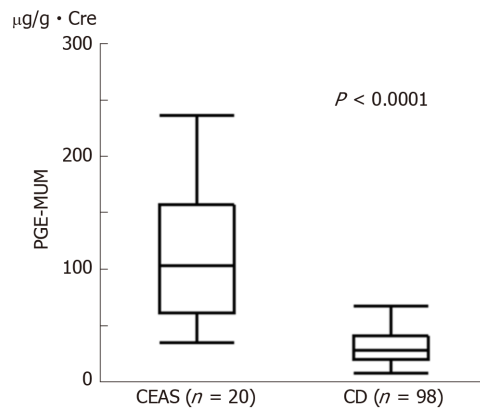


Figure 1 Comparison of Prostaglandin E-major urinary metabolites concentrations between chronic enteropathy associated with *SLCO2A1* gene ($n = 20$) and Crohn's disease ($n = 98$) groups. Prostaglandin E-major urinary metabolite concentrations in the chronic enteropathy associated with *SLCO2A1* gene group were significantly higher than those in the Crohn's disease group [median (interquartile range): 102.7 (62.0-155.0) $\mu\text{g/g} \times \text{Cre}$ vs 27.9 (19.6-40.0) $\mu\text{g/g} \times \text{Cre}$, $P < 0.0001$]. Mann-Whitney *U*-test. CEAS: Chronic enteropathy associated with *SLCO2A1* gene; CD: Crohn's disease; PEG-MUM: Prostaglandin E-major urinary metabolite.

overabundance of PGE2. Although PGE2 is protective against gastrointestinal mucosal injuries^[35,42], multiple ileal ulcers occur in patients with CEAS, in whom systemic levels of PGE2 are elevated. Considering our previous result that the prostaglandin transporter was expressed on the cellular membrane of vascular endothelial cells^[10], it can be presumed that impaired prostaglandin use in the intestinal mucosa caused by mutation of the *SLCO2A1* gene is a major factor in the pathogenesis of intestinal ulcers in CEAS.

Cryptogenic multifocal ulcerous stenosing enteritis (CMUSE) is another disease entity that causes gastrointestinal ulcerations resembling CEAS^[43,44]. Recently, recessive mutations in the *PLA2G4A* gene, encoding cytoplasmic phospholipase A2- α (cPLA2 α), which hydrolyses cellular membrane phospholipids into arachidonic acids, have been identified as a cause of CMUSE^[44,45]. Because the loss-of-function of cPLA2 α decreases systemic levels of PGE2 (approximated by PGE-MUM) and thromboxane A2^[45], multiple small bowel ulcers, as well as the dysfunction of platelet aggregation are observed in patients with CMUSE^[46]. Although precise analyses of the morphologic features of gastrointestinal lesions in CMUSE have not been reported yet, it seems likely that CEAS and CMUSE share morphologic features regarding the gastrointestinal lesions. In this sense, the measurement of PGE-MUM concentrations can be assumed to be useful to differentiate CEAS from CMUSE, although genetic testing is mandatory to confirm the diagnosis.

This study had several limitations. First, the sample size of the patients with CEAS was relatively small because CEAS is a rare disease. Therefore, we could not validate the cut-off value for the distinction between the two diseases. Second, because most of our CD patients were in clinical remission, the cut-off value may not be appropriate for the distinction of CEAS from active CD. Indeed, some patients with quiescent CD had markedly high PGE-MUM concentrations. Third, we could not completely rule out the possibility that the patients with CD had recessive mutations in the *SLCO2A1* gene. Although we checked the major six mutations of the *SLCO2A1* gene in patients with CD, 9.8% of the mutations might be overlooked based on our previous result^[10].

In conclusion, the measurement of PGE-MUM might be a convenient, non-invasive and useful test to differentiate CEAS from CD, although genetic analysis is mandatory for the confirmation of CEAS. Further studies are necessary to clarify the pathogenesis of CEAS to explore therapeutic targets of this disease.

Table 3 Convert odds ratio for prostaglandin E major urinary metabolite

	Model 1	Model 2	Model 3
Odds ratio of 1 log unit change	7.3	6	29.6
(95%CI)	(3.2-16.7)	(2.6-13.9)	(4.7-185.7)
AUC (95%CI)	0.90 (0.82-0.94)	0.93 (0.87-0.96)	0.95 (0.86-0.98)

CI: Confidence interval; AUC: Area under the curve; Model 1: Prostaglandin E-major urinary metabolite; Model 2: Prostaglandin E-major urinary metabolite + Age + Gender; Model 3: Prostaglandin E-major urinary metabolite + Age + Gender + Medical history of pulmonary disease + History of surgery + Disease duration+ C reactive protein.

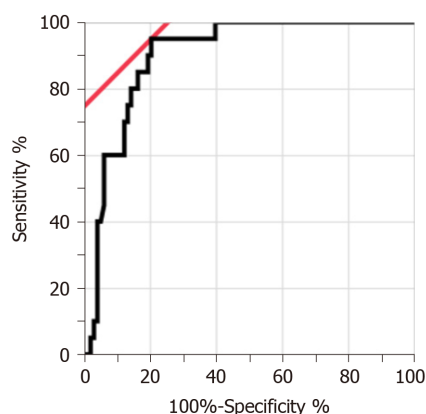


Figure 2 Receiver operating characteristic curve of Prostaglandin E-major urinary metabolites concentrations for differentiation between chronic enteropathy associated with *SLCO2A1* gene and Crohn's disease. The area under the receiver operating characteristic curve was 0.90 (95% confidence interval, 0.82-0.95). The optimal cut-off value was 48.9 $\mu\text{g/g} \times \text{Cre}$.

ARTICLE HIGHLIGHTS

Research background

Chronic enteropathy associated with *SLCO2A1* gene (CEAS) is a rare small intestinal disease, but distinct clinical condition from Crohn's disease (CD). To date, we can make a correct diagnosis of CEAS by combination of clinical features and genetic analysis. However, CEAS is sometimes misdiagnosed as CD, because these diseases have some clinical features in common.

Research motivation

A more convenient and non-invasive screening test will help to diagnose CEAS correctly.

Research objectives

To investigate the usefulness of prostaglandin E-major urinary metabolites (PGE-MUM) to distinguish CEAS from CD.

Research methods

Participants were diagnosed CEAS and CD by clinical diagnostic criteria and genetic analysis. All participants' PGE-MUM concentrations were measured by radioimmunoassay. We analyzed differentiating ability of PGE-MUM measurement between CEAS and CD.

Research results

Twenty patients with CEAS and 98 patients with CD were enrolled. It was found that the PGE-MUM concentrations of patients with CEAS were significantly higher than those of patients with CD and this correlation was still statistically significant after adjusting the possible confounding factors. Additionally, the present study showed the provisional cut-off value (48.9 $\mu\text{g/g} \times \text{Cre}$) of PGE-MUM had a differentiating ability with 95.0% sensitivity and 79.6% specificity (area under the curve 0.90).

Research conclusions

The measurement of PGE-MUM can serve as a useful biomarker to differentiate CEAS from CD, although genetic analysis is mandatory for the diagnosis of CEAS.

Research perspectives

Our study showed the usefulness of PGE-MUM to differentiate CEAS from CD. In the present research, the sample size of the patients with CEAS were relatively small, the cut-off value for

the distinction of CEAS from CD should be validated with large sample size of patients with CEAS in the future research.

ACKNOWLEDGEMENTS

We appreciate the patients for participating in this study. We also appreciate Ms. Risa Tsuneyoshi for technical assistance and Drs. Tomohiko Moriyama, Shin Fujioka, Naoya Kubokura, Yoichiro Nuki, Ema Washio, and Shinichi Kawano for their assistance with clinical characterization.

REFERENCES

- Iddan G, Meron G, Glukhovskiy A, Swain P. Wireless capsule endoscopy. *Nature* 2000; **405**: 417 [PMID: 10839527 DOI: 10.1038/35013140]
- Yamamoto H, Sekine Y, Sato Y, Higashizawa T, Miyata T, Iino S, Ido K, Sugano K. Total enteroscopy with a nonsurgical steerable double-balloon method. *Gastrointest Endosc* 2001; **53**: 216-220 [PMID: 11174299 DOI: 10.1067/mge.2001.112181]
- Matsumoto T, Moriyama T, Esaki M, Nakamura S, Iida M. Performance of antegrade double-balloon enteroscopy: Comparison with push enteroscopy. *Gastrointest Endosc* 2005; **62**: 392-398 [PMID: 16111958 DOI: 10.1016/j.gie.2005.04.052]
- Matsumoto T, Kudo T, Esaki M, Yano T, Yamamoto H, Sakamoto C, Goto H, Nakase H, Tanaka S, Matsui T, Sugano K, Iida M. Prevalence of non-steroidal anti-inflammatory drug-induced enteropathy determined by double-balloon endoscopy: A Japanese multicenter study. *Scand J Gastroenterol* 2008; **43**: 490-496 [PMID: 18365915 DOI: 10.1080/00365520701794121]
- Esaki M, Matsumoto T, Watanabe K, Arakawa T, Naito Y, Matsuura M, Nakase H, Hibi T, Matsumoto T, Nouda S, Higuchi K, Ohmiya N, Goto H, Kurokawa S, Motoya S, Watanabe M. Use of capsule endoscopy in patients with Crohn's disease in Japan: A multicenter survey. *J Gastroenterol Hepatol* 2014; **29**: 96-101 [PMID: 24354993 DOI: 10.1111/jgh.12411]
- Matsumoto T, Iida M, Matsui T, Yao T, Watanabe H, Yao T, Okabe H. Non-specific multiple ulcers of the small intestine unrelated to non-steroidal anti-inflammatory drugs. *J Clin Pathol* 2004; **57**: 1145-1150 [PMID: 15509673 DOI: 10.1136/jcp.2003.015735]
- Matsumoto T, Iida M, Matsui T, Yao T. Chronic nonspecific multiple ulcers of the small intestine: A proposal of the entity from Japanese gastroenterologists to Western enteroscopists. *Gastrointest Endosc* 2007; **66**: S99-107 [PMID: 17709045 DOI: 10.1016/j.gie.2007.01.004]
- Matsumoto T, Kubokura N, Matsui T, Iida M, Yao T. Chronic nonspecific multiple ulcer of the small intestine segregates in offspring from consanguinity. *J Crohns Colitis* 2011; **5**: 559-565 [PMID: 22115375 DOI: 10.1016/j.crohns.2011.05.008]
- Esaki M, Umeno J, Kitazono T, Matsumoto T. Clinicopathologic features of chronic nonspecific multiple ulcers of the small intestine. *Clin J Gastroenterol* 2015; **8**: 57-62 [PMID: 25788296 DOI: 10.1007/s12328-015-0559-x]
- Umeno J, Hisamatsu T, Esaki M, Hirano A, Kubokura N, Asano K, Kochi S, Yanai S, Fuyuno Y, Shimamura K, Hosoe N, Ogata H, Watanabe T, Aoyagi K, Ooi H, Watanabe K, Yasukawa S, Hirai F, Matsui T, Iida M, Yao T, Hibi T, Kosaki K, Kanai T, Kitazono T, Matsumoto T. A Hereditary Enteropathy Caused by Mutations in the SLCO2A1 Gene, Encoding a Prostaglandin Transporter. *PLoS Genet* 2015; **11**: e1005581 [PMID: 26539716 DOI: 10.1371/journal.pgen.1005581]
- Umeno J, Esaki M, Hirano A, Fuyuno Y, Ohmiya N, Yasukawa S, Hirai F, Kochi S, Kurahara K, Yanai S, Uchida K, Hosomi S, Watanabe K, Hosoe N, Ogata H, Hisamatsu T, Nagayama M, Yamamoto H, Abukawa D, Kakuta F, Onodera K, Matsui T, Hibi T, Yao T, Kitazono T, Matsumoto T; CEAS study group. Clinical features of chronic enteropathy associated with SLCO2A1 gene: A new entity clinically distinct from Crohn's disease. *J Gastroenterol* 2018; **53**: 907-915 [PMID: 29313109 DOI: 10.1007/s00535-017-1426-y]
- Seifert W, Kühnisch J, Tüysüz B, Specker C, Brouwers A, Horn D. Mutations in the prostaglandin transporter encoding gene SLCO2A1 cause primary hypertrophic osteoarthropathy and isolated digital clubbing. *Hum Mutat* 2012; **33**: 660-664 [PMID: 22331663 DOI: 10.1002/humu.22042]
- Zhang Z, Xia W, He J, Zhang Z, Ke Y, Yue H, Wang C, Zhang H, Gu J, Hu W, Fu W, Hu Y, Li M, Liu Y. Exome sequencing identifies SLCO2A1 mutations as a cause of primary hypertrophic osteoarthropathy. *Am J Hum Genet* 2012; **90**: 125-132 [PMID: 22197487 DOI: 10.1016/j.ajhg.2011.11.019]
- Zhang Z, He JW, Fu WZ, Zhang CQ, Zhang ZL. Mutations in the SLCO2A1 gene and primary hypertrophic osteoarthropathy: A clinical and biochemical characterization. *J Clin Endocrinol Metab* 2013; **98**: E923-E933 [PMID: 23509104 DOI: 10.1210/jc.2012-3568]
- Okayasu I, Ohnishi H, Sarandi I, Shojima J, Komatsu J, Oritsu M, Sasabe M, Nanami KO, Matsuura M, Azumi J, Ito S, Fujiwara M. Significant increase of prostaglandin E-major urinary metabolite in male smokers: A screening study of age and gender differences using a simple radioimmunoassay. *J Clin Lab Anal* 2014; **28**: 32-41 [PMID: 24375858 DOI: 10.1002/jcla.21640]
- Hirano A, Yamazaki K, Umeno J, Ashikawa K, Aoki M, Matsumoto T, Nakamura S, Ninomiya T, Matsui T, Hirai F, Kawaguchi T, Takazoe M, Tanaka H, Motoya S, Kiyohara Y, Kitazono T, Nakamura Y, Kamatani N, Kubo M. Association study of 71 European Crohn's disease susceptibility loci in a Japanese population. *Inflamm Bowel Dis* 2013; **19**: 526-533 [PMID: 23388546 DOI: 10.1097/MIB.0b013e31828075e7]
- Yamazaki K, Umeno J, Takahashi A, Hirano A, Johnson TA, Kumasaka N, Morizono T, Hosono N, Kawaguchi T, Takazoe M, Yamada T, Suzuki Y, Tanaka H, Motoya S, Hosokawa M, Arimura Y, Shinomura Y, Matsui T, Matsumoto T, Iida M, Tsunoda T, Nakamura Y, Kamatani N, Kubo M. A genome-wide association study identifies 2 susceptibility Loci for Crohn's disease in a Japanese population. *Gastroenterology* 2013; **144**: 781-788 [PMID: 23266558 DOI: 10.1053/j.gastro.2012.12.021]
- Matsumoto T, Nakamura S, Esaki M, Yada S, Koga H, Yao T, Iida M. Endoscopic features of chronic nonspecific multiple ulcers of the small intestine: Comparison with nonsteroidal anti-inflammatory drug-

- induced enteropathy. *Dig Dis Sci* 2006; **51**: 1357-1363 [PMID: [16868823](#) DOI: [10.1007/s10620-006-9080-x](#)]
- 19 **Hosoe N**, Ohmiya N, Hirai F, Umeno J, Esaki M, Yamagami H, Onodera K, Bamba S, Imaeda H, Yanai S, Hisamatsu T, Ogata H, Matsumoto T; CEAS Atlas Group. Chronic Enteropathy Associated With SLCO2A1 Gene [CEAS]-Characterisation of an Enteric Disorder to be Considered in the Differential Diagnosis of Crohn's Disease. *J Crohns Colitis* 2017; **11**: 1277-1281 [PMID: [28510689](#) DOI: [10.1093/ecco-jcc/jjx068](#)]
 - 20 **Hisabe T**, Hirai F, Matsui T, Watanabe M. Evaluation of diagnostic criteria for Crohn's disease in Japan. *J Gastroenterol* 2014; **49**: 93-99 [PMID: [23546557](#) DOI: [10.1007/s00535-013-0798-x](#)]
 - 21 **Ware JS**, Wain LV, Channavajjhala SK, Jackson VE, Edwards E, Lu R, Siew K, Jia W, Shrine N, Kinnear S, Jalland M, Henry AP, Clayton J, O'Shaughnessy KM, Tobin MD, Schuster VL, Cook S, Hall IP, Glover M. Phenotypic and pharmacogenetic evaluation of patients with thiazide-induced hyponatremia. *J Clin Invest* 2017; **127**: 3367-3374 [PMID: [28783044](#) DOI: [10.1172/JCI89812](#)]
 - 22 **Fujiwara M**, Okayasu I, Oritsu M, Komatsu J, Yoshitsugu M, Katoh Y, Bandoh T, Toyoshima H, Kase Y, Sugihara K, Kanno J, Hayashi Y. Significant increase in prostaglandin E-main urinary metabolite by laxative administration: Comparison with ulcerative colitis. *Digestion* 2000; **61**: 201-206 [PMID: [10773726](#) DOI: [10.1159/000007758](#)]
 - 23 **Horikiri T**, Hara H, Saito N, Araya J, Takasaka N, Utsumi H, Yanagisawa H, Hashimoto M, Yoshii Y, Wakui H, Minagawa S, Ishikawa T, Shimizu K, Numata T, Arihiro S, Kaneko Y, Nakayama K, Matsuura T, Matsuura M, Fujiwara M, Okayasu I, Ito S, Kuwano K. Increased levels of prostaglandin E-major urinary metabolite (PGE-MUM) in chronic fibrosing interstitial pneumonia. *Respir Med* 2017; **122**: 43-50 [PMID: [27993290](#) DOI: [10.1016/j.rmed.2016.11.017](#)]
 - 24 **Satsangi J**, Silverberg MS, Vermeire S, Colombel JF. The Montreal classification of inflammatory bowel disease: Controversies, consensus, and implications. *Gut* 2006; **55**: 749-753 [PMID: [16698746](#) DOI: [10.1136/gut.2005.082909](#)]
 - 25 **Fuyuno Y**, Yamazaki K, Takahashi A, Esaki M, Kawaguchi T, Takazoe M, Matsumoto T, Matsui T, Tanaka H, Motoya S, Suzuki Y, Kiyohara Y, Kitazono T, Kubo M. Genetic characteristics of inflammatory bowel disease in a Japanese population. *J Gastroenterol* 2016; **51**: 672-681 [PMID: [26511940](#) DOI: [10.1007/s00535-015-1135-3](#)]
 - 26 **Okabe H**, Sakimura M. "Hi Tokui-sei Tahatsu-sei Shouchou Kaiyou-shou". *Stomach Intest* 1968; **3**: 1539-1549
 - 27 **Yamaguchi S**, Yanai S, Nakamura S, Kawasaki K, Eizuka M, Uesugi N, Sugai T, Umeno J, Esaki M, Matsumoto T. Immunohistochemical differentiation between chronic enteropathy associated with SLCO2A1 gene and other inflammatory bowel diseases. *Intest Res* 2018; **16**: 393-399
 - 28 **Yanai S**, Yamaguchi S, Nakamura S, Kawasaki K, Toya Y, Yamada N, Eizuka M, Uesugi N, Umeno J, Esaki M, Okimoto E, Ishihara S, Sugai T, Matsumoto T. Distinction of Chronic Enteropathy associated with SLCO2A1 Gene from Crohn's Disease. *Gut Liver* 2018; **13**: 62-66
 - 29 **Jabr S**, Gartner S, Milne GL, Roca-Ferrer J, Casas J, Moreno A, Gelpi E, Picado C. Quantification of major urinary metabolites of PGE2 and PGD2 in cystic fibrosis: Correlation with disease severity. *Prostaglandins Leukot Essent Fatty Acids* 2013; **89**: 121-126 [PMID: [23791427](#) DOI: [10.1016/j.plefa.2013.06.001](#)]
 - 30 **Arai Y**, Arihiro S, Matsuura T, Kato T, Matsuoka M, Saruta M, Mitsunaga M, Matsuura M, Fujiwara M, Okayasu I, Ito S, Tajiri H. Prostaglandin E-major urinary metabolite as a reliable surrogate marker for mucosal inflammation in ulcerative colitis. *Inflamm Bowel Dis* 2014; **20**: 1208-1216 [PMID: [24846719](#) DOI: [10.1097/MIB.0000000000000062](#)]
 - 31 **Arai Y**, Matsuura T, Matsuura M, Fujiwara M, Okayasu I, Ito S, Arihiro S. Prostaglandin E-Major Urinary Metabolite as a Biomarker for Inflammation in Ulcerative Colitis: Prostaglandins Revisited. *Digestion* 2016; **93**: 32-39 [PMID: [26788915](#) DOI: [10.1159/000441665](#)]
 - 32 **Johnson JC**, Schmidt CR, Shrubsole MJ, Billheimer DD, Joshi PR, Morrow JD, Heslin MJ, Washington MK, Ness RM, Zheng W, Schwartz DA, Coffey RJ, Beauchamp RD, Merchant NB. Urine PGE-M: A metabolite of prostaglandin E2 as a potential biomarker of advanced colorectal neoplasia. *Clin Gastroenterol Hepatol* 2006; **4**: 1358-1365 [PMID: [16996805](#) DOI: [10.1016/j.cgh.2006.07.015](#)]
 - 33 **Otani T**, Yamaguchi K, Scherl E, Du B, Tai HH, Greifer M, Petrovic L, Daikoku T, Dey SK, Subbaramaiah K, Dannenberg AJ. Levels of NAD(+)-dependent 15-hydroxyprostaglandin dehydrogenase are reduced in inflammatory bowel disease: Evidence for involvement of TNF-alpha. *Am J Physiol Gastrointest Liver Physiol* 2006; **290**: G361-G368 [PMID: [16195422](#) DOI: [10.1152/ajpgi.00348.2005](#)]
 - 34 **Hatazawa R**, Ohno R, Tanigami M, Tanaka A, Takeuchi K. Roles of endogenous prostaglandins and cyclooxygenase isozymes in healing of indomethacin-induced small intestinal lesions in rats. *J Pharmacol Exp Ther* 2006; **318**: 691-699 [PMID: [16699067](#) DOI: [10.1124/jpet.106.103994](#)]
 - 35 **Takeuchi K**, Kato S, Amagase K. Prostaglandin EP receptors involved in modulating gastrointestinal mucosal integrity. *J Pharmacol Sci* 2010; **114**: 248-261 [PMID: [21041985](#) DOI: [10.1254/jphs.10R06CR](#)]
 - 36 **Kunikata T**, Tanaka A, Miyazawa T, Kato S, Takeuchi K. 16,16-Dimethyl prostaglandin E2 inhibits indomethacin-induced small intestinal lesions through EP3 and EP4 receptors. *Dig Dis Sci* 2002; **47**: 894-904 [PMID: [11991626](#) DOI: [10.1023/A:1014725024519](#)]
 - 37 **Uppal S**, Diggle CP, Carr IM, Fishwick CW, Ahmed M, Ibrahim GH, Helliwell PS, Latos-Bieleńska A, Phillips SE, Markham AF, Bennett CP, Bonthron DT. Mutations in 15-hydroxyprostaglandin dehydrogenase cause primary hypertrophic osteoarthropathy. *Nat Genet* 2008; **40**: 789-793 [PMID: [18500342](#) DOI: [10.1038/ng.153](#)]
 - 38 **Nakanishi T**, Tamai I. Roles of Organic Anion Transporting Polypeptide 2A1 (OATP2A1/SLCO2A1) in Regulating the Pathophysiological Actions of Prostaglandins. *AAPS J* 2017; **20**: 13 [PMID: [29204966](#) DOI: [10.1208/s12248-017-0163-8](#)]
 - 39 **Kanai N**, Lu R, Satriano JA, Bao Y, Wolkoff AW, Schuster VL. Identification and characterization of a prostaglandin transporter. *Science* 1995; **268**: 866-869 [PMID: [7754369](#) DOI: [10.1126/science.7754369](#)]
 - 40 **Nomura T**, Lu R, Pucci ML, Schuster VL. The two-step model of prostaglandin signal termination: *In vitro* reconstitution with the prostaglandin transporter and prostaglandin 15 dehydrogenase. *Mol Pharmacol* 2004; **65**: 973-978 [PMID: [15044627](#) DOI: [10.1124/mol.65.4.973](#)]
 - 41 **Harada S**, Nagy JA, Sullivan KA, Thomas KA, Endo N, Rodan GA, Rodan SB. Induction of vascular endothelial growth factor expression by prostaglandin E2 and E1 in osteoblasts. *J Clin Invest* 1994; **93**: 2490-2496 [PMID: [8200985](#) DOI: [10.1172/JCI117258](#)]
 - 42 **Rao R**, Redha R, Macias-Perez I, Su Y, Hao C, Zent R, Breyer MD, Pozzi A. Prostaglandin E2-EP4 receptor promotes endothelial cell migration via ERK activation and angiogenesis in vivo. *J Biol Chem*

- 2007; **282**: 16959-16968 [PMID: [17401137](#) DOI: [10.1074/jbc.M701214200](#)]
- 43 **Shoesmith JH**, Tate GT, Wright CJ. Multiple Strictures Of The Jejunum. *Gut* 1964; **5**: 132-135 [PMID: [14159400](#) DOI: [10.1136/gut.5.2.132](#)]
- 44 **Perlemuter G**, Guillevin L, Legman P, Weiss L, Couturier D, Chaussade S. Cryptogenetic multifocal ulcerous stenosing enteritis: An atypical type of vasculitis or a disease mimicking vasculitis. *Gut* 2001; **48**: 333-338 [PMID: [11171822](#) DOI: [10.1136/gut.48.3.333](#)]
- 45 **Adler DH**, Cogan JD, Phillips JA, Schnetz-Boutaud N, Milne GL, Iverson T, Stein JA, Brenner DA, Morrow JD, Boutaud O, Oates JA. Inherited human cPLA(2alpha) deficiency is associated with impaired eicosanoid biosynthesis, small intestinal ulceration, and platelet dysfunction. *J Clin Invest* 2008; **118**: 2121-2131 [PMID: [18451993](#) DOI: [10.1172/JCI30473](#)]
- 46 **Brooke MA**, Longhurst HJ, Plagnol V, Kirkby NS, Mitchell JA, Rüschendorf F, Warner TD, Kelsell DP, MacDonald TT. Cryptogenic multifocal ulcerating stenosing enteritis associated with homozygous deletion mutations in cytosolic phospholipase A2- α . *Gut* 2014; **63**: 96-104 [PMID: [23268370](#) DOI: [10.1136/gutjnl-2012-303581](#)]



Prospective Study

Endoscopic response to tumor necrosis factor inhibitors predicts long term benefits in Crohn's disease

Ignacio Alfaro, Maria Carme Masamunt, Nuria Planell, Alicia López-García, Jesús Castro, Marta Gallego, Rebeca Barastegui, Angel Giner, Alejandro Vara, Azucena Salas, Elena Ricart, Julián Panés, Ingrid Ordás

ORCID number: Ignacio Alfaro (0000-0002-1823-3182); Maria Carme Masamunt (0000-0001-8736-1623); Nuria Planell (0000-0001-7550-2433); Alicia López-García (0000-0001-9268-4259); Jesús Castro (0000-0002-2269-7385); Marta Gallego (0000-0001-9761-3070); Rebeca Barastegui (0000-0002-8370-8498); Angel Giner (0000-0001-8314-1172); Alejandro Vara (0000-0003-2218-0535); Azucena Salas (0000-0003-4572-2907); Elena Ricart (0000-0003-3354-1594); Julián Panés (0000-0002-4971-6902); Ingrid Ordás (0000-0001-7632-0340).

Author contributions: Alfaro I, Salas A, Ricart E, Panés J and Ordás I contributed to study conception and design; Masamunt MC, López-García A, Castro J, Gallego M, Barastegui R, Giner A and Vara A contributed to patients recruitment and data acquisition; Planell N contributed to data analysis and interpretation; Alfaro I contributed to writing of article; Panés J and Ordás I contributed to editing and reviewing; all authors approve the final version of the article.

Supported by the Leona M. and Harry B Helmsley Charitable Trust, No. 2015PG-IBD005.

Institutional review board statement: The study was reviewed and approved by the Hospital Clinic of Barcelona Institutional Review Board.

Informed consent statement: All study participants or their legal

Ignacio Alfaro, Maria Carme Masamunt, Alicia López-García, Jesús Castro, Marta Gallego, Rebeca Barastegui, Angel Giner, Alejandro Vara, Elena Ricart, Julián Panés, Ingrid Ordás, Gastroenterology Department, Hospital Clínic de Barcelona, Barcelona 08036, Spain

Nuria Planell, Azucena Salas, Institut d'Investigacions Biomèdiques August Pi i Sunyer (IDIBAPS), University of Barcelona, Barcelona 08036, Spain

Corresponding author: Ingrid Ordás, MD, PhD, Staff Physician, Gastroenterology Department, Hospital Clínic de Barcelona, Villarroel 170, Barcelona 08036, Spain. iordas@clinic.cat

Telephone: +34-932275418

Fax: +34-932275454

Abstract

BACKGROUND

Identifying predictors of therapeutic response is the cornerstone of personalized medicine.

AIM

To identify predictors of long-term mucosal healing (MH) in patients with Crohn's disease (CD) treated with tumor necrosis factor α (TNF- α) inhibitors.

METHODS

Prospective single center study. Consecutive patients with clinically active CD requiring treatment with a TNF- α inhibitor were included. A baseline segmental CD Endoscopic Index of Severity (CDEIS) ≥ 10 in at least one segment or the presence of ulcerations were required for inclusion. Clinical, biological and endoscopic data were obtained at baseline, weeks 14 and 46. Endoscopic response (ER) was defined as a decrease $\geq 50\%$ from baseline CDEIS and MH as partial CDEIS ≤ 5 in all segments.

RESULTS

Of 62 patients were included. At baseline, median CD Activity Index and CDEIS were 201 and 6.7, respectively with a significant reduction after one year of treatment (53 and 3.0 respectively, $P < 0.001$). At week 14, 56% of patients achieved ER and 34% MH. At week 46, the corresponding percentages were 52% and 44%. Baseline disease characteristics or biomarkers did not predict MH. A decrease from baseline CDEIS at week 14 of at least 80% was the best predictor of MH at week 46 (59% sensitivity and 91% specificity; area under the curve = 0.778).

guardian provided informed written consent about personal and medical data collection prior to study enrolment.

Conflict-of-interest statement: All the Authors have no conflict of interest related to the manuscript.

Data sharing statement: All available data can be obtained by contacting the corresponding author

CONSORT 2010 statement: The authors have read the CONSORT 2010 Statement, and the manuscript was prepared and revised according to the CONSORT 2010 Statement.

Open-Access: This article is an open-access article which was selected by an in-house editor and fully peer-reviewed by external reviewers. It is distributed in accordance with the Creative Commons Attribution Non Commercial (CC BY-NC 4.0) license, which permits others to distribute, remix, adapt, build upon this work non-commercially, and license their derivative works on different terms, provided the original work is properly cited and the use is non-commercial. See: <http://creativecommons.org/licenses/by-nc/4.0/>

Manuscript source: Unsolicited manuscript

Received: November 9, 2018

Peer-review started: November 12, 2018

First decision: January 30, 2019

Revised: February 26, 2019

Accepted: March 1, 2019

Article in press: March 1, 2019

Published online: April 14, 2019

P-Reviewer: Sipahi AM, Tahan V

S-Editor: Yan JP

L-Editor: A

E-Editor: Song H



CONCLUSION

Clinical and biomarker data are not useful predictors of response to TNF- α inhibitors in CD, whereas ER to induction therapy, defined as 80% reduction in global CDEIS, is a robust predictor of long-term MH. Achievement of this endoscopic endpoint may be considered as a therapeutic target for anti-TNF- α therapy.

Key words: Crohn's disease; Endoscopy; Mucosal healing; Crohn's Disease Endoscopic Index of Severity; Tumor necrosis factor

©The Author(s) 2019. Published by Baishideng Publishing Group Inc. All rights reserved.

Core tip: In our study we report that endoscopic response after completion of induction treatment with a tumor necrosis factor inhibitor predicts mucosal healing at long term in patients with Crohn's disease, and that endoscopic evaluation at this time point may be considered in clinical practice to predict long term outcomes and could contribute to perform treatment adjustments.

Citation: Alfaro I, Masamunt MC, Planell N, López-García A, Castro J, Gallego M, Barastegui R, Giner A, Vara A, Salas A, Ricart E, Panés J, Ordás I. Endoscopic response to tumor necrosis factor inhibitors predicts long term benefits in Crohn's disease. *World J Gastroenterol* 2019; 25(14): 1764-1774

URL: <https://www.wjgnet.com/1007-9327/full/v25/i14/1764.htm>

DOI: <https://dx.doi.org/10.3748/wjg.v25.i14.1764>

INTRODUCTION

Crohn's disease (CD) is a chronic inflammatory bowel disease (IBD) characterized by a wide spectrum of disease phenotypes that typically alternates periods of active inflammation and remission. Persistent inflammation leads to the accumulation of intestinal damage and loss of function in the affected intestinal segments, resulting in disability in many patients^[1]. The main treatment goal in CD is to achieve healing of inflammatory lesions to prevent damage progression by introducing highly effective therapies early during the course of the disease. Tumor necrosis factor α (TNF- α) inhibitors are one of the most effective therapies for induction and maintenance of remission in patients with CD^[2].

Response to anti-TNF therapy is heterogeneous. In patients with CD several predictors of clinical response have been described, including age^[3,4], disease duration^[5], inflammatory phenotype^[6], and smoking status^[6-10], but the effect size of these factors is small and not sufficient to guide clinical practice. Furthermore, predictors of endoscopic healing remain to be definitively established. In the field of biomarkers, normalization of C reactive protein (CRP) and calprotectin has been associated with mucosal healing (MH)^[6,11]. With regard to endoscopic lesions, achievement of MH after three months of treatment with a TNF- α inhibitor has been identified as a predictor of long-term endoscopic response^[12,13]. However, to date, no observational prospective studies have been specifically designed to identify predictors of MH, which should be the therapeutic target^[14].

The availability of new treatment agents with mechanisms of action different from TNF- α inhibition, has brought about the need for identifying predictors of efficacy, in particular predictors of MH, in order to individualize treatment strategies and facilitate a more personalized medicine. The aim of this study was to identify predictors of MH after one year of treatment with TNF- α inhibitors.

MATERIALS AND METHODS

Study design and patients

This is a prospective observational single center study. Recruitment of patients was performed from November 2012 until May 2016. The study was approved by the local ethics committee of Hospital Clinic de Barcelona on November 22 of 2012, and was performed according to the good clinical practice guidelines of the European

Medicines Agency (CMPM/ICH/135/95, July 2002). All patients provided written informed consent before inclusion. Eligibility criteria were patients with clinically active luminal CD requiring treatment with an anti-TNF for induction of remission. At baseline, all patients underwent a colonoscopy for assessment of endoscopic disease activity. A baseline segmental CD Endoscopic Index of Severity (CDEIS) ≥ 10 in at least one segment, or the presences of ulcerations, was required for inclusion. Exclusion criteria were formal contraindication for anti-TNF therapy, intolerance or contraindication for undergoing an ileocolonoscopy, absence of endoscopic activity as described above or a patient's refusal to participate.

Anti-TNF treatment

The induction therapy for infliximab was 5 mg/kg at weeks 0, 2 and 6; for adalimumab 160 mg and 80 mg at weeks 0 and 2, respectively, followed by 40 mg every other week. For maintenance, 5 mg/kg infliximab was administered every 8 weeks and 40 mg of adalimumab every other week. Intensification of treatment was performed reactively when loss of clinical response was documented in association with objective evidence of active disease (increased fecal calprotectin or

CRP or presence of endoscopic lesions) and drug levels below recommended thresholds (infliximab $< 3 \mu\text{g/mL}$, adalimumab $< 7 \mu\text{g/mL}$). If remission was documented by endoscopy, no modification of treatment was performed.

Clinical and biomarker data

Clinical evaluation was performed at baseline, and at weeks 6, 14, 30 and 46. At each visit the CD Activity Index (CDAI) was determined. Blood and fecal samples were also collected at each visit for assessment of biomarkers (CRP and calprotectin). Monitoring for adverse events and use of concomitant medications was registered at each visit, including unscheduled visits performed if the patient developed symptoms between scheduled visits. Drug levels and anti-drug antibodies were analyzed at baseline, week 14, week 46, and in case of loss of clinical response.

Endoscopic examination

Ileocolonoscopy was performed at baseline, week 14 and week 46. All examinations were performed under anesthesia by an endoscopist experienced in the assessment of IBD (ER, IA, IO). Quantification of endoscopic disease activity was based on the CDEIS, with measurement of segmental and global scores. Investigators evaluating the endoscopic lesions were blinded to the patient's symptoms. Endoscopic response was defined as a decrease of at least 50% from baseline in the global CDEIS and MH as segmental CDEIS ≤ 5 in all segments, which implies the disappearance of mucosal ulcerations.

Statistical analysis

A formal sample-size calculation was not performed. Precision of the predictors identified is provided by 95% confidence intervals. Quantitative variables are expressed as mean. Percentages are given for discrete variables. Analyses were performed according to the intention-to-treat principle including all recruited patients. Patients with missing data were classified as non-responders for clinical and endoscopic outcomes (Non-response imputation). Missing quantitative data at different time points was imputed using the last observation carried forward. For identification of clinical, biological and endoscopic predictors of endoscopic response, logistic regression analysis was performed. A receiver operating characteristic (ROC) curve was constructed to determine the best cut-off value for predicting MH after one year of treatment. Spearman rank-order correlation coefficient was performed to identify association between variables. Statistical significance was set at $P < 0.05$ for all tests. Statistical analysis was performed using the statistical package SPSS V.23. The Statistical methods of this study were review by one of the authors (Ingrid Ordas).

RESULTS

From 100 potentially eligible patients with clinically active disease, 62 were finally included. Thirty eight patients were excluded for the following reasons: colonoscopy could not reach the affected area ($n = 14$), absence or mild endoscopic activity with all segmental CDEIS < 10 ($n = 8$), patient's refusal to participate ($n = 7$), spontaneous patient's improvement without need of anti-TNF treatment initiation ($n = 7$) or because anti-TNF treatment was initiated for complex perianal disease without significant luminal activity ($n = 2$).

Seven patients dropped out from the study, three of them during induction and four during the maintenance period. In 5 cases because surgery was required, in one

patient treatment was switched to another anti-TNF due to immunogenicity with secondary loss of response and in one case treatment was stopped due to an adverse event (infusion reaction). All seven cases were imputed as non-responders. Fifty-nine patients (95.2%) completed the 14 wk induction period. Of these, 53 underwent endoscopic evaluation. Fifty-six patients (90.3%) completed one year of follow up of whom forty-seven underwent endoscopic evaluation (Figure 1). Endoscopic assessment was not performed in some patients at weeks 14 or 46 due to patient's refusal; all of them were considered as non-responders.

Demographic and baseline disease characteristics are summarized in Table 1. A majority of patients received combination therapy (86%). The proportion of patients achieving MH at week 46 under IFX and ADA were similar (46% *vs* 42%), the subsequent analysis was therefore performed in the pooled population.

Clinical, biological, pharmacokinetic, and endoscopic data at baseline and during follow up are presented in Table 2. At baseline, median CDAI was 201; treatment with anti-TNF resulted in a significant decrease in CDAI to 60 ($P < 0.001$) at week 14 and to 53 at week 46 ($P < 0.001$). Changes in biomarkers are summarized in Table 2. Calprotectin levels decreased progressively with significant differences relative to baseline at weeks 14 and 46. CRP value also decreased during follow-up reaching statistical significance at week 46 in the whole study population and also in the subgroup of patients with elevated CRP (> 1.0 mg/dL) at baseline ($n = 26$; 41%). Hemoglobin and albumin concentrations significantly increased at weeks 14 and 46 relative to baseline ($P < 0.05$).

Median infliximab and adalimumab concentrations at week 14 were 3.1 µg/mL and 8.9 µg/mL, respectively. After one year of treatment median serum drug concentrations were 1.8 µg/mL and 9.9 µg/mL, respectively. At baseline 8% of patients presented antidrug antibodies to infliximab (ATIs) and 10% to adalimumab (ATAs); of them 60% and 50% respectively were naïve to anti-TNF therapy. In all cases, antibody levels were in the low range (3.9-98 µg/mL). At week 14, ATIs were detected in only one patient (3%) and ATAs in none of them (the test used, ELISA, cannot detect antibodies in the presence of circulating drug). After one year of treatment, ATIs were detected in 4 patients (13%) and ATAs in one patient (4%). All of them were under concomitant immunomodulatory therapy. Median CDEIS at baseline was 6.7 with significant decreases up to 3.2 at week 14 ($P < 0.001$) and up to 3.0 ($P < 0.001$) after one year of treatment. As illustrated in Figure 2, at week 14, 56% of patients achieved endoscopic response and 34% were on MH. At week 46, the corresponding percentages for endoscopic response and MH were 52% and 44%, respectively.

Predictors of endoscopic remission

None of the demographic or baseline disease characteristics predicted endoscopic response or remission at week 14. Baseline disease characteristics with predictive value of long-term endoscopic response (wk46) in the univariate analysis included disease duration, CDAI and CDEIS. The week 14 variables that predicted endoscopic response at week 46 were: CRP, a decrease from baseline CDAI of 100 points, CDEIS, the percentage of CDEIS reduction from baseline and the achievement of endoscopic response or MH. Due to an elevated rate of missing values (35% at baseline and 42% at week 14), calprotectin was not included in the logistic regression analysis. In the multivariate analysis, only disease duration and the percentage of CDEIS reduction at week 14, independently predicted MH on the long term.

Predictors of MH after 46 wk of treatment were identified only at week 14 in the univariate analysis, including the CRP and the adalimumab concentration, the CDEIS score, the percentage of CDEIS reduction from baseline and the achievement of endoscopic response or MH at week 14. In the multivariate analysis all the endoscopic variables independently predicted MH at week 46.

The changes in clinical or biomarker variables from baseline to week 14 did not predict MH on the long term. Adalimumab or infliximab serum concentrations at week 14 were not associated with clinical or endoscopic outcomes at this time point of evaluation. Serum drug concentration at week 14 did not predict clinical outcomes or endoscopic response at week 46. Only adalimumab concentration at week 14 achieved statistical significance to predict MH on the long term (week 46). A concentration of at least 10 µg/mL at week (area under the curve: 0.76) predicts MH with moderate sensitivity (61%) and good specificity (84%). Drug concentration and anti-drug antibodies at week 46 were not correlated with clinical or endoscopic outcomes at that time of evaluation.

In our cohort, only 19% of patients required treatment intensification before achieving the endpoint of week 46. In the logistic regression analysis treatment intensification did not achieve statistical significance as a predictor of MH. To define the best cutoff value for predicting MH after one year of treatment, ROC curves were constructed for CDEIS scores at week 14 and for the percentage of CDEIS reduction

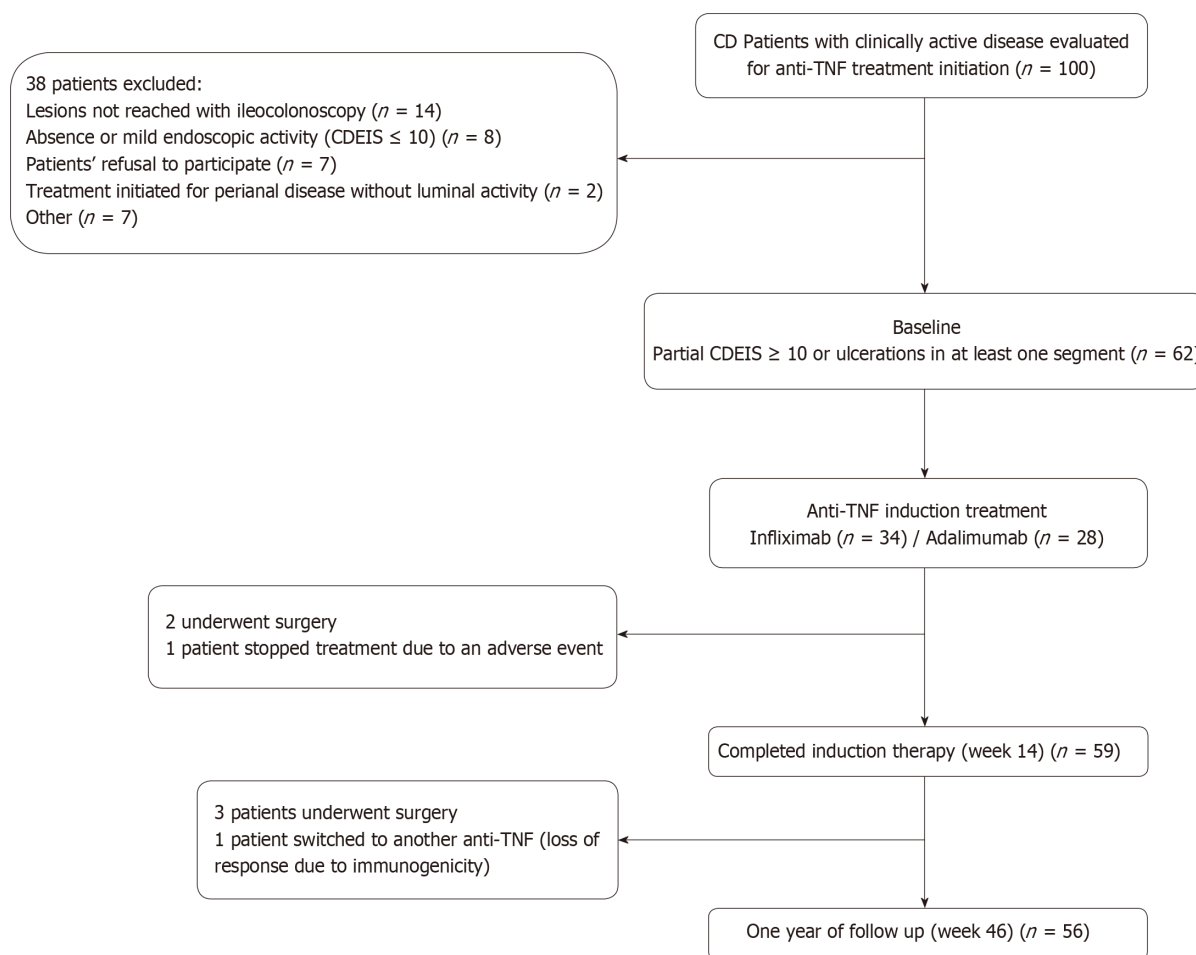


Figure 1 Flow-chart of the study. CD: Crohn's Disease; CDEIS: Crohn's Disease Endoscopic Index of Severity; TNF: Tumor necrosis factor.

from baseline to week 14. Sensitivity and specificity were also calculated for achievement of endoscopic response and MH at week 14 as predictors of long-term MH (Table 3). Relative changes in the endoscopic score from baseline to week 14 had higher accuracy in predicting MH at week 46 than absolute CDEIS values at week 14. Based on the clinical relevance of the evaluated cutoff values, a decrease of at least 80% from baseline CDEIS at week 14 was the best discriminative cutoff value for predicting MH at week 46 with a sensitivity of 59% and 91% specificity (Figure 3). As shown in Table 4, at week 14, a reduction of $\geq 80\%$ from baseline CDEIS was documented in 19 patients (31%) with a positive predictive value (PPV) of 84% and a negative predicted value of 74%. Table 5 shows the comparison of diagnostic accuracy between 50% and 80% CDEIS reduction from baseline to week 14 as a predictor of MH at week 46.

DISCUSSION

In this prospective observational study, we identified predictors of long-term MH in patients with CD treated with TNF- α inhibitors. After completing 14 weeks of treatment, we found that the absolute CDEIS value, the percentage of CDEIS reduction from baseline and the achievement of endoscopic response or MH significantly predict MH after one year of treatment. Of these four predictive factors, achievement of MH after induction treatment with an anti-TNF has already been described as a predictor of long-term MH in a series of patients retrospectively evaluated and prospectively validated in a subsequent study^[12,13]. In this study, 42 patients with active luminal CD (defined as a SES-CD ≥ 3) treated with an anti-TNF were followed clinically and endoscopically after 3 months and one year of treatment. The authors concluded that MH (defined as a SES-CD ≤ 2) after 3 mo of treatment predicted long-term MH with 88% of sensitivity and 64% of specificity. Our study shows that not only achievement of MH is a predictor of long term MH, but also achievement of endoscopic response after completing induction predicts MH on the

Table 1 Patient's demographic characteristics (n = 62) n (%)

Patient's demographic characteristics (n = 62)	
Female, n (%)	31 (50)
Age at inclusion, mean (min-max)	39 (18-72)
Disease duration (yr), mean (min-max)	9 (0-33)
Location	
Terminal ileum	32 (52)
Colonic	15 (24)
Ileocolonic	15 (24)
Associated upper involvement	3 (5)
Phenotype	
Inflammatory	39 (63)
Stricturing	14 (22)
Penetrating	9 (15)
Associated structuring + penetrating	4 (7)
Perianal disease	16 (26)
Current smokers	19 (31)
Anti-TNFdrug used	
Infliximab	34 (55)
Adalimumab	28 (45)
Prior anti-TNF exposure	16 (26)
Immunomodulators at baseline	53 (86)
Steroids at baseline	13 (21)
Previous CD surgery	9 (15)

TNF: Tumor necrosis factor; CD: Crohn's disease.

long term, expanding thus the number of patients in whom a recommendation of continued anti-TNF therapy is made after induction with high probability of achieving the therapeutic target of MH at week 46.

The percentage of CDEIS reduction as a predictor of clinical outcomes has been evaluated in a post-hoc analysis of the SONIC trial^[15]. In this study, a decrease from the baseline CDEIS of at least 50% at week 26 predicted steroid-free clinical remission at week 50 with a sensitivity of 73% and a specificity of 46 %. We consider, though, that objective demonstration of MH by endoscopy is a more robust endpoint than steroid-free clinical remission. In addition, a specificity of 46% can lead to a high rate of false positives.

In our cohort, a decrease of at least 50% from baseline CDEIS at week 14 had a sensitivity of 85% and moderate specificity (66%). In our study, we chose a reduction of 80% from baseline CDEIS as a predictor of long term MH since it has better diagnostic accuracy, with moderate sensitivity (59%) but excellent specificity (91%). Moreover, compared with a 50% reduction, it demonstrated a better PPV and positive likelihood ratio. In cases in which sensitivity is more relevant, a 50% reduction can be chosen as the endpoint. In the current study, we observed that changes in CDEIS in response to induction therapy are better predictors of long-term efficacy of anti-TNF drugs than absolute values. Absolute values are highly influenced by disease location and extension, whereas a percentage reduction relative to baseline may be preferable because it is a dynamic parameter of response and integrates the magnitude of response to induction therapy.

In this cohort, 84% of patients that achieved an 80% reduction in CDEIS from baseline to week 14 were in MH after one year of treatment. In patients who do not achieve this endpoint, potential treatment optimization might be considered by the addition of immunosuppressive agents in case of anti-TNF monotherapy, intensification of anti-TNF treatment or by considering alternative treatment strategies other than TNF- α inhibitors. The effectiveness of these type of interventions remains to be assessed in prospective clinical trials. In our study neither demographic nor disease characteristic predicted achievement of endoscopic response at week 14, or MH after induction or at week 46. This was also true for clinical disease activity and CRP. Disease duration has been reported to be a predictor of clinical response^[5] and in our study was identified as a predictor of endoscopic response in the long term

Table 2 Biological, pharmacokinetic, clinical and endoscopic data at baseline and during follow up

	Baseline, <i>n</i> = 62	Week 14, <i>n</i> = 59	<i>P</i> value (week 14-baseline)	Week 46, <i>n</i> = 56	<i>P</i> value (week 46-baseline)
CDAI, median (IQR)	201 (114-236)	60 (28-94)	<i>P</i> < 0.001	53 (26-94)	<i>P</i> < 0.001
CDEIS, median (IQR)	6.7 (5-11.3)	3.2 (0.8-5)	<i>P</i> < 0.001	3.0 (0.2-4.4)	<i>P</i> < 0.001
CRP mg/dL, median (IQR)	0.66 (0.16-1.72)	0.2 (0.03-0.71)	<i>P</i> = 0.125	0.19 (0.03-0.76)	<i>P</i> < 0.05
Hemoglobin g/L, median (IQR)	127 (113-140)	135 (121-141)	<i>P</i> < 0.05	134 (123-143)	<i>P</i> < 0.05
Albumin g/L, median (IQR)	41 (40-43)	43 (40-45)	<i>P</i> < 0.05	43 (40-45)	<i>P</i> < 0.05
Serum TNF-alpha pg/mL, median (IQR)	5.5 (3.3-8)	20 (11-36)	<i>P</i> < 0.001	17 (8.25-30)	<i>P</i> < 0.001
Fecal Calprotectin µg/g, median (IQR)	1044 (685-1800)	610 (209-1646)	<i>P</i> < 0.05	940 (233-1747)	<i>P</i> < 0.05
Infliximab µg/mL, median (IQR)	0 (0-0)	3.1 (1.2-5.6)	<i>P</i> < 0.001	1.8 (1-6.6)	<i>P</i> < 0.001
ATIs, % patients (<i>n</i>)	8 (5/62)	3 (1/34)	<i>P</i> = 0.327	13 (4/32)	<i>P</i> = 0.230
Adalimumab µg/mL, median (IQR)	0 (0-0)	8.9 (5.6-12)	<i>P</i> < 0.001	9.9 (7-12)	<i>P</i> < 0.001
ATAs, % patients (<i>n</i> /total)	10 (6/62)	0 (0/25)	<i>P</i> = 0.117	4.1 (1/24)	<i>P</i> = 0.408

IQR: Interquartile range; CRP= C reactive protein; TNF-alpha: Tumor necrosis factor alpha; ATIs: Anti-infliximab antibodies; ATAs: Anti-adalimumab antibodies; CDAI: Crohn's Disease Activity Index; CDEIS: Crohn's Disease Endoscopic Index of Severity.

(the longer the disease duration the less probabilities to achieve endoscopic response).

In our cohort, adalimumab serum concentration after completing treatment induction has predictive value for the long term MH diagnosis. Previous reports have described an association between adalimumab serum levels and achievement of MH. The cutoff point of this parameter has been situated in at least 4.9 µg/mL^[16] and some retrospective studies or studies with non-systematic measurement of adalimumab serum concentration suggest that the concentration needed to achieve this endoscopic outcome are even higher (> 7.1 µg/mL)^[17-19]. In our prospective cohort, an adalimumab concentration of at least 10 µg/mL after induction was best correlated with long term MH with a moderate sensitivity and good specificity, suggesting that patients may need even higher concentrations than previously reported. Measurement of serum drug concentration after induction could be considered as a time point to perform this evaluation for predicting long term endoscopic outcomes. Infliximab serum concentration were not predictive of MH; lack of statistical power, and the fact that a considerable number of patients had low serum infliximab concentrations may have prevented the identification of the relationship between drug levels and therapeutic response.

When we analyzed the subgroup of patients that achieved MH at weeks 14 and 46, a recommended concentration of infliximab (equal or higher than 3.0 µg/mL) was observed in a 73% and 29% of patients respectively. The high proportion of patients in MH and low anti-TNF serum concentration during maintenance might indicate that lower drug levels may be sufficient after achieving healing. The current study has several strengths. It has been prospectively performed and all patients had documented endoscopic active disease at baseline. In addition, monitoring of disease activity was prospectively registered using clinical, biological, and endoscopic variables. Our cohort has a lower clinical activity at baseline compared to pivotal registration trials. Indeed, our population probably better reflects clinical practice, where anti-TNF therapies are used not only in patients with severe disease as in pivotal trials, but also in patients with milder forms.

This study has also some limitations that should be acknowledged. It is a single center study with a limited sample size. With regard to biomarkers as predictors of endoscopic response, calprotectin could not be incorporated in the analysis due to a considerable proportion of missing samples, despite proactively reminding the patients to collect them. This is an inherent limitation of this monitoring modality. Escalation of drug doses was triggered by clinical symptoms. This could be considered as a limitation, however, there is no evidence at this moment supporting that treatment intensification based on a target serum drug concentration^[20,21] is superior to clinically based dosing. In this scenario, treatment intensification based on

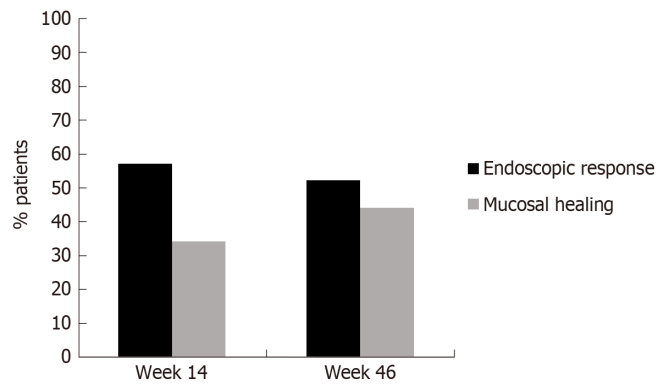


Figure 2 Endoscopic response and mucosal healing during follow-up.

clinical decisions represent the current clinical practice in the majority of centers until new evidence is available.

In summary, in patients with CD treated with an anti-TNF, endoscopic evaluation following completion of induction treatment should be considered for determining endoscopic response and predicting long-term outcomes. After 14 weeks of treatment, achievement of a reduction of 80% from baseline CDEIS may be considered a target for optimization of anti-TNF therapy in clinical practice.

Table 3 Sensitivity and specificity of variables at week 14 as predictors of long-term mucosal healing

Variable	Sensitivity	Specificity
CDEIS < 3	69	67
CDEIS < 4	62	78
80% reduction of CDEIS (baseline to week 14)	59	91
Endoscopic response at week 14	85	66
Endoscopic remission at week 14	59	85

CDEIS: Crohn's Disease Endoscopic Index of Severity.

Table 4 Diagnostic accuracy of 80% Crohn's Disease Endoscopic Index of Severity reduction at week 14 for the diagnosis of long-term mucosal healing

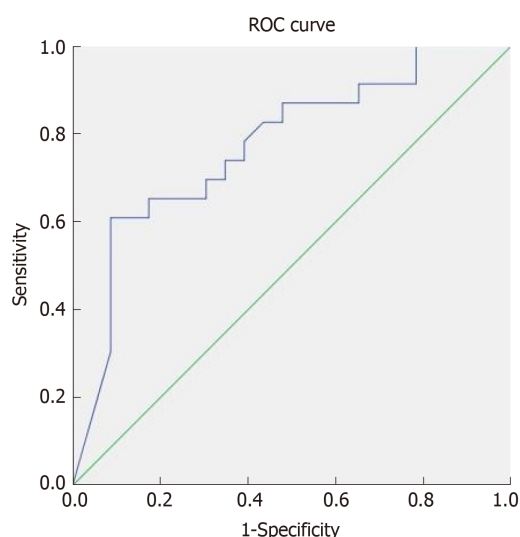
			Mucosal healing at week 46	
			No	Yes
≥ 80% reduction in CDEIS at week 14 from baseline	No	<i>n</i> (%)	32 (74.4)	11 (25.6)
	Yes	<i>n</i> (%)	3 (15.8)	16 (84.2)

CDEIS: Crohn's Disease Endoscopic Index of Severity.

Table 5 Comparison between 50 and 80% Crohn's Disease Endoscopic Index of Severity reduction from baseline to week 14 as predictors of long-term mucosal healing

CDEIS reduction	Sensitivity (95%CI)	Specificity (95%CI)	PPV (95%CI)	NPV (95%CI)	LR+ (95%CI)	LR- (95%CI)
50%	85 (66%-96%)	66 (48%-81%)	66 (54%-76%)	85 (69%-93%)	2.5 (1.5-4)	0.23 (0.09-0.57)
80%	59 (39%-77%)	91 (77%-98%)	84 (63%-94%)	74 (65%-82%)	6.9 (2.24-21)	0.45 (0.28-0.72)

CDEIS: Crohn's Disease Endoscopic Index of Severity; CI: Confidence interval; PPV: Positive predictive value; NPV: Negative predictive value; LR+: Positive likelihood ratio; LR-: Negative likelihood ratio.

**Figure 3 Receiver operating characteristics curves depicting the endoscopic response at week 14 as a predictor of mucosal healing after one year of anti-tumor necrosis factor treatment. Area under the curve = 0.778, $P = 0.001$; ROC: Receiver operating characteristics.****ARTICLE HIGHLIGHTS****Research background**

Tumor necrosis factor (TNF) inhibitors are one of the most effective therapies for induction and maintenance of remission in patients with Crohn's disease (CD), however, to date, no observational prospective studies have been specifically designed to identify predictors of mucosal healing (MH), which should be the therapeutic target.

Research motivation

Improve knowledge about the predictive factors of response to TNF inhibitors and try to provide more tools to perform a personalized treatment.

Research objectives

The aim of this study was to identify predictors of MH after one year of treatment with TNF- α inhibitors.

Research methods

Prospective observational single center study. Consecutive patients with clinically active CD requiring treatment with a TNF- α inhibitor were included. Clinical, biological and endoscopic data were obtained at baseline, weeks 14 and 46.

Research conclusions

Endoscopic response to induction therapy, defined as 80% reduction in global CD Endoscopic Index of Severity (CDEIS), is a robust predictor of long-term MH. Endoscopic response is a predictor of MH. Achievement endoscopic response after induction may be considered as a therapeutic target for anti-TNF- α therapy. None, it was an observational study to identify predictors. After induction of remission with a TNF inhibitor perform a colonoscopy should be considered to predict long-term outcomes. Endoscopic response predict long-term outcomes. There were no hypotheses. After induction of remission with a TNF inhibitor perform a colonoscopy should be considered to predict long-term outcomes in patients with CD.

Research perspectives

Clinical and biomarker data are not useful predictors of response to TNF- α inhibitors in CD, whereas endoscopic response to induction therapy, defined as 80% reduction in global CDEIS, is a robust predictor of long-term MH. Achievement of this endoscopic endpoint may be considered as a therapeutic target for anti-TNF- α therapy.

ACKNOWLEDGEMENTS

This work has been founded in part by Helmsley Charitable Trust 2015PG-IBD005.

REFERENCES

- 1 **Pariente B**, Cosnes J, Danese S, Sandborn WJ, Lewin M, Fletcher JG, Chowers Y, D'Haens G, Feagan BG, Hibi T, Hommes DW, Irvine EJ, Kamm MA, Loftus EV, Louis E, Michetti P, Munkholm P, Oresland T, Panés J, Peyrin-Biroulet L, Reinisch W, Sands BE, Schoelmerich J, Schreiber S, Tilg H, Travis S, van Assche G, Vecchi M, Mary JY, Colombel JF, Lémann M. Development of the Crohn's disease digestive damage score, the Lémann score. *Inflamm Bowel Dis* 2011; **17**: 1415-1422 [PMID: [21560202](#) DOI: [10.1002/ibd.21506](#)]
- 2 **Hazlewood GS**, Rezaie A, Borman M, Panaccione R, Ghosh S, Seow CH, Kuenzig E, Tomlinson G, Siegel CA, Melmed GY, Kaplan GG. Comparative effectiveness of immunosuppressants and biologics for inducing and maintaining remission in Crohn's disease: A network meta-analysis. *Gastroenterology* 2015; **148**: 344-354.e5; quiz e14-15 [PMID: [25448924](#) DOI: [10.1053/j.gastro.2014.10.011](#)]
- 3 **Grover Z**, Biron R, Carman N, Lewindon P. Predictors of response to Infliximab in children with luminal Crohn's disease. *J Crohns Colitis* 2014; **8**: 739-746 [PMID: [24445015](#) DOI: [10.1016/j.crohns.2013.12.017](#)]
- 4 **Sandborn WJ**, Melmed GY, McGovern DP, Loftus EV, Choi JM, Cho JH, Abraham B, Gutierrez A, Lichtenstein G, Lee SD, Randall CW, Schwartz DA, Regueiro M, Siegel CA, Spearman M, Kosutic G, Pierre-Louis B, Coarse J, Schreiber S. Clinical and demographic characteristics predictive of treatment outcomes for certolizumab pegol in moderate to severe Crohn's disease: Analyses from the 7-year PRECISE 3 study. *Aliment Pharmacol Ther* 2015; **42**: 330-342 [PMID: [26031921](#) DOI: [10.1111/apt.13251](#)]
- 5 **Ding NS**, Hart A, De Cruz P. Systematic review: Predicting and optimising response to anti-TNF therapy in Crohn's disease - algorithm for practical management. *Aliment Pharmacol Ther* 2016; **43**: 30-51 [PMID: [26515897](#) DOI: [10.1111/apt.13445](#)]
- 6 **Kiss LS**, Szamosi T, Molnar T, Miheller P, Lakatos L, Vincze A, Palatka K, Barta Z, Gasztonyi B, Salamon A, Horvath G, Tóth GT, Farkas K, Banai J, Tulassay Z, Nagy F, Szenes M, Veres G, Lovasz BD, Vegh Z, Golovics PA, Szathmari M, Papp M, Lakatos PL; Hungarian IBD Study Group. Early clinical remission and normalisation of CRP are the strongest predictors of efficacy, mucosal healing and dose escalation during the first year of adalimumab therapy in Crohn's disease. *Aliment Pharmacol Ther* 2011; **34**: 911-922 [PMID: [21883326](#) DOI: [10.1111/j.1365-2036.2011.04827.x](#)]
- 7 **Cohen RD**, Lewis JR, Turner H, Harrell LE, Hanauer SB, Rubin DT. Predictors of adalimumab dose escalation in patients with Crohn's disease at a tertiary referral center. *Inflamm Bowel Dis* 2012; **18**: 10-16 [PMID: [21456032](#) DOI: [10.1002/ibd.21707](#)]
- 8 **Triantafyllidis JK**, Mantzaris G, Karagiannis J, Papavasiliou E, Papatheodoridis G, Fouskas J, Malgarinos G, Gikas A, Papamichael K, Mathou N, Symbolakis E, Karamanolis D. Similar response to adalimumab in patients with active Crohn's disease either naive to biologic agents or with prior loss of response or intolerance to infliximab. *Rev Med Chir Soc Med Nat Iasi* 2010; **114**: 85-90 [PMID: [21456032](#) DOI: [10.1002/ibd.21707](#)]

- 20509281]
- 9 **Chaparro M**, Panes J, García V, Mañosa M, Esteve M, Merino O, Andreu M, Gutierrez A, Gomollón F, Cabriada JL, Montoro MA, Mendoza JL, Nos P, Gisbert JP. Long-term durability of infliximab treatment in Crohn's disease and efficacy of dose "escalation" in patients losing response. *J Clin Gastroenterol* 2011; **45**: 113-118 [PMID: [21242747](#) DOI: [10.1097/MCG.0b013e3181ebae9f](#)]
- 10 **Arnott ID**, McNeill G, Satsangi J. An analysis of factors influencing short-term and sustained response to infliximab treatment for Crohn's disease. *Aliment Pharmacol Ther* 2003; **17**: 1451-1457 [PMID: [12823146](#) DOI: [10.1046/j.1365-2036.2003.01574.x](#)]
- 11 **Roseth AG**, Aadland E, Grzyb K. Normalization of faecal calprotectin: A predictor of mucosal healing in patients with inflammatory bowel disease. *Scand J Gastroenterol* 2004; **39**: 1017-1020 [PMID: [15513345](#) DOI: [10.1080/00365520410007971](#)]
- 12 **af Björkstén CG**, Nieminen U, Sipponen T, Turunen U, Arkkila P, Färkkilä M. Mucosal healing at 3 months predicts long-term endoscopic remission in anti-TNF-treated luminal Crohn's disease. *Scand J Gastroenterol* 2013; **48**: 543-551 [PMID: [23477356](#) DOI: [10.3109/00365521.2013.772230](#)]
- 13 **af Björkstén CG**, Nieminen U, Turunen U, Arkkila PE, Sipponen T, Färkkilä MA. Endoscopic monitoring of infliximab therapy in Crohn's disease. *Inflamm Bowel Dis* 2011; **17**: 947-953 [PMID: [20860048](#) DOI: [10.1002/ibd.21439](#)]
- 14 **Peyrin-Biroulet L**, Sandborn W, Sands BE, Reinisch W, Bemelman W, Bryant RV, D'Haens G, Dotan I, Dubinsky M, Feagan B, Fiorino G, Geary R, Krishnareddy S, Lakatos PL, Loftus EV, Marteau P, Munkholm P, Murdoch TB, Ordás I, Panaccione R, Riddell RH, Ruel J, Rubin DT, Samaan M, Siegel CA, Silverberg MS, Stoker J, Schreiber S, Travis S, Van Assche G, Danese S, Panes J, Bouguen G, O'Donnell S, Pariente B, Winer S, Hanauer S, Colombel JF. Selecting Therapeutic Targets in Inflammatory Bowel Disease (STRIDE): Determining Therapeutic Goals for Treat-to-Target. *Am J Gastroenterol* 2015; **110**: 1324-1338 [PMID: [26303131](#) DOI: [10.1038/ajg.2015.233](#)]
- 15 **Ferrante M**, Colombel JF, Sandborn WJ, Reinisch W, Mantzaris GJ, Kornbluth A, Rachmilewitz D, Lichtiger S, D'Haens GR, van der Woude CJ, Danese S, Diamond RH, Oortwijn AF, Tang KL, Miller M, Cornillie F, Rutgeerts PJ. International Organization for the Study of Inflammatory Bowel Diseases. Validation of endoscopic activity scores in patients with Crohn's disease based on a post hoc analysis of data from SONIC. *Gastroenterology* 2013; **145**: 978-986.e5 [PMID: [23954314](#) DOI: [10.1053/j.gastro.2013.08.010](#)]
- 16 **Roblin X**, Marotte H, Rinaudo M, Del Tedesco E, Moreau A, Phelip JM, Genin C, Peyrin-Biroulet L, Paul S. Association between pharmacokinetics of adalimumab and mucosal healing in patients with inflammatory bowel diseases. *Clin Gastroenterol Hepatol* 2014; **12**: 80-84.e2 [PMID: [23891927](#) DOI: [10.1016/j.cgh.2013.07.010](#)]
- 17 **Yarur AJ**, Jain A, Hauenstein SI, Quintero MA, Barkin JS, Deshpande AR, Sussman DA, Singh S, Abreu MT. Higher Adalimumab Levels Are Associated with Histologic and Endoscopic Remission in Patients with Crohn's Disease and Ulcerative Colitis. *Inflamm Bowel Dis* 2016; **22**: 409-415 [PMID: [26752470](#) DOI: [10.1097/MIB.0000000000000689](#)]
- 18 **Zittan E**, Kabakchiev B, Milgrom R, Nguyen GC, Croitoru K, Steinhart AH, Silverberg MS. Higher Adalimumab Drug Levels are Associated with Mucosal Healing in Patients with Crohn's Disease. *J Crohns Colitis* 2016; **10**: 510-515 [PMID: [26783345](#) DOI: [10.1093/ecco-jcc/jjw014](#)]
- 19 **Ungar B**, Levy I, Yavne Y, Yavzori M, Picard O, Fudim E, Loebstein R, Chowers Y, Eliakim R, Kopylov U, Ben-Horin S. Optimizing Anti-TNF- α Therapy: Serum Levels of Infliximab and Adalimumab Are Associated With Mucosal Healing in Patients With Inflammatory Bowel Diseases. *Clin Gastroenterol Hepatol* 2016; **14**: 550-557.e2 [PMID: [26538204](#) DOI: [10.1016/j.cgh.2015.10.025](#)]
- 20 **Vande Casteele N**, Ferrante M, Van Assche G, Ballet V, Compernelle G, Van Steen K, Simoons S, Rutgeerts P, Gils A, Vermeire S. Trough concentrations of infliximab guide dosing for patients with inflammatory bowel disease. *Gastroenterology* 2015; **148**: 1320-1329.e3 [PMID: [25724455](#) DOI: [10.1053/j.gastro.2015.02.031](#)]
- 21 **D'Haens G**, Vermeire S, Lambrecht G, Baert F, Bossuyt P, Pariente B, Buisson A, Bouhnik Y, Filippi J, Vander Woude J, Van Hooft P, Moreau J, Louis E, Franchimont D, De Vos M, Mana F, Peyrin-Biroulet L, Brixi H, Allez M, Caenepeel P, Aubourg A, Oldenburg B, Pierik M, Gils A, Chevret S, Laharie D, GETAID. Increasing Infliximab Dose Based on Symptoms, Biomarkers, and Serum Drug Concentrations Does Not Increase Clinical, Endoscopic, and Corticosteroid-Free Remission in Patients With Active Luminal Crohn's Disease. *Gastroenterology* 2018; **154**: 1343-1351.e1 [PMID: [29317275](#) DOI: [10.1053/j.gastro.2018.01.004](#)]



Application of a 3D-printed "fistula stent" in plugging enteroatmospheric fistula with open abdomen: A case report

Zi-Yan Xu, Hua-Jian Ren, Jin-Jian Huang, Zong-An Li, Jian-An Ren

ORCID number: Zi-Yan Xu (0000-0001-9027-1282); Hua-Jian Ren (0000-0002-2205-4072); Jin-Jian Huang (0000-0002-8951-8935); Zong-An Li (0000-0002-3580-5891); Jian-An Ren (0000-0002-4697-4762).

Author contributions: Xu ZY, Ren HJ, and Ren JA designed this report; Ren HJ and Huang JJ implanted the fistula stent; Xu ZY and Li ZA fabricated this 3D-printed fistula stent; Xu ZY and Ren HJ followed the patient and recorded his medical information; Xu ZY wrote the paper; Xu ZY and Ren HJ contributed equally to this paper.

Informed consent statement: Written informed consent was obtained from the patient.

Conflict-of-interest statement: We declared no potential conflicts of interest with respect to the research, authorship, and publication of this article.

CARE Checklist (2016) statement: The authors have read the CARE Checklist (2016), and the guidelines of the CARE Checklist (2016) have been adopted.

Open-Access: This article is an open-access article which was selected by an in-house editor and fully peer-reviewed by external reviewers. It is distributed in accordance with the Creative Commons Attribution Non Commercial (CC BY-NC 4.0) license, which permits others to distribute, remix, adapt, build upon this work non-commercially, and license their derivative works on different terms, provided the

Zi-Yan Xu, Hua-Jian Ren, Jin-Jian Huang, Jian-An Ren, Research Institute of General Surgery, Jinling Hospital, Nanjing 210002, Jiangsu Province, China

Zi-Yan Xu, School of Medicine, Nanjing University, Nanjing 210008, Jiangsu Province, China

Zong-An Li, NARI School of Electrical and Automation Engineering, Nanjing Normal University, Nanjing 210042, Jiangsu Province, China

Corresponding author: Jian-An Ren, MD, FACS, PhD, Chief Doctor, Professor, Surgeon, Research Institute of General Surgery, Jinling Hospital, 305 East Zhongshan Road, Nanjing 210002, Jiangsu Province, China. jiananr@gmail.com

Telephone: +86-13605169808

Fax: +86-25-80860376

Abstract

BACKGROUND

Open abdomen (OA) has been generally accepted for its magnificent superiority and effectiveness in patients with severe trauma, severe intra-abdominal infection, and abdominal compartment syndrome. In the meantime, OA calls for a mass of nursing and the subsequent enteroatmospheric fistula (EAF), which is one of the most common complications of OA therapy, remains a thorny challenge.

CASE SUMMARY

Our team applied thermoplastic polyurethane as a befitting material for producing a 3D-printed "fistula stent" in the management of an EAF patient, who was initially admitted to local hospital because of abdominal pain and distension and diagnosed with bowel obstruction. After a series of operations and OA therapy, the patient developed an EAF.

CONCLUSION

Application of this novel "fistula stent" resulted in a drastic reduction in the amount of lost enteric effluent and greatly accelerated rehabilitation processes.

Key words: 3D printing; Enteroatmospheric fistula; Open abdomen; Isolation technique; Case report

©The Author(s) 2019. Published by Baishideng Publishing Group Inc. All rights reserved.

Core tip: Few methods can be utilized to control enteroatmospheric fistulas (EAFs)

original work is properly cited and the use is non-commercial. See: <http://creativecommons.org/licenses/by-nc/4.0/>

Manuscript source: Unsolicited manuscript

Received: February 17, 2019

Peer-review started: February 18, 2019

First decision: February 26, 2019

Revised: March 7, 2019

Accepted: March 16, 2019

Article in press: March 16, 2019

Published online: April 14, 2019

P-Reviewer: Gupta R, Lara FJ, Misiakos EP, Okumura K, Skierucha M

S-Editor: Yan JP

L-Editor: Wang TQ

E-Editor: Song H



which are unlikely to achieve spontaneous closure. The 3D-printed “fistula stent” presented here can be implanted to close EAF in the early stage of open abdomen. We think that this report could start the train of thought for plugging EAF to reduce the lost enteric effluent as well as avoid water electrolyte imbalance, corrosion on the wound surface, and intra-abdominal infection.

Citation: Xu ZY, Ren HJ, Huang JJ, Li ZA, Ren JA. Application of a 3D-printed “fistula stent” in plugging enteroatmospheric fistula with open abdomen: A case report. *World J Gastroenterol* 2019; 25(14): 1775-1782

URL: <https://www.wjgnet.com/1007-9327/full/v25/i14/1775.htm>

DOI: <https://dx.doi.org/10.3748/wjg.v25.i14.1775>

INTRODUCTION

The open abdomen (OA) therapy has been commonly recognized as a crucial treatment in settling severe trauma, severe intra-abdominal infection (sIAI) and abdominal compartment syndrome (ACS). The World Society of ACS has formulated a classification for OA in which frozen OA with fistula is classified as grade 4 (Table 1)^[1]. Meanwhile, fistula, which is one of the most common complications of OA, remains a nightmare for all surgeons and intensive care unit doctors, and urgently needs to be solved^[2].

Enteroatmospheric fistula (EAF) is a type of fistula different from enterocutaneous fistula (ECF). The occurrence rate of EAFs is reported to be 25% in patients receiving OA with an associated mortality rate of 42%^[3]. Various reasons result in these openings between the atmosphere and the lumen within the gastrointestinal tract. Unlike ECF, EAF has neither connective fistulous tract or overlying soft tissue such as the skin, subcutaneous tissue, omentum majus and other gastrointestinal tract which leads to high flow of enteric fistula effluent and makes it unlikely to reach spontaneous closure. In addition to fluid and electrolyte imbalance, acid-base imbalance and gastrointestinal dysfunction, enteric fistula effluent from EAF can cause more disastrous effects^[4]: enteric fistula effluent contaminates the exposed wound and exacerbates the infection condition which can lead to sepsis in severe cases. Besides, high and continuous output of digestive juices raises the difficulty in fistula closure, prolongs the length of hospital stay along with medical expense^[3], and increases mortality tremendously.

To date, multiple techniques have been come up with to solve EAF such as silicone fistula plug^[5], collapsible EAF isolation device^[6], polyethylene glycol tube^[7], and covered self-expanding metal stent^[8]. However, these techniques can only be used after the formation of frozen abdomen or the adhesion between the bowel and the abdominal wall. On the other hand, they can hardly reach accurate match with the trend of bowel or the shape of the orifice of the fistulous tract. Furthermore, after the labiate fistula is formed, the outcomes usually get worse^[9]. In order to carry out enteral nutrition (EN) as early as possible and shorten the waiting time before definitive gastrointestinal reconstruction, our team applied a 3D-printed “fistula stent”, which is a combination of 3D printing with traditional isolation technique, to control enteric fistula effluent at the early stage of OA.

CASE PRESENTATION

Patient information

A 33-year-old male patient complaining of abdominal pain and distension was initially diagnosed as bowel obstruction and went through enterolysis and omentum majus biopsy (Table 2). Several days after the first surgery, the patient appeared a relapse of abdominal pain and received exploratory laparotomy and bypass operation. Then, the patient’s physical condition turned to go downhill with intermittent fever and cachexia. Afterwards, the patient was referred to our clinic with sIAI, hypoalbuminemia, hydrothorax, poor incisions healing, and suspected fistula with intestinal juice flowing from the incision.

After the patient was admitted to our hospital, he presented with intermittent high fever (39 °C) and cachexia. Anti-infection therapy, acid suppression therapy, digestive

Table 1 Open abdomen classification from the World Society of the Abdominal Compartment Syndrome

OA classification from the WSACS	
Grade 1A	Clean without fixation
Grade 1B	Contaminated without fixation
Grade 1C	Enteric leak without fixation
Grade 2A	Clean with developing fixation
Grade 2B	Contaminated with developing fixation
Grade 2C	Enteric leak with developing fixation
Grade 3A	Clean with frozen abdomen
Grade 3B	Contaminated with frozen abdomen
Grade 4	Formed EAF with frozen abdomen

OA: Open abdomen; WSACS: World Society of the Abdominal Compartment Syndrome; EAF: Enteroatmospheric fistula.

juices secretion suppression therapy, total parenteral nutrition (PN), and double-pipe drainage were utilized to maintain the patient's homeostasis. To relieve the symptoms, we decided to carry out OA to locate the source of enteric fistula effluent and control the IAI. During the procedure of exploration, the fistula was found situated at the place where the side-to-side anastomosis was carried out during the bypass operation (Figure 1A). The volume of enteric fistula effluent reached a peak of approximately 2500 mL/d, corroding surrounding tissue and incision continuously, thus making the orifice of the fistulous tract and incision unlikely to heal spontaneously. Afterwards, high-resolution computed tomography and contrast-mediated fistula angiography confirmed the existence of the EAF (Figure 1B), the area of which reached 8.5 cm², thus making most other isolation techniques inapplicable and invalid^[9].

Interventions

With the intention of blocking the enteric effluent to improve fistula healing, restoring EN, and carrying out definitive surgeries earlier, we attempted to implant a "fistula stent" to plug the EAF. After investigating the anatomy of EAF from fistulography and measuring the actual inner diameter and tortuosity of the bowel with fingers, we utilized Solidwork software to build the model of a hollow and curving pipe stent with a small protuberance and integrated wall. The following data were collected: inner diameter of 14 mm, thickness of pipe wall of 0.5 mm, length of 14 cm, and bend pipe instead of combined two straight ones. The whole model was saved in Standard Template Library (STL) form to be recognized by 3D printer (Figure 2A).

Thermoplastic polyurethane (TPU) is a synthetic and biocompatible material with strong tenacity and good flexibility, which has been applied widely in medical devices such as catheter and vascular graft. Our team has been investigating the properties and biocompatibility of TPU for years and the safety of TPU-made stent is assured^[10]. We collaborated with Nanjing Normal University and utilized Fused Deposition Modeling (FDM), which is one of the most classic and mature techniques of 3D printing, to build the "fistula stent" from STL file (Figure 2B).

Nine days after carrying out OA, the stent was implanted into the bowel through the orifice of the fistulous tract and proved to suit the trend of bowel ideally (Figure 3A-E). No obstruction was observed around the orifice of the fistulous tract. Then, contrast-mediated fistula angiography was conducted to verify the effectiveness of the stent with the contrast agent flowing past the stent without obstruction (Figure 3F). The protuberance was fixed with threads to avoid displacement due to peristalsis or postural changes (Figure 4). After the implantation, there was an obvious decrease in the amount of enteric fistula effluent and increase in stool frequency and capacity. Four days after implantation, we restored the patient's EN by nasal feeding, which was started from 500 mL and increased to 1500 mL during the following 3 d. No abnormal or subjective discomfort was observed during the whole process.

Several indexes of the patient were recorded in which we regarded the amount of lost enteric effluent (V_{loss}) as the most significant one. In the duration of therapy, V_{loss} was equal to the amount of drainage fluid from the fistula orifice minus the amount of fistula irrigation fluid. EAF in this patient belonged to high flow fistula (> 500 mL/d) because the scope of the orifice of the fistulous tract occupied nearly half of the intestinal wall (Figure 5A). Though it was still higher than 400 mL/d, leakage of

Table 2 Patient's previous surgeries		
Timing	Diagnosis	Surgeries
Initial	Bowel obstruction	Enterolysis and omentum majus biopsy
4 wk later	Abdominal pain	Exploratory laparotomy and bypass operation for bowel obstruction
7 wk later	Hydrothorax	Bilateral thoracentesis
2 mo later	Fistula and sIAI	OA

OA: Open abdomen; sIAI: Severe intra-abdominal infection.

enteric effluent was notably reduced after the implantation. With the increase in the amount of EN per day from 500 mL to 1500 mL, V_{loss} floated upwards within a short time and gradually turn to decrease by degrees.

Outcomes

Seven days after implantation, no sign of pyrexia or obvious infection existed and the general condition of the patient was improved with frozen abdomen formed steadily and drainage unobstructed. Considering the good physical condition of the patient and the blocked EAF, skin grafting on the abdominal wall was conducted successfully. Timely blocking of EAF laid the foundation of the skin graft healing. Ten days after skin grafting, the abdomen had granulated around the EAF and the orifice of the fistulous tract had also decreased to a very small size (Figure 6). During the follow-up, we observed that the orifice of the fistulous tract was enlarged due to the change in abdominal incision and body position, so we used butterfly-shaped adhesive to strain the bilateral abdominal walls to control the V_{loss} further. The patient is receiving EN in good condition and waiting for definitive intestinal anastomosis and abdominal closure, in which the “fistula stent” will be drawn from the orifice of the fistulous tract.

FINAL DIAGNOSIS

EAF, sIAI, and hypoalbuminemia.

TREATMENT

Fistula stent; anti-infection therapy; total PN and double-pipe drainage.

OUTCOME AND FOLLOW-UP

The patient has passed the crisis and received skin grafting. The patient is receiving EN in good condition and waiting for definitive intestinal anastomosis and abdominal closure.

DISCUSSION

What we introduce in this case report is a hollow and curving pipe stent with integrated wall, which is a combination of isolation technique with 3D printing^[1], and can be applied to plug EAF at the very early stage of OA. Unlike silicone fistula plug reported by Ozer *et al*^[5] or PEG tube reported by Miranda *et al*^[7], 3D-printed “fistula stent” can be used to block EAF as soon as the EAF is discovered or formed. In other words, successfully plugging EAF from inside can transform some grade 4 OA to grade 1C or 2C in a sense, rather than simply blocking fistulous tract or ECF after the formation of frozen abdomen or skin grafting. We think that our report could start the train of thought for plugging EAF at the early stage to reduce the amount of lost enteric effluent as well as avoid water electrolyte imbalance, corrosion on wound surface, and IAI. Furthermore, “fistula stent” functions as a temporary tract to restore EN and improve bowel function, which can accelerate the process of rehabilitation. In addition, a stent which can block nearly all the orifice of the fistulous tract saves a lot of work of drainage and succus entericus reinfusion.

We regard our 3D-printed “fistula stent” as a strong and ideal supplement to

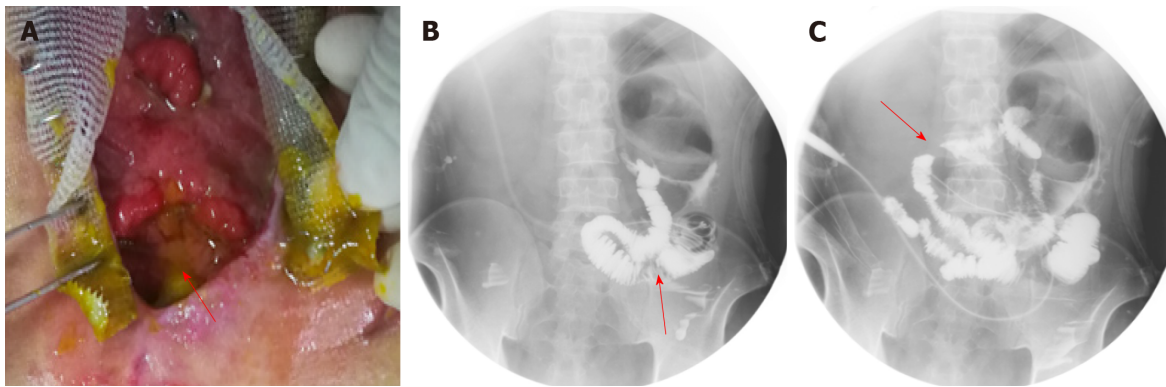


Figure 1 Clinical picture and imaging materials of the patient. A: The enteroatmospheric fistula (EAF) happened at side-to-side anastomosis was exposed and visible after open abdomen (red arrow); B: Contrast-mediated fistula angiography through the orifice of the fistulous tract (red arrow); C: The location of initial obstruction was shown (red arrow).

negative pressure wound therapy, total PN, and somatostatin therapy, which are the key techniques to close an EAF^[12]. And it has the potential to be combined with advanced technique of bio-printed 3D human intestinal tissues^[13]. However, several deficiencies exist with FDM based 3D-printed “fistula stent”. When adhesion between the bowel and the abdominal wall or the frozen abdomen formed, the size and shape of the orifice of the fistulous tract may change, thus causing the stent unfit with the bowel tract. On the other hand, the “fistula stent” has the risk of enlarging the EAF size, reducing the rate of spontaneous closure. Further, the sample size is still very limited and more well-designed trials are required to verify the effectiveness of 3D-printed plugs.

CONCLUSION

EAFs in OA patients continue to be a challenge. Our 3D-printed “fistula stent” is presented to offer an effective and applicable method to block EAF at the early stage to simplify the management of OA with EAF, thus providing conditions for definitive surgeries.

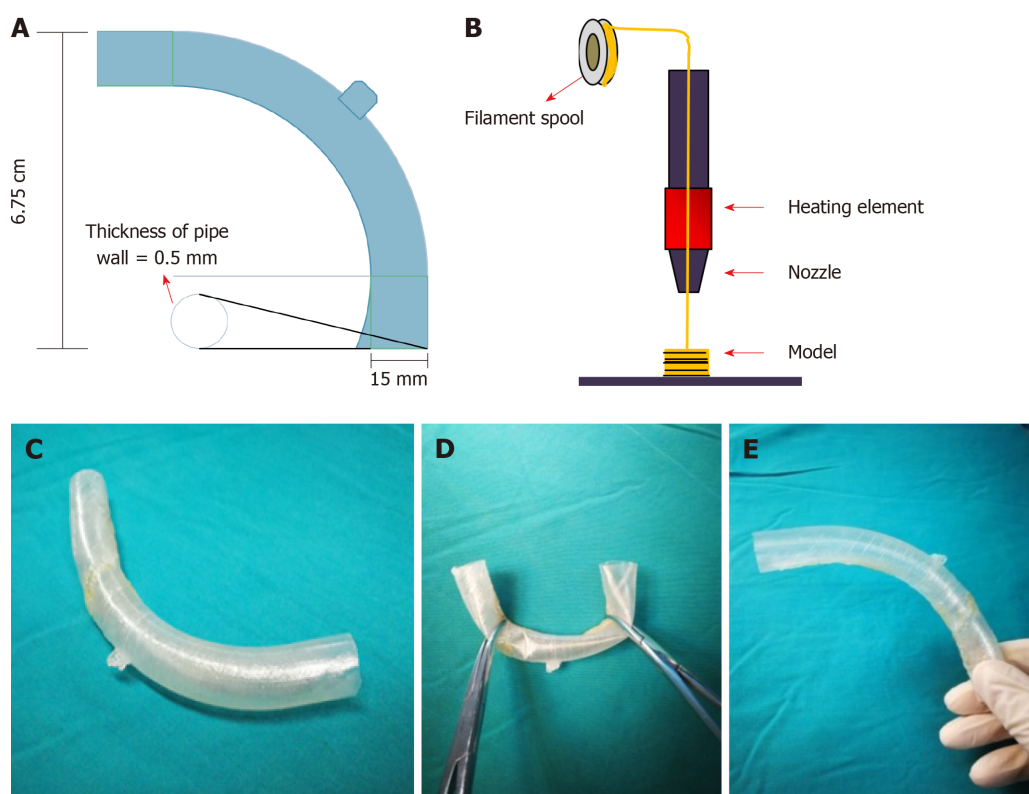


Figure 2 Manufacturing process of the “fistula stent”. A: The blueprint of “fistula stent” was built with Solidwork software and saved in Standard Template Library (STL) form; B: Fused Deposition Modeling is a process where thermoplastic filaments are driven with a motorized heated nozzle; C: Build model of a hollow and curving pipe stent with a small protuberance and integrated wall; D: Flexibility of the “fistula stent”; E: Shape memory of the “fistula stent” after application of an external force.

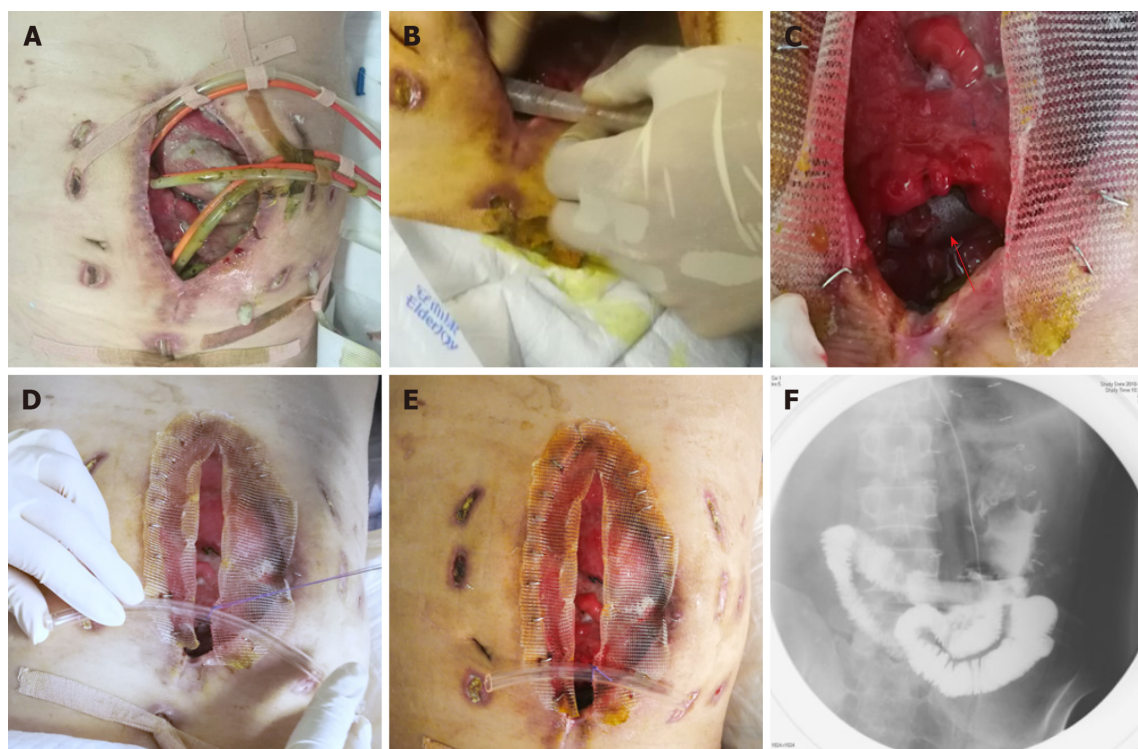


Figure 3 Process of the implantation and fixation of the “fistula stent”. A: Four double pipes were used to drainage enteric fistula effluent before implantation ; B: The process of implantation; C: After the implantation the stent can still be seen (red arrow); D: The process of fixation by suturing the small protuberance with a latex tube overhanging the abdominal wall; E: After the accomplishment of implantation, only one double pipe was needed for drainage; F: Contrast-mediated fistula angiography was conducted to verify the effectiveness of the stent and the contrast agent flowed past the stent without obstruction.

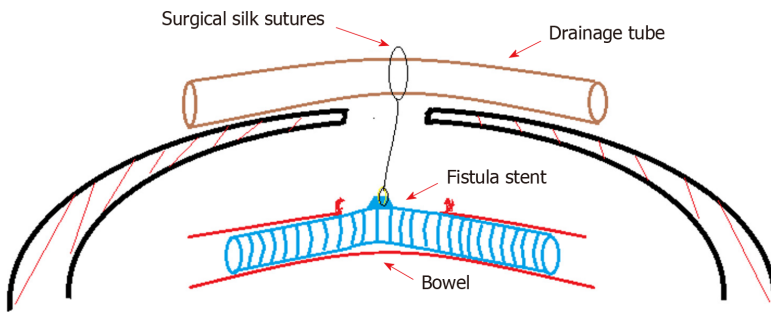


Figure 4 Concept graph of how is the “fistula stent” fixed in the bowel. The protuberance is connected with a latex drainage tube hanging over the abdominal wall in order to prevent the sliding due to peristalsis.

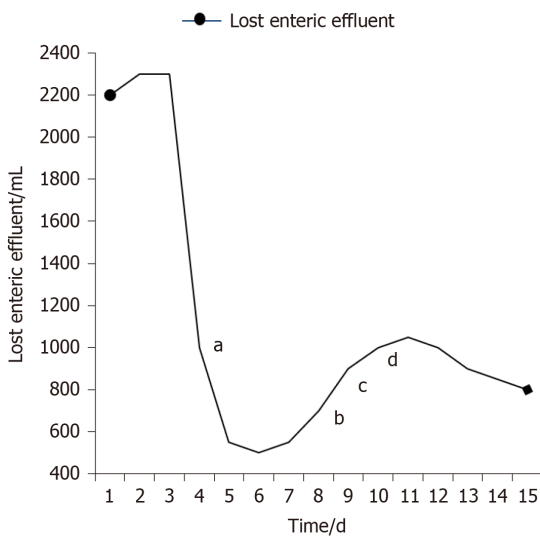


Figure 5 Recorded amount of lost enteric effluent. ^aThe day of implantation; ^bStarting enteral nutrition (EN) of 500 mL; ^cEN of 1000 mL; ^dEN of 1500 mL.

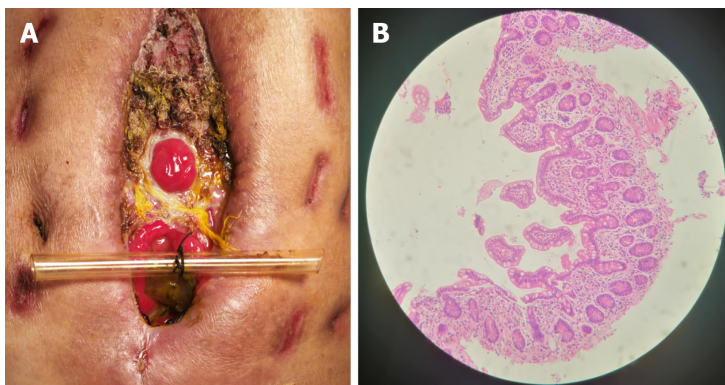


Figure 6 Follow-up after the implantation. A: After skin grafting, the abdomen had granulated around the enteroatmospheric fistula (EAF) and the orifice of the fistulous tract had also decreased to a very small size; B: Atrophic intestinal mucosa in the distal end of the EAF before restoring enteral nutrition.

REFERENCES

- 1 **Kirkpatrick AW**, Roberts DJ, De Waele J, Jaeschke R, Malbrain ML, De Keulenaer B, Duchesne J, Bjorck M, Leppaniemi A, Ejike JC, Sugrue M, Cheatham M, Ivatury R, Ball CG, Reintam Blaser A, Regli A, Balogh ZJ, D'Amours S, Debergh D, Kaplan M, Kimball E, Olvera C; Pediatric Guidelines Sub-Committee for the World Society of the Abdominal Compartment Syndrome. Intra-abdominal hypertension and the abdominal compartment syndrome: Updated consensus definitions and clinical practice guidelines from the World Society of the Abdominal Compartment Syndrome. *Intensive Care Med* 2013; **39**: 1190-1206 [PMID: 23673399 DOI: 10.1007/s00134-013-2906-z]
- 2 **Schechter WP**, Hirshberg A, Chang DS, Harris HW, Napolitano LM, Wexner SD, Dudrick SJ. Enteric

- fistulas: Principles of management. *J Am Coll Surg* 2009; **209**: 484-491 [PMID: [19801322](#) DOI: [10.1016/j.jamcollsurg.2009.05.025](#)]
- 3 **Boele van Hensbroeck P**, Wind J, Dijkgraaf MG, Busch OR, Goslings JC. Temporary closure of the open abdomen: A systematic review on delayed primary fascial closure in patients with an open abdomen. *World J Surg* 2009; **33**: 199-207 [PMID: [19089494](#) DOI: [10.1007/s00268-008-9867-3](#)]
- 4 **Cristaudo AT**, Jennings SB, Hitos K, Gunnarsson R, DeCosta A. Treatments and other prognostic factors in the management of the open abdomen: A systematic review. *J Trauma Acute Care Surg* 2017; **82**: 407-418 [PMID: [27918375](#) DOI: [10.1097/TA.0000000000001314](#)]
- 5 **Ozer MT**, Sinan H, Zeybek N, Peker Y. A simple novel technique for enteroatmospheric fistulae: Silicone fistula plug. *Int Wound J* 2014; **11** Suppl 1: 22-24 [PMID: [24851733](#) DOI: [10.1111/iwj.12308](#)]
- 6 **Heineman JT**, Garcia LJ, Obst MA, Chong HS, Langin JG, Humpal R, Pezzella PA, Dries DJ. Collapsible Enteroatmospheric Fistula Isolation Device: A Novel, Simple Solution to a Complex Problem. *J Am Coll Surg* 2015; **221**: e7-14 [PMID: [26122589](#) DOI: [10.1016/j.jamcollsurg.2015.04.015](#)]
- 7 **Miranda LE**, Miranda AC. Enteroatmospheric fistula management by endoscopic gastrostomy PEG tube. *Int Wound J* 2017; **14**: 915-917 [PMID: [28198100](#) DOI: [10.1111/iwj.12726](#)]
- 8 **Rebibo L**, Wacrenier A, Thiebault H, Delcenserie R, Regimbeau JM. Combined endoscopic and surgical covered stent placement: A new tailored treatment for enteroatmospheric fistula in patients with terminal ileostomy. *Endoscopy* 2017; **49**: E35-E36 [PMID: [28068698](#) DOI: [10.1055/s-0042-121489](#)]
- 9 **Blair SG**, Fayard NJ, Ahmed N, Rogers EA, Simmons JD. Early use of split-thickness skin graft allows separation of the wound into different compartments facilitating the collection of enteroatmospheric fistulae output. *Am Surg* 2015; **81**: E96-E98 [PMID: [25760178](#)]
- 10 **Huang JJ**, Ren JA, Wang GF, Li ZA, Wu XW, Ren HJ, Liu S. 3D-printed "fistula stent" designed for management of enterocutaneous fistula: An advanced strategy. *World J Gastroenterol* 2017; **23**: 7489-7494 [PMID: [29151703](#) DOI: [10.3748/wjg.v23.i41.7489](#)]
- 11 **Huang J**, Li Z, Hu Q, Chen G, Ren Y, Wu X, Ren J. Bioinspired Anti-digestive Hydrogels Selected by a Simulated Gut Microfluidic Chip for Closing Gastrointestinal Fistula. *iScience* 2018; **8**: 40-48 [PMID: [30273911](#) DOI: [10.1016/j.isci.2018.09.011](#)]
- 12 **Terzi C**, Egeli T, Canda AE, Arslan NC. Management of enteroatmospheric fistulae. *Int Wound J* 2014; **11** Suppl 1: 17-21 [PMID: [24851732](#) DOI: [10.1111/iwj.12288](#)]
- 13 **Madden LR**, Nguyen TV, Garcia-Mojica S, Shah V, Le AV, Peier A, Visconti R, Parker EM, Presnell SC, Nguyen DG, Retting KN. Bioprinted 3D Primary Human Intestinal Tissues Model Aspects of Native Physiology and ADME/Tox Functions. *iScience* 2018; **2**: 156-167 [PMID: [30428372](#) DOI: [10.1016/j.isci.2018.03.015](#)]



Published By Baishideng Publishing Group Inc
7041 Koll Center Parkway, Suite 160, Pleasanton, CA 94566, USA
Telephone: +1-925-2238242
Fax: +1-925-2238243
E-mail: bpgoffice@wjgnet.com
Help Desk: <http://www.f6publishing.com/helpdesk>
<http://www.wjgnet.com>

